

# High-dynamic-range displays : contributions to signal processing and backlight control

## ***Citation for published version (APA):***

Hammer, M. (2014). *High-dynamic-range displays : contributions to signal processing and backlight control*. [Phd Thesis 2 (Research NOT TU/e / Graduation TU/e), Electrical Engineering]. Technische Universiteit Eindhoven. <https://doi.org/10.6100/IR773243>

## ***DOI:***

[10.6100/IR773243](https://doi.org/10.6100/IR773243)

## ***Document status and date:***

Published: 01/01/2014

## ***Document Version:***

Publisher's PDF, also known as Version of Record (includes final page, issue and volume numbers)

## ***Please check the document version of this publication:***

- A submitted manuscript is the version of the article upon submission and before peer-review. There can be important differences between the submitted version and the official published version of record. People interested in the research are advised to contact the author for the final version of the publication, or visit the DOI to the publisher's website.
- The final author version and the galley proof are versions of the publication after peer review.
- The final published version features the final layout of the paper including the volume, issue and page numbers.

[Link to publication](#)

## ***General rights***

Copyright and moral rights for the publications made accessible in the public portal are retained by the authors and/or other copyright owners and it is a condition of accessing publications that users recognise and abide by the legal requirements associated with these rights.

- Users may download and print one copy of any publication from the public portal for the purpose of private study or research.
- You may not further distribute the material or use it for any profit-making activity or commercial gain
- You may freely distribute the URL identifying the publication in the public portal.

If the publication is distributed under the terms of Article 25fa of the Dutch Copyright Act, indicated by the "Taverne" license above, please follow below link for the End User Agreement:

[www.tue.nl/taverne](http://www.tue.nl/taverne)

## ***Take down policy***

If you believe that this document breaches copyright please contact us at:

[openaccess@tue.nl](mailto:openaccess@tue.nl)

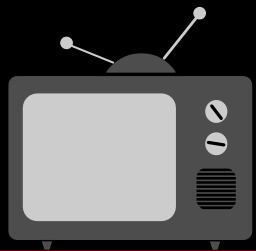
providing details and we will investigate your claim.

Once you go HDR, you never go back.

In daily life, a large range of light intensities can occur. For example, the sun at noon is up to 100 million times brighter than a starlit night. The human visual system is capable of adapting to this full intensity range of as much as 10 orders of magnitude. In comparison, the dynamic range of a typical liquid-crystal display (LCD) is only 3 orders of magnitude and the peak luminance is usually around  $500 \text{ cd/m}^2$ , which is substantially lower than the average luminance on a sunny day ( $100.000 \text{ cd/m}^2$ ) or even on a cloudy day ( $20.000 \text{ cd/m}^2$ ). These obvious discrepancies between real-world and display leaves ample room for improvement.

In this dissertation, the poor contrast and peak luminance (also referred to as dynamic range) of LCDs is addressed. The light efficiency of conventional LCDs is typically 5-7% due to the crossed polarisers, small pixel aperture, and the presence of colour filters. In order to achieve high system efficiency, we investigated three options; (1) an LC-panel with RGBW subpixel layout and local backlight boosting, (2) a colour-sequential display with local luminance boosting, and (3) a 120 Hz, 2-field colour-sequential system. Finally, we investigated the contrast requirements for high-contrast display systems by considering human-eye glare the limiting factor. In order to enable the described research, a versatile high-dynamic range display system was built.

This thesis contributes primarily to the field of display systems engineering with novel video processing and backlight control algorithms. A sophisticated backlight with HDR capabilities was constructed to facilitate the research and to demonstrate the performance of the proposed concepts. Existing methods for visualising HDR images consider display luminance and contrast characteristics constant. This thesis contributes by demonstrating that, by considering such characteristics dynamic, it is possible to increase both contrast and luminance without physically modifying the display system.



High-Dynamic-Range Displays

Martin Hammer

# High-Dynamic-Range Displays

Contributions to  
Signal Processing and Backlight Control



Martin Hammer



# **High-Dynamic-Range Displays**

Contributions to  
Signal Processing and Backlight Control

Martin Hammer

The work described in this thesis has been carried out at the *Philips Research Laboratories* and the *Philips Business-Unit Television* (later *TP Vision*) as part of the regular research programme.

Hammer, Martin

High-Dynamic-Range Displays

— Contributions to Signal Processing and Backlight Control

Technische Universiteit Eindhoven

Proefschrift

ISBN: 978-90-386-3621-4

Cover design: Martin Hammer.

Copyright © 2014 TP Vision Netherlands

All rights reserved. No part of the material protected by this copyright notice may be reproduced or utilised in any form or by any means, electronic or mechanical, including photocopying, recording or by any information storage and retrieval system, without permission from the copyright holder.

A catalogue record is available from the Eindhoven University of Technology Library: ISBN: 978-90-386-3621-4

Printed by Ipskamp Drukkers, Enschede, the Netherlands.

# High-Dynamic-Range Displays

Contributions to  
Signal Processing and Backlight Control

## PROEFSCHRIFT

ter verkrijging van de graad van doctor aan de  
Technische Universiteit Eindhoven, op gezag van de  
rector magnificus, prof.dr.ir. C.J. van Duijn, voor  
een commissie aangewezen door het College voor  
Promoties in het openbaar te verdedigen op  
donderdag 8 mei 2014 om 16.00 uur

door

Martin Hammer

geboren te Horsens, Denemarken

Dit proefschrift is goedgekeurd door de promotor en de samenstelling van de promotiecommissie is als volgt:

voorzitter: prof.dr.ir. A.C.P.M. Backx  
promotor: prof.dr.ir. G. de Haan  
copromotor: dr. E.H.A. Langendijk (Liquavista)  
leden: prof.dr. P.H.N. de With  
prof.dr. I.E.J. Heynderickx  
prof.dr. J. Biemond (Technische Universiteit Delft)  
prof.dr. S. Süssstrunk (Ecole Polytechnique Fédérale de Lausanne)

*Til An for hendes støtte  
Til Mona og Jeppe for deres livslyst*



# Acknowledgements

I would like to thank the many people who have offered help, advice, and support through the completion of this dissertation. First and foremost, I would like to thank my co-promoter, dr. Erno Langendijk, who has contributed tremendously to the work described in this thesis. As a project leader, co-inventor, co-author, co-promotor, and as a friend. Thank you for your support and tutoring.

Secondly, I thank my promotor, prof.dr. Gerard de Haan, for providing me the opportunity to write this dissertation. Also I would like to express my gratitude to the committee members for their efforts.

Thanks to all past and present colleagues at Philips Research. In particular I am indebted to Frank Vossen, Jürgen Vogt, and Hakan Gokgurler for their efforts creating the HDR display prototypes. To Danny Ruijzendaal for excellent help with raw video playback. To Remco Muijs for introducing me to display processing and to Yuning Zhang and Fang-Cheng Lin for many interesting discussions on colour-sequential displays. Thanks to my colleagues at Philips BU-TV (TP Vision), in particular thanks to Marc Lambooi, Chris Varekamp, Ramachandra Rao, Jeroen Stessen, Hans van Mourik, Aleksandar Sevo, Age van Dalen, Marcel Peeters, Kees Kortekaas, Pierre de Greef, Rimmert Wittebrood, and Kees Teunissen.

A very special thanks to Karel Hinnen, with whom I had the pleasure to share office for more than six years. It has truly been a pleasure working with you. Also I extend my thanks and appreciation to my many students, in particular thanks to Teun Baar. Honestly, there is not enough space to thank everyone, so if I should not have mentioned you, please do not think I forgot you.

Lastly and most importantly, my most sincere thank you to my wife for her understanding and support. For many hours spent alone with our wonderful children Mona and Jeppe, while I was occupied writing this dissertation.





# Summary

## High-Dynamic-Range Displays

In daily life, a large range of light intensities can occur. For example, the sun at noon is up to 100 million times brighter than a starlit night. The human visual system is capable of adapting to this full intensity range of as much as 10 orders of magnitude. In comparison, the dynamic range of a typical liquid-crystal display (LCD) is only 3 orders of magnitude and the peak luminance is usually around  $500 \text{ cd/m}^2$ , which is substantially lower than the average luminance on a sunny day ( $100\,000 \text{ cd/m}^2$ ) or even on a cloudy day ( $20\,000 \text{ cd/m}^2$ ). These obvious discrepancies between real-world and display leaves ample room for improvement.

In this dissertation, the poor contrast and peak luminance (also referred to as dynamic range) of LCDs is addressed. The light efficiency of conventional LCDs is typically 5-7% due to the crossed polarisers, small pixel aperture, and the presence of colour filters. In order to achieve high system efficiency, we investigated three options; (1) an LC-panel with RGBW subpixel layout and local backlight boosting, Chapter 3, (2) a colour-sequential display with local luminance boosting, Chapter 4, and (3) a 120 Hz, 2-field colour-sequential system, Chapter 5. Finally, we investigated the contrast requirements for high-contrast display systems by considering human-eye glare the limiting factor (Chapter 6). In order to enable the described research, a versatile high-dynamic range display system was built (Chapter 2).

A prototype display with a backlight consisting of individually-addressable light-emitting diodes (LEDs) has been constructed. By using the backlight as a second modulator, which creates a low-resolution approximation of the desired image, the contrast can be increased by about 2 orders of magnitude. Furthermore, the 1125 segments of individually-addressable and tightly-packed RGB high-power LED triplets allowed us to raise the peak luminance of a standard LCD to more than  $4000 \text{ cd/m}^2$ . By careful design, the backlight segments were optically separated, yet slightly overlapping, allowing a very large modulation

depth and high uniformity of full-screen luminance. The prototype display has served as a research vehicle to a majority of the work described in this thesis and is described in detail in Chapter 2.

Compared to a conventional RGB subpixel layout, the transmission of an RGBW LCD is 150%, yet colourful images may be perceived as dull and unattractive. When reproducing saturated colours, such as primary red, the transmission is namely reduced to 75% due to a reduction of subpixel aperture. In order to address the luminance shortage of bright saturated pixels, a method is introduced in Chapter 3 in which a spatially-modulated backlight is locally boosted in regions of bright, saturated colours. Whereas state-of-the-art methods for deriving backlight drive levels either results in high contrast or temporal stability, we additionally present a reformulation of backlight modulation control which results in both superior contrast and temporal stability. By employing local backlight boosting, the colour error (99.5%-percentile of  $\Delta E_{94}$ ) is reduced from 12.3 JND to 4.3 JND on average. Power consumption is reduced by 18% compared to an RGB LCD with local backlight dimming. Additionally, it is proposed to increase luminance of desaturated pixels in regions of backlight boosting, which results in an average luminance increase of 16% for pixels which are boosted.

Colour-sequential LCDs eliminate the need for colour filters. Colour is made temporally using a flashing backlight of red, green, and blue primary colours. Such a display is 3-4 times more efficient than a regular colour-filter based LCD. In addition to this transmission gain, it is possible to further increase peak luminance up to a factor three for images of limited colour variation. In order to achieve this, the primary colours are locally adjusted by means of mixing the RGB triplet of a backlight segment. When the primaries are close-to identical, the gamut becomes very tall and allows significant increase of luminance. In Chapter 4, a backlight control strategy which utilises this insight is presented. The results show an average luminance increase of 143% for a display with 240 backlight segments.

While the increased transmission of colour-sequential LCDs is attractive, commercial breakthrough has been impeded by requirements for fast LC-panel optical response time. Conventional displays use at least three primaries for full-colour image reproduction and colour-sequential LCDs are therefore traditionally based on at least three fields per frame. In Chapter 5, a display system is presented which is based on only two fields. A backlight with locally-addressable LED RGB-triplets is used to produce local and temporally varying primaries. On a local basis, the two primaries that minimises the colour error in a total least-squares sense are chosen. Colour reproduction of natural images is very good for a majority of images given a sufficient amount of addressable backlight segments. A statistical analysis shows that excellent colour reproduction ( $\Delta u'v' < 0.020$ ) for more than 99.0% of the pixels per frame) can be achieved for 74.2% of the frames using 9216 backlight segments. When the display system op-

erates at 2 fields rather than 3 fields, the requirements for LC-panel response time is relaxed by 33% without affecting the high-transmission advantage ascribed to colour-sequential displays.

In Chapter 6, we investigate the contrast requirements for high-contrast display systems by considering human-eye glare. Displays based on organic-light emitting diodes (OLEDs) promises perfect dark-room black level. However, light scatter in the human eye leads to an increase in retinal black level and suggests that a close-to-zero black level is not required for natural images. The local increase of black level caused by human-eye glare is estimated. With a spatially-modulated backlight, an LCD can make enough contrast provided a sufficient number of addressable segments, in the order of 2000, is used.

In a final contribution (Chapter 7), OLED displays are considered for HDR image reproductions. Whereas the contrast characteristics of state-of-the-art OLED displays exceed those of most other display technologies, the luminance is still lower than that of LCDs. As large-sized OLED displays have only recently been commercialised, the next decade is likely to bring several improvements on light output. Meanwhile, it is necessary to consider alternative methods in order to maximise light output. In this chapter, an early-stage study showing experimental data of luminance and thermal characteristics of some OLED displays is reported. Furthermore, a method is presented which is expected to allow improvements of luminance by explicitly modelling heat conduction.

In conclusion, this thesis contributes primarily to the field of display systems engineering with novel video processing and backlight control algorithms. A sophisticated backlight with HDR capabilities was constructed to facilitate the research and to demonstrate the performance of the proposed concepts. Existing methods for visualising HDR images consider display luminance and contrast characteristics constant. This thesis contributes by demonstrating that, by considering such characteristics dynamic, it is possible to increase both contrast and luminance without physically modifying the display system.



# Contents

<b>Acknowledgements</b>	<b>I</b>
<b>Summary</b>	<b>III</b>
<b>1 Introduction</b>	<b>1</b>
1.1 HVS and Dynamic Range Capabilities . . . . .	1
1.2 Dynamic Range and Amplitude Resolution . . . . .	4
1.3 Reproduction of Real-World Scenes . . . . .	5
1.4 State-of-The-Art Liquid-Crystal Display Systems . . . . .	16
1.5 Temporal Response of Liquid Crystal Displays . . . . .	22
1.6 Objectives of this Thesis . . . . .	24
1.7 Thesis Outline and Beyond . . . . .	26
<b>2 A Versatile High-Dynamic Range Display System</b>	<b>31</b>
2.1 Optical Design . . . . .	33
2.2 Electrical, Mechanical, and Thermal Design . . . . .	37
2.3 Characterisation and Calibration of RGB LEDs . . . . .	44
2.4 Characterisation of Segment Point-Spread Function . . . . .	49
2.5 Display Applications and Summary of Performance . . . . .	57
2.6 Model- and Metrology-Based Evaluation of Contrast and Luminance	59
2.7 Conclusions . . . . .	69

<b>3</b>	<b>Local Luminance Boosting of an RGBW LCD</b>	<b>71</b>
3.1	Introduction . . . . .	72
3.2	Related Work . . . . .	73
3.3	Motivation . . . . .	78
3.4	Methods . . . . .	81
3.5	Results . . . . .	88
3.6	Discussion . . . . .	93
3.7	Conclusion . . . . .	93
<b>4</b>	<b>Local Luminance Boosting of a Colour-Sequential Display</b>	<b>95</b>
4.1	Introduction . . . . .	95
4.2	Boosting Method . . . . .	102
4.3	Results . . . . .	110
4.4	Discussion . . . . .	114
4.5	Conclusions . . . . .	114
<b>5</b>	<b>Colour Reproduction on a 120-Hz Two-Field Color-Sequential LCD</b>	<b>117</b>
5.1	Introduction . . . . .	118
5.2	Related Work . . . . .	119
5.3	Methods . . . . .	121
5.4	Refinements of the Proposed Method . . . . .	122
5.5	Results . . . . .	123
5.6	Statistical Justification . . . . .	129
5.7	LCD Demonstrator . . . . .	132
5.8	Discussion . . . . .	132
5.9	Conclusions . . . . .	133
<b>6</b>	<b>Display Contrast Requirements Based on Human Eye Glare</b>	<b>135</b>
6.1	Introduction . . . . .	135
6.2	Methods . . . . .	137
6.3	Results . . . . .	138
6.4	Discussion . . . . .	140
6.5	Conclusions . . . . .	141



<b>7</b>	<b>What About OLED Displays?</b>	<b>143</b>
7.1	Introduction . . . . .	143
7.2	Observations of OLED Display Luminance . . . . .	144
7.3	Observations of OLED Display Temperature . . . . .	145
7.4	Suggestions for Improvements of Luminance . . . . .	148
7.5	Conclusions . . . . .	151
<b>8</b>	<b>Conclusions and Future Work</b>	<b>153</b>
	<b>Bibliography</b>	<b>165</b>
	<b>List of Publications</b>	<b>177</b>
	<b>Curriculum Vitae</b>	<b>179</b>



# Introduction

The work presented in this thesis is motivated by the discrepancy between real world light levels and those which can be reproduced by state-of-the-art displays. To that end, the dynamic range capabilities of the human visual system (HVS) is reviewed and compared to the capabilities of state-of-the-art displays in this chapter. The principles behind the liquid-crystal display (LCD), the most common display type of today, is introduced and recent advancements in LCD technology is reviewed. Finally the objectives of this thesis are accounted for and a thesis outline is presented.

## 1.1 HVS and Dynamic Range Capabilities

In the world around us, variations in light intensity span over 10 orders of magnitude. For example, the sun at noon may be up to 100 million times brighter than a starlit night (Reinhard, Ward, *et al.*, 2006). The human visual system (HVS) is capable of adapting to this range of lighting conditions through a variety of adaptation mechanisms including the pupil, the duplex retina of rods and cones, photopigment bleaching, and neural gain controls (Ferwerda, 2001; Rieke and Rudd, 2009). Figure 1.1 shows the luminance of a sheet of white paper under different natural illumination conditions. The intensity of light reflected of the paper may vary from  $10^{-3}$  cd/m<sup>2</sup> at starlight to  $10^5$  cd/m<sup>2</sup> at a sunny day. Whereas instantaneous discrimination of intensity of the HVS is limited to about 3-4 orders of magnitude (Kunkel and Reinhard, 2010), the system functions over a stunning 10 orders of magnitude, thanks to the coordinated action of the adaptation mechanisms (Ferwerda, 2001).

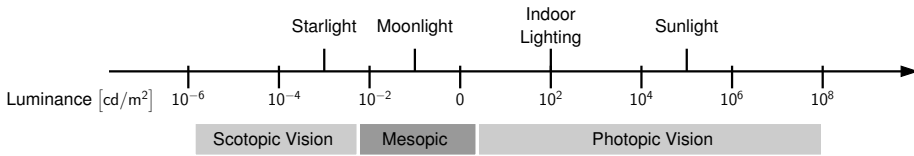


**Figure 1.1:** Illustration of the reflected luminance of a white sheet of paper at different illumination conditions. The ranges of vision is divided into scotopic (rods dominant), photopic (cones dominant), and mesopic (both active). Whereas the human visual system can function across 10 orders of magnitude, it can only discriminate across about 3 orders of magnitude at any instance in time. Reproduced from (Ferwerda, 2001; Reinhard, Ward, *et al.*, 2006).

As illustrated in Figure 1.1, at luminance levels up to about  $10^{-2} \text{ cd/m}^2$ , the vision of rods will be dominating (scotopic vision). At luminance levels from  $10^0 \text{ cd/m}^2$  and higher, the vision of cones will be dominating (photopic vision). In between is called mesopic vision, which is a combination of scotopic and photopic vision where both rods and cones are active.

Whereas the HVS system is capable of adapting to varying illumination conditions this does not happen instantaneously. When entering a tunnel or when the lights are switched from on to off, it may take many minutes before the visual system has completely adjusted to the new (much darker) level of illumination. This process is known as dark adaptation and can take more than a minute for level differences of 1-2 orders of magnitude and more than 10 minutes for adaptation levels above 2 orders of magnitude (Wyszecki and Stiles, 1982, chap. 7.3; Ferwerda, 2001). The time course of dark adaptation is shown in Figure 1.2. In this study, the observer is first adapted to a bright background luminance (expressed in retinal illuminance, measured in trolands). The detection threshold is then measured at regular intervals after the observer is put into darkness. When adapting to darkness from a very bright surround,  $400\,000 \text{ Td}$ , improvements in contrast threshold detection can be observed for up to 35 minutes. When adapting coming from a relatively dark surround,  $263 \text{ Td}$ , the recovery is significantly faster. Notice the kinked curve when adapting from a bright surround. This is a result of the different speed of recovery of the cone and rod sensitivity. The first minutes the threshold drops rapidly while the sensitivity of the cone system is recovering. The following minutes, the detection threshold is relatively constant because, although the cone system has recovered, the rod system has not recovered significantly. The inverse of dark adaptation is light adaptation. This process is much quicker compared to dark adaptation and may take up to a few minutes (Ferwerda, 2001).

Whereas temporal changes in intensity from day to night can be really extreme, light intensity variations within a natural scene can also be quite substantial. The HVS must also be able to quickly adapt to these intensity variations

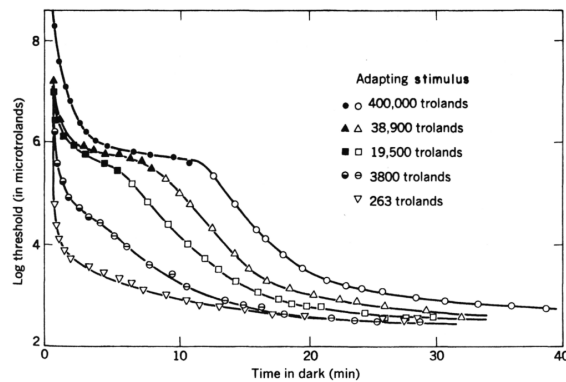


**Figure 1.2:** Time course of dark adaptation expressed as log-threshold of contrast visibility. Reproduced from (Wyszecki and Stiles, 1982).

when exploring a single visual scene. From highlights to shadows, the dynamic range of *natural scenes* may span from a few orders of magnitude (Jones and Condit, 1941), up to five orders of magnitude (Fairchild, 2007; van Hateren, 2006), and even larger if direct-view light sources are involved. Within a scene, the HVS is known to function across a range of about five orders of magnitude (Reinhard, Ward, *et al.*, 2006). Compared to instantaneous contrast discrimination, this range is extended due to the adaptation of the neural gain of the photoreceptors associated with the photoreceptors in the retina. The neural gain can be adjusted fast enough to match the changes in light intensity produced as the eyes move from one location to another within a single visual scene. It has been established that a set of computational principles translates the individual photoreceptor signals into rapid and reliable adaptation levels by means of receptor pooling and adaptation to the local mean intensity and contrast (van Hateren, 2006; Rieke and Rudd, 2009).

Despite the ability to adapt to different levels of illumination, the visual performance is not equally good under all adaptation states. At low luminance levels, scotopic vision in particular, the visual acuity, contrast sensitivity, and colour discrimination are all substantially reduced (Ferwerda, 2011).

Natural scenes of extremely large dynamic range may also have a significant impact on vision. A bright light source in the visual field can lead to reduced retinal contrast in the proximity of the bright light source due to intra-ocular reflections and scattering (Vos, 1984; Vos and van den Berg, 1999; Murdoch and Heynderickx, 2012). This effect is called glare and impairs detail perception near high-contrast boundaries. In Figure 1.3 an illustration on how a desk lamp could be perceived with and without human-eye glare. In the left illustration, the light bulb is a small bright object and the text inside the reflector (Luxo) is clearly readable. This is normally not the case when looking directly into a desk lamp. In the

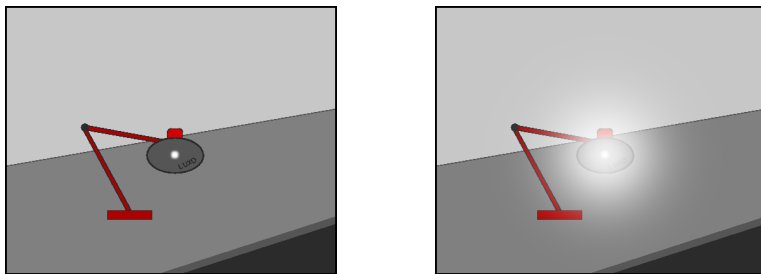


**Figure 1.3:** Illustration of how glare may impair detail perception near high-contrast boundaries. In the left illustration of a Luxo-lamp on the table, the light bulb is represented by a small bright spot and the text inside the reflector is readable. In the right illustration a simulation of human-eye glare has been added showing the more common experience of a large halo around bright objects.

right illustration, we have added a large halo around the bright light bulb. This is meant to illustrate human-eye glare and corresponds better to the experience of looking into a desk lamp. Notice that the text is now barely readable.

## 1.2 Dynamic Range and Amplitude Resolution

The term *dynamic range* is used in engineering to define the ratio between the largest and the smallest quantity under consideration (Myszkowski, Mantiuk, and Krawczyk, 2008). Depending on the technical field of expertise, different measures may be used. When considering real world light levels, the ratio between the largest and the smallest amount of light in a scene is often expressed as orders of magnitude. This is called log-range and defined as the base-10 logarithm.

Besides the base-10 logarithm, a number of other definitions of dynamic range are in use. Signal-to-noise ratio (SNR) is defined as peak signal intensity in relation to noise level intensity and is often employed by camera manufacturers to characterise camera sensors. The unit for SNR is decibel [dB] and expressed as 20 times base-10 logarithm. Occasionally, scene dynamic range is referred to as exposure latitude expressed in *f*-stops (base-2 logarithm). This is a legacy from analogue film and generally discouraged (Myszkowski, Mantiuk, and Krawczyk, 2008). In display systems, dynamic range is commonly expressed directly in terms of contrast ratio. It is defined as the ratio between the peak white luminance and the darkest luminance (black level). For example peak luminance of  $300 \text{ cd/m}^2$  and black level of  $0.6 \text{ cd/m}^2$  results in a contrast ratio of 500:1. In this thesis we will use orders of magnitude and contrast ratio as measures of dynamic range, consistent with common use in the computer graphics and the display community, respectively.

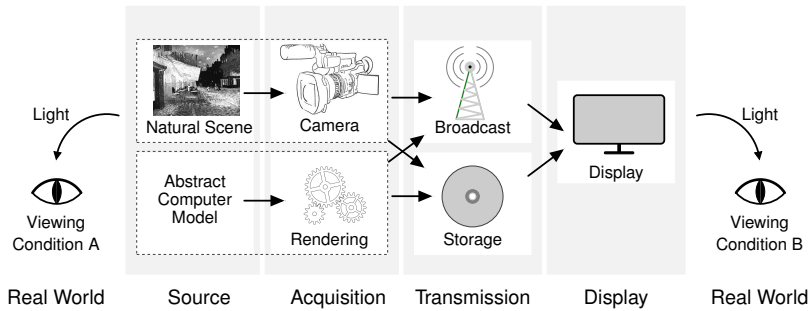


**Figure 1.4:** Illustration of a video reproduction pipeline from acquisition and transmission to display. The pipeline basically converts light into a digital signal and back into light. Adapted from (Mantiuk, Krawczyk, *et al.*, 2007).

Dynamic range is often confused with *amplitude resolution*, which is defined as the number of distinct levels that can be recorded by a camera, or portrayed by a display device. For digital devices, amplitude resolution is often expressed as the bit depth of the associated signal. There is no obvious relationship between amplitude resolution and dynamic range, the application of a device governs the necessary amplitude resolution. For an imaging device, such as a display, it is a good practice to ensure that each individual amplitude step corresponds to at most 1 just-noticeable difference (JND) for the human visual system. Obviously devices of high dynamic range require a high amplitude resolution in order to prevent large clearly distinguishable amplitude steps, but high bit depth does not warrant high dynamic range capabilities.

### 1.3 Reproduction of Real-World Scenes

Considering the enormous dynamic range encountered in the real world and the impressive adaptability of the human visual system, modern digital imaging devices are in comparison quite limited. The dynamic range of typical devices, such as front projectors, cathode ray tubes (CRT), plasma screens, and liquid crystal displays (LCD), ranges from as low as 10:1 for projectors up to 5000:1 for the best CRTs. For LCDs the typical range is around 500:1 for monitors, and up to 3000:1 for high-fidelity screens. The full-white luminance ranges from about 30 cd/m<sup>2</sup> for a cheap projector, and up to 600 cd/m<sup>2</sup> for a high-fidelity LCD. When the capabilities of the HVS is compared to the capabilities of a display system, it becomes clear that conventional display technologies leave ample room for improvement

This discrepancy can partly be ascribed to technological limitations of display systems, but is also largely related to other elements of video reproduction. In Figure 1.4, a typical video reproduction pipeline is illustrated. The pipeline consists of three activities; acquisition, transmission, and display. Traditionally, video



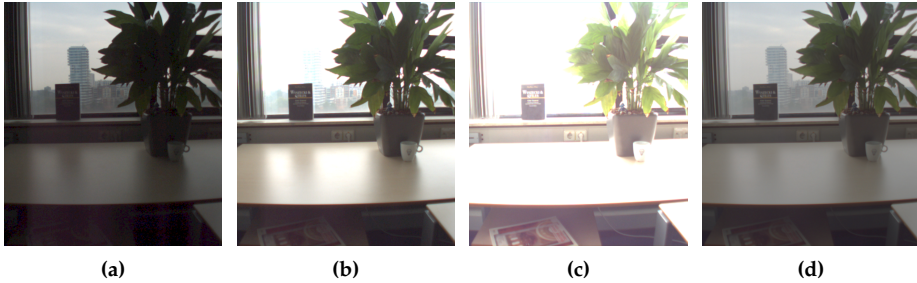


**Figure 1.5:** In (a-c) a short, medium, and long exposure. Notice how none of the exposures allows to see the book (bottom atop the drawer) and the building simultaneously. In (d) the combined exposures is shown. The tonal range of the HDR photograph has been compressed.

reproduction consists of capturing light of a natural scene using a video camera, transmission of the video signal by broadcasting or hard-copy distribution, and reproduction of the light of the scene using a display device. This corresponds to the top row of Figure 1.4. The past 20 years, visual special effects generated by computer graphics rendering has won popularity. Abstract computer models of texture, lighting conditions, and shading information is used to generate photo-realistic virtual scenes which may be mixed with footage in post processing or completely replace the traditional camera acquisition. This is illustrated in the bottom row in Figure 1.4. We review each element of video reproduction in the following sections.

### 1.3.1 Acquisition: Capturing and Rendering in HDR Scenes

Electronic acquisition of motion picture using analogue film dominated up until the 2000's, after which digital acquisition won out. Photographic film offers a dynamic range of around 4 orders of magnitude, commonly expressed as 12-13 *f*-stops, while digital sensors offer a slightly lower dynamic range of 3-3.5 orders of magnitude, commonly expressed as 65 dB (10-11 *f*-stops) (Reinhard, Ward, *et al.*, 2006). In practice, the dynamic range is reduced, in particular in the vicinity of bright objects, such as light sources or the sun, due to optical flare. Jones and Condit (1941) reported a factor four reduction of dynamic range for cameras at that time, while Fairchild (2007) reported a reduction by a factor of 1.4 for a modern digital single-lens reflex (DSLR) still-image camera.

The inherent limitations of dynamic range of image sensors, makes it impossible to capture the full dynamic range of a natural scene in a single exposure. The photographer will have to choose which pixels to leave saturated, i.e. clipped to black or white. However, by taking multiple exposures of a scene with

different shutter times, each pixel will be correctly exposed in one or more images in the sequence. Based on this observation, and assuming a linearised camera response, it is possible to combine the exposures in order to generate a photograph of extended dynamic range (Reinhard, Ward, *et al.*, 2006). This method, often referred to as *exposure bracketing*, has been particularly popular in amateur photography and is frequently applied to capture scene illumination using a mirror-ball for physically-based rendering of photo-realistic virtual scenes.

In order to demonstrate exposure bracketing, we captured three photographs in an office setting. The exposures are shown in Figure 1.5(a)-(c). The challenge of the scene lies in the large intensity difference between the sky and buildings in the background and the book located on the drawer at the bottom of the photograph. A CCD-sensor-based IDS Imaging UI-2230ME camera was used and exposure time was set to 1 ms, 8 ms, and 64 ms, respectively (3 *f*-stops apart). This particular camera unit provides a linear camera response (Rüfenacht, 2011). The HDR photograph shown in Figure 1.5(d) is constructed by shifting the intensity of the individual exposures according to their relative exposure time and computing a weighed average of the measured pixel intensities. In the resulting HDR photograph, in which mid-tones have been compressed (frequently referred to as global tone mapping), both the building and the book are recognisable.

Whereas a sequence of exposures is useful for still photography, it is impractical for capturing video. Kang *et al.* (2003) have demonstrated a camera setup with temporally-varying exposure settings. This limits maximum frame rate and may induce motion blur due to the time-difference between the frames of low- and high exposure. Nevertheless, RED, a US-based manufacturer of digital cinema cameras, has commercialised a camera based on this concept. Unger and Gustavson (2007) have demonstrated a camera system capable of rapid exposures within one frame (25 fps) using a rolling-shutter CMOS-system. With up to 8 exposures per frame, the system can capture a wide dynamic range of up to 140 dB. However, the extremely short exposure times require very sensitive image sensors, or a boosted sensitivity using amplifiers, which unfortunately often leads to increased noise levels.

Rather than using multiple frames to create different exposures, it is possible to simultaneously capture differently exposed images using multiple image sensors (Myszkowski, Mantiuk, and Krawczyk, 2008). Light entering a single lens is split using beam-splitters and relayed through neutral-density filters resulting in simultaneously recording of radiometrically-offset images. Absorptive neutral density filters are typically applied resulting in poor optical efficiency and requiring sensitive image sensors. Tocci *et al.* (2011) have proposed to use beam-splitters of different reflective coefficients and redirect reflected light back into the optical pathway thereby increasing optical efficiency to close-to 100%. At the ACM SIGGRAPH conference 2010, the German-based Spheron VR, a manu-

facturer of cameras used for special effects applications, demonstrated an HDR video camera operating in real time. The concept of this camera was not disclosed at the conference.

Besides the multiplexed HDR capture concepts described above, a considerable amount of research has focused on enlarging the intrinsic dynamic range of the image sensors. Some of this research has resulted in commercialised single-sensor HDR cameras, which are primarily applied in surveillance and industrial computer-vision applications.

### 1.3.2 Transmission: Image and Video Formats

Irrespective of the HDR acquisition technology used, it is important to consider the format used for storage and transmission of the resulting HDR image. Traditional image formats were designed in a time where CRTs were the dominating display technology and consequently the limited capabilities of such displays have dictated the characteristics of popular colour encoding systems typically used in image formats such as BMP, PNG, JPEG, TIFF, etc. It is typical to use 8-bit integers to represent each colour (RGB) and consequently the dynamic range is limited to a few orders of magnitude in order to avoid visible banding (Reinhard, Ward, *et al.*, 2006).

Besides limitations on usable dynamic range, traditional image formats do not specify a mapping between digital values and photometric units. Consequently, the maximum digital value is often simply mapped to the maximum luminance of a display device and the minimum value is mapped to the minimum luminance value. From a mathematical point-of-view, the range of an 8-bit encoded RGB signal is around 5 orders of magnitude,  $(1/255)^{2.2} : 1$ , which will lead to significant visible banding. If each individual step is kept below the visible threshold, the dynamic range is closer to 1 order of magnitude.<sup>1</sup> This is, however, a very conservative use of the 8-bit encoding, and the dynamic range is likely to be closer to 2 orders of magnitude (Reinhard, Ward, *et al.*, 2006).

According to HDR-imaging pioneer Greg Ward, the dynamic range capability of an HDR format should cover at least 4 orders of magnitude (Greg Ward, 2005). Besides dynamic range, it is desirable that an HDR format encompasses the full range of visible colours, either with wide-gamut primaries, by allowing negative primaries, or by using CIE XYZ tri-stimulus coordinates (Berns, 2000). Lastly, it is desirable that an HDR format can be compressed in order to occupy the least possible data volume (fewest bits).

<sup>1</sup>We have made use of the standard display function, which is tabulated in (DICOM Part 14, Supp. 28, 1998), and relates luminance to a JND index. For a display device of 100 cd/m<sup>2</sup> peak luminance, the minimum luminance is 10.6 cd/m<sup>2</sup>, resulting in a dynamic range of 1 order of magnitude.

A large variety of lossless HDR image formats have been proposed (Mantiuk, 2006; Reinhard, Ward, *et al.*, 2006). Of these formats, the Radiance HDR (RGBE and XYZE) format was the first. The format covers well beyond 70 orders of magnitude, but suffers from colour artefacts of saturated colours due to lack of de-coupling of intensity and chromaticity. The integer-based LogLUV encoding solves these issues and covers well beyond 30 orders of magnitude, while maintaining the maximum relative step size below 0.3% (Greg Ward, 2005). Finally, the OpenEXR format, is a half-precision floating-point type with a 10-bit mantissa and 5-bit exponent, allowing a dynamic range of more than 10 orders of magnitude while keeping the relative step size below 0.1% (Greg Ward, 2005).

Interestingly, the half-precision format used in the OpenEXR format, has won wide-spread use in graphics processing units and has served as the basis for an digital film interchange framework called ACES. The ACES format is used to store intermediate data before the final video is colour-graded for a particular display device. For consumer applications it may be beneficial to trade off quality for lower bandwidth by applying a lossy compression scheme, such as JPEG for LDR images. Recently, the JPEG committee have approved an extended-range JPEG format named JPEG-XR (Dufaux, Sullivan, and Ebrahimi, 2009).

Without a display device with HDR capabilities, it is necessary to map the tonal range of the HDR data to the display device. A comprehensive study on tone-mapping operators for compressing the dynamic range of still images can be found in (Devlin *et al.*, 2002), (Reinhard and Devlin, 2005), and (Reinhard, Ward, *et al.*, 2006). A recent study by Eilertsen *et al.* (2013), in which tone-mapping operators were applied to video, indicates that with few exceptions, tone-mapping operators are either sensitive to noise or causing visible flicker. Another problem is that tone-mapping operators often change the image appearance and may require considerable processing power. As a solution to this problem, it has been argued to make a backwards-compatible format which contains a low-dynamic range image and a residual signal to reconstruct the HDR image. The methods by Ward and Simmons (2005) and Mantiuk, Efremov, *et al.* (2006) are examples of such an approach.

When an HDR image has been acquired, it is obviously desirable to have a display with HDR capabilities in order to faithfully reproduce the HDR image. In fact, in a psychophysical experiment on observer preference it was found that tone-mapped HDR images viewed on an LDR display are no better than the best LDR exposure (Akyüz *et al.*, 2007). This provides evidence, that in order to truly benefit from HDR technology one would need an HDR display.

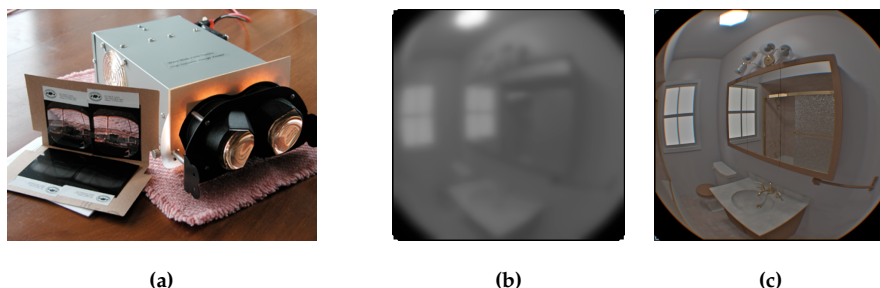


**Figure 1.6:** A photograph of a wide-viewing angle stereoscopic viewer with high-dynamic range capabilities was presented by Ward in 2002. In (a) a photograph of the viewer, in (b) and (c), the transparency base- and detail-layer, respectively.

### 1.3.3 Display: Reproducing HDR Scenes

Printed photography reproduced on paper is generally characterised by a low dynamic range considerably less than 100:1 due to the relatively low light absorption of the printed dyes. Being a reflection print, the image quality depends greatly on the paper, the dyes used, and, in particular, the ambient light under which the print is observed. A transparency print, such as those used in overhead and slide projectors, however, largely decouples the light source from the ambient light. The contrast ratio may be up to 10 times higher than for reflection prints if viewed in a perfectly darkened room (Reinhard, Ward, *et al.*, 2006). Nevertheless, both printed photography and projected transparent slides exhibit insufficient dynamic range to reproduce HDR imagery.

In 2002, Ward presented a still-image stereographic viewer with high-dynamic range capabilities. The system is based on stacking a set of transparency prints in combination with a bright light source. When the printed transparencies are stacked, the density of the dyes is doubled and consequently the dynamic range is doubled in log-terms. Whereas the dynamic range capabilities of the film recorder used was close to 1000:1, the desire to keep all intensity steps below the visible threshold forced the authors to limit the individual prints to about 100:1 (Ledda, Ward, and Chalmers, 2003). The dynamic range of the transparency stack was about 10000:1. A pair of 50 W lamps was used as light source and ensured a peak luminance of about 5000 cd/m<sup>2</sup>. The input images were digitally divided across the transparencies using a square-root operation and in order to avoid alignment problems, one transparency was slightly blurred, while the other was compensated, such that the product would yield the desired HDR image.

In Figure 1.6(a) a photograph of the still-image viewer is seen. Note the wide-viewing angle optics and the dual-barrel design for stereoscopic reproduction. To the left in the photograph two pairs of transparencies can be seen. In Figures 1.6(b)-(c), the contrast of a photo-realistic rendering has been divided across



**Figure 1.7:** A projector-illuminated LC-panel is simple, yet very effective way of creating a HDR display. A photograph of a prototype by Seetzen, Heidrich, *et al.* (2004) is seen in (a). For this photograph the housing, which is used to reduce unintended light leakage, has been removed. In (b) a photograph of the display described by Daly *et al.* (2013a).

two transparencies. The rear transparency has been made monochrome and slightly blurred, the other transparency contains details and colour. In an observer preference study, where reproductions of a naked-eye natural scene on a CRT (tone-mapped) and on the HDR prototype were compared, the HDR reproduction was favoured (Ledda, Ward, and Chalmers, 2003).

Seemingly inspired by the concept of stacking transparencies, Seetzen, Heidrich, *et al.* (2004) constructed an HDR display using a modified projector and a conventional LC-panel. A photograph of the display system is seen in Figure 1.7(a). A conventional LC-panel is being illuminated by a projector, rather than a set of parallel-mounted fluorescent tubes, as was normal at that time. In addition to the optical modulation of the LC-panel, the high resolution of the DMD-based projector allows a second modulating layer. In this way, two stacked modulating layers are combined in order to create a display with an extended dynamic range. Note that the housing which should prevent unintended light leakage has been removed for the photograph. In the still-image viewer, the densities of the transparent prints were added to allow dual modulation of a uniform light source. In comparison, the projector-based system is a non-uniform light source illuminating a variable transparent media.

In order to operate efficiently, a number of modifications were carried out by the authors. The light output of the projector was tripled by removing the colour-filter wheel. Consequently, the projector could only create monochromatic images, similar to the approach of Ward (2002). Also, the rear-image (on the projector) was blurred slightly in order to avoid alignment issues and potential moiré. Light output towards the viewer was increased by using a fresnel lens in front of the LC-panel. The contrast ratio of the LC-panel and projector, was 300:1 and 800:1, respectively. In practice a maximum contrast of 54 000:1 was measured,

slightly lower than the theoretical 240 000:1. Peak luminance was measured to be  $2700 \text{ cd/m}^2$ .

Interpretation of the reported contrast level should be done with care. Display system such as the stereographic viewer of Ward (2002) and projector-illuminated LC-panels are both based on the combination of a low and a high resolution modulator. The local contrast will depend on the distance to nearby bright objects due to light scattering from the low resolution modulator. Typically contrast is computed based on sequential measurements of a white and black image, or by measurements of a  $5 \times 5$  checkerboard pattern. Consequently, the reported contrast levels are not representative for the performance to be expected when depicting natural images.

The projector-illuminated LC-panel was one of the first designs proposed for a video-capable HDR display, but due to its large form factor and the high power consumption, it never gained much popularity outside of academic research laboratories. Because of the scarcity of commercially-available HDR displays and the simplicity of this approach, the recipe has been followed by other research laboratories, such as Munsell Colour Science Laboratory (Ferber and Luka, 2009), Bangor University (Wanat, Petit, and Mantiuk, 2012), and most recently Dolby Laboratories (Daly *et al.*, 2013a). In this most recent design, a cinema-grade projector, intended for illuminating screens of 30 metres or wider, was combined with a 23 inch LC-panel. Consequently, the display system has a peak luminance close to  $20000 \text{ cd/m}^2$  and a dynamic range covering about 6 orders of magnitude (Daly *et al.*, 2013a). Notice that the colour reproduction method is reversed compared to the previous design, as the LC-panel is monochrome and the projector is providing colour. A photograph of the display system is shown in Figure 1.7(b). The housing which is used to prevent unintended light leakage has been removed for the photograph.

### LED-Illuminated LC-panel

HDR display prototypes based on a LC-panel with projector illumination are typically fairly small (up to about 20 inch), but not thin. In order to illuminate a large TV-sized LC-panel with a projector, a certain throw distance is needed. This limits the minimum thickness of such a display. Further, the projector luminous flux is roughly proportional to the square-root of the display diagonal. Consequently, with today's projectors the display diagonal must be small to obtain a high peak brightness.

As an alternative to a rear-projection setup, it has been proposed to replace the projector with a matrix of individually-addressable light-emitting diodes (LEDs) (Seetzen, Whitehead, and Ward, 2003; Seetzen, Heidrich, *et al.*, 2004; Trentacoste *et al.*, 2007). Similar to the aforementioned HDR display concepts, the backlight



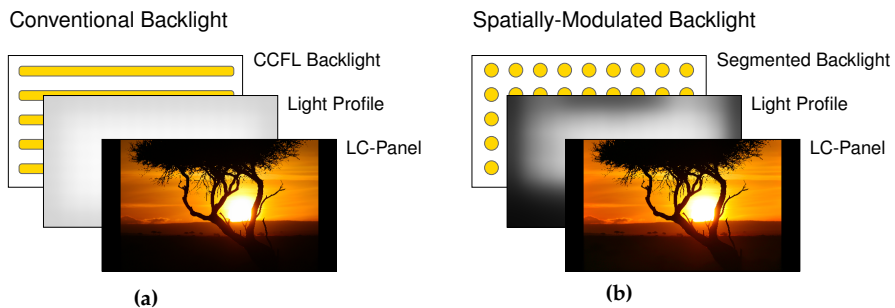


**Figure 1.8:** Illustration of a conventional LCD with a backlight consisting of parallel-mounted CCFL and a spatially-modulated backlight, for example by means of LEDs. The light profile illuminating the LC-panel is illustrated behind the LC-panel. Notice the correspondence between dark areas in the image and dark areas in the light profile of the spatially-modulated backlight.

creates a low-resolution approximation of an image, while ensuring enough light intensity for all pixels. The LC-panel can then be used to modulate the intensity to the desired light level and colour. However, the resolution of the segmented backlight is typically well below that of the LC-panel and smooth optical segment profiles are characteristic for an LED-based design. It is therefore *not* necessary to initially blur the rear-image as it will be low resolution by nature. The optical profiles, i.e. the point-spread function, of each backlight segment are desirably smooth enough to provide sufficient uniformity for a full-white image. Typically a luminance ripple of about 1 to 2 percent is perceptually acceptable (Vogels, Heynderickx, and Swinkels, 2003). As a consequence of the smooth segment profiles, segments generating light for a specific bright object may also illuminate adjacent dark areas, which may result in unintended bright halo artefacts due to light leakage through the LC-panel.

An illustration of a conventional LCD is shown in Figure 1.8(a). A conventional LCD is illuminated by parallel-mounted cold-cathode fluorescent lamps (CCFL) which ensure uniform illumination on the LC-panel, as is illustrated behind the LC-panel. Notice that the light profile is slightly sponge-shaped, with light intensity dropping towards the edges of the display. Typically the intensity drops by 20 to 50 percent, however the low frequency of the intensity change makes the reduction perceptually acceptable (Vogels, Heynderickx, and Swinkels, 2003).

Figure 1.8(b) gives an illustration of a spatially-modulated backlight in which the light profile can be modulated according to the video content by means of individually addressable LEDs. The light profile is consequently dark in corresponding dark image regions and bright in bright image regions.

The first reporting of a HDR display with a spatially-modulated LED backlight consisted of a 18.1 inch LC-panel and 760 high-power LEDs resulting in a



**Figure 1.9:** The 18.1 inch prototype HDR display from Sunnybrook Technologies (2004) is shown in (a). The display features 760 high-power LEDs and a peak luminance of  $8500 \text{ cd/m}^2$  (Seetzen, Heidrich, *et al.*, 2004). The 37 inch HDR display from Brightside Technologies Inc. (2005, former Sunnybrook Tech.) with a peak luminance of  $3000 \text{ cd/m}^2$  is shown in (b).

peak luminance of  $8500 \text{ cd/m}^2$  and a contrast ratio of about 280 000:1 (Seetzen, Heidrich, *et al.*, 2004). In Figure 1.9(a) a photograph of this display is seen. A larger design was created by Brightside Technologies Inc. (Canada), a spinout of University of British Columbia (Canada). This prototype was based on a 37 inch LC-panel, 1380 LEDs arranged in a hexagonal pattern, and featured a peak luminance of  $3000 \text{ cd/m}^2$  and a contrast ratio of 200 000:1 (Brightside Technologies, 2012). Due to the high power consumption, the peak luminance was achieved for about 1/3 of the LEDs at maximum intensity corresponding to a power consumption of 1.6 kW (about the limits of a regular circuit breaker). A photograph of this display is seen in Figure 1.9(b).

Similar to other display technologies using low and high resolution modulators, the reported contrast levels should be interpreted with care. Whereas the contrast between two sequential images (white and black, respectively) may be very large, the local contrast of adjacent pixels (white and black, respectively) may approach the contrast of the high-resolution modulator. This is a consequence of the lower resolution of the second modulator. With an insufficient number of backlight segments, LED-illuminated LC-panels are therefore known to suffer from visibly annoying spatially-varying contrast levels, sometimes referred to as backlight halo artefacts.

This first commercially-available HDR display was made by Brightside Technologies Inc. Only a small series was produced, of which most were distributed across academic research laboratories around the world. In 2009, Italian-based SIM2 Multimedia presented a 47 inch HDR display product (co-developed by Dolby Laboratories) which featured 2206 addressable segments and a peak luminance of  $4000 \text{ cd/m}^2$ .

The HDR displays are typically used in research labs and the film industry. For consumer products, most television manufacturers have high-end products

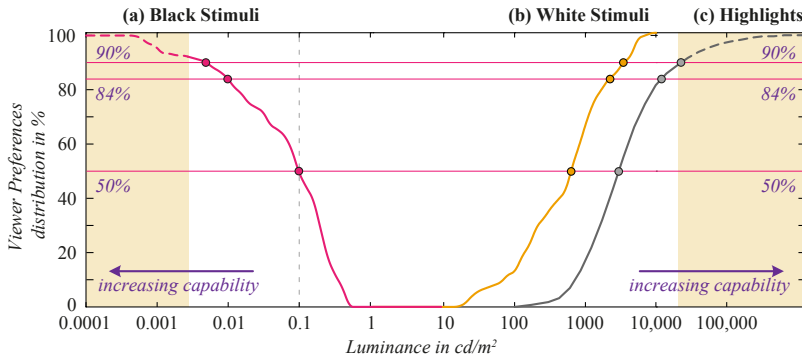


**Figure 1.10:** Observer preference for black luminance, diffuse-range peak luminance (reflective objects), and highlights luminance (specular reflections and emissive objects). In particular the preference for the 50% (average) observer, the 84% observer, and the 90% observer is highlighted in the figure. Courtesy of Timo Kunkel (Daly *et al.*, 2013b).

based on the concept of spatially-modulated backlights using LEDs. Such displays are characterised by a large contrast ratio, but the peak luminance is typically limited (up to 1000  $\text{cd/m}^2$ ). The displays are promoted as *local dimming* LCDs and exhibit up to a few hundred backlight segments.

### 1.3.4 Observer Preference of Contrast and Luminance

From scene acquisition (camera) to reproduction (display), technological progress has been made in order to improve the dynamic range. However, how much dynamic range is actually needed? Rather than letting technological limitations define the answer, it may be more pertinent to explore observer preference for contrast and luminance.

It has been observed that subjects prefer a bright image (high luminance) in the first order, and high contrast in the second order (A Yoshida *et al.*, 2006; Akyüz *et al.*, 2007). In an experiment relating peak luminance to image quality, Seetzen, Li, *et al.* (2006) found that for each contrast level, the image quality increases with increasing luminance until a particular level has been reached, whereafter image quality decreases. For example for a contrast ratio of 2500:1, the optimal luminance is about 800  $\text{cd/m}^2$ , whereas for a contrast ratio of 5000:1, the optimal luminance is about 1800  $\text{cd/m}^2$ .

Daly *et al.* (2013a) have rigorously investigated observer preferences limits for black luminance and peak luminance (split in diffusive white luminance and specular highlights luminance). In order to avoid the HDR display being a limiting factor, a custom-built display with a peak luminance of 20000  $\text{cd/m}^2$  and a contrast ratio of about 6 order of magnitude was constructed. The participants

were not allowed to adapt to the scene luminance, rather stimuli and a uniform inter-stimulus was changed with an interval of 4 s.

The main results of this study are shown in Figure 1.10. The average observer preference for dark luminance is  $0.1 \text{ cd/m}^2$  and diffusive white luminance  $650 \text{ cd/m}^2$  (contrast of 6500:1). Note that state-of-the-art consumer TVs exhibit a peak luminance and contrast range close to the average observer preference. However, the 90-percentile observer preferred a dark luminance of  $0.005 \text{ cd/m}^2$  and a diffusive luminance of  $3800 \text{ cd/m}^2$  (contrast 760000:1). This range is orders of magnitude larger than state-of-the-art displays.

For the study on luminance of image highlight (specular reflections and emissive sources), the average observer preference was  $4000 \text{ cd/m}^2$ , however considerable inter-stimuli variation was observed. The preference ranged from about  $18000 \text{ cd/m}^2$  to  $1400 \text{ cd/m}^2$ . In an analysis on the subject demographics, it was revealed that users experienced with HDR technology preferred a diffuse luminance more than twice as high as the naïve observer (Daly *et al.*, 2013b). This may suggest that as users become familiar with HDR technology, the luminance preference may increase.

## 1.4 State-of-The-Art Liquid-Crystal Display Systems

Whereas spatially-modulated backlights in combination with an LC-panel can increase both the luminance and the contrast range, only the contrast improvement has found widespread use. A modulated backlight may be used to increase contrast and achieve reduced power consumption, however, increasing the luminance range results in a significant increase in power consumption. HDR displays have therefore been limited to experimental research laboratory setups. As the light efficiency of conventional LCDs is rather low (typically in the order of 5-7%), we expect that higher transmittance will facilitate commercial uptake of HDR display technology. In the following sections we review state-of-the-art LCD technology. We limit the review to transmissive LCD suited for large-size screens and exclude projector technology.

### 1.4.1 Operation of Liquid-Crystal Displays

Liquid-crystal panels are transmissive flat panels which modulate light from a backlight unit. A stack of components makes it possible to control the transmissivity thereby modulating the light level of the backlight. In Figure 1.11, a typical stack of components in an LCD is illustrated.

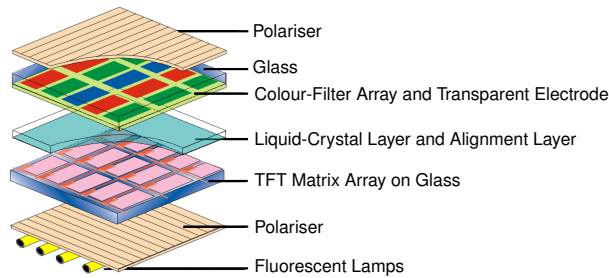


**Figure 1.11:** Illustration of the optical stack in a liquid-crystal display. The LC material is confined between glass substrates whose inner surface is coated with an alignment layer. Crossed polarisers ensure the electro-optical properties of the stack. A first polariser ensures incoming plane-polarised light, while the second polariser absorbs light which has not undergone a phase change. The transmittance level is controlled by the TFT matrix in combination with the transparent electrode. The colour filter array divides the LC cells into red, green, and blue coloured pixels. At the bottom a backlight unit with parallel-mounted fluorescent lamps is shown. Adapted from (Klompshouwer, 2006).

The opto-electronic effect of a liquid-crystal panel is mediated by a layer of liquid-crystal molecules aligned between electrodes. With application of an electrical field, the liquid-crystal molecules tend to re-orient accordingly. Plane-polarised light will propagate along the molecular orientation of the liquid-crystal molecules and result in a change of polarisation state. A first polariser is used to absorb light that is not plane-polarised, while a second (crossed) polariser absorbs the remaining light that has not been changed in polarisation state by the LC-cell. Consequently, varying the electrical field across the LC-cell will result in varying the intensity of the light.

The liquid-crystal material is confined between two glass substrates of about 0.5-1.0 mm each. The inner surface of the glass is covered by a thin layer of transparent indium tin oxide (ITO), which is used as an electrode. The cell gap is about 3.5-4.0  $\mu\text{m}$  (Lee, Liu, and Wu, 2008). It is important to anchor the liquid-crystal material in an initial state (no external electrical field applied). This is done using an alignment layer, traditionally mechanically rubbed polyimide, about 80-100 nm thick, is coated on the inside of the electrodes (Lee, Liu, and Wu, 2008).

The liquid-crystal alignment mode and the electrode configuration is characteristic for the performance of an LC-panel. The most popular alignment modes for large-sized LCDs are twisted nematic (TN), in-plane switching (IPS), fringe-field switching (FFS), multi-domain vertical alignment (M-VA), and optically-bend cell (OCB). The transmittance is voltage dependent and often follows an S-shaped curve. The curve is either normally black (IPS, M-VA, FFS) or normally white (TN, OCB) depending on transmittance at 0 V. Perpendicular to the display surface, the contrast ratio may be around 100:1 to 2000:1. At oblique angles this is significantly lower (less than 10:1), and often susceptible to visible discoloura-

tions. Lastly, the transmittance of an LC-panel does not change instantaneously following a change in applied electrical field. The response time depends on the liquid-crystal compound (viscosity, in particular), cell thickness, alignment mode, and the electrodes. We will return to this in Section 1.5.

In order to improve light efficiency of LCDs, optical sheets are typically positioned between the backlight and the LC-panel. Most important is a reflective polariser film, which allows recycling of light with a polarisation state orthogonal to the first polariser (light would normally be absorbed). Secondly, micro-prismatic films which reflect light at angles higher than  $35\text{--}40^\circ$  are employed, such that light output toward the viewer is increased, while light at larger angles is reduced. Both a vertically- and horizontally-oriented micro-prism sheet is often used in high-end LCDs.

In order to individually control the transmittance of the millions of pixels, a matrix-addressing scheme is used. Transistor switches allow each pixel to be applied a different voltage and a capacitor is used to maintain this voltage until the next addressing moment. Column and row drivers are used to sequentially address a row of pixels. Amorphous silicon-based thin-film-transistors (TFT) are most common, but metal-oxide TFTs are gaining popularity due to larger electron mobility resulting in smaller TFTs and larger pixel aperture.

Reproducing colour images on conventional LCDs is made possible by colour filters patterned to the front glass substrate, as illustrated in Figure 1.11. In the following section we review alternative methods for reproducing colour images on an LCD.

### 1.4.2 Colour Reproduction on LCDs

In order to reproduce colour images, conventional LCDs rely on red, green, and blue colour filters patterned on the front glass substrate. This effectively reduces resolution by a factor of three as three LC-cells are needed to form a white pixel. These three cells are commonly referred to as sub-pixels. By individually controlling the transmittance of the sub-pixels, a wide range of colours can be reproduced.

In Figure 1.12(a), colour reproduction of a conventional colour-patterned LCD is shown. The white backlight illuminating the LCD is shown behind the LC-panel. The colour-filter matrix is depicted clearly to emphasise the method of colour reproduction. Typically the operating frequency is 60 Hz or higher in order to preclude visible flicker. This is in accordance with the critical flicker frequency of the human visual system for an achromatic stimulus (Wyszecki and Stiles, 1982). However, in order to improve motion portrayal, operating frequencies of 120 Hz, 240 Hz, and even 480 Hz have been reported.

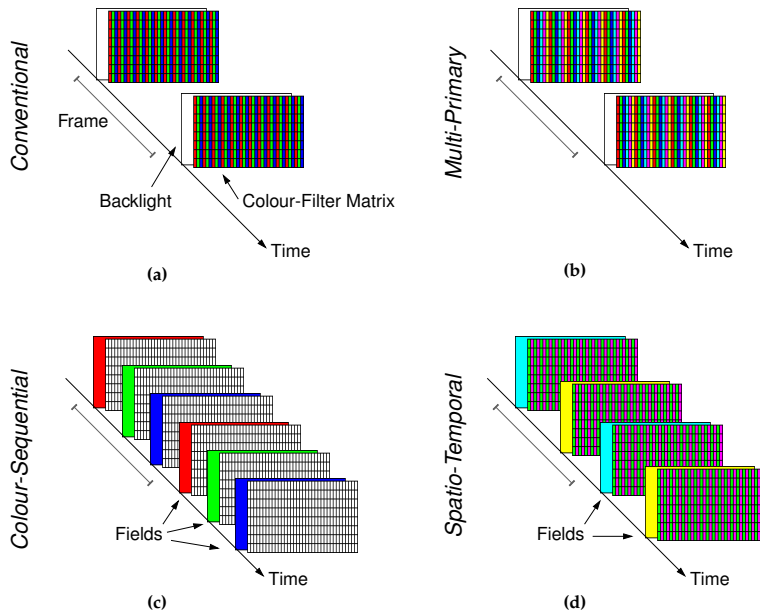


**Figure 1.12:** Illustration of LCD colour reproduction methods. In (a), a conventional LCD with patterned RGB colour filters and a white backlight unit. In (b), a multi-primary LCD with RGBCMY colour filters. The wide-band colour filters CMY results in increase light efficiency. In (c) and (d) colour is created timely, using several fields per frame. In the colour-sequential scheme (c), a flashing backlight of RGB is combined with a colour-filter-less LC-panel. The operating frequency is seen to be three times that of a conventional LCD. The spatio-temporal scheme (d) combines colour filters with temporally changing backlight spectrum. In this example a green-magenta colour filter is combined with a cyan-yellow backlight. With only two fields per frame, the frequency is lower than colour-sequential displays, but at least twice the frequency of a conventional LCD.

The range of reproducible colours is defined by the colour of the sub-pixels (the primaries). These are in turn depending on the backlight spectrum, the wavelength-dependent transmittance of the LC-panel, and the transmission spectrum of the colour filters. Often displays are engineered to have a colour gamut corresponding to a standard, such as the ITU Rec. 709 sRGB. In such a standard, the chromaticity coordinates of the primaries and the white point are defined.

The colour gamut is always defined for the sub-pixel in the brightest state (high transmittance). However, for dark colours, the colour gamut of an LCD may be significantly different. For an LCD with fixed-intensity white-coloured backlight, the small light leakage in the dark state will pollute the darkest colours. Consequently the darkest colours are desaturated toward the native black point (colour of the small light leakage in the dark state). By applying modulation of the backlight, either globally or locally, this can be improved by reducing the relative contribution of the light leakage (Luka and Ferwerda, 2009; Cheng and Shieh, 2009).

## Multi-Primary LCDs

It is not possible to reproduce all naturally-occurring colours using a standard colour gamut such as ITU Rec. 709 sRGB. This particular gamut only covers 59% of the colours of the real-surface objects measured by Pointer (Hinnen and Langendijk, 2010; Pointer, 1980). Consequently, it is interesting to increase the colour gamut in order to span a large chromaticity area. This class of displays is referred to as wide gamut displays. In order to increase the gamut, one could use RGB colour filters with a narrow transmission spectrum, however, this reduces light efficiency. Another option is to narrow the RGB peaks in the backlight spectrum using RGB LED emitters, or a RGBCY LED emitters (Hinnen, Hammer, and Langendijk, 2011; Sano, Nonaka, and Baba, 2012). Such a backlight is relatively expensive. It has therefore been proposed to introduce additional subpixels with colour filters that have a wider spectra, such as yellow (RG), cyan (GB), or white (RGB). This class of displays are referred to as multi-primary displays.

In Figure 1.12(b), a colour-reproduction of a multi-primary LCD is shown. The operating frequency is identical to a conventional LCD and the backlight illumination is also white.

Interestingly, multi-primary displays exhibits increased light transmittance. For example, by adding a fourth, white subpixel, light transmittance can be improved with 50% (Elliott, Credelle, and Higgins, 2005; Lee, Park, *et al.*, 2003; Lee, Song, *et al.*, 2004; Langendijk, Belik, *et al.*, 2007). Compared to a conventional RGB subpixel layout, the transmittance is 150%. However, such systems also have disadvantages. When reproducing a saturated colour, such as primary red, the transmittance is 75% (25% area compared to 33% area) of that of an RGB subpixel layout. Generally speaking desaturated colours will exhibit improved light efficiency, whereas saturated colours will exhibit reduced light efficiency (Hinnen and Langendijk, 2010). Furthermore, multi-primary displays also increase complexity due to gamut mapping, multi-primary conversion (3-to-N primaries), and subpixel rendering for increased resolution (Hinnen, Klompenhouwer, *et al.*, 2009; Teragawa *et al.*, 2011).

## Colour-Sequential and Spatio-Temporal LCDs

In LCDs, the presence of colour filters contributes significantly to the low light efficiency. A colour-sequential LCD, operating without colours filters, can increase the efficiency by 3-4 times (Lee, Liu, and Wu, 2008). With an RGB-coloured backlight, one can sequentially flash a red, green, and blue backlight and accordingly adjust a colour-filter less LCD to create colours temporally (Hasebe and Kobayashi, 1985; Yamada *et al.*, 2002). This is illustrated in Figure 1.12(c). Notice that the frame rate has tripled in our illustration and that each frame consists of three fields.



Colour-sequential LCDs have two major issues to overcome; 1) the slow optical response of LC-panels, and 2) the presence of visible colour breakup. Colour-sequential LCDs use at least three fields per frame and requires a fast LC-panel response time in order to preclude visible flicker. It has been estimated that between 180 Hz and 240 Hz is required in order to provide flicker-free operation (Silverstein, Roosendaal, and Jak, 2006). With relative motion between the human eye and the LCD (tracking moving objects, scanning image scene, or eye saccades), the temporal colour changes are translated into spatial colour changes, which causes bright, coloured fringes around high-contrast areas. This phenomena is known as colour breakup. In order to reduce colour breakup below the threshold of visibility, field rates as high as 1 000 Hz are needed (Post *et al.*, 1998).

Colour breakup may be reduced by other means than increased frame rate. For example, motion-compensated field-rate up-conversion (Leyvi and van Zon, 2004), inserting black frames, known as the RGB-KKK scheme, (Sekiya, Miyashita, and Uchida, 2006), or desaturation of the backlight primaries (mixing RGB with white) to match the smallest possible chromaticity distribution of the image (Bergquist and Wennstam, 2006). It has also been proposed to dynamically choose a fourth field (cyan, yellow, magenta, or white) (Huang *et al.*, 2011). The authors noted that a backlight segmentation (4 by 4) was instrumental in suppressing colour breakup. Using further backlight segmentation (665 segments) and three fields with locally-optimised primaries (XXX), it has been shown to reduce colour breakup to acceptable levels (Lin, Zhang, and Langendijk, 2011; Zhang, Lin, and Langendijk, 2011).

Operating a colour-sequential display has been complicated by the slow response time of LC-panels. In order to address this issue so-called spatio-temporal displays combine high-transmittance colour filters with sequential colour reproduction. This results in a trade-off between field rate and increasing light efficiency (Langendijk, Roosendaal, *et al.*, 2005; Langendijk, 2005; Silverstein, Roosendaal, and Jak, 2006). The basic principle is to generate one set of primaries with one illuminant in field 1 and another set of primaries with another illuminant in field 2. As an example of such a system we provide Figure 1.12(d). The colour filter configuration is in our example green and magenta, resulting in a blue and green primary when the cyan backlight is flashed, and a red and green primary when the yellow backlight is flashed. Notice that only two fields per frame are necessary, which means that the response-time requirements are relaxed. Further, we note that many more configurations are possible, see for example (Zhang, Langendijk, Hammer, and Lin, 2011b), several of which will have four, rather than three, distinct primaries. Such systems will, similar to multi-primary displays, require multi-primary conversion.

## 1.5 Temporal Response of Liquid Crystal Displays

Ideally transmittance of an LC-panel should change instantaneous to changes in the applied electrical field. However, upon a change in electrical field, the re-alignment of the LC molecules is slowed due to internal flow in the LC-layer. Common LC-alignment modes, with the exception of OCB-mode, are susceptible to this backflow effect causing slow response times (Mori, 2005).

The optical response of an LC-panel is typically characterised by means of the duration it takes to change the transmittance from 10% to 90% of the nominal transmittance level. However, as transitions between different electrical levels are frequently occurring, the same definition of 10% to 90% (or 90% to 10%) is used to characterise the response time for any grey-to-grey level transition. Furthermore, it is important to separate the optical response time (described above) from the electrical refresh rate. The latter is a merit of the voltage-controlling circuit and a fast refresh rate does not warrant a short response time.

The response time may be up to 50 ms, however, state-of-the-art LC-panels exhibit shorter response times. For example, an M-VA-mode LC-panel with 10 ms response time has been demonstrated (Lyu *et al.*, 2007). Similar, an IPS-mode LC-panel with a response time of less than 8 ms has been reported (Hong, Shin, and Chung, 2007). Recognising that these numbers reflect changes from 10% to 90% (or 90% to 10%), we realise that the response time is too long for colour-sequential operation (5.6 ms at 180 Hz).

In order to illustrate the optical response of LCDs, we provide Figure 1.13(a). Measured using a calibrated photo-diode, the light output of an LC-panel with a backlight operating in continuous mode is measured as a function of time. When the externally-applied voltage is changed, the transmittance of the LC-panel increases. The IPS-mode panel measured is engineered for 60 Hz operation, however, the transmittance is seen to increase over a much longer period than 16.7 ms (the duration of one frame at 60 Hz).

The measurement of the IPS-mode panel shows an increase in rate of change at each addressing instance (vertical blue lines at 0 ms, 16.7 ms, and 33.3 ms). This is not caused by discharge of the switching-circuit capacitor. Rather, this is caused by the capacitive effect which results in a slight decrease in transmissivity toward the end of a frame (Bitzakidis, 1994).<sup>2</sup> This effect can be observed in most LC-panels.

Besides slow temporal response, the continuous illumination is the cause of inter-frame crosstalk. Sluyterman and Boonekamp (2005) proposed to allow each pixel to respond to the changed electrical field and only illuminate the LC-panel

---

<sup>2</sup>When the LC-molecules re-orient according to the externally applied voltage, the di-electrical properties of the LC-layer also change resulting in a change of capacitance of the LC-layer.

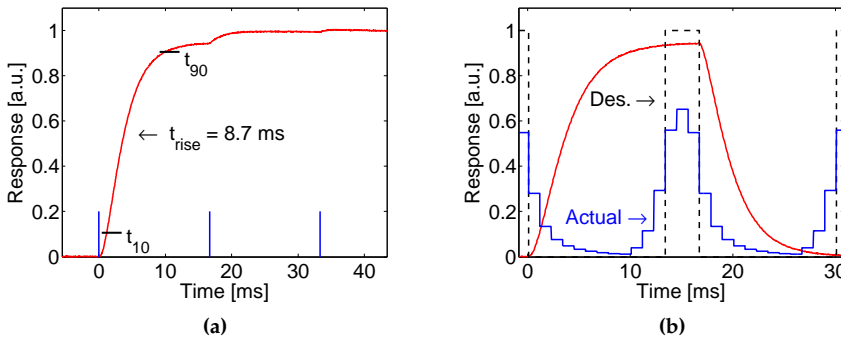


**Figure 1.13:** In 1.13(a), change in transmittance of an IPS-mode LC-panel at a refresh rate of 60 Hz. The 10%-90% rise time is about 8.7 ms. In 1.13(b), illustration of backlight scanning. The transmittance of an LC-panel (two frames white, two frames black) is shown in red. The desired backlight response is shown black-dashed, whereas the actual scanning backlight temporal response (blue-solid) is seen to be a combination of the vertically-scanning segments. Figure adapted from (Hammer and Langendijk, 2010).

for a short time instance. In Figure 1.13(b), the transmittance of an LC-panel is shown (red-solid) for two frames white and two frames black. This corresponds to a continuously-operating backlight. A pulsing backlight is illustrated (black-dashed) which is timely aligned with the addressing of the following frame. It can be seen that this will significantly reduce inter-frame cross-talk. However, the intensity of the pulse should be increased inverse proportionally to the reduction in pulse-width in order to keep the brightness level identical.

The above-mentioned pulsed backlight is not suitable for the TFT addressing scheme of LC-panels which operates row-per-row. Sluyterman and Boonekamp (2005) therefore propose to use a backlight with vertical segments and apply the pulsing in a scanning pattern matched to the addressing of the LC-panel. In practise, backlight light sources are overlapping, with each lamp contributing to about 30% of the total amount of light directly above it. Consequently, the scanning backlight will be slightly smeared as illustrated in Figure 1.13(b) in blue-solid.

With breakthrough achievements in LCD technology, a significantly shorter response time may be obtained. For example, a polymer-stabilised LC blue-phase-mode have demonstrated sub-millisecond response time (Kikuchi *et al.*, 2007; Ge *et al.*, 2009; Y Chen *et al.*, 2011), and a device using the  $\pi$ -cell structure (OCB-mode) has been demonstrated with a maximum response time of  $650 \mu\text{s}$  (at 10 V) and potentially an order of magnitude faster at higher voltages (Cheng, Bhowmik, and Bos, 2013). A fringe-field-switching alignment mode with a response time of maximum 1.29 ms has been demonstrated (Xu *et al.*, 2013), and, employing a new electrode design, the response time of the wide-spread VA-

mode has also been demonstrated an order of magnitude faster than normally (Iwata *et al.*, 2013).

## 1.6 Objectives of this Thesis

The discrepancy between the real-world light levels and those reproduced by state-of-the-art displays can be explained by historical choices (technical standards) and technological limitations, on the one hand, and human visual perception, on the other hand. Despite that the real-world observer is adapted to the real-world light levels, and the display observer is adapted to the limited dynamic range of the display, the display observer still perceives the reproduced scene as realistic. Nevertheless, scientific literature shows observer preference for image reproductions with higher dynamic range than conventional displays can deliver.

In response to a desire for increased contrast and luminance, several different HDR prototypes have been constructed. Such HDR displays are typically based on an LC-panel and a spatially-modulated backlight (projector or matrix of LEDs). A spatially-modulated backlight can lead to increased contrast (deeper blacks), whereas increased luminance is achieved by increasing backlight intensity and consequently increasing power consumption. Existing HDR display prototypes exhibit 3-9 times higher luminance compared to conventional displays. This results in a significant increase in power consumption.

Existing HDR displays have been constructed using conventional LC-panels which exhibit a low light efficiency (typically in the order of 5-7%). High-transmittance LC-panel technologies, such as multi primary or colour sequential, can improve the light efficiency. The potential efficiency improvement of high-transmittance LC-panels is expected to be an enabler for bringing HDR displays to the consumer. Therefore, it is a goal of the research described in this thesis to investigate how advancements in LC-panel transmittance can be utilised to create brighter HDR displays with high image fidelity and without increasing power consumption.

With respect to advancements in LC-panel transmittance, two major improvements have been proposed that relate to light absorption in the colour filters. The first is multi-primary in which more efficient colour filters are added to the existing RGB colour filters. For example by adding a “white” (wide spectrum) colour filter. A second improvement is to get rid of the colour filters entirely by using colour sequential technology in which a sequence of coloured (backlight) fields are modulated to obtain the desired colour. Both solutions have substantial contributions to the light efficiency of a display system, but introduce artefacts that reduce the image fidelity. This will be discussed further in the following paragraphs.

In comparison with a conventional LCD, a multi-primary LCD provides up to about 50% higher transmittance, but suffers from colour distortions. This is caused by the gamut mapping necessary to transform the source signal defined in a three-primary gamut volume to the multi-primary gamut volume. Depending on the additional primaries, the gamut mapping can be designed to reduce saturation and/or reduce luminance for colours close to the multi-primary gamut boundary. A multi-primary LCD may consequently appear of inferior image fidelity in comparison with a conventional LCD. With respect to multi-primary LCDs, it is an objective of this thesis to realise 50% higher luminance compared to a conventional LCD, while preserving same image fidelity and power consumption.

A colour-sequential LCD does not have colour filters and therefore exhibits about three times higher transmittance in comparison with a conventional LCD. An objective of this thesis with respect to colour sequential displays is to realise three times higher luminance compared to a conventional LCD with RGB colour filters with the same power consumption and comparable image fidelity.

Although the relative high transmittance of colour-sequential LCDs is an attractive means of increasing luminance, two problems should be considered; 1) the response time of state-of-the-art LC-panels is too long, which may result in colour distortions due to inter-field crosstalk, and; 2) existing colour-sequential LCD prototypes suffer from visibly annoying colour breakup due to relatively low frame rate.

With respect to colour breakup, it has recently been demonstrated (Lin, Zhang, and Langendijk, 2011; Zhang, Lin, and Langendijk, 2011) that by employing spatially- and temporally-varying primaries using a segmented backlight with RGB LEDs and advanced backlight control, the colour breakup can be reduced below the threshold of visible annoyance. It is an objective of this thesis to realise colour-sequential display with spatially- and temporally-varying primaries as a means of reducing colour breakup artefacts.

Conventional colour-sequential display systems operate at a minimum field rate of 180 Hz to avoid visible flicker. In order to reduce the field rate to 120 Hz without flicker, it has been proposed to use two wide-band colour filters with two colour fields. This will trade off transmittance for a lower field rate. Typically the transmittance of such spatio-temporal LCDs is about 50%-150% higher than a conventional LCD. It is an objective of this thesis to investigate solutions with only two colour fields and no colour filters which would demonstrate three times higher luminance and same image fidelity compared to conventional LCDs.

The limited intrinsic contrast of LC-panels is about 3-orders of magnitude and is insufficient for HDR reproductions. A spatially-modulated backlight is a solution to increase contrast and extend the dynamic range with about 1-3 orders of magnitude. Typically such a backlight is constructed using a matrix of locally

addressable white LEDs and in response to the video signal, the intensity of the LEDs is controlled to match the necessary spatial distribution of light. Due to the resolution mismatch between the backlight and the video pixels, both spatial and temporal smoothing is applied. This reduces the modulation depth and the potential contrast improvement. With respect to display contrast, it is an objective of this thesis to realise LCD solutions which utilise spatially-modulated backlights in order to improve the contrast with at least 2-3 orders of magnitude. Furthermore, optimisation techniques should be explored which can increase the modulation depth while providing sufficient temporal stability.

In order to facilitate the research, a prototype display must be constructed. The display system should consist of a segmented backlight with RGB LEDs and an LC-panel. As both multi-primary and colour-sequential displays are targeted, it is desirable to allow easy exchange of the LC-panel. The number of backlight segments should be at least on par with state-of-the-art research prototypes and provide better spatial light separation than conventional mixing-in-air designs utilising segments of LEDs. Furthermore, it must be possible to control signal amplitude and signal timing for each backlight segment colour individually.

Finally, the overall objective of this thesis can be summarised as follows: Investigate display system solutions in combination with video processing and backlight control algorithms in order to improve the luminance and contrast of HDR displays with high-transmittance LC-panels and spatially-modulated backlights.

In the following section, an outline of the thesis is presented based on the main contributions of the described research.

## 1.7 Thesis Outline and Beyond

In Chapter 2, a custom-built HDR backlight system is described which facilitated a majority of the research described in this thesis. In Chapter 3 we aim at improving luminance using a multi-primary display. Chapters 4 and 5 concern colour-sequential display operations and aim at luminance increase beyond the improvement in transmittance and reducing the field-rate, respectively. Chapter 6 describes the contrast requirements for displays while considering human-eye glare, while Chapter 7 concerns the use of OLED displays for HDR image reproductions. Finally, in chapter 8 a general conclusion is provided and some directions for future work introduced.

Directly below is a brief overview of the subjects treated in this thesis including the main contributions. It also provides references to the publications that have been produced based on the work described in this thesis.

**A display prototype with high-dynamic range capabilities** (Chapter 2) which allows a peak luminance of more than  $4000 \text{ cd/m}^2$ . The 42 inch backlight unit had 1125 segments each consisting of a triplet of high-power RGB LEDs. From 2007 to 2012, the backlight unit has been mounted with 5 different LC-panels ranging from fast VA-mode, over IPS-mode with patterned retarder, to fast-response OCB-mode panel type. The prototype served as research vehicle and was instrumental in several research projects.

**A method for boosting luminance of an RGBW LC-display** (Chapter 3) An LC-display system with RGBW-colour filters typically suffers from dark saturated colours. In order to improve colour reproduction, a local backlight boosting scheme was presented which exhibit good temporal stability (Hammer and Hinnen, 2014). Whenever the backlight was boosted in order to restore luminance of bright, saturated colours it was also possible to apply luminance enhancement of desaturated colours. This has also been disclosed in (Hinnen, Hammer, and Langendijk, 2012).

**Boosting luminance of a colour-sequential display** (Chapter 4) such that up to a factor-three luminance increase can be realised using a conventional spatially-modulated RGB-LED backlight unit. The method utilises dynamic adjustment of local primaries. The method was disclosed in (Hinnen, Hammer, and Langendijk, 2012) and described in the articles (Hammer, Hinnen, and Langendijk, 2012) and (Hammer, Hinnen, and Langendijk, 2013).

**A display with 2-field colour sequential mode** (Chapter 5) which allowed full colour reproduction by dynamically adjusting two local primaries per frame to the chromaticity statistics. Such a system can operate at 120 Hz field rate, whereas a conventional, 3-field colour sequential display requires 180 Hz field rate in order to suppress visible flicker. The method was described in the following publications (Hammer *et al.*, 2011) and (Hammer *et al.*, 2012) and disclosed in (Hammer, Baar, Hinnen, *et al.*, 2013).

**Study of contrast requirements for high-contrast displays systems** (Chapter 6) while considering human-eye glare. In particular it investigates the visibility of contrast modulations with different spatial frequencies and of contrast variations in natural images and applies this to the contrast requirements of LCD and OLED displays. The method and results were published in (Langendijk and Hammer, 2010)

**OLED displays for HDR reproductions** (Chapter 7). Whereas the contrast characteristics of state-of-the-art OLED displays exceed those of most other display technologies, the luminance is still lower than that of LCDs. An early-stage study showing experimental data of luminance and thermal behaviour is reported. A method for improved luminance, previously disclosed in (Hammer and de Greef, 2012), is presented.

Besides the work described in this thesis, a number of publications were generated on subjects which relate to the presented work. Below is a brief overview of these contributions.

**Spatio-Temporal LC-Displays:** In order to balance increased transmittance and the presence of colour breakup, spatio-temporal displays with two fields and two colour filters have been proposed (Langendijk, Cennini, and Belik, 2009). However, as visible colour breakup remains present, we proposed mixing the backlight colours locally such that smaller colour gamuts would be created resulting in less colour and contrast difference between the fields. With two fields and two colour filters, the system effectively exhibits four spatially-varying primaries such that dynamic multi-primary conversion must be applied. Based on simulations, the proposed methods was verified to reduce the perceived colour breakup. This work was published in (Zhang, Langendijk, Hammer, and Lin, 2011a) and (Zhang, Langendijk, Hammer, and Lin, 2011b).

**Colour-Breakup Metric:** Colour sequential display systems suffer from colour breakup, an artifact occurring with relative motion between display and the eyes of the observer. We established a computational metric based on the presented fields, which could predict the perceived level of colour breakup. In a psychophysical study, it was established that colour difference and relative contrast between fields have a strong effect on perceived colour breakup, whereas correlation with absolute luminance levels, as is often used in colour-breakup metric, is less pronounced. The proposed method was verified to have a high correlation with the subjective scores of the psychophysical experiment. This work was published in (Zhang, Langendijk, Hammer, and Hinnen, 2012).

**Wide-Gamut Displays:** Natural colours cover a much larger colour gamut, than can be reproduced by most commercial display systems (Hinnen and Langendijk, 2010). In order to reproduce the full range of colours, we proposed a multi-spectral backlight LC-display system with 5 different types of LEDs (RGBCY). Based on the spectra of the LEDs and the colour filters, a model was derived to describe the local multi-spectral backlight system. This was published in (Hinnen, Hammer, and Langendijk, 2011).

**Visibility threshold levels for binocular crosstalk** (3D perception) has only been established for limited contrast and luminance levels (up to 100:1 and up to  $100 \text{ cd/m}^2$ ). We investigated the impact of higher contrast and luminance levels, respectively with an HDR display which allowed independent adjustments of luminance, contrast, and binocular crosstalk. It was found that an increase in luminance resulted in a slight reduction of the visibility threshold for binocular crosstalk, whereas contrast was found to have no



impact on threshold for contrast levels above 100:1. This work was published in (Lambooj and Hammer, 2013).

A comprehensive list of technical publications has been included in the List of Publications at the end of the thesis.



# A Versatile High-Dynamic Range Display System

As illustrated in Chapter 1, both contrast and luminance of state-of-the-art displays are considerably lower than the capabilities of the human visual system and what can be experienced in daily life. In order to facilitate research with primary focus on improvements of contrast and luminance, a unique display system has been constructed at Philips Research Laboratories. The display system is based on an LC-panel illuminated by an HDR backlight unit consisting of locally-addressable RGB LEDs. For different applications, the backlight unit could be configured with different LC-panels. Depending on the configuration, the peak luminance was between  $3000 \text{ cd/m}^2$  and  $7000 \text{ cd/m}^2$  while the corner-box contrast (ICDM, 2012) ratio was about 7800000:1.

The display system was instrumental for the work described in this dissertation, either allowing a physical demonstration of a novel concept (Chapter 4 and 5) or as a source of inspiration (Chapter 3 and 6).

In the following sections, we describe the applications of the display system and provide a summary of the key performance characteristics. The resulting design and the considerations behind the design choices are covered in Section 2.1 (optical design), Section 2.2 (electrical, mechanical, thermal), and Section 2.2.4 (backlight control software). In order to use the display, it was necessary to carry out a calibration of the RGB LED intensity and to characterise the segment spatial profile (point-spread function), which is treated in Section 2.3 and Section 2.4.

Finally, in Section 2.6 two computational methods are introduced in order to evaluate the contrast and luminance performance of a display system. We found

these methods particularly useful in the design of the optical stack. These methods, however, rely on detailed characterisation of the backlight segment point-spread function. To that end, we review display metrology methods and show the result of a comparative study on contrast and luminance in Section 2.6.4.

## Targeted Specifications

The HDR display was constructed in order to demonstrate state-of-the-art contrast and luminance performance. We had the following applications in mind during the design: 1) colour-sequential operation using a fast-switching colour-filter-less LC-panel, 2) wide-gamut demonstrations and investigation of novel colour-gamut mapping algorithms, 3) tone-mapping operations of either HDR video or legacy video to the displayable dynamic range, 4) vehicle for psychophysical studies on contrast and colour perception, and 5) support to Philips Television product development, for example by means of emulations of high-contrast display concepts. Consequently, the HDR display should exhibit high peak luminance, high contrast ratio, large colour gamut, whereas the backlight halos should be kept below a level of perceptability. The form factor, in particular display thickness, was considered a less important design parameter.

In the following, the high-level specifications of the display system together with motivation for each choice is listed. The specifications are shown in Table 2.1.

The display size and complexity were important design constraints. At the time of the design, high-end LC-based display systems were either 42 inch or 46 inch. The power consumption of a larger display system would result in a lower peak luminance due to limitations of the wall-plug circuit breaker. It was therefore chosen to construct a 42 inch display. Due to the considerable amount of custom-built electronics, it was opted for a modular construction of the backlight unit, which would allow several design iterations on a small-scale prototype at manageable costs.

The peak luminance of high-end display systems is about  $500 \text{ cd/m}^2$ . As the response of the human visual system to increase of light intensity can be roughly described by a logarithmic relationship, a doubling of the perceived amount of light corresponds to an increase in light intensity with a factor 6. It was therefore chosen to aim for at least  $3000 \text{ cd/m}^2$  peak luminance.

The number of backlight segments and the luminance profile is known to play an important role on the image quality. Both the spatial frequency and the presence of bright objects (glare) may reduce contrast perception. In a user-preference study, Swinkels *et al.* (2006) measured preference scores for simulated backlight segmentation on a double-LCD display setup, and found that preference scores increased up to about 2500 segments. Langendijk and Hammer (2010) estimated the increase of perceived black level due to human-eye glare and found that

**Table 2.1:** Design choices for the HDR display.

Parameter	Value	Remarks
Peak Luminance	3000 cd/m <sup>2</sup>	Constrained by circuit-breaker (3 kW)
Panel Contrast	1500:1	or higher
Backligh Segments	1125	About 2 cm pitch, 25 × 45 segments.
Colour Gamut	120% NTSC ( $u'v'$ )	Use of RGB LEDs will maximise gamut.
Screen Size	42-inch	Trade-off between display size and luminance.

about 2304 backlight segments would perform comparable to an ideal HDR display. Both the experimental and the modelling-based results indicate a limit of a few thousand backlight segments. However, more backlight segments result in increased cost of materials and increased complexity of the backlight design. We therefore settled for a design with 1125 backlight segments.

Lastly, the colour gamut should be at least 120% NTSC (CIE  $u'v'$ ) in order to facilitate research on novel wide-colour gamut algorithms and psychophysical studies on colour perception. The wide gamut was achieved by using RGB LEDs.

## 2.1 Optical Design

In this section, we elaborate on the choice of light source, LED RGB emitters, and the design of the optical stack governing the local profile shape, yet ensuring full-white uniformity.

### 2.1.1 Light Source

In order to guide the backlight design, the following reasoning was applied. With a desire for 3000 cd/m<sup>2</sup> front-of-screen luminance, assuming 5% LC-panel transmittance, the backlight should be 60000 cd/m<sup>2</sup> corresponding to a luminous emittance of 189000 lm/m<sup>2</sup>. For a 42-inch backlight the flux should be 89000 lm. For about 1000 LED triplets and assuming a relative contribution of red, green, and blue of 20%, 70%, and 10%, the luminous flux should be 62 lm, 18 lm, and 9 lm, respectively.

Philips Lumiled Rebels LEDs were chosen as light sources. The specifications of the red, green, and blue LEDs can be seen in Table 2.2. The luminous flux is seen to be larger than the desired level. Furthermore, the dominant wavelength was chosen based on simulations of the resulting colour gamut. In Figure 2.1 the transmission levels of the red, green, and blue colour filter of a conventional LC-panel is shown with dashed lines. The chosen spectra, extracted from (Philips,

**Table 2.2:** Characteristics of the Philips Lumileds Luxeon Rebel LEDs used in the HDR backlight.

	Red	Green	Blue
Part Number	LXML-PD01	LXML-PM01	LXML-PR01
Type – Bin	040 - G4C	080 - M3D	275 - D5F
Peak $\lambda$ [nm]	620.5-631.0	530-535	450-455
Luminous Flux [lm]	40-50	90-100	350-425 mW (~11 lm)
Forward Voltage [V]	2.79-3.03	3.03-3.27	3.51-3.75

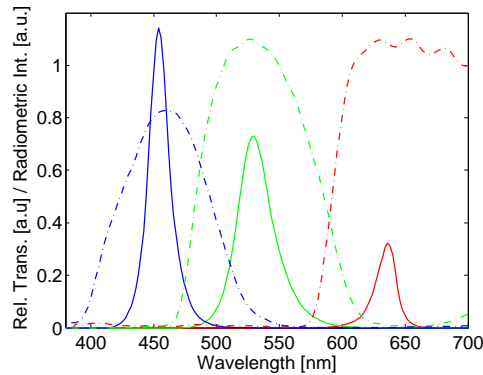


**Figure 2.1:** Measured spectra of the RGB LEDs (solid lines) and the colour filters of the “VA-mode 1” panel (dashed lines). Note, that the blue LED spectrum has been scaled by 1/3. The peak wavelength of red, green, and blue was 454 nm, 530 nm, and 636 nm, well in correspondence with the specifications in Table 2.2.

2009) and shown in solid, is seen to match well with the colour filters. As the HVS is most sensitive to light around 550 nm, the dominant wavelength will impact the peak luminance. It is therefore important to balance the choice of the dominant wavelength (wide-colour gamut) and the peak luminance.

In Table 2.2 the LED bin type is listed. The backlight unit was constructed with LEDs of the same type. Each LED had been tested by the manufacturer to exhibit dominant wavelength, luminous flux, and forward voltage to within a given range (seen in Table 2.2). Using a single bin type has several advantages. Variations in luminous flux and dominant wavelength would require significant calibration to the worst-performing LED. Besides being undesirable, it would also make the resulting specifications less predictable. The forward voltage is the voltage necessary to keep the diode in a saturated regime. Large variations would require a significant buffer-voltage to ensure correct voltage to all LEDs and consequently lead to undesirable resistive losses.

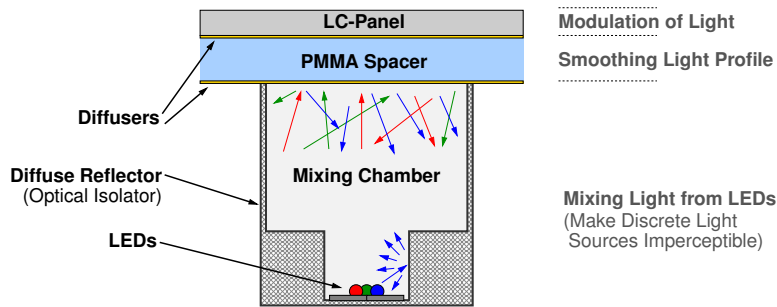


**Figure 2.2:** Illustration of the optical stack for a single segment. A light-mixing chamber is responsible for masking the discrete positions of the LEDs and create a wide emission profile limited by the optical isolator (walls). Two diffusers separated by a transparent (PMMA) spacer are positioned atop the mixing chamber. The dual-diffuser design is intended to mask the optical isolator and create a smooth spatial light profile. Finally, the LC-panel is seen at the very top.

## 2.1.2 Optical Stack

A unique optical concept was developed in order to deliver superior backlight modulation. In a good backlight design, the spatial light profile of a backlight segment is confined to a small region, while allowing sufficient mixing with adjacent segment in order to guarantee good uniformity. Conventional backlight units are based on a matrix of LEDs and an open air cavity for light mixing. However, this results in a significant cross-talk between the backlight segments. In our design, it was opted for a backlight structure with optical isolators, that first transform the coloured point light sources (RGB) into a white area light source using a mixing chamber, and then control the spatial light overlap between the backlight segments using a diffuser–PMMA–diffuser stack.

In Figure 2.2 an illustration of the optical stack of a single segment is shown (side view). At the bottom, the RGB LEDs are positioned with the light-emitting dies as centrally-positioned as possible. The segments are optically isolated by a diffuse reflector, which creates a light-mixing chamber. The efficiency of the mixing chamber is improved by a diffuser-sheet lid, forcing a fraction of the light to bounce up and down. The mixing chamber is divided in two, a smaller mixing chamber located closely to the LEDs, and a wider upper chamber. The two-chamber structure was a preferred design option, in which the bottom chamber would mask the discrete positions of the RGB emitters, and the upper chamber would enlarge the light-emitting area of the segment. It was experimentally found that a height of 20 mm for the mixing chamber provided sufficient light mixing. Two diffusers separated by a transparent spacer (PMMA) are positioned atop the mixing chamber. The dual-diffuser design is intended to mask the optical isolator (walls) and create a smooth spatial light profile that overlaps

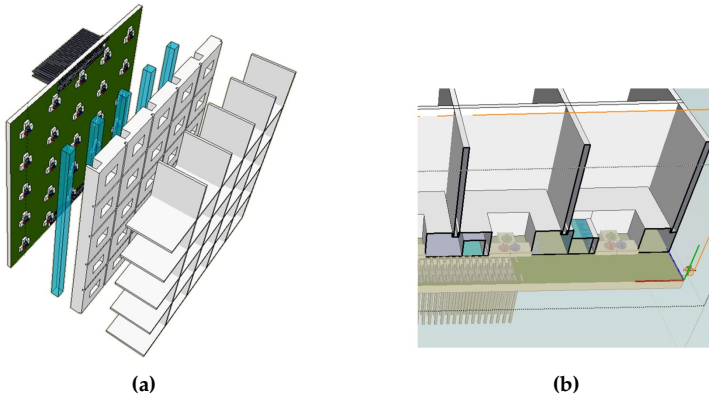


**Figure 2.3:** A CAD drawing of an LED tile with the optical structure is shown in (a). The LED tile, the lower and upper mixing chamber is clearly seen. The transparent (blue) rods were meant for sense-and-control in an early design, but not included in the final design. In (b) a CAD drawing showing the assembled structure. Notice how the light-emitting dies of the RGB LEDs are position centrally as close as possible.

substantially with its neighbouring segments, but has no long tails. Finally, the LC-panel is shown at the very top.

In Figure 2.3, two CAD drawings of an LED tile are shown. It was opted for a modular design consisting of tiles of  $5 \times 5$  LED triplets in order to manage cost and design complexity. In Figure 2.3(a), the PCB with LEDs, the small mixing chamber, and the large (wider) mixing chamber is shown. The vertically-oriented glass-looking sticks, were PMMA-based light guides intended for real-time calibration. However, in an early prototype it was established that the light guide would sacrifice backlight modulation depth as it would enable vertical light-transfer between segments. Secondly, intensity drift of the LEDs proved less of an issue as initially assumed.

The performance, segment profile shape and uniformity were experimentally verified in a number of design cycles by constructing small prototypes of  $5 \times 5$  segments. In Figure 2.4(a), a photograph of such a prototype is shown. The LEDs were connected such that the intensity of three circular regions could be adjusted independently. In Figure 2.4(b) a photograph of the backlight prototype without the PMMA spacer and second diffuser is shown. The circular pattern of white-yellow-red can easily be recognised. Also notice the slightly visible optical separation walls framing each segment. In Figure 2.4(c) a photograph of the backlight prototype including PMMA spacer and second diffuser are shown. Notice that the walls are no longer visible, yet the colours of each segment have been preserved illustrating good optical isolation between each segment.

In the full-sized backlight, the modules, such as that shown in Figure 2.4(a), were tiled 9 horizontally and 5 vertically resulting in 45 by 25 segments. In Fig-



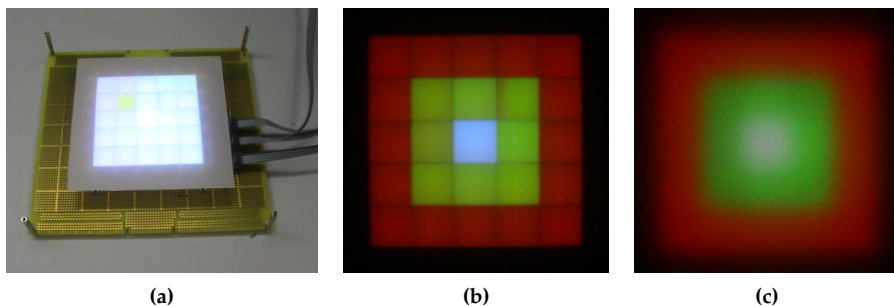


**Figure 2.4:** Photographs of an early prototype backlight tile. In (a) a LED tile with drive electronics, the optical isolators and a single diffuser is seen. In (b) the same setup is seen up close showing three circles of different colour. Notice the distinct separation of the outer segments from the inner segments. In (c) the PMMA-spacer and a second diffuser has been position. Notice how the segments are less distinct, yet distinguishable, while allowing a smooth transition between the differently-coloured segments.

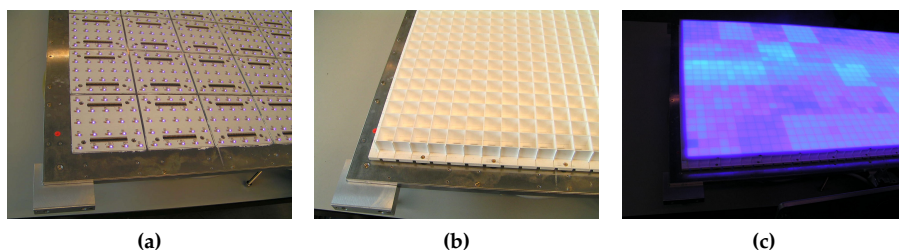


**Figure 2.5:** Photographs of the HDR display during build-up. In (a) a close-up of the 5 by 9 LED tiles with 25 segments each. Each LED tile is clearly visible at this stage. In (b) the structure for optical isolation and light mixing has been mounted and in (c) a single diffuser has been placed. As the photograph is from an early stage, neither hardware nor software calibration has been carried out, which is causing the irregular pattern.

ure 2.5(a) a photograph of the backlight unit with the LED tiles mounted on the aluminium carrier plate is shown. In Figure 2.5(b) the optical isolator structure has been positioned. In Figure 2.5(c) the first-level diffuser has been placed and the backlight is emitting light. The backlight is in an uncalibrated state, hence the large segment-to-segment variations.

## 2.2 Electrical, Mechanical, and Thermal Design

In this section, we introduce a split design using an LED tile for the  $5 \times 5$  LEDs, and a driver tile holding the corresponding driver and power converter ICs. Secondly, the backlight power supply module and thermal management system is

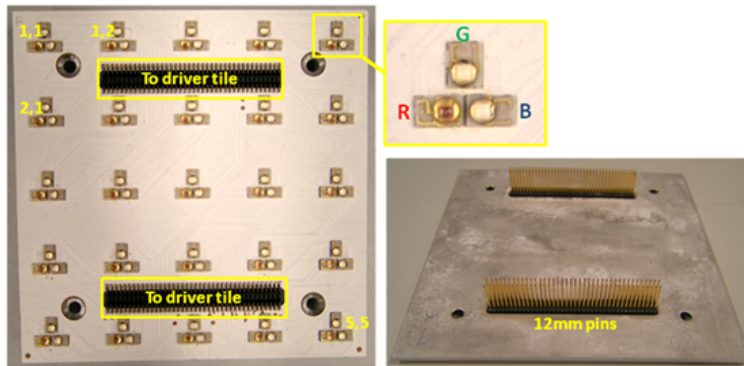


**Figure 2.6:** LED driver tile top and bottom view. To the left the front view of the tile is depicted. A matrix of  $5 \times 5$  RGB triplets are uniformly distributed over a  $10 \text{ cm} \times 10 \text{ cm}$  metal core board. In order to plug it in the accompanying driver tile, two connectors are mounted at the back of the tile (see lower-right photograph). In the inset, top-right, a close up of the layout of the RGB LEDs is shown.

treated. Lastly, the backlight data and timing control needed for real-time adjustments of the backlight is discussed.

### 2.2.1 LED Tile

The modular design of the backlight is centred around a LED tile and a driver tile. The LED tile consists of a matrix of  $5 \times 5$  RGB triplets equally distributed over a  $10 \text{ cm} \times 10 \text{ cm}$  metal-core printed circuit board (PCB). A photograph of a LED tile is shown in Figure 2.6. In the small inset at the top, the discrete position of the Philips Lumileds Luxeon Rebels can be seen. Notice that the die of each LED is located as close as possible to the centre of a segment. This is important in order to have the best colour mixing between the three LEDs.

The design included a metal-core PCB in order to dissipate heat away from the LEDs and towards the water-cooled aluminium carrier plate, which is discussed in Section 2.2.3. This would ensure a more stable LED temperature, which may extend LED lifetime and increase luminous efficacy. Since metal-core PCBs can only be soldered on one side, a cavity allowed a long-pin connector to be soldered to the front and stretch to the back. In Figure 2.6(right) these connectors are seen (back view). The benefit of this mounting method is that a flat front-surface is realised while gaining maximum thermal conductivity through the metal-core PCBs.

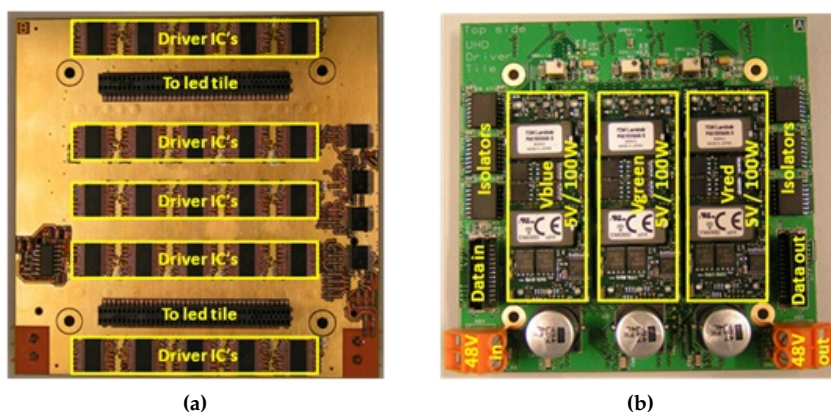


**Figure 2.7:** Driver tile bottom and top view in (a) and (b), respectively. The bottom side is facing the LED tile, which will be plugged in the two slim-shaped connectors. Each LED triplet corresponds to a driver IC, adding up to 5 times 5 ICs. The top view reveals the drivers, the power supply (chained, in/out), and the data connection to serially connect the driver tiles. Supply and logic signals are daisy-chained from left-to-right using the “data in”-“data out” connectors.

## 2.2.2 Driver Tile

A driver tile is capable of driving a  $5 \times 5$  matrix of RGB LEDs (75 LEDs in total). In order to provide sufficient current to the 3 W high-power LEDs, one driver IC (Texas Instruments TLC5940) was needed per RGB triplet. In Figure 2.7(a), this matrix of  $5 \times 5$  drivers is shown spread evenly over the bottom side of the driver tile. The copper on this side of the PCB will take care of directing the heat away from the driver ICs towards the aluminium carrier plate. In the two slim-shaped connectors, the LED tile can be inserted.

For controlling the LED intensity a driver IC from Texas Instruments was used. It allows serial programming of pulse-width modulation (PWM) and amplitude modulation (AM) of 16 current sinks capable of up to 120 mA constant current. Several outputs were connected in parallel in order to achieve the desired driving current. To roughly match the desired display white point, the following current levels were hard-wired; blue LEDs at 600 mA, green LEDs at 840 mA, and red LEDs at 480 mA. The final white-point adjustment was done using AM based on a post-assembly calibration (Section 2.3).

All LEDs were supplied by similar power supply modules. The green LED with a maximum current of 840 mA and a forward voltage of about 4 V was used as target. Despite the lower maximum current for blue and red, identical power supply modules were used for all colours for simplicity. In Figure 2.7(b) a photograph of the driver tile front is seen (this side will face away from the carrier plate).

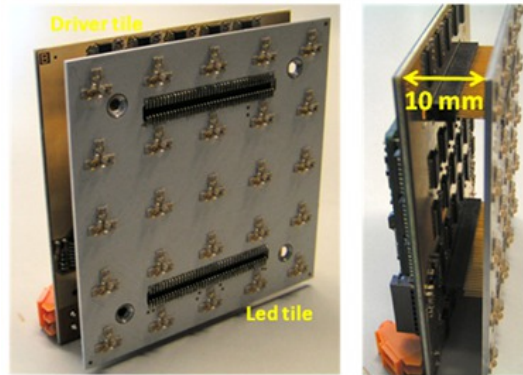


**Figure 2.8:** A photograph of the LED tile connected to the driver tile (left). The 10 mm gap between the driver tile and the LED tile is clearly visible in the photograph (right). This gap is filled by the 42 inch aluminium plate (not shown) with water channels for active cooling.

The left side of the PCB may be regarded as the receiving side for power supply (48 V) and logic signals (data in). At the right side, the next board in line can be wired and this can be continued to create a chain of tiles. As the programming of pulse-width and current (amplitude) of the driver ICs is done in a serial manner, making long chains of driver tiles translates into a long programming time. On the other hand, a separate cable for each driver tile will result in cable clutter. We opted for daisy-chaining three tiles which resulted in 15 groups (cables) of 225 LEDs.

In Figure 2.8, a photograph of the LED tile connected to the driver is shown. Notice the gap between the tiles which is reserved for the aluminium carrier plate.

**2.2.3 Power Supply and Thermal Management**

For practical and aesthetic reasons, it was decided to put the power supply and thermal management system in a separate box next to the display, because the large power and current requirements of the HDR display system together with the water-cooling unit, would make a combined system bulky and very heavy. The power box is shown in the photograph of Figure 2.9(c).

The amount of power conducted from the power box to the display unit can be very high. In order to balance losses and safety of use, the supply voltage was 48 V. Each driver tile was equipped with separate power converters for the red, green, and blue LEDs, respectively. As the forward voltage of each LED colour is different (see Table 2.2), this proved useful to adjust the voltage across each LED colour independently, helping a reduction in losses in the driver ICs.

The amount of energy dissipated in the LEDs would result in an considerable temperature of the LED dies, which eventually may result in device failure. Con-



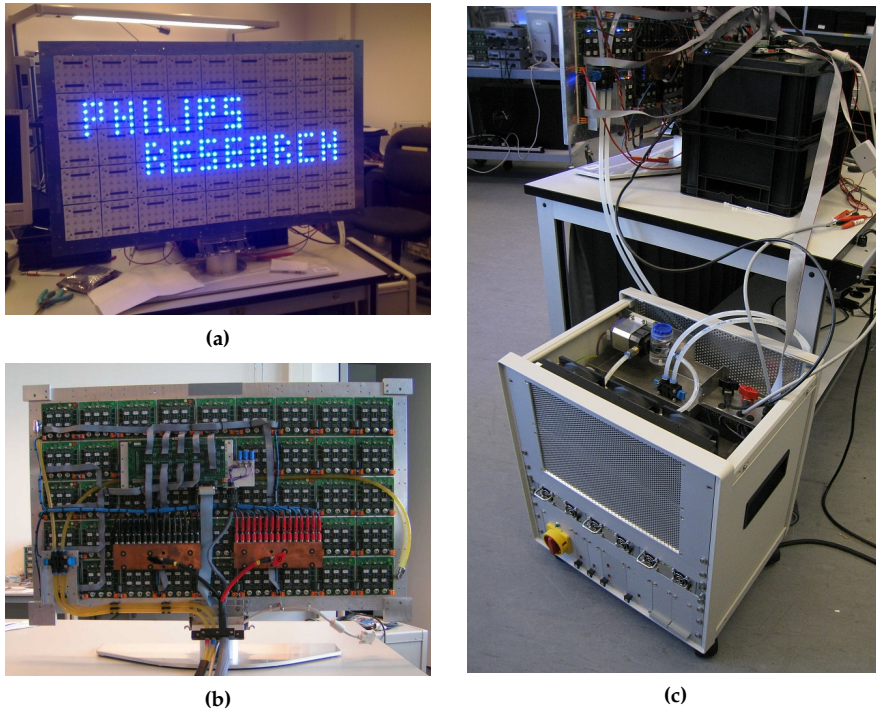


**Figure 2.9:** Photographs of the HDR display during build-up. In (a) a front-view of the 5 by 9 LED tiles is shown. The blue LEDs are acknowledging the Research Laboratories at Philips. In (b) a rear-view of the backlight unit. Notice the modular build-up based on PCB tiles of drivers, equivalent to the LED driver tiles on the front, mounted on an aluminium carrier for cooling. The pressure tubes used for the water cooling are seen in the bottom-left corner. In (c) the power supply unit is seen. The unit supplied all necessary voltage levels for LED drivers to digital logic. The water pump and radiator cooling is located at the top of the power supply unit.

sequently, a thermal management system was constructed consisting of a large, thick aluminium carrier plate with internal water flow. The carrier plate will ensure heat spread, while the water flow is responsible for heat extraction.

The full-sized 42 inch backlight unit is based on the aluminium carrier plate onto which the driver tiles and LED tiles are mounted. The dimensions of the carrier plate are 1000 mm  $\times$  600 mm and 10 mm thick. The layout consisted of 5 vertical and 9 horizontal tiles resulting in a total of 25 by 45 segments. In Figure 2.9(a) and Figure 2.9(b), photographs are shown of the backlight unit front and back during buildup, respectively.

Water channels (40 mm) were milled out in the carrier plate, creating a zig-zagging flow of water from top to bottom. The water channels are located directly beneath each tile between the connector openings. Furthermore, extensive milling is used to match the uneven topography of the driver tile surface. Gap-

pads are used to avoid short circuits and damp vibrations, and to reduce thermal resistance (by eliminating air gaps). The thermal resistance between the LED tiles and the carrier plate was reduced using heat compound.

In the power box, the water flow for thermal management is created using a small 12 V water pump. The water is cooled using two radiators equipped with 6 fans to facilitate sufficient air-flow. The radiators and fans are mounted behind the perforated part of the power box and the water pump is located at the top in Figure 2.9(c).

### 2.2.4 Backlight Data and Timing Control

In order to adjust the backlight intensity to the video data, each LED should be updated synchronously with the video data. It was chosen to embed the backlight data into the video signal and use an FPGA to extract the desired pulse-width and amplitude modulation. Each of the 15 areas (of 225 LEDs on 3 driver tiles) would then be programmed in parallel.

The embedded video signal consists of 16 lines; 1 header line with per-row on-time (for backlight scanning; see next section) and 15 data lines, one row per area of 3 driver tiles. The driver ICs could adjust the intensity by 6-bit AM and 12-bit PWM. The AM-range was only used for calibration of segment-to-segment variations of intensity based on a set of static calibration values. The entire PWM-range could then be used for real-time backlight modulation.

The high peak luminance of the display system made 12-bit PWM necessary. It was initially estimated that peak luminance would become close to  $9000 \text{ cd/m}^2$  in a colour-sequential operation. As it is desired to also support operation at  $500 \text{ cd/m}^2$  it was necessary to retain about 8-bit resolution ( $562.5 \text{ cd/m}^2$  corresponds to 8-bits in this example).

Embedding the backlight control data into the video signal turned out to provide problems. Small objects such as the mouse cursor could mistakenly be interpreted as the backlight control signal. This could lead to spurious light generation when the mouse cursor would move in and out of the region of embedded data. Each row was therefore equipped with an 8-bit cyclic redundancy check based on the following generator polynomial:  $x^8 + x^7 + x^4$ . If the check failed, the embedded modulation values would be neglected and a safe state used instead.

### Backlight Scanning

LCDs are known to suffer from motion blur due to the slow temporal response of the LC-panel and continuous backlight illumination. The slow temporal response is the cause of inter-frame cross-talk, i.e. wrong transmission levels due to insufficient settling time, whereas continuous illumination results in sample-and-hold

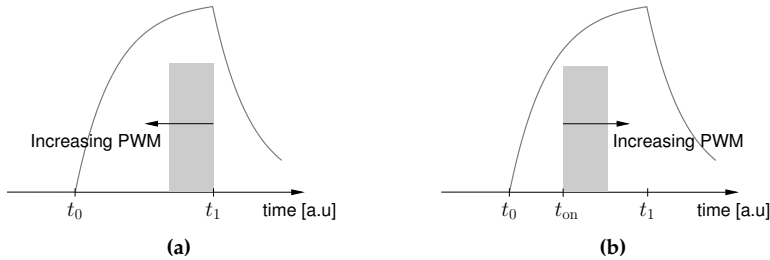


**Figure 2.10:** Illustration of options for pulse-width modulation provided by LED drivers. A simple black-white-black LC-panel response is shown, the frame synchronisation indicated by  $t_0$  and  $t_1$ . In (a), the pulse-width and the off-time is used, such that increasing pulse width extends backward in time w.r.t.  $t_1$ . In 2.10(b), the pulse-width and the on-time,  $t_{on}$ , is used, such that increasing pulse width extends forward in time w.r.t.  $t_{on}$ . The first method is better suited for backlight applications.

behaviour. In a colour-sequential operation both effects will contribute to colour errors. In this section, it is described how these issues have been addressed.

Improved motion portrayal for LC-displays has been extensively investigated, see for example Klompenhouwer (2006). Reduced illumination duty cycle is among the most effective remedies and can be achieved using PWM of the backlight LEDs. This is illustrated in Figure 2.10(a). An LC-panel is switched to high transmission at  $t_0$  and to low transmission at  $t_1$ . The grey-block illustrates the light generation from the backlight and is aligned with  $t_1$ . If the pulse-width is increased, the off-time is not changed.

As demonstrated by Sluyterman and Boonekamp (2005), a short duty cycle is not sufficient, the illumination period should also be timely aligned to the addressing of the LC-cells. The LC-cells in an LCD are addressed row-sequentially, typically from top-to-bottom. The time needed to address all rows is approximately equal to the frame time. When the illumination period of each row of backlight LEDs is timely aligned to the addressing of the corresponding row(s) of LC-cells, the backlight will also operate in a scanning sequence.

Whereas typical LED driver ICs for backlight applications allow specifying the desired off-time ( $t_1$  in Figure 2.10(a)), the chosen driver IC only provides specifying the on-time. This is illustrated in Figure 2.10(b). In this example, the light generation is not aligned with  $t_1$  and one would have to take the (variable) pulse-width into account when determining the  $t_{on}$  which would align the light generation with  $t_1$ . If the pulse-width is frequently adjusted,  $t_{on}$  should also be adjusted frequently. Using the embedded backlight data protocol, it is possible to adjust the on-time for each of the 25 rows of LEDs in the backlight.

## 2.3 Characterisation and Calibration of RGB LEDs

Due to LED-to-LED variations in luminance, colour, forward voltage, and driving current, it is expected that each LED needs careful calibration after the system has been assembled. This section describes this automated calibration procedure using an imaging colourimeter.

### 2.3.1 Methods

The calibration procedure was split in two. First the intensity of each LED was levelled such that all LEDs of the same colour were at the same intensity resulting in a per-colour (red, green, blue) uniform backlight. Secondly, the global relative intensity of the colours was adjusted to achieve the desired display white point. The latter depends on the LC-panel and the colour filter, whereas the per-LED calibration pertains to the backlight unit only. As the white point adjustment is rather trivial, we will not treat this further in this section.

Rather than manually re-positioning and re-aiming a spot colourimeter, we made use of an imaging colourimeter. Such a device is based on a scientific-grade image sensor and a colour-filter wheel which allows sequential measurements of CIE tri-stimulus values. Each measurement consists of one of the tri-stimulus values, depending on the position of the colour-filter wheel. Hence, three measurements are necessary to obtain a tri-stimulus colour description.

The transmission spectra of the colour-filter wheel are (typically) approximations to the 2° CIE 1931 color matching functions  $\bar{x}(\lambda)$ ,  $\bar{y}(\lambda)$ , and  $\bar{z}(\lambda)$  (Berns, 2000). Let the transmission spectra of the colour-filter wheel be given by,  $\tilde{x}_R(\lambda)$ ,  $\tilde{y}_G(\lambda)$ , and  $\tilde{z}_B(\lambda)$ . The spectrum of a red LED is denoted by  $S_R(\lambda, I, p)$ , where  $I$  is current and  $0 \leq p \leq 1$  is pulse width. Then the measured tri-stimulus value of the red LED is:

$$\tilde{X}_R = \int_{\lambda} \tilde{x}_R(\lambda) T(\lambda) S_R(\lambda, I, p) d\lambda, \quad (2.1)$$

$$\tilde{Y}_R = \int_{\lambda} \tilde{y}_G(\lambda) T(\lambda) S_R(\lambda, I, p) d\lambda, \quad (2.2)$$

$$\tilde{Z}_R = \int_{\lambda} \tilde{z}_B(\lambda) T(\lambda) S_R(\lambda, I, p) d\lambda. \quad (2.3)$$

The LC-panel transmission,  $T(\lambda)$ , depends on the drive levels and the colour filters. However, for calibration of the backlight uniformity,  $T(\lambda)$  can be neglected. Similar, we have neglected the slight wavelength shift of LEDs with elevated temperatures (Harbers, Bierhuizen, and Krames, 2007).

For simplicity it is assumed that the spectra of all LEDs of a particular colour are identical. As the backlight is constructed from LEDs which have been



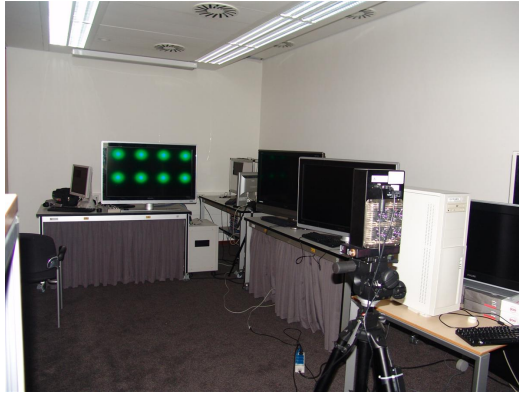


**Figure 2.11:** Photograph of the display calibration setup. The imaging colourimeter can be seen in the front, while the display, with 8 green LEDs turned on, is located at the back of the room.

factory-measured (binned) to be within a 10 nm range, this is a reasonable assumption (see Table 2.2). Furthermore, the narrow spectra of the red LEDs and the location of the peak wavelength means that  $\tilde{X}_R \gg \{\tilde{Y}_R, \tilde{Z}_R\}$ . Under the assumption that the spectra of all red LEDs are identical, it is therefore possible to only measure and calibrate  $\tilde{X}_R$  in order to achieve a uniform backlight. Following the same reasoning for the green and blue LEDs, it is only necessary to measure and calibrate  $\tilde{Y}_G$  and  $\tilde{Z}_B$ , respectively.

The calibration values are conveyed to the backlight unit by means of the amplitude modulation signal which leaves the full range of pulse-width modulation to signal processing purposes. However, LEDs do not exhibit a linear relationship between current and intensity (Philips, 2009). To that end it is assumed that  $S_R(\lambda, I, p) \approx S_R(\lambda)f(I)p$ , where  $f(I)$  is a characterisation of LED current versus intensity. This curve can be characterised by measuring the response from an LED. Based on an initial current and a desired linear correction coefficient, an inverse lookup can be used to determine the calibrated current.

The post-measurement processing is done in a number of steps targeting to achieve a uniform backlight. Obtain the measured intensities (image) of a segment, for example measured  $\tilde{X}_R$  for a red LED. Apply a low-pass filter of small-support (about 3-4 mm) and extract the intensity at the centre of the profile, which is known a priori<sup>1</sup>. The result is a per-LED scalar representing the measured (averaged) intensity per segment. Determine the desired intensity, say the median of the intensities of the red LEDs, and compute the needed relative adjustments. Using an inverse-lookup in the current vs. intensity characteristic,  $f^{-1}(I)$ , the new current level can be computed.

<sup>1</sup>A geometric calibration relating each image pixel coordinate in the measurement to the coordinates of the display had been carried out using a projective transformation.

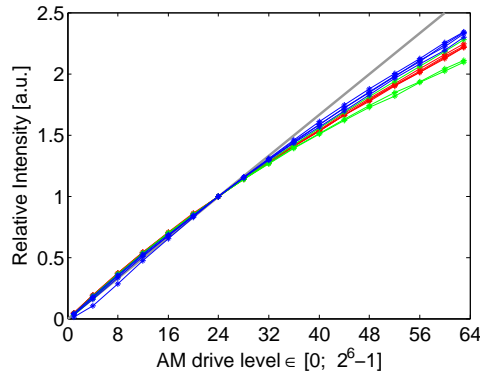


**Figure 2.12:** Luminous flux as a function of current (amplitude modulation) for 4 red, green, and blue LEDs. Up to level 28, the intensity is seen to be approximately linear.

In order to verify the result, a second set of measurements can be carried out using the measurement procedure. It was found that two measurements and a verification step was necessary in order to obtain satisfactory results.

The strong optical separation of the backlight segments can be exploited to speed up the measurement process. It was verified, that segments separated by more than 4 segments, had an inter-segment cross-talk level below 1 promille. This error is considered acceptable and a pattern based on this criterion can contain up to 8 segments reducing the time of measurement by a factor eight. In Figure 2.11, the calibration setup can be seen with the backlight having eight green LEDs on.

The imaging colourimeter was a Radiant Imaging ProMetric, type 1423E-1 with a resolution of 1024 by 768. This device comes with an interactive software package for device adjustments and control. For the large amount of regular measurements, it was chosen to design an automated procedure based on the proprietary software API. The fully-automated procedure would iteratively adjust the backlight and capture and store a measurement.

2.3.2 Results

In order to apply the calibration to the amplitude modulation, it was necessary to characterise the current vs. intensity relation. In Figure 2.12, the response for 4 LEDs is shown. The curve was measured at 17 of the 64 intensity steps (6 bit signal). Notice that the curves have been normalised at level 24, which corresponds to the initial current level for all colours. This also allows comparison between the characteristic curves. Up to level 28, the curve is approximately linear, for higher levels the intensity increases less with increased current. Good consistency for the blue and red LEDs can be observed, whereas curves for the green

LED are less consistent. The larger absolute current of the green LED may explain this behaviour. A per-colour average of these curves was successfully used to do inverse-lookup for the colour uniformity correction.

Three measurement iterations were carried out. Two for calibration and a last one for verification. In Figure 2.13, the results of the first measurement procedure (before any calibration) and the verification procedure are shown. Each segment is represented by a pixel and the intensity is normalised to the average. In the left column, the initial measurement results are shown, whereas in the right column the results of the verification measurements are shown. From top to bottom, the figures correspond to the red, green, and blue LEDs.

In Figure 2.13(a) and Figure 2.13(c), the measurement of red and green can be seen. The data is dominated by a low-frequency pattern showing peak intensity in the centre and a fall-off towards the edges. In comparison, the result of the blue LEDs seen in Figure 2.13(e), shows significantly larger variations. Blocks of LEDs are significantly brighter than their surroundings. Besides this, a similar low-frequency pattern can be observed. The bright blocks corresponds to  $5 \times 5$  LEDs on the same LED tile. It was speculated that either two LED wavelength bins had been used (rather than one) or the LEDs were of different efficacy bins. By inspection it was verified that the LEDs had similar spectra and the variation was assumed to be caused by differences in efficacy.

In the second column of Figure 2.13 showing the resulting uniformity, the red and green uniformity are seen to be within a variation of 10%. The uniformity of the blue LEDs is comparable, although 5 LEDs were left with a variation above 10%. Due to optical mixing this is not visible when all segments are turned on. The resulting full-white uniformity was judged visibly imperceptible by a group of expert viewers.

A histogram of the data of Figure 2.13 is shown in Figure 2.14. The large variation in intensity of the blue LEDs before calibration is clear from Figure 2.14(c). The bin-size of the histogram is 2.5% relative intensity. With the exception of a few outliers for the blue LEDs, all LEDs have been calibrated to within a 10% range. The standard deviation of the intensity relative average before and after calibration was 7.8% and 0.9% for red, 9.1% and 1.5% for green, and 22.6% and 2.1% for blue, respectively.

The final result can be seen in Figure 2.15 showing the display before and after calibration. The regions with a low contribution from the blue LEDs can readily be seen in Figure 2.15(a). It was judged by expert viewers that the resulting calibration state seen in Figure 2.15(b) was sufficiently uniform to be suitable for demos

The automated procedure resulted in fast and robust calibration results. It was estimated, that manual measurement of all LEDs would take about three days of

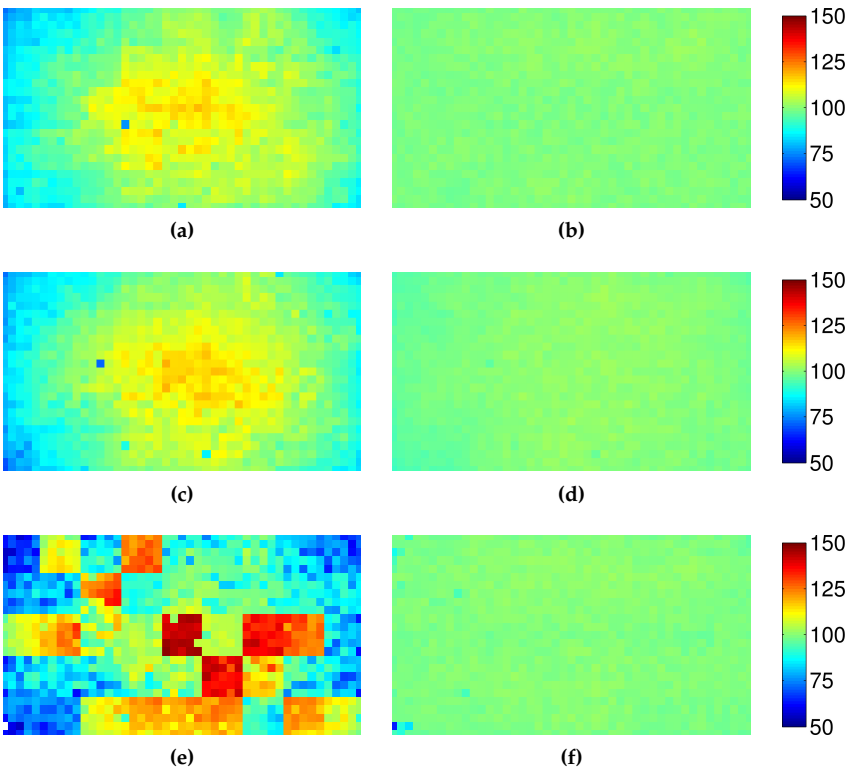


**Figure 2.13:** Measurement results of relative intensity of red, green, and blue LEDs (top-to-bottom). In the left column the initial un-calibrated state is shown, whereas the right column shows the calibrated state. In 2.13(a) and 2.13(c), the high-frequency noise was slightly visible. In 2.13(e), the strong intra-tile variation was visibly very annoying. By utilising the AM range, a calibration was achieved which was judged visibly imperceptible by expert viewers. In this result, 5 blue LED outliers were left with a per-segment variation above 10%. Due to optical mixing this was not visible when all segments were turned on (full white).

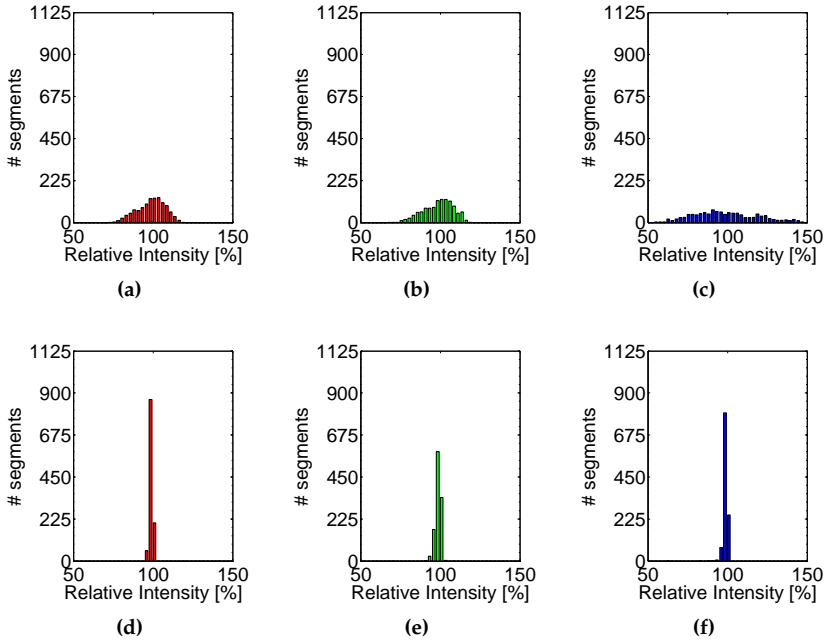


**Figure 2.14:** Histogram of the measured red, green, and blue LEDs before calibration is seen in the top row. The corresponding histograms after calibration is seen in the bottom row. The large variation in blue-LED intensity can be observed in ((c)). The standard deviation before and after was (7.8%, 0.9%), (9.1%, 1.5%), and (22.6%, 2.1%), respectively.

work, excluding the time needed to initially setup the measurement equipment. The automated measurement approach could do the task in half a day and when measuring up to 8 segments per measurement the total measurement time was reduced to less than an hour. In the end, the entire calibration procedure, including setting up the system, carrying out the measurements and post-measurement processing steps, takes about one day.

## 2.4 Characterisation of Segment Point-Spread Function

Careful characterisation of the locally addressable backlight segments is necessary in order to make use of the modulating properties of the backlight. The light from a single backlight segment is engineered to emit light to neighbouring segments in order to provide acceptable uniformity. Consequently it is necessary to take these light contributions into account when modulating the backlight segments.



**Figure 2.15:** Photograph of the HDR display before, (a), and, (b) calibration. Note that the white-point correction of the camera has caused the yellowish background due the blueish white point of the HDR display.

For a LC-display with  $N$  addressable backlight segments, the light level illuminating the  $i$ -th pixels can be described by:

$$L_i = \sum_{j=0}^{N-1} d_j h_{i,j} , \quad (2.4)$$

where  $0 \leq d_j \leq 1$  is the backlight drive level of the  $j$ -th backlight segment and  $h_{i,j}$  the contribution of the  $j$ -th segment on the  $i$ -th pixel. In the above equation, the light level at a particular pixel,  $L_i$ , is described by the combined contributions from all backlight segments. Considering all contributions from a single segment to all pixels is called the point-spread function (PSF) and is comparable to an image of the backlight segment.

The shape and width of the PSF depends on the optical design of the backlight unit. It is likely the most critical parameter in accurate rendering of images on a spatially-modulated HDR LCD (Trentacoste *et al.*, 2007). In this section we therefore describe the procedure for measurement of the PSF of our HDR backlight unit.

### 2.4.1 Methods

In order to measure the optical profile of a backlight segment, it is necessary to make use of a flat-field calibrated image sensor. Such a sensor is calibrated for any geometric and intensity distortions, such that an intensity variation in the measurement can be directly related to a variation of the backlight intensity. An imaging colourimeter, which comprises a high-quality image sensor and a colour-filter wheel, can be supplied with such a flat-field calibration. For our

measurements we made use of a Radiant Imaging Prometric, type 1423E-1 imaging colourimeter.

Despite the actively cooled image sensors, the dynamic range was found limited to capture the intensity variations from the bright centre to the dark tails of a segment profile. The capture was therefore split in two exposures. A first exposure would capture the bright details, whereas a second longer exposure would capture the details in the tails. Consistently with established methods, the two exposures could be merged in post-processing to obtain a single PSF.

Bright objects may reduce the image quality of nearby features due to lens flare. Consequently, the measurement of the second exposure would be polluted by light from the brightest regions of the image. This would be unacceptable. It was found that the modulating properties of the LCD panel could be utilised to reduce the intensity of the centre region of the segment profile. In the second longer exposure, a square region of low LC-panel transmittance was created by setting the drive levels to 0, while the remainder of the LC-panel was at maximum transmittance.

In an early stage, it was established that the profile for a red, green, and blue LED was identical. The following measurement steps were therefore carried out for each backlight segment:

1. Turn on all LEDs (red, green, and blue) of a single backlight segment.
2. Record the position of this segment.
3. Leave the LC-panel in full transmission mode, i.e. a white image.
4. Measure the spatial profile with a short exposure (depends on lens, distance, neutral-density filter, etc.).
5. Reduce transmittance of the LC-panel in a small square region directly above the segment in question in order to block the bright peak directly above the LED.
6. Measure the spatial profile with a long exposure time (to accurately measure the segment profile tails).
7. Carry out steps 1-6 for all segment positions.

In the measurement (step 4), a fixed exposure of 1 s and no neutral-density filter was used for the short exposure.

In order to acquire the segment profiles consistently, it was necessary to have the entire display in the field of view. The camera was therefore positioned about three meters from the display, as we did not have access to a calibrated wide-angle lens. Furthermore, a geometric calibration was carried out. This was

done by recording an image with fiduciaries of known locations and determining the projective transformation that would relate display coordinates to camera coordinates.

## 2.4.2 Results

All backlight segments were measured and the two exposures merged to obtain one PSF per segment. The geometric calibration made it possible to accurately crop the measured region to the correct size. Considering the low-frequency nature of the PSFs, the measurements were transformed and re-sampled at a resolution of  $480 \times 270$  pixels, i.e. one-fourth of full-HD resolution.

In Figure 2.16(a), the PSF of a centre segment is shown. The PSF is seen to consist of a small bright spot, with short tails and a large almost-black region. Whereas the centre of the segment appears squared, the tails appear circular symmetric. In Figure 2.16(b) the combined result of all segments turned on (full-white) is shown. This result is based on the individually measured PSFs and was verified with the actual display. The variation at full-white (uniformity) was about 2.7%. The reader is referred to a digital copy of the thesis to appreciate the data of Figure 2.16(a) and Figure 2.16(b).

A horizontal cross-cut of the PSFs of three centrally positioned segments is shown in Figure 2.16(c). Above the PSFs, the segment pitch is indicated by crosses. At the intersection of the segments, the PSF is at 70% of the peak intensity. This does, however, not warrant good optical separation. The contribution of one PSF to the combined output of all PSFs (full-white) is only about 25%. Therefore, small image features will be significantly darker than large image features when spatial modulating is applied. We will return to this in Section 2.6.2.

## 2.4.3 Analytical Approximation of PSF

Measurements of the PSF typically contain noise and some form of noise reduction is often applied. The most simple approach is a low-pass filter kernel of small support applied to the data. However, the risk of changing the PSF is high. A better approach is to approximate the data by fitting an analytical function. An advantage of this approach is the possibility to evaluate the analytical function, rather than reading large amounts of data into memory. Existing systems have successfully been modelled using a weighted set of Gaussians (Trentacoste *et al.*, 2007; Seetzen, Heidrich, *et al.*, 2004). A third option is a filter pyramid, where filtering with a small-sized kernel followed by upsampling is applied iteratively. If the filter coefficients of the small-sized kernel and the coefficients of the upsampling step are optimised to the measured PSF, it creates a good balance between memory and computational load (Liao and Huang, 2010).



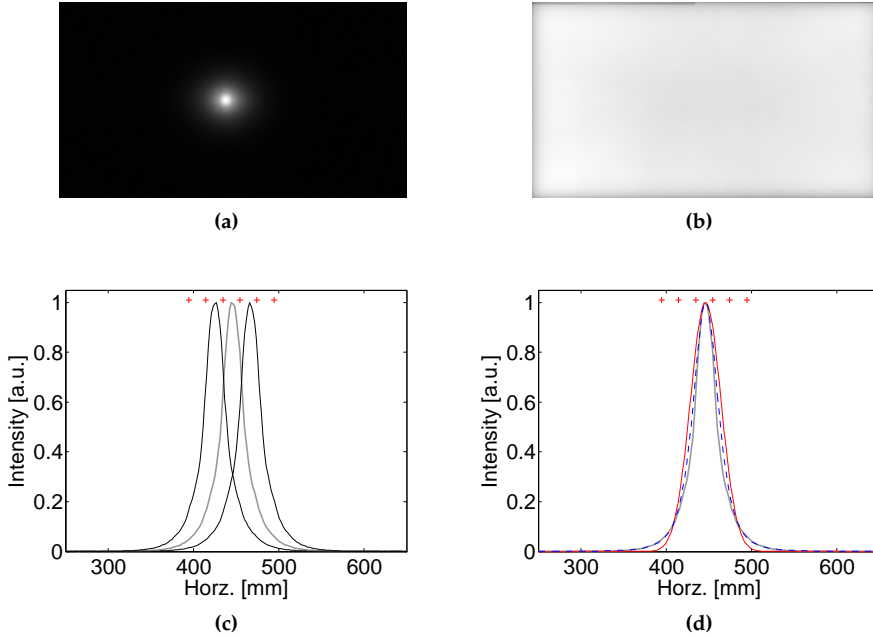


**Figure 2.16:** In (a), the measured unfiltered point-spread function of a single centrally-located segment. When all LEDs are on, a small imperceptible ripple is present, as illustrated in (b) - data scaled to make ripple visible. A 1D-plot of three adjacent segments is shown in (c), while in (d) a single profile is compared to a synthetic Gaussian (solid-red) and Quadratic Lorentzian profile (dashed-blue).

In Figure 2.16(d), the PSF of the display system is compared to two common mathematical descriptions of PSFs; 1) a Gaussian function, and 2) a Quadratic Lorentzian function. For the comparison, the width of the functions were optimised using the  $25 \times 45$  segment layout and ensuring a full-white uniformity of about 1%. The Gaussian function (solid-red) is seen to have slightly wider slopes at the centre and very steep tails tapering faster than the measured PSF. The Quadratic Lorentzian function (dashed-blue) is seen to match the slope better than the Gaussian function. The tails of the measured PSF are also seen to match well. However, when carefully evaluated, neither of the functions approximate the PSF sufficiently.

A poor approximation may lead to visible artefacts. The predicted light level falling onto the LC-panel is compensated in order to create the desired intensity. Consequently any mismatch between the predicted and actual backlight intensity may lead to visible artefacts. For example, a uniform gray box on a white surround may show visible shadows close to the boundary of the intensity transition.

In the following section, an optimisation procedure is introduced which was used to approximate the PSFs. Besides the procedure, the analytical functions tested are also presented.

## Methods

The problem of obtaining an approximation of the PSF of the  $j$ -th segment,  $q_j(i)$ , by means of a sum of analytical expressions,  $p_k(i)$ , can be defined as:

$$\underset{\mathbf{p}}{\operatorname{argmin}} \left\| \sum_k p_k(i) - q_j(i) \right\|^2, \quad (2.5)$$

where  $\mathbf{p}$  is a stacked vector of parameters for the candidate functions,  $p_k(i)$ . This problem can be solved by means of a numerical non-linear solver.

Rather than obtaining individual approximations for each PSF, the procedure is used to obtain an approximation of a centre segment. When the approximation is sufficiently accurate, these parameters are used to determine the error for all PSFs.

A good approximation is not the only important objective, it is also important to ensure a uniform result. To that end, it is possible to apply a regularisation penalty to the optimisation problem of (2.5). Let the desired level of uniformity be given by  $u_{\text{tgt}}$ , then the penalty could be defined by:

$$w = \frac{u}{u_{\text{tgt}}}, \quad (2.6)$$

where  $u$  is the uniformity of the current approximation. The penalty,  $w$ , was simply multiplied to the error vector of (2.5).

In practise it proved necessary to use three functions (2.5) to approximate the measured PSF. All three functions were Gaussian functions. The uniformity of the approximation was close to 1%. Only approximations in linear light were performed.

## Candidate Functions for Modelling the PSF

In Figure 2.17 a sketch of the tested candidate functions is shown. As can be seen, some profiles are smooth and rather flat in the centre, while others have a rather fast fall-off farther away from the centre. Visual inspection of the measured PSF, shown in Figure 2.16, does not directly reveal which function is a good candidate.

The first function described is the Gaussian:

$$p_g(x, y, \sigma_x, \sigma_y) = g \exp \left\{ -\frac{1}{2} \left( \left( \frac{x}{\sigma_x} \right)^2 + \left( \frac{y}{\sigma_y} \right)^2 \right) \right\}, \quad (2.7)$$

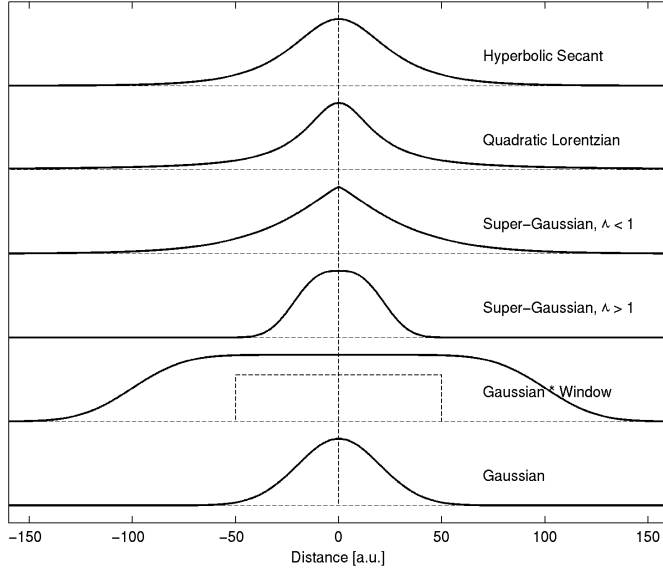


**Figure 2.17:** Example of candidate functions for the analytical approximation of the back-light PSF. Notice how one profile is rather flat, while another has a steeper fall-off. From the sketch above it is rather difficult to decide which function forms the best basis.

where  $g$  is the overall gain, and the parameters  $\sigma_x$  and  $\sigma_y$  are spatial scaling parameters. Its short tails (very close to zero) make it difficult to realise a Gaussian PSF in practice. An alternative function is the super-Gaussian function:

$$p_{sg}(x, y, \sigma_x, \sigma_y, \lambda_x, \lambda_y) = g \exp \left\{ -\frac{1}{2} \left( \left( \frac{x}{\sigma_x} \right)^{\lambda_x} + \left( \frac{y}{\sigma_y} \right)^{\lambda_y} \right) \right\}, \quad (2.8)$$

Where the power of two functions in the Gaussian distribution are variables of  $x$  and  $y$ . Another often-used function is the Quadratic Lorentzian distribution which is wider than the Gaussian function.

$$p_{ql}(x, y, \sigma_x, \sigma_y) = \frac{g}{1 + \left( \frac{x}{\sigma_x} \right)^2 + \left( \frac{y}{\sigma_y} \right)^2}, \quad (2.9)$$

where  $g$  is the overall gain, and the parameters  $\sigma_x$  and  $\sigma_y$  are spatial scaling parameters. The quadratic Lorentzian is a description of a Lambertian diffuser, and so, this function is a good candidate for backlights based on the principles of mixing-in-air. For the HDR backlight the tails of the approximation showed to be too large compared to the PSF of the display. Yet another candidate is the hyperbolic secant.

$$p_{hs}(x, y) = g \operatorname{sech} \left\{ \left( \frac{x}{\sigma_x} \right)^2 + \left( \frac{y}{\sigma_y} \right)^2 \right\}, \quad (2.10)$$

where  $g$  is the overall gain, and the parameters  $\sigma_x$  and  $\sigma_y$  are spatial scaling parameters. This also did not turn out to be a good fit. We noticed that the super-Gaussian profiles were sometimes optimised with a power-function larger than two and decided to include a very flat candidate function. The following function describes the convolution between a Gaussian function and a window function.

$$p_{gw}(x, y, \sigma_x, \sigma_y, b_x, b_y) = g g_N \left\{ -\operatorname{erf} \left( \frac{x - b_x}{\sqrt{2}\sigma_x} \right) + \operatorname{erf} \left( \frac{x + b_x}{\sqrt{2}\sigma_x} \right) \right\} \left\{ -\operatorname{erf} \left( \frac{y - b_y}{\sqrt{2}\sigma_y} \right) + \operatorname{erf} \left( \frac{y + b_y}{\sqrt{2}\sigma_y} \right) \right\} \quad (2.11)$$

where

$$g_N = \frac{1}{4 \operatorname{erf} \left( \frac{b_x}{\sqrt{2}\sigma_x} \right) \operatorname{erf} \left( \frac{b_y}{\sqrt{2}\sigma_y} \right)}. \quad (2.12)$$

The offset parameters  $b_x$  and  $b_y$  define the half-width of the window function, while  $g$  is the overall gain, and the parameters  $\sigma_x$  and  $\sigma_y$  are spatial scaling parameters. As can be seen in Figure 2.17, this function can represent large flat surfaces while maintaining smooth tails.

## Results

It was expected that at least two analytical functions should be used to approximate the measured PSFs. One narrow profile to describe the local shape and one wider profile for the contributions farther away toward the display edge. Based on (2.5) with the PSF in linear light, a non-linear optimisation technique was applied. Approximations using one, two, or three functions were tested. In practise it proved necessary to use three Gaussian functions to approximate the measured spatial segment profile. Visual inspection on the prototype showed, that images generated using the result of this fit were indistinguishable from images generated using the original measurements directly. Due to the well-defined edges of the PSFs, it was necessary to control the overall uniformity in order to prevent introduction of visible noise at a frequency matching the pitch of the segments. To that end, the weighing of (2.6) was necessary in order to achieve 1% uniformity.

## 2.5 Display Applications and Summary of Performance

In this section, the display demonstrator is presented. For different applications, the HDR backlight was equipped with several different LC-panels over the time. The performance in terms of peak luminance and colour gamut is compared for a number of different configurations.

### 2.5.1 Display demonstrator

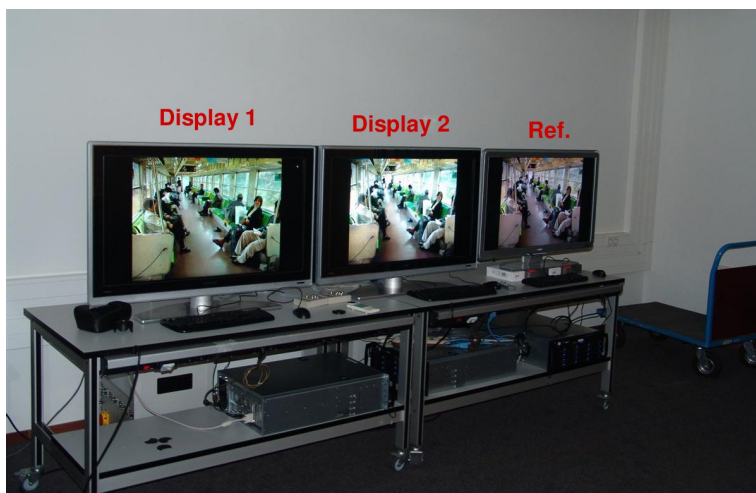


**Figure 2.18:** Line up of the two 42 inch HDR displays (leftmost) together with a reference Philips TV set (rightmost). The three large PCs at the shelf below are used for uncompressed video playback. In this photograph, both HDR displays are mounted with a commercially available 42 inch LC-panel. The power boxes can barely be seen behind the tables. The centre HDR display is bright, while the luminance of the right HDR display was adjusted to the luminance of the reference display.

In Figure 2.18, a photograph of the two HDR displays (left and middle) in a line-up with a reference Philips TV set (right) is shown. The reference display was 40 inch whereas the HDR displays were both 42 inch. The LC-panels mounted on the HDR backlight were different, one being an IPS-mode panel and the other an VA-mode panel. In the photographed setup, the centre HDR display was bright, while the luminance of left HDR display was adjusted to the luminance of the reference display. Below the table, three large PCs can be seen. These custom-built systems provide uncompressed playback of video using hard drives providing very high bandwidth. As the backlight amplitude and pulse-width modulation signals are embedded in the video signal, uncompressed video is necessary. In

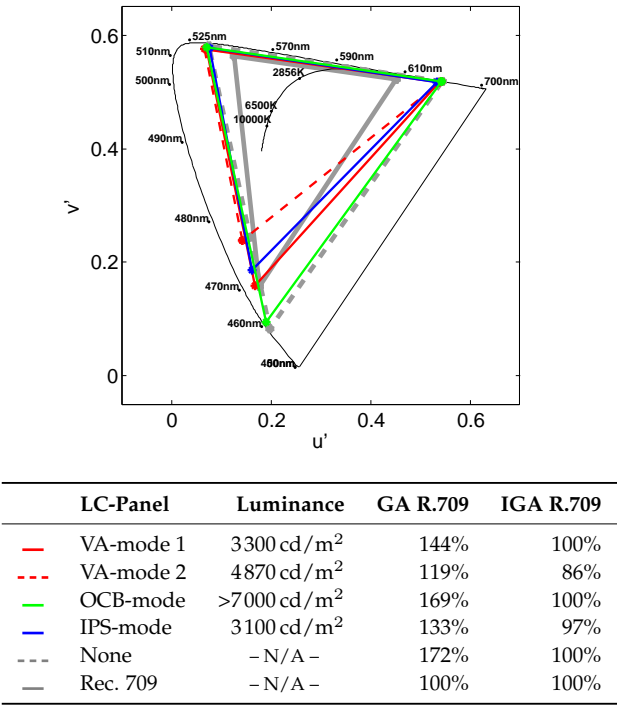


**Figure 2.19:** Specifications for different HDR display configurations using five different LC-panels (tabulated right). In the 1976 CIE  $u'v'$  chromaticity diagram, the primaries of the combinations of LC-panel and backlight is shown. In the table the peak luminance is shown. Besides four LC-panels, the backlight unit without LC-panel (“none”) and a reference gamut “Rec. 709” is also shown.

the photograph, the two power boxes with water cooling are just visible behind the table.

2.5.2 Performance

For different applications, the HDR backlight was equipped with several different LC-panels over the time. The initial configuration was based on conventional LC-panels with VA-mode and IPS-mode. A fast-switching OCB-mode LC-panel replaced the IPS-mode LC-panel in order to facilitate research on colour-sequential operation. In 2010, the VA-mode LC-panel was replaced by a state-of-the-art VA-mode LC-panel. A number of less notable configurations has also existed for a period of time.

In Figure 2.19, the colour gamut and peak luminance of four different configurations and the bare backlight (no LC-panel) is shown. The initial configuration consisted of *VA-mode 1* and *IPS mode* with a peak luminance slightly

above  $3000 \text{ cd/m}^2$ . The improved *VA-mode 2* resulted in a peak luminance of  $4870 \text{ cd/m}^2$ . The *OCB-mode LC-panel*, which does not have any colour filters, resulted in a much higher peak luminance of more than  $7000 \text{ cd/m}^2$ .

In Figure 2.19, the colour gamut spanned by the different display configurations is shown expressed in CIE 1976  $u'v'$  chromaticity coordinates. The area of each triangle compared to the area of a reference gamut (ITU Rec. 709) is reported in the table as *GA R.709* (gamut area). As a larger gamut does not warrant that all colours in the reference gamut can be reproduced, the area of the triangle intersection with the reference triangle is also reported as *IGA R.709* (intersection gamut area).

The colour gamut spanned by the bare backlight (LEDs only; shown in grey-dashed) is extremely wide and encompasses the Rec. 709 (grey-solid). The *VA-mode 1* configuration is seen to reduce the gamut, in particular the saturation of the blue primary is reduced. This is likely caused by the spectral cross-talk between the green LED and the blue-colour filter. Despite this, the colour gamut was 144% (*GA R.709*) and covered the entire Rec. 709 gamut. The colour gamut for the *IPS-mode* configuration and the *VA-mode 2* configuration resulted in a reduction of colour gamut. For the latter, the colour gamut was very limited for bluish-colours and covered only 86% of the Rec. 709 gamut (*IGA R.709*). Measurements on the spectral cross-talk between the LEDs and the colour filters revealed that a wide transmission band of the blue colour filter was the cause of the reduction in gamut area. The increased transmission of green may also explain the increased peak luminance. Finally, notice how the colour-filter less *OCB-mode LC-panel* has no significant reduction of colour gamut compared to LEDs only (169% compared to 172% *GA R.709*).

The maximim corner-box contrast ratio (ICDM, 2012) of the display system was close to 10 million to 1. In Section 2.6.4 this will be treated in detail with a comparative study on contrast and luminance in relation to other HDR display technologies.

## 2.6 Model-Based and Metrology-Based Evaluation of Contrast and Luminance

During the design of the HDR display, a number of computational models were used in order to evaluate the front-of-screen performance in terms of contrast. Light generated by a backlight segment should be spatially confined in order to maximise modulation depth, i.e. contrast increase. Full-white uniformity may suffer from this requirement, however, due to segment-to-segment variations in light and colour. Therefore, the backlight segments were designed to have an optimum in spatial confinement and uniformity.

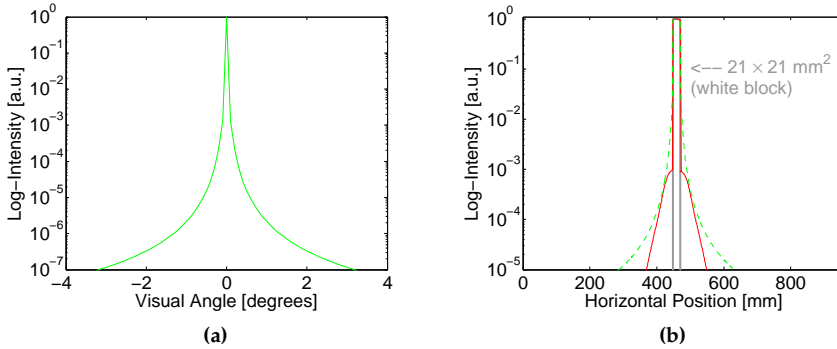


**Figure 2.20:** In 2.20(a) the point-spread function of human-eye glare. In 2.20(b) and ideal HDR display (solid-gray), the retinal luminance of the ideal HDR display by considering human-eye glare (green-dashed), and the HDR backlight response (red-solid). The image stimuli was a white block of 21 mm by 21 mm.

## 2.6.1 Human-Eye Glare and Visibility of Backlight Halos

The presence of bright objects may reduce detail perception near high contrast boundaries. When a backlight segment is at maximum intensity due to a small white image feature, the light may leak to surrounding dark image regions. These backlight halos are particularly annoying as they do not correlate with the image content. Secondly, image motion may cause apparently random halo flicker. On the other hand, the visibility of backlight halos may be masked by intra-ocular glare causing an increase of retinal luminance near bright objects. The human-eye glare can be described by a point-spread function. The PSF described by Vos and van den Berg (1999) is shown in Figure 2.20(a).

The PSF can be used to estimate the increase in retinal luminance, similar to the study described in Chapter 6. A small white block on a black background was used as test image. The white block was 21 mm by 21 mm, i.e. the same size as a backlight segment, and phase-aligned with the backlight segment. We assumed a viewing distance of 3 times the screen height (42 inch). The display luminance was converted to a retinal image (expressed in visual angle) by assuming that the flat-field emitter (the display) could be represented by a curved-emitter (at constant distance from the human observer). This assumption was in practise irrelevant, as only a small-centre part of the display emitted significant amounts of light. By convolving the PSF of Figure 2.20(a) with the retinal image, shown in grey-solid in Figure 2.20(b), the resulting retinal luminance could be obtained (green-dashed). This retinal image of an ideal HDR display may be compared with the reproduced retinal image from the HDR display (red-solid). It can be seen that the backlight halo is masked by the glare. This result has been confirmed for a similar design (Seetzen, Heidrich, *et al.*, 2004). We have for this ex-



periment assumed a modest 1000:1 contrast ratio of the LC-panel. In practise the contrast ratio of state-of-the-art LC-panels is higher making the backlight halos even smaller.

When the white block is increased in size, the retinal luminance will increase significantly, however, this also holds for the backlight halo due to the increased amount of backlight segments needed in order to illuminate the white-image region. Moreover, when the white-image region is reduced in size, the retinal luminance will reduce revealing the backlight halo. In conclusion, the backlight design of the HDR display will make the halos imperceptible for most natural images. Only images with small, bright image features on a black background, such as a starlight sky, will result in visible halos.

## 2.6.2 Direct Contribution

Whereas the light profile of a backlight segment should be confined in order to avoid visibility of halos, it is advantageous to include sufficient amounts of segment-to-segment light mixing in order to mask variations in light intensity and colour. Spatially smooth segment profiles can ensure significant light mixing. However, when the spatial extent of light from a backlight segment becomes large, insufficient amounts of light will be generated locally. Consequently many neighbouring segments are needed in order to achieve a sufficient light output.

We found the direct contribution, the light contribution of a particular backlight segment to the full white situation, a useful measure. This can easily be established by turning on a centre segment, measure the luminance right above this segment, then turn on all segments and measure the luminance at the same location. The ratio of the numbers is the direct contribution. In our experience, direct contribution is between 20% and 40% in most designs.

Direct contribution is, however, a poor measure of the shape and spatial extent of the light profile from a backlight segment. We therefore found it useful to plot the relative intensity measured right above a particular segment and sequentially turn on the neighbouring segments in a radial pattern. In this way, the contribution of close-by and far-away segments can be distinguished. Although the direct contribution is often only 20%-40%, the relative intensity of a good design should increase close to 100% using only the neighbouring segments.

In Figure 2.21, the light intensity right above a centre segment ( $n$  segments on) relative to a full-white image (all segments on) is plotted against the distance to the centre segment. Besides the measured data from our HDR display (black-solid line), the following backlight division have been simulated:  $16 \times 9$  (144),  $32 \times 18$  (576),  $24 \times 44$  (1056), and  $64 \times 36$  (2304). These simulations were based on a quadratic Lorentzian segment profile. With more backlight segments, a particular relative light intensity can be reached using a smaller backlight area. For

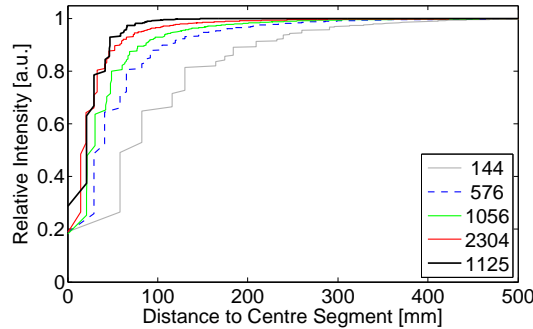


**Figure 2.21:** The light intensity relative to a full-white image right above a centre segment as a function of the amount of segments turned on (expressed in distance). Four virtual backlights based on a quadratic-Lorentzian segment profile with  $16 \times 9$  (144),  $32 \times 18$  (576),  $24 \times 44$  (1056),  $64 \times 36$  (2304), and  $25 \times 45$  (1125) backlight segments (the latter is our HDR display design) are shown. With more backlight segments, it is possible to achieve a desired intensity, say 80%, using only neighbouring segments. Consequently, such designs may exhibit a smaller, more narrow halo. Our HDR display is seen to perform equal to a display with twice the number of segments.

example, 80% relative intensity can be achieved at 60 mm distance with 1056 segments, while with 144 segments 130 mm is necessary. Consequently the halos for the latter system may be more visible. Comparing our HDR display to a display with quadratic Lorentzian backlight profiles and 1056 segments, it can be seen that a significantly smaller area of backlight segments is necessary in order to achieve a particular intensity. In fact, our design is comparable to the system with 2304 Quadratic Lorentzian segments, which has twice as many segments as our system.

2.6.3 Contrast Gain of Sinusoidal Patterns

Whereas direct contribution and Figure 2.21 are instrumental in designing a backlight, it is not easy to translate the results into expected performance for natural images. Therefore, it has been proposed to take a signal processing approach. Simulating the resulting backlight modulation as follows from a set of horizontally-oriented sinusoidal patterns (Langendijk, Muijs, and Beek, 2008).

In Figure 2.22(a), a cross-cut of the simulated backlight response to a horizontally-oriented sinusoid of 6 cycles-per-screen width is shown. Similar to the previous study on direct contribution, the following backlight division has been included:  $16 \times 9$  (144),  $32 \times 18$  (576),  $24 \times 44$  (1056), and  $64 \times 36$  (2304). The backlight profiles were described by a quadratic Lorentzian profile. The input sinusoid is shown in gray (ranging from 0 to 1). The modulation depth with 144 backlight segments can be seen to be very poor, whereas 1056 segments allows close

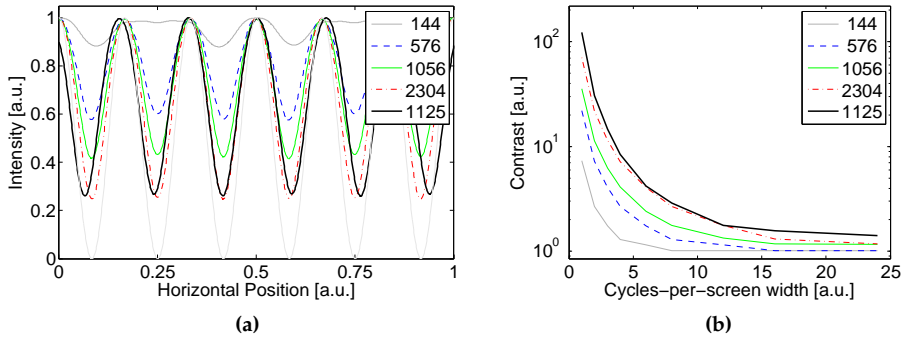


**Figure 2.22:** In 2.22(a), the reproduced backlight profile in response to a sinusoidal input (light-grey) is shown. The more backlight segments, the better the sinusoid can be reproduced, and the larger the contrast improvement. In 2.22(b) the modulation depth (contrast) as function of cycles-per-screen width is shown. Notice that our HDR display performs comparable to a display system with twice as many backlight segments (2304) up to 12 cycles-per-screen width. Moreover, for higher frequencies, our HDR display outperforms this system. The applied method was presented in (Langendijk, Muijs, and Beek, 2008).

to a factor 2.5 in contrast. Our HDR display with 1125 segments performs equal to the simulated system with 2304 segments when we compare the modulation depth. We further observe a slight phase offset for the HDR display for this sinusoidal test pattern. For natural images, however, this is unlikely to give rise to visibly-annoying halo artefacts.

In Figure 2.22(b), the modulation depth (contrast) of a sinusoidal reproduction is plotted against the cycles-per-screen width. As shown in Figure 2.22(a), the contrast of the HDR display is comparable to the contrast of the simulated system with 2304 segments for 6 cycles-per-screen width. The results shown in Figure 2.22(b) further show that the contrast of the HDR display is comparable or higher for all reproductions from 1 to 24 cycles-per-screen width.

## 2.6.4 Metrology-Based Evaluation of Contrast and Luminance

It is frequently necessary to compare the contrast and luminance characteristics of a set of HDR displays. This can be done without knowledge of display-technology specific operational principles in an unobtrusive way by using a spot photometer (or colourimeter).

Classically, a black and a white image is used to characterise the maximum and minimum luminance level. The ratio of these is the contrast definition. However, despite a finite display contrast ratio, this may lead to reporting of infinite contrast ratios suggesting that the display can show natural images with a high contrast (ICDM, 2012). For example, in an LCD with global backlight modulation,

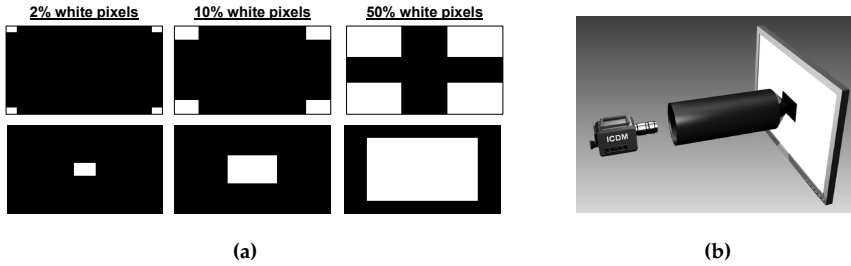


**Figure 2.23:** In (a), an illustration of the corner-box stimuli. The luminance of the screen centre is measured by a spot photometer for, 1) the black target in the upper row, and 2) the white target in the bottom row. From left to right 2%, 10%, and 50% white pixels are set to full white. In (b), the spot photometer is seen located perpendicular to the screen and covered by a frustum to prevent stray light entering the lens. Illustration in (b) is reproduced from (ICDM, 2012).

the backlight LEDs will turn off for the black image resulting in no measurable light and consequently infinite contrast ratio.

As sequential measurements of luminance and contrast can lead to deceptive results, a checkerboard of white and black (ANSI contrast pattern) is often used. The presence of white checkers avoids the problem of zero-luminance black. The method is generally also better in predicting the maximum contrast in natural images rendered on the display. However, spatially-modulated LCDs are known to exhibit increased black luminance in the vicinity of bright regions, and OLEDs are known to show reduced white luminance when the average pixel value increases. For these situations, the checkerboard contrast pattern is not very suitable. Although the number of checkers can be adjusted, this does not provide sufficient control over the distance between white and black pixels. Secondly, the checkerboard pattern has 50% white and 50% black pixels by design, such that the average pixel value does not change.

In the following section we describe the corner-box contrast stimuli (ICDM, 2012) and apply this measure to 5 different display systems.

## Methods

Both peak luminance and contrast are important characteristics of an HDR display and both characteristics can be captured by using the corner-box contrast stimuli (ICDM, 2012). Furthermore, the measurement method can reveal if display peak luminance and/or contrast depend on the spatial composition of an input image.

The corner-box contrast measurement consists of black and white stimuli pairs. Each pair has a fixed amount of white pixels, either located in the centre, or loc-

**Table 2.3:** Five displays (products and prototypes) that have been measured using the corner-box contrast method. Display 1 and 2 are regular desktop monitors, display 3 is a professional studio monitor, while display 4 and 5 are HDR display prototypes.

	Display Type	Model	Screen Diag.
1	CRT Monitor	iiyama HM 204DT A	20 inch
2	LCD Monitor	Philips 190P	19 inch
3	OLED Monitor	SONY PVM-2541	25 inch
4	HDR Philips	LED-illum. LCD, Philips	42 inch
5	HDR Bangor	Proj.-illum. LCD, Bangor Univ. (UK)	15 inch

ated in the four corners. Three such black and white image pairs is illustrated in Figure 2.23(a). The measurement procedure consists in measuring the luminance in the centre of the display for all six test images. The contrast ratio is then calculated by dividing the measured luminance of the centre white and the centre black for all three image pairs.

The particular large dynamic range of HDR displays may result in a very low luminance level of the black image. In order to prevent stray light from the bright corners of the image to enter the aperture of the measurement equipment, it has been recommended by the International Committee for Display Metrology to cover the lens with a frustum (ICDM, 2012). Furthermore, the photometer should be positioned perpendicular to the screen surface at a distance close to the normal viewing distance. For recreational viewing, such as television applications, this is typically 3 times the screen height. It is advisable to use a angular aperture of 1 degree or less. Such a setup is illustrated in Figure 2.23(b).

Results

In our experiment, we have included five different display technologies, of which two are HDR displays. The displays are listed in Table 2.3. The first two selected displays are regular desktop monitors based on LCD and CRT technology, respectively. The third monitor is a professional studio monitor based on an organic-light-emitting diode (OLED) display. The fourth and fifth display are based on different HDR technologies using LED illumination (Philips) and projector illumination (Bangor University, UK).

In Figure 2.24, the measured luminance is shown as a function of the relative amount of white pixels in the corner-box stimuli. The luminance of the LCD ( $170\text{ cd/m}^2$ ) and the CRT ( $80\text{ cd/m}^2$ ) can be seen to be independent of the amount of white pixels. This can also be seen for the luminance of the projector-illuminated HDR LCD ( $2200\text{ cd/m}^2$ ). The luminance of the OLED reduces from  $210\text{ cd/m}^2$  to  $165\text{ cd/m}^2$  starting at 25% white pixels, whereas the LED-illuminated

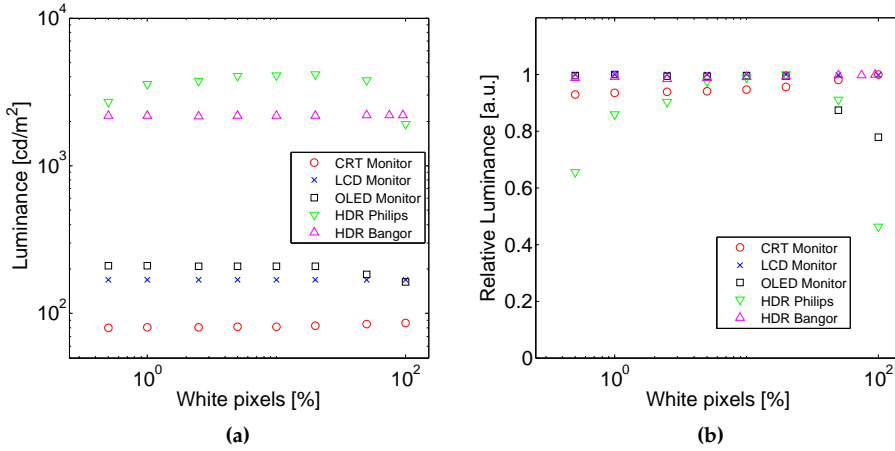


**Figure 2.24:** Measured luminance of white corner-box stimuli surrounded by black as a function of the relative amount of white pixels. In (a) the absolute luminance levels are seen. The conventional displays are seen to be between  $80 \text{ cd/m}^2$  and  $200 \text{ cd/m}^2$ , whereas the HDR displays are several factors brighter. In (b), the luminance data is plotted relative the maximum luminance. Consequently, it can be observed the the luminance of the CRT and OLED is reduced with increasing amount of white pixels. The Philips HDR display shows maximum luminance for a load of about 10% to 20%. Measurements “HDR Bangor” are courtesy of Robert Wanat.

LCD varies from  $2700 \text{ cd/m}^2$  at 0.5% white pixels to  $1910 \text{ cd/m}^2$  at 100% white pixels.

The luminance of the LED-illuminated LCD peaks at  $4140 \text{ cd/m}^2$  for 20% white pixels. The initial increase from  $2700 \text{ cd/m}^2$  to  $4140 \text{ cd/m}^2$  can be explained by the low contribution of light from a single LED to the total level of generated light, see Section 2.6.2. This behaviour is inherent to an LED-illuminated LCD display system and independent of the peak luminance. With more than 50% white pixels, the luminance in the centre is reduced because the maximum power consumption is reached while more LEDs (off centre) need to be turned on). This luminance reduction is not inherent to the display principle and can be reduced with a more energy-efficient design or a lower peak luminance.

The reduction in luminance of the OLED display for a large amount of white pixels is typical, because it also has a total power limiter. The size and the application of an OLED display is known to dictate the luminance characteristics. Recent demonstrations of large-sized OLED displays (55 inch) have revealed a peak luminance of  $400 \text{ cd/m}^2$  and a full-white luminance of  $100 \text{ cd/m}^2$  (Nam *et al.*, 2013; Yoon *et al.*, 2013).. A full-white luminance reduction to about 50% to 20% of the peak luminance is commonly observed.

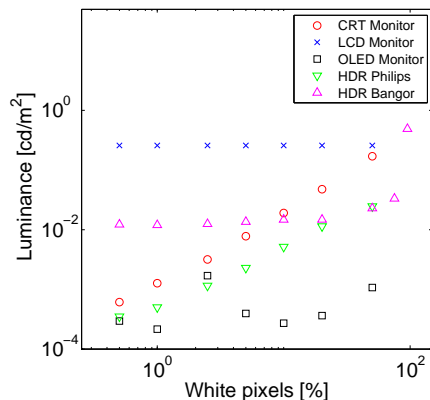


**Figure 2.25:** Measured luminance of a black corner-box stimuli surrounded by white as a function of the relative amount of white pixels. It is seen that the black luminance is highest for the LCD ( $0.25 \text{ cd/m}^2$ ) and independent of the amount of white pixels. For the other displays, the black luminance increases with increasing amount of white pixels. Measurements “HDR Bangor” are courtesy of Robert Wanat.

In order to compare the changes of luminance across the display types, the luminance data is plotted relative the maximum luminance in Figure 2.24(b). The variation in luminance of the OLED and LED-illuminated LCD becomes obvious in this figure.

In Figure 2.25, the measured luminance of a black corner-box stimulus surrounded by white is shown as a function of the relative amount of white pixels. It can be seen that only the conventional LCD exhibits a constant black luminance of  $0.25 \text{ cd/m}^2$ . The projector-illuminated HDR LCD shows a constant black luminance of  $0.012 \text{ cd/m}^2$  up to 20%, after which it rises to up to  $0.5 \text{ cd/m}^2$ , corresponding to a factor 40. The black luminance of the CRT is seen to rise from  $0.0012 \text{ cd/m}^2$  to  $0.17 \text{ cd/m}^2$  (factor 140), and the black luminance of the LED-illuminated HDR LCD is seen to rise from  $0.00026 \text{ cd/m}^2$  to  $0.25 \text{ cd/m}^2$  (factor 960). The lowest black luminance is measured from the OLED display. The luminance is between  $0.0002 \text{ cd/m}^2$  and  $0.0009 \text{ cd/m}^2$ , with the exception of an out-lier of  $0.002 \text{ cd/m}^2$  at 2.5% white pixels. OLED displays are renowned for having a very low black luminance. The slight luminance increase in our measurements of the OLED display may be a consequence of imperfect measurement conditions, in particular the frustum is a typical source of errors. The rise of luminance for the projector-illuminated HDR LCD is not ascribed to measurement errors, as these displays are known to exhibit deliberate smoothing of the projector-illumination signal to prevent alignment errors.

The measurements of white and black luminance can be used to determine the contrast ratio. In Figure 2.26, the contrast ratio of the five measured displays

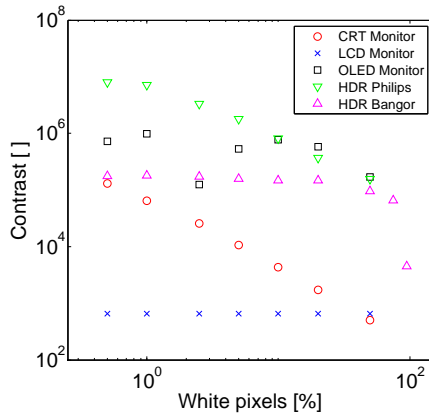


**Figure 2.26:** Dark-room contrast of different displays as a function of amount of white pixels. It can be seen that older display technologies, such as CRT and LCD, perform worse than modern HDR prototypes. Dark-room contrast is typically lower for an image with many bright pixels.

can be seen as a function of the relative amount of white pixels. The LCD shows the lowest contrast ratio of about 600:1. The contrast ratio of the CRT decreases from 63 000:1 to 500:1 when increasing the amount of white pixels. This relation between contrast and amount of white pixels can also be observed for the LED-illuminated HDR LCD, which varies from 7 800 000:1 to 154 000:1, i.e. from close to 8 orders of magnitude to 5 orders of magnitude. The projector-illuminated HDR LCD can be seen to exhibit a rather constant contrast ratio of about 180 000:1, which reduces from 20% white pixels down to 5000:1. The contrast ratio of the OLED display varies between 700 000:1 and 150 000:1, including the out-lier on the curve at 2.5%.

In conclusion, the white luminance and black luminance varies depending on the relative amount of white pixels in the stimuli. The OLED display exhibits a very good contrast ratio, but the absolute white luminance is comparable to existing display technologies. The two HDR displays exhibit both high contrast and high luminance, however, the LED-illuminated HDR LCD was superior for both attributes. For particular applications, such as psychophysical studies, the constant contrast ratio of the projector-illuminated HDR LCD may prove beneficial.

The results above illustrate the importance of considering complex stimuli, rather than a black and white image when characterising contrast and luminance for display systems. The corner-box stimuli successfully reveal spatial interactions between dark and nearby white regions. However, it is not clear how these results relate to natural images of complex spatial composition and if particular



parameters are more important than others. We encourage fellow researchers to consider this topic of future research.

## 2.7 Conclusions

In this chapter, the design of a 42 inch HDR display with 1125 backlight segments of RGB LEDs has been introduced. The display system has been instrumental for the work described in this dissertation. The many backlight segments with individually-adjustable colour, the well-defined light profiles, and the exceptional performance characteristics allowed a large amount of flexibility when experimenting and exploring options for signal processing and backlight control.

The optical design of the display system, in which the goal was to balance overall uniformity and local light generation, was realised using a structure of optical isolators and a diffuser-PMMA-diffuser stack. The electrical, mechanical, and thermal design was described including real-time control of PWM, AM, and backlight scanning using data embedded into the video signal.

After assembling the HDR display, the backlight intensity and colour was irregular and required a uniformity calibration. An automated procedure using an imaging colourimeter was presented to calibrate the 3375 individual LEDs. With this method, the variation in intensity was reduced to less than 10% and expert viewers judged the display to be sufficiently uniform.

As the backlight is of lower resolution than the LC-panel, it is necessary to characterise the PSF of the backlight segments in order to correct for this difference using the LC-panel. A method for characterisation of the PSF using an imaging colourimeter and multiple imaging exposures was presented. The measured PSF was compared to simulated profiles and a modelling approach described.

For different applications, the HDR backlight was equipped with different LC-panels over the time. The contrast was close to 10 million to 1 for all configurations. The peak luminance was between 3100 cd/m<sup>2</sup> for a conventional VA-mode LC-panel configuration and up to 7000 cd/m<sup>2</sup> for a colour-sequential OCB-mode LC-panel configuration. The colour gamut area varied from 119% up to 169% compared to Rec.709 in CIE 1976  $u'v'$  coordinates.

During the design phase of the backlight unit, several computational models were used to evaluate contrast and luminance performance. Human-eye glare was estimated and shown to perceptually mask the backlight halos for a simple image with a small white block. The direct contribution, a measure of the light intensity directly above one segment relative to the full-white image (all segments on), was presented. It was shown that the HDR display with 1125 segments performs comparable to a simulated system with 2304 segments of Quadratic Lorentzian shape. In a last model, a set of horizontally-oriented sinusoids was

used to gain insight into the frequency-dependent modulation depth (contrast) of the backlight system. Again, the HDR display systems was demonstrated to have comparable performance to the simulated display system with 2304 segments.

Finally, a metrology-based evaluation of contrast and luminance was described, in which a simple photometer was used to compare the performance of different display systems. The corner-box contrast stimuli were used and the performance of the HDR display compared to alternative display technologies.

# Local Luminance Boosting of an RGBW LCD

## Abstract

Compared to a conventional RGB LCD, an RGBW LCD is known to result in 50% higher light transmission. However, the reduced aperture for the RGB subpixels lead to reduced luminance for saturated pixels. Consequently, colorful images may appear dull due to a lack of sufficient luminance. In this work it is proposed to address the luminance shortage for bright saturated pixels by boosting a spatially modulated backlight. Whereas best-in-class methods for deriving backlight drive levels either results in high contrast *or* temporal stability, we propose a reformulation which provide superior contrast and temporal stability. By employing local backlight boosting, the 99.5%-percentile of  $\Delta E_{94}$  is reduced from 12.3 JND to 4.3 JND on average. Power consumption is reduced by 18% compared to an RGB LCD with local backlight dimming. Additionally, we propose to increase luminance of desaturated pixels in regions of backlight boosting, which results in an average luminance increase of 16% for pixels which are boosted.

---

Reproduced from M Hammer and KJG Hinnen (2014). „Local Luminance Boosting of an RGBW LCD”. in: *IEEE/OSA J. Display Technol.* 10.1, pp. 33–42.

### 3.1 Introduction

Conventional LC-displays are inherently inefficient with a light transmission level of about 5-8% due to polarizers, color filters, and the presence of TFT circuitry and black matrix. In an ideal case, a light loss of 33% can be ascribed to the use of RGB color filters. By adding a fourth, white subpixel, transmission can be improved with 50% (Elliott, Credelle, and Higgins, 2005; Lee, Park, *et al.*, 2003; Lee, Song, *et al.*, 2004; Langendijk, Belik, *et al.*, 2007). Compared to a conventional RGB subpixel layout, the transmission at white is 150%. However, when reproducing a saturated color, such as primary red, the transmission is 75% (25% area compared to 33% area) of that of an RGB subpixel layout.

An illustration of an RGB gamut projected on its R-G plane is shown in Figure 3.1(a) (black-square) together with a set of input colors (yellow-shape). An RGBW gamut is shown (black-hexagon) assuming primaries of identical chromaticity and with white point matched to RGB gamut white point. It may happen that particular input colors, such as point P, cannot be reproduced by the RGBW gamut due to aforementioned limitations on maximum luminance.

Elliott, Credelle, and Higgins (2005) has argued, that bright and saturated colors are infrequently occurring in natural images. We confirmed this by processing the 17,988 frames of the IEC 62087 sequence (IEC, 2008) and determining the out-of-gamut colors based on the RGBW gamut illustrated in Figure 3.1(a). The frequency of occurrence for out-of-gamut colors was 2.2%. Langendijk, Belik, *et al.* (2007) reversed the argument and suggested to apply global backlight boosting in those infrequent situations. Global boosting of a white backlight will enlarge the RGBW gamut to encompass all input colors, including the point P, as shown in the illustration of Figure 3.1(b). Notice that with backlight boosting the intensity of the white point has also been significantly increased.

Bright and saturated colors may be infrequently occurring, however, we will argue that reduction of luminance and/or saturation will inevitably lead to a reduction in perceived image quality. Wang *et al.* (2007) studied a number of RGB-to-RGBW conversion algorithms and concluded, based on a preference experiment, that the preferred method strongly depends on the image, and in particular colorful images are preferably reproduced by an RGB display, rather than an RGBW display due to the loss of bright saturated colors.

In this paper we propose to combine local backlight dimming and local backlight boosting in order to locally address the luminance shortage for saturated pixels in an RGBW LCD system. Our work is aimed at correct color reproduction, while maximizing contrast and minimize power consumption. In Section 3.2 we review related work and show that existing methods for deriving backlight drive levels provides either high contrast or good temporal stability. In Section 3.4

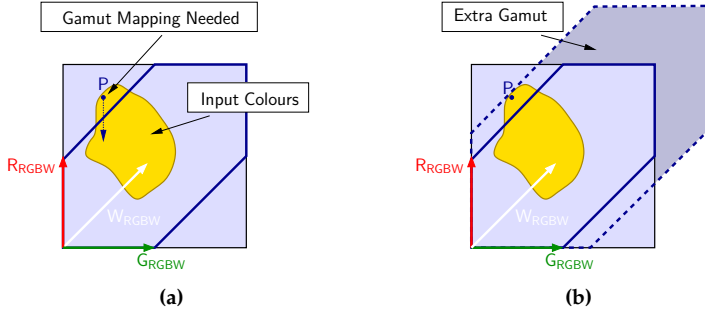


**Figure 3.1:** In (a) an illustration of an RGB gamut projected on its R-G plane (black-square) and corresponding RGBW gamut (blue-hexagon). Particular colors, such as P, may require gamut mapping as it is out of gamut. In (b) it is illustrated that with backlight boosting, the RGBW gamut can be made sufficiently large gamut to include the point P.

we propose a new concept which provides both temporal stability and high contrast. Further we propose a method to increase luminance of non-saturated pixels (which *do not* need boosting) in regions of saturated pixels (which *do* need boosting). In Section 3.5, the performance of the proposed methods is quantified in terms of contrast, luminance increase, and power consumption.

## 3.2 Related Work

### 3.2.1 LC-Displays with an RGBW-Subpixel Layout

With four subpixels per pixel rather than three, an RGBW display belongs to the class of multi-primary display systems. Due to the differences in gamut and the presence of metameric colors, such displays require special processing (Hinnen, Klompenhouwer, *et al.*, 2009). Most importantly, gamut mapping in order to compress or expand the input gamut to match the display gamut, and multi-primary conversion in order to convert the RGB-primaries to RGBW-primaries (1 degree of freedom).

Let the  $3 \times 4$  matrix  $\mathbf{A}_4$  represent the CIE-XYZ tri-stimulus values for the red, green, blue, and white subpixels measured through the LC-panel. Transmission levels of the panel,  $0 \leq \mathbf{p}_i^4 \leq 1$ , in linear light is defined as  $\mathbf{p}_i^4 = [p_i^R \ p_i^G \ p_i^B \ p_i^W]$  for the  $i$ -th subpixel. Then the tri-stimulus output,  $\mathbf{o}_i^4 = [X_i \ Y_i \ Z_i]$ , of an RGBW display can be defined as:

$$\mathbf{o}_i^4 = \mathbf{A}_4 \mathbf{p}_i^4, \quad (3.1)$$

where we have used superscript 4 to indicate that the system has 4 primaries. We will assume  $\mathbf{A}_4 [1 \ 1 \ 1 \ 0]^T = \mathbf{A}_4 [0 \ 0 \ 0 \ 1]^T$  throughout this paper, which means

the white subpixel chromaticity and luminance equals the sum of the RGB subpixels as illustrated in Figure 3.1.

The RGB-to-RGBW conversion should establish  $p_i^4$  of (3.1) for a particular input color,  $\mathbf{q}_i^3 = [q_i^R \ q_i^G \ q_i^B]$  in linear light. Early algorithms proposed to make the white subpixel equal the luminance of RGB, or to set:

$$p_i^W = \min(q_i^R, q_i^G, q_i^B) , \quad (3.2)$$

without correcting the RGB values (Elliott, Credelle, and Higgins, 2005). Consequently, the reproduced output would appear desaturated. By combining either method with:

$$p_i^k = q_i^k - p_i^W , \quad k = \{R, G, B\} , \quad (3.3)$$

the color will be reproduced at correct chromaticity, albeit not necessarily in-gamut. In order to ensure in-gamut solutions, it has been proposed to reduce intensity and/or saturation of bright, saturated colors (Lee, Park, *et al.*, 2003; Lee, Song, *et al.*, 2004; Wang *et al.*, 2007; Elliot *et al.*, 2008; Miller and Murdoch, 2009). With a slight modification, all of the above methods are also suited for dealing with a white-subpixel chromaticity and/or luminance level different than that of the sum-of-RGB (Murdoch, Miller, and Kane, 2006; Kao, Hsieh, and Lin, 2010).

Elliott *et al.* (2008) extended the work of Lee, Park, *et al.* (2003; 2004) by applying local reduction of intensity and/or saturation only in regions of frames with out-of-gamut colors, thereby leaving all in-gamut colors unmodified. They also proposed to apply global backlight dimming to reduce power consumption. Kao, Hsieh, and Lin (2011) noted that the backlight dimming parameter should depend on image saturation, such that desaturated images would result in significant power savings. However, they explicitly suggested not to apply backlight boosting, which would have allowed reproduction of bright, saturated colors.

Langendijk, Belik, *et al.* (2007) proposed to correctly reproduce colors on an RGBW display using global backlight adjustments. By analysis of out-of-gamut colors, the backlight consisting of red, green, and blue LEDs would be boosted to sufficiently enlarge the gamut volume. Individual adjustment of the backlight primaries effectively leads to a skewed gamut volume in which the white point may be off-white.

### 3.2.2 Local Backlight Dimming and Boosting

Dynamic adjustment of the (global) backlight intensity for grayish images is known to lead to reduced power consumption and improved temporal contrast, while maintaining sufficient brightness (Raman and Hekstra, 2005; Greef *et al.*, 2006).

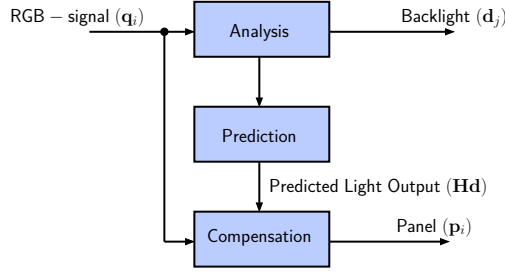


**Figure 3.2:** Block diagram for local backlight dimming consist of; 1) establish backlight drive levels based on input frame analysis; 2) predict backlight light output taking into account inter-segment spatial cross-talk; and, 3) compensate input frame drive levels to account of actual light output of the backlight.

Whenever the backlight intensity is reduced, it is important to increase the transmission level of the LC-panel proportionally in order to ensure correct intensity. This follows from the global-dimming forward model for an RGB display:

$$\hat{\mathbf{o}}_i^3 = g \mathbf{A}_3 \mathbf{p}_i^3, \quad (3.4)$$

where  $0 \leq g \leq 1$  is the global backlight dimming factor,  $\mathbf{p}_i^3 \in \mathbb{R}^3$ , the LC-panel drive levels of the red, green, and blue channel of the  $i$ -th pixel, and  $\hat{\mathbf{o}}_i^3 \in \mathbb{R}^3$ , the resulting CIE XYZ tri-stimulus value. All values are defined in linear light. The corrected drive levels of the LC-panel can be determined by:

$$p_i^k = \frac{q_i^k}{g}, \quad k = \{R, G, B\}, \quad (3.5)$$

where  $q_i^k$  is an element of  $\mathbf{q}_i^3$ .

The concept of global backlight dimming can be extended to local dimming, by applying the step of dimming per backlight segment (Seetzen, Whitehead, and Ward, 2003; Seetzen, Heidrich, *et al.*, 2004). For an LC-display with  $N$  addressable backlight segments, the tri-stimulus output can be described as follows:

$$\hat{\mathbf{o}}_i^3 = \left( \sum_{j=0}^{N-1} d_j h_{i,j} \right) \mathbf{A}_3 \mathbf{p}_i^3, \quad (3.6)$$

where  $0 \leq d_j \leq 1$  is the backlight drive level of the  $j$ -th segment. The weight factor  $h_{i,j}$  is included in order to account for optical cross-talk between the  $j$ -th backlight segment and the  $i$ -th pixel. Rather than a scalar value, the local backlight intensity depends on all backlight drive levels and the crosstalk factor, cf. (3.4). It is trivial to see that (3.5) also holds for (3.6).

A typical block diagram of local backlight dimming is provided in Figure 3.2. The backlight drive levels,  $d_j$ , are determined based on analysis of the input

frame. The resulting signals are used to predict the amount of light falling onto the LC-panel, taking the point-spread function of each segment into account. Finally, it is necessary to increase the transmission of the LC-panel proportionally to the reduction of the (local) backlight intensity.

The notoriously present light leakage of LC-panels makes local backlight dimming and attractive method for increasing display contrast ratio. The number of individually addressable segments is known to strongly affect the resulting increase of contrast (Langendijk, Muijs, and Beek, 2008; Langendijk and Hammer, 2010). Optical segment profiles need to be engineered with a sufficiently local profile in order to allow modulation for high-frequency patterns, while at the same time it needs to be sufficiently smooth in order to provide acceptable uniformity for a full-white image. Increasing the number of addressable backlight segments is known to improve viewer preference (Swinkels *et al.*, 2006) and display systems with well over 1,000 segments have been constructed (Seetzen, Heidrich, *et al.*, 2004). However, a system with 100 segments or more is already preferred by close to 90% of observers over global backlight dimming (Swinkels *et al.*, 2006).

It is possible to re-state (3.6) in a linear algebra form:

$$\begin{aligned}\hat{\mathbf{o}}^k &= \mathbf{p}^k \circ \mathbf{H} \mathbf{d}, \quad k = \{R, G, B\} \\ 0 &\leq \mathbf{p}^k, \mathbf{d} \leq 1,\end{aligned}\tag{3.7}$$

where  $\hat{\mathbf{o}}^k, \mathbf{p}^k \in \mathbb{R}^Q$  are stacked vectors of the output pixels and the LC-panel drive levels, respectively.  $\mathbf{H} \in \mathbb{R}^{Q \times N}$  is the cross-talk matrix between the  $Q$  pixels and the  $N$  backlight segments, and  $\mathbf{d} \in \mathbb{R}^N$  is a stacked vector of the backlight drive levels. The operator  $\circ$  denotes the Hadamard product.

Zhai and Llach (2009) and Shu, Wu, and Forchhammer (2013) have formulated a cost function based on (3.7) and propose solve for LC-panel transmission levels and the backlight drive levels in an integral manner. However, with significant less addressable segments than image pixels, i.e.  $Q \gg N$ , and as the point-spread function of the backlight segments is typically quite smooth, it is attractive to separately solve the problem of establishing backlight drive levels and establishing LC-panel transmission levels (Trentacoste, 2006; Trentacoste *et al.*, 2007). In our work, it has been chosen to follow the more traditional approach of separately determining backlight drive levels and LC-panel transmission levels.

### 3.2.3 Deriving Backlight Drive Levels

Early methods (Seetzen, Heidrich, *et al.*, 2004; Trentacoste *et al.*, 2007) of establishing backlight drive levels are based on dividing an image frame into non-overlapping regions,  $B_j$ , and computing the backlight drive level corresponding



to the  $j$ -th segment as:

$$d_j = \max (q_m^R, q_m^G, q_m^B)^\alpha, \quad m \in B_j. \quad (3.8)$$

Often the maximum ( $\alpha = 1$ ) or square-root of maximum ( $\alpha = 0.5$ ) is used. Alternatively, the maximum operator can be replaced with a block-wise average or a block-wise percentile. In order to increase backlight contrast Lin, Huang, *et al.* (June 2008) proposed to use the inverse cumulative distribution function of the input frame, quite similar to histogram equalization. And, Kim *et al.* (2009) and Hong, Kim, and Song (2010) used heuristic measures of contrast and clipping in order to create a differently balanced solution.

Equation (3.6) illustrates that each backlight segment cannot be established separately. The presence of optical inter-segment crosstalk may result in too little or too much light. Consequently, it is important to explicitly take the crosstalk into account when establishing the backlight drive levels. To that end, Li *et al.* (2007a; 2007b) provided two approaches.

The first method is based on minimization of the power consumption. Using the notation of (3.7) we have:

$$\begin{aligned} & \underset{\mathbf{d}}{\operatorname{argmin}} \mathbf{c}^T \mathbf{d} \\ & \text{subject to } \mathbf{H} \mathbf{d} \geq \mathbf{b} \\ & 0 \leq \mathbf{d} \leq \mathbf{1}. \end{aligned} \quad (3.9)$$

The desired backlight profile,  $\mathbf{b} \in \mathbb{R}^N$ , is defined to be equal to the solution of (3.8) ( $\alpha = 1$ ) with one sample per addressable segment, such that  $\mathbf{H}$  in (3.9) is  $N \times N$ , i.e.  $Q = N$ . The vector  $\mathbf{c} \in \mathbb{R}^N$  is a vector of ones. Notice the explicit constraint on minimum and maximum backlight drive level. The optimization problem formulated in (3.9), with linear constraints, can be solved by linear programming. In order to reduce the computational load, Albrecht, Karrenbauer, and Xu (2009), simplified the problem by neglecting far-away cross-talk and demonstrated real-time performance, however, the simplification obviously leads to a sub-optimal solution. An alternative formulation of lower computational load, also using the notation of (3.7), is proposed in (Li *et al.*, 2007a; Li *et al.*, 2007b):

$$\underset{\mathbf{d}}{\operatorname{argmin}} \|\mathbf{b} - \mathbf{H} \mathbf{d}\|^2, \quad (3.10)$$

and an iterative solution is provided based on a steepest-descent approach:

$$\begin{aligned} \mathbf{d}_{k=0} &= \beta \mathbf{b} \\ \mathbf{d}_{k+1} &= \mathbf{d}_k + \beta (\mathbf{b} - \mathbf{H} \mathbf{d}_k). \end{aligned} \quad (3.11)$$

The constant  $\beta$  is a step-wise weighting factor. The constraint  $0 \leq \mathbf{d} \leq \mathbf{1}$  is explicitly enforced after each iteration. The authors conclude, that the approach

of steepest descent works better than a simple per-segment operator. However, for narrow-support highlights, the method of linear programming outperforms the simpler method of steepest descent.

Whereas local backlight dimming is known to improve display contrast, it is important to address any undesirable side-effects such as temporal flicker. When bright objects move between adjacent segments, the backlight profile may cause clicking behavior, as neighboring segments turn off and on, respectively, resulting in viewer annoyance. This sudden change in black level is frequently occurring and can be reduced by temporal filtering (H Chen *et al.*, 2007; Kerofsky and Zhou, 2008). Unfortunately the filtering may cause the backlight to lag behind the image. This can be remedied by a 1-st order recursive filter with adaptive parameters based on scene-cut detection of pixel-wise difference (H Chen *et al.*, 2007) or correlated histograms (Kerofsky and Zhou, 2008). However, it may be more attractive to create an intrinsic more temporally-stable solution.

Muijs, Langendijk, and Vossen (2008) have proposed to impose spatial constraints on (3.8). They establish the backlight drive level based on overlapping regions, including the neighboring segments, such that the region,  $B_j$ , covers 9 rather than 1 segment, and apply spatial weighing:

$$\hat{d}_j = \max (W_m (q_m^R, q_m^G, q_m^B))^\alpha, \quad m \in B_j. \quad (3.12)$$

The weight,  $W_m$ , is defined in LC-panel resolution, following from  $B_j$ , such that backlight segments will gradually increase in intensity proportional to the distance to bright objects. The spatial weight should be tailored to each backlight design such that the backlight will approximate a shift-invariant backlight profile response to small image details. A slight loss of contrast and a widening of the profiles (due to the shift-invariant design) are typical disadvantages of this spatio-temporal method.

### 3.3 Motivation

The plurality of methods for deriving local backlight drive levels all have their merits. However, it is not obvious which method is most suited for our application. In the following section we provide a quantitative study of modulation depth (contrast) and temporal stability in order to motivate the need for a new approach.

#### 3.3.1 Quantification of Backlight Contrast

In order to quantitatively compare the contrast performance of different display systems with local backlight dimming, Langendijk, Muijs, and Beek (2008) have

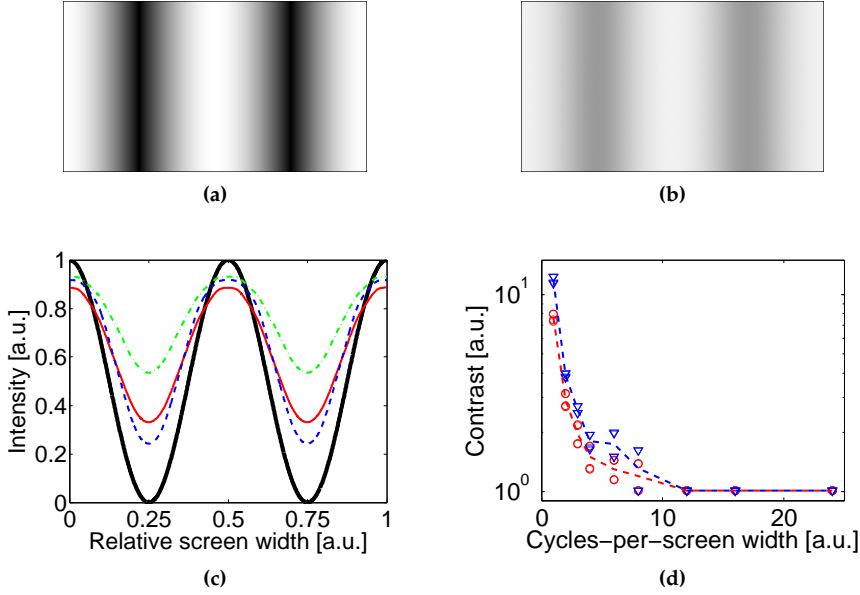


**Figure 3.3:** Illustration of backlight modulation for a horizontally-oriented sinusoidal pattern of 2 cycles-per-screen width, shown in (a), and corresponding output, processed using (3.8), shown in (b). In (c), a cross-cut of the test pattern (black-solid), and the backlight profile by the maximum method (red-solid), square-root method (green-dotted), and steepest-descent (blue-dashed) is shown. The contrast ratio of the backlight profile as a function of cycles-per-screen width is shown for the maximum method (red-circles) and steepest-descent method (blue-triangles) in (d).

introduced a method based on horizontally-oriented sinusoidal patterns. Their study was in particular focused on contrast performance for displays systems with different amount of addressable segments. We propose to use their method to investigate the impact of different methods for deriving backlight drive levels for a fixed number of addressable segments.

In Figure 3.3(a) a sinusoidal test pattern of 2 cycles-per-screen width is shown. We defined a backlight system with 9 vertical by 16 horizontal addressable segments and a quadratic Lorentzian profile shape designed for a full-white uniformity of  $\pm 1\%$ . The backlight profile based on the maximum-method of (3.8) ( $\alpha = 1$ ) is shown in Figure 3.3(b). Compared to the input, both contrast and maximum intensity is lower. Note that the modulation of the LC-panel has been disregarded.

In Figure 3.3(c) a cross-cut of both figures is shown together with the output using the square-root method of (3.8) ( $\alpha = 0.5$ ), red-solid line, and the method of steepest descent (3.11), blue-dashed line. The square-root method leads to a reduction of contrast, whereas brightness is increased, compared to the maximum

method. However, the method of steepest descent allows an increase in both contrast and brightness.

We note that a reduction of intensity is characteristic to systems with addressable backlight segments due to low direct contribution. To that end, it has been proposed to use a roll-off in the tone-scale for close-to-clipping drive levels such that details are preserved (Kerofsky and Daly, 2006; Morovič, 2008).

Following the method of Langendijk, Muijs, and Beek (2008), we recorded the maximum contrast of the backlight profile from sinusoidal stimuli from 1 to 24 cycles-per-screen width. The resulting contrast levels are depicted in Figure 3.3(d) for  $\alpha = 1$  (red-circles) and steepest-descent (blue-arrows). The lines represent the average of four phases of the sinusoidal pattern. We have added this in order to reduce the effect of correlation between location of horizontal segmentation and sinusoidal input pattern. It can be seen that up to 12 cycles-per-screen width, the method of steepest-descent provides the largest contrast ratio. In an attempt to capture the contrast characteristics in one number, the authors proposed to use the sum (maximum: 19.6, and steepest-descent: 26.3). The average power consumption was 0.63 for  $\alpha = 1$  and 0.62 for steepest-descent. We conclude that for two display systems with identical number of addressable segments and identical profile shape, the method of deriving backlight drive levels can significantly improve contrast without increasing average power consumption.

### 3.3.2 Quantification of Backlight Temporal Stability

To the knowledge of the authors no quantitative method for evaluation of temporal stability exists. We therefore propose a method based on a pair of orbiting circles, as illustrated in Figure 3.4. As the circles move about, the black level at each pixel location will change. We assert that the derivative of this change will be constant for temporally stable solutions.

Using the notation from (3.7) the average temporal difference for the  $k$ -th frame can be defined as

$$\mathcal{E}_k = \mathbf{c}^T |\mathbf{H}\mathbf{d}_k - \mathbf{H}\mathbf{d}_{k-1}| / Q, \quad (3.13)$$

where  $\mathbf{c} \in \mathbb{R}^Q$  is a vector of ones. The stimuli consisting of 25 frames for one rotation has been processed by re-using the backlight design with 9 vertical by 16 horizontal addressable segments. The resulting  $\mathcal{E}_k$  is shown in Figure 3.4(b) for the maximum method of (3.8) with  $\alpha = 1$  (red-circles), the spatio-temporal method (3.12) (green-crosses), and the method of steepest descent (3.11) (blue-arrows). It can be seen that the method of Muijs, Langendijk, and Vossen (2008), which was designed for temporal stability, outperforms the other two methods. This can be summarized with the standard deviation of change of  $152 \cdot 10^{-4}$  and

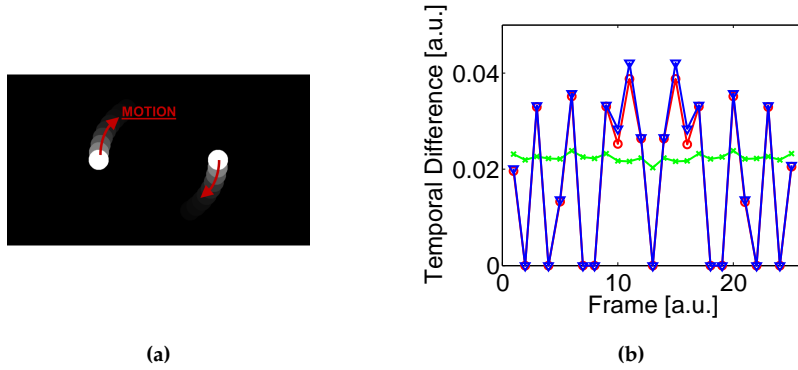


**Figure 3.4:** In (a) the stimuli for the method for quantifying temporal stability is shown consisting of a pair of white circles orbiting with a fixed radius. In (b) the resulting pixel-wise temporal difference of backlight intensity for maximum method (3.8)(red-circles), spatio-temporal method (3.12) (green-crosses), and steepest-descent method (3.11) (blue-arrows) is shown. Observe how the spatio-temporal method provides a constant change of average intensity, while the in terms of contrast more optimal method of steepest descent results in a temporal less stable solution.

$159 \cdot 10^{-4}$  for the maximum- and steepest-descent method, whereas this is only  $8 \cdot 10^{-4}$  with the spatio-temporal method.

In conclusion, whereas some methods of deriving backlight drive levels are better than others in achieving high contrast results, these methods are often temporally instable. In the following section we introduce a local dimming and boosting method which exhibits both high contrast and temporal stability. We combine this with an RGBW LC-panel and apply boosting in order to reproduce saturated colors at the correct intensity. Furthermore, in regions of backlight boosting, we propose to apply luminance boosting of desaturated colors in order to create bright, vivid images.

## 3.4 Methods

### 3.4.1 RGB-to-RGBW Conversion with Min-Max Criterion

Prior studies on the combination of an RGBW LC-display with a (local) backlight dimming have been reported to reduce power consumption compared to either technology separate (Elliot *et al.*, 2008; Kao, Hsieh, and Lin, 2011). However, typically RGB-to-RGBW conversion has been based on minimum-RGB as shown in (3.2). We argue, that in order to minimize power consumption (and maximize backlight dimming), it is necessary to maximize the benefit of the increased

transmission level of an RGBW LC-display. We here propose an RGB-to-RGBW conversion with a min-max drive level criterion (minimize the maximum drive level) in order to facilitate reduction of power consumption.

Let the linear-light input color be defined by  $\mathbf{q}_i^3 = [q_i^R \ q_i^G \ q_i^B]$ , then we propose the following RGB-to-RGBW conversion strategy:

$$\hat{p}_i^W = \min(q_i^{\min}, q_i^{\max}/2) \quad (3.14)$$

$$\hat{p}_i^k = q_i^k - \hat{p}_i^W, \quad k = \{R, G, B\}, \quad (3.15)$$

where

$$\begin{aligned} q_i^{\max} &= \max(q_i^R, q_i^G, q_i^B) \\ q_i^{\min} &= \min(q_i^R, q_i^G, q_i^B). \end{aligned}$$

For saturated colors, with  $q_i^{\max}/2 \geq q_i^{\min}$ , Equation (3.14) will be identical to (3.2). In Figure 3.5 we provide a sketch illustrating the rationale behind (3.14). The drive level of the white primary is expressed as a function of the RGB primary drive level. In this example, the green primary will limit the white primary drive level at  $q_i^{\min}$ . For  $\mathbf{q}_i^3 = [1 \ 1 \ 1]$  we may choose  $\hat{p}_i^W = 1$  and set  $\hat{p}_i^k = 0$ , however, this does not allow any backlight dimming. Subsequently, we limit  $\hat{p}_i^W$  to  $q_i^{\max}/2$ , such that  $\hat{p}_i^W = 1/2$  and  $\hat{p}_i^k = 1/2$ . This solution obviously allows significant backlight dimming.

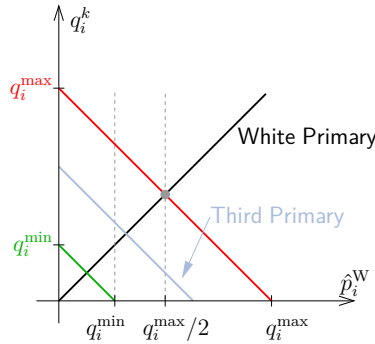


**Figure 3.5:** Sketch of white-primary drive level as a function of RGB-primary drive level. For saturated colors, with  $q_i^{\max}/2 \geq q_i^{\min}$ ,  $q_i^{\min}$  will determine the white primary drive level. For desaturated colors, the white primary drive level is limited to  $q_i^{\max}/2$ .

As this strategy results in a minimization of the maximum drive level, this method of RGB-to-RGBW conversion is particular suited for local backlight dimming. We note that it is possible to extend the min-max RGB-to-RGBW conversion method to situations where the white subpixel white point is different than the sum of RGB. Consequently, the curves for red, green, and blue will no longer be parallel.

### 3.4.2 Local Backlight Dimming and Boosting

In Section 3.3.1 it was illustrated, that local backlight dimming strategies which explicitly included the optical crosstalk of the backlight segments can lead to an increase of the contrast at a comparable level of power consumption. However, temporal stability of the backlight profile may occur, as is demonstrated in Section 3.3.2. In this section we introduce a method for achieving high local contrast while reducing visibly annoying spatio-temporal artifacts and maintaining low power consumption.

Assume the white point of the RGBW display is matched to the white point of the RGB display, such that, using (3.14) and (3.15), any primary color (red, green, or blue) will result in a drive level of 2. Without backlight boosting, this will obviously result in clipping by the RGBW display.

Let the cost function be the squared difference between the desired (based on maximum of RGBW drive levels of (3.14) and (3.15)) and actual (predicted) backlight profile, then:

$$\begin{aligned} & \underset{\mathbf{d}}{\operatorname{argmin}} \|\mathbf{H}\mathbf{d} - \mathbf{b}\|^2 + c & (3.16) \\ & \text{subject to } \mathbf{H}\mathbf{d} \geq \mathbf{b} - c \\ & 0 \leq \mathbf{d} \leq d_{\max} \\ & 0 \leq c \leq c_{\max} . \end{aligned}$$

A squared-error cost function is chosen as it is assumed that power consumption will implicitly be minimized for best possible approximation of the desired backlight profile. Relaxation with  $c$  was found necessary for the constraint  $\mathbf{H}\mathbf{d} \geq \mathbf{b} - c$  to avoid the problem to be infeasible. Both the backlight drive levels and the relaxation parameter are constrained. We found  $c_{\max} = 10$  to work well, but this depends on normalization of a.o. the backlight segments. In order to compensate for loss of luminance for bright saturated colors, we set  $d_{\max} = 2$ . The formulation in (3.16) can be solved by quadratic programming. We have made use of an open-source package SeDuMi v. 1.3 in our work (Pólik, Terlaky, and Zinchenko, 2013).

Whereas formulating local backlight dimming as an optimization problem may seem attractive, it essentially shifts the problem to determination of the desired backlight profile,  $\mathbf{b}$ . We found the maximum-method effective, see Eq. (3.8), however, the spatio-temporal method, Equation (3.12), will greatly increase the temporal behavior of the results. To that end, we note that it can be beneficial to pre-condition the input image by a simple noise reduction filter a few pixels wide.

Li *et al.* (2007a; 2007b) suggested to pre-distort the desired backlight level,  $\mathbf{b}$ , to account for visually imperceptible vignetting, which is present in most backlight

design. As the vignetting is caused by the measured segment profile data in  $\mathbf{H}$ , we suggest to rather ensure that each row of  $\mathbf{H}$  equals to one, such that the total contribution for all backlight segments to one pixel locations sums up to exactly one. This procedure needs only to be done once and not for each frame.

We further found it very useful to decouple the resolution of the desired backlight profile,  $\mathbf{b}$ , and the actual backlight segmentation to, for example,  $(3 \times 3)$  sample points (virtual segments) per addressable segment. Consequently the crosstalk matrix will also increase in samples per segment such that  $\mathbf{b} \in \mathbb{R}^{9N}$  and  $\mathbf{H} \in \mathbb{R}^{9N \times N}$ . The low resolution of the backlight compared to the resolution of the LC-panel, means that using more sample points per addressable segment will increase accuracy of approximation. We also found that temporal artifacts were largely suppressed by increasing the resolution of  $\mathbf{b}$  and  $\mathbf{H}$ .

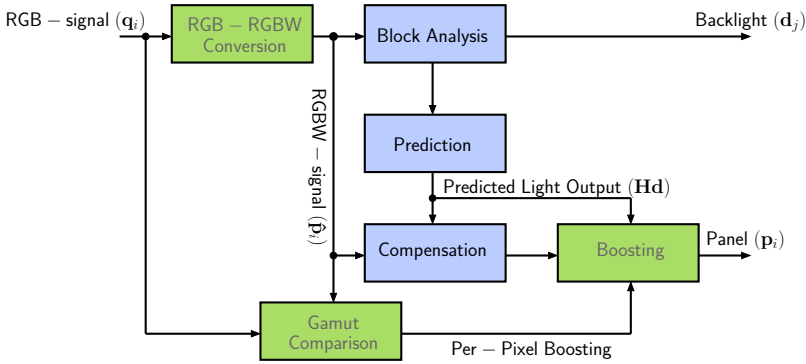


**Figure 3.6:** Extended block diagram based on Figure 3.2. The new blocks are marked in green. To facilitate the RGBW subpixel layout an RGB-to-RGBW conversion is added. In regions where the backlight is boosted due to the presence of saturated colours, we propose to increase the luminance of the desaturated pixels. This operation involves a computing the maximum luminance for the colour in question and comparing to the actual backlight intensity level. When gamut and backlight allows, a pixel can be boosted.

### 3.4.3 Gamut-Dependent Local Tone-Mapping

When the backlight is boosted in order to allow correct reproduction of saturated colors on an RGBW LC-display, it is possible to increase the intensity of desaturated colors as well. In Figure 3.7 an input image with a red block on a greenish-white background is shown. In order to reproduce the bright red at location  $P_1$ , the backlight is boosted (seen top-right). At adjacent, non-saturated pixels, points  $P_2$  and  $P_3$ , the maximum display luminance is larger than required. This is illustrated in the three insets at location,  $P_1$ ,  $P_2$ , and  $P_3$ , respectively. Close to the red block, it is possible to enhance the intensity of the white region. In the following, we describe a method for such a local tone mapping.



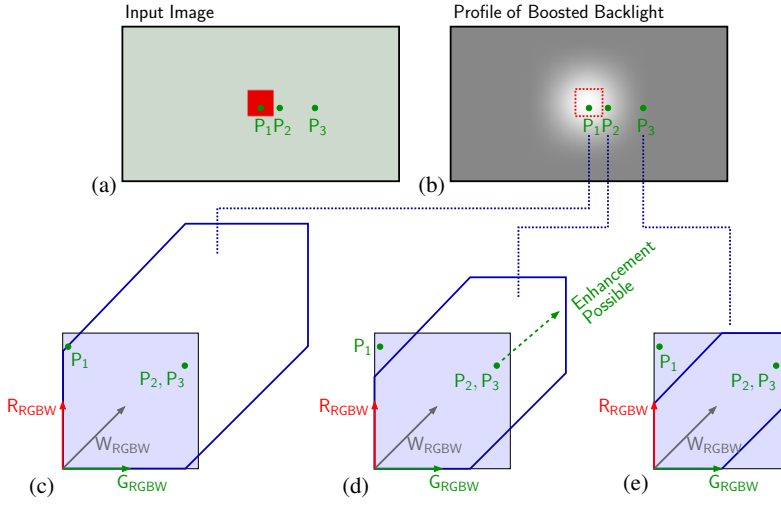


**Figure 3.7:** Illustration of the local boosting step. In (a) an input image with a small saturated central block. In (b) the corresponding backlight, where the centre is boosted. In (c-e) the size of the gamut and the potential boost of the desaturated regions is illustrated.

We will utilize the spatially smooth characteristics of the backlight profile in order to create a smooth transition between boosted and non-boosted image regions. Whereas pixels of high saturation will require the boosted backlight intensity in order to be reproduced at the correct intensity, other de-saturated pixels may benefit from the boosted backlight intensity. Thus, the pixel-wise gain will depend on its chromaticity and n possible backlight headroom.

Let the maximum luminance (or relative intensity), without backlight boosting or dimming, of the  $i$ -th pixel in the RGB gamut be given by  $Y_{\hat{Q}_i}$  and in the RGBW gamut by  $Y_{\hat{P}_i}$ . Then the needed boosting will be given by:

$$\mathcal{I}_i = Y_{\hat{Q}_i} / Y_{\hat{P}_i} , \quad (3.17)$$

where  $1 \leq \mathcal{I}_i \leq 2$  in our example. For white  $\mathcal{I}_i = 1$  and for the primary colors  $\mathcal{I}_i = 2$ . From Equation (3.6) the intensity of the backlight at the  $i$ -th pixel is defined as  $\mathcal{B}_i = \sum_{j=0}^{N-1} (d_j h_{i,j})$ . The output luminance can then be defined as:

$$\hat{Y}_i = \begin{cases} f(\mathcal{B}_i / \mathcal{I}_i, Y_i) Y_i & \mathcal{B}_i / \mathcal{I}_i \geq 1 , \\ Y_i & \text{otherwise} . \end{cases} \quad (3.18)$$

The tone mapping is limited to regions where the backlight intensity is larger than the necessary chromaticity-dependent boosting factor. It may be undesirable to apply this linear enhancement to all pixels, in particular pixels of low intensity should remain dark in order to preserve the contrast impression. Therefore, it

**Table 3.1:** Quantification of Contrast, Mean-Square-Error, Power Consumption, and Temporal Stability for 5 Different Methods for Deriving Backlight Drive Levels ( $d_{\max} = 1.00$ )

Method	Eq.	Sinusoids			Natural			Smoothness
		CR	MSE	Pow	CR	MSE	Pow	Std. dev.
maximum	(3.8)	4.90	0.21	81.5	38.8	0.15	61.4	$240 \cdot 10^{-4}$
spatio-temporal	(3.12)	4.75	0.22	82.4	28.8	0.16	63.8	$11 \cdot 10^{-4}$
steepest-descent	(3.11)	6.57	0.19	77.6	42.1	0.14	60.1	$244 \cdot 10^{-4}$
linear prog.	(3.9)	8.54	0.17	74.8	28.1	0.14	58.5	$763 \cdot 10^{-4}$
qp.-1 (max)	(3.16)	6.74	0.24	85.2	26.4	0.20	67.7	$668 \cdot 10^{-4}$
qp.-1 (spat-temp.)	(3.16)	6.70	0.24	85.5	26.3	0.20	68.0	$547 \cdot 10^{-4}$
qp.-9 (max)	(3.16)	8.80	0.13	69.1	41.5	0.10	54.3	$59 \cdot 10^{-4}$
qp.-9 (spat-temp.)	(3.16)	8.83	0.14	69.7	40.3	0.11	55.3	$57 \cdot 10^{-4}$

may be beneficial to define the local tone mapping function,  $f(\cdot, \cdot)$ , as being dependent on the current pixel intensity before enhancement. For dark pixels, no enhancement will be performed, while for bright pixels, full enhancement will be performed. A smooth transition between two modes in a tone mapping function is typically done using a knee function (Morovič, 2008).

In Figure 3.6, the complete block diagram of the proposed display system is seen. The relative intensity of the gamuts, corresponding to (3.17), is combined with the backlight intensity, in order to apply the per-pixel boosting of the output RGBW drive levels.

In order to apply (3.17), it is necessary to know the maximum luminance of the RGB gamut and the RGBW gamut. For the RGB gamut, the maximum luminance is simply found by maximizing the largest subpixel:

$$\mathcal{Q}_i = \mathbf{q}_i / \max(\mathbf{q}_i) . \quad (3.19)$$

For the RGBW gamut this is not straightforward due to the presence of metamers. However, it turns out that the min-max constraint of (3.14) and (3.15) will always yield the maximum luminance by normalizing the largest subpixels.

$$\hat{\mathcal{P}}_i = \hat{\mathbf{p}}_i / \max(\hat{\mathbf{p}}_i) . \quad (3.20)$$

This can be used in (3.17). We provide this statement on (3.20) without proof. In the following section a series of examples are included in order to illustrate the effectiveness of the proposed methods.

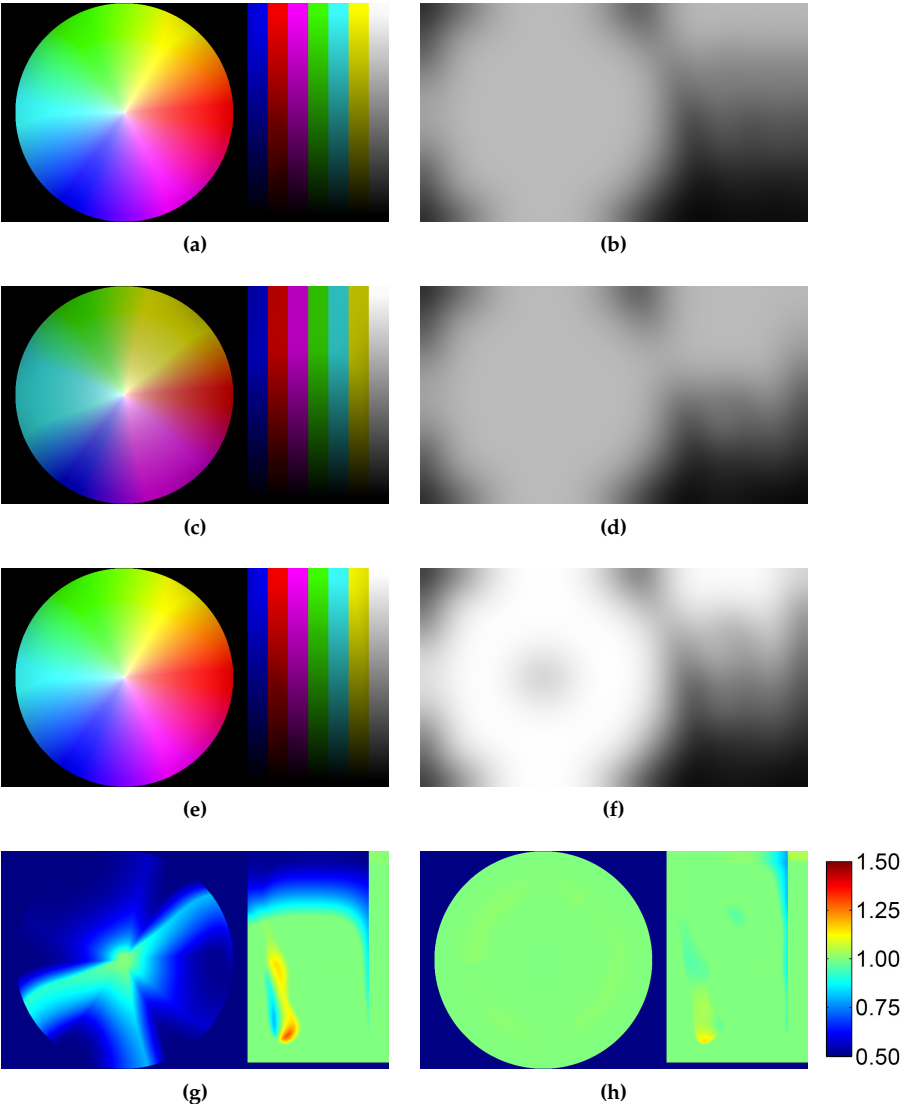


**Figure 3.8:** Simulations of front-of-screen performance for RGB and RGBW with local backlight dimming and RGBW with local backlight boosting, is show in (a), (c), and (e), respectively. The corresponding backlight profiles are shown in (b), (d), and (f). Relative luminance of RGB compared to RGBW (no boosting) is shown in (g). Notice the lack of luminance for saturated colours. The relative luminance for RGB compared to RGBW (with boosting) is shown in (h).

## 3.5 Results

### 3.5.1 Contrast Increase and Temporal Stability

The methods for deriving backlight drive levels described in Section 3.2.3 and in Section 3.4.2 have been applied to a set of test methods in order to determine the best option. First, the methods of Section 3.3.1 based on a set of horizontally-oriented sinusoidal patterns ranging from 1 to 24 cycles-per-screen width and with 4 phases is tested. Secondly, a set of 8 natural images as shown in the first row of Table 3.2 is applied. For both experiments, the average contrast increase, the mean square error, and the power consumption has been recorded. The mean-square-error has been defined as:

$$1/Q \sum_{i=0}^{Q-1} \left( \left\| \max(q_i^R, q_i^G, q_i^B) - \sum_{j=0}^{N-1} (d_j h_{i,j}) \right\|^2 \right).$$

The results of the investigated methods have been tabulated in Table 3.1. The first four methods are based on literature (Seetzen, Heidrich, *et al.*, 2004; Trentacoste *et al.*, 2007; Li *et al.*, 2007a; Li *et al.*, 2007b; Muijs, Langendijk, and Vossen, 2008). The following four options are variations on the in Section 3.2.3 proposed method based on quadratic programming. The method is based on the maximum (max.) or the spatio-temporal (spat.-temp.) methods as desired backlight profile, **b**, in the cost function. Either the backlight profile is based on 1 sample per segment (qp.-1) or 9 samples per segment (qp.-9).

Linear programming performs well for sinusoidal input, while steepest-descent is best performing for the set of natural images. It is seen that the maximum and the spatio-temporal method is never well performing with both high MSE and low CR. Also, the power consumption is highest for these methods. For the method of quadratic programming with 1 sample per segment, the performance is poor compared to linear programming and steepest-descent, both in terms of CR and MSE. However, when using 9 samples per segment, the methods compares favorably to all methods for sinusoids, and all but steepest-descent for natural images. However, steepest descent has a significant higher MSE, than the methods based on quadratic programming.

In terms of power consumption, the method of quadratic programming with 9 samples per segment is always preferred. The undesirable temporal instability has been quantified using the method of orbiting circles presented in Section 3.3.2. The lower the standard deviation, the more stable the change of backlight intensity is. The spatio-temporal method is an order of magnitude lower than the other reference methods. The proposed method of quadratic programming is significantly improved by including neighboring segments. The result is only affected to a small extend by the use of the spatio-temporal method in the cost-function.

In the following section we compare a conventional RGB system with local dimming with an RGBW system with and without local backlight boosting.

### 3.5.2 Example of Improved Color Reproduction

A test image consisting of mostly saturated colours has been processed for an RGB reference system with local backlight dimming. The simulated output is seen in Figure 3.8(a) and the corresponding backlight is seen in Figure 3.8(b). Similar in Figure 3.8(c) and Figure 3.8(d) the output and backlight of an RGBW display system with local backlight dimming and without boosting, is shown. The backlight profile is largely identical to the RGB reference system. However, in Figure 3.8(g) the relative luminance of the RGBW system compared to the RGB system is shown. All bright saturated colours are reproduced at about 50%, whereas the white bar (right-most) has been reproduced at the correct intensity.

In Figure 3.8(e) and Figure 3.8(f) the output and backlight of an RGBW display system with local backlight dimming and boosting is shown. The backlight is clearly boosted in order to compensate for the reduced transmission of saturated colours in an RGBW display system. Notice in Figure 3.8(f) that the white bar (rightmost) and the innermost area of the circle has not been boosted. The relative intensity of the RGBW system with backlight boosting compared to the RGB system is shown in Figure 3.8(h). The intensity of the saturated colours has largely been restored with exception of a small area (right-top) in the yellow bar close to the white bar. As the white bar can be reproduced without backlight boosting, the nearby yellow bar will suffer in intensity. The problem of locality is an inherent problem to local backlight dimming and boosting.

### 3.5.3 Gamut-Dependent Local Tone-Mapping

The method of local tone mapping is based on gamut headroom in regions of backlight boosting for pixels which do not need boosting. In Figure 3.9(a) the backlight of the image shown in Figure 3.10(a) is shown. The above-nominal contours are marked in red, green, and blue, for 100%, 125%, and 150%, respectively. In Figure 3.9(b) the per-pixel needed boosting,  $\mathcal{I}_i$ , is shown. The chromaticity of the blue sky and the red building is seen to require boosting (note that this does not mean that a pixel is bright and saturated, just saturated). Combining these results in a per-pixel gain map,  $\mathcal{B}_i/\mathcal{I}_i$  from (3.18), shown in Figure 3.9(c). Regions such as the window casements and the trees in the foreground are seen to be candidates for luminance boosting. Whereas bright regions should be enhanced, it is undesirable to enhance the dark trees. By applying a knee-function suppressing enhancement of dark pixels, the resulting gain map is seen in Figure 3.10(d). The input, output, and zoomed insets are shown in Figure 3.10(c). In order to

fully appreciate the added value of the propose method, we suggest the reader to compared the images on a high-quality digital copy.

On average the luminance of Figure 3.10(a) has been increased with 3.95% compared to Figure 3.10(b). As only some pixels are enhanced, the average luminance increase for enhanced pixels ( $\mathcal{B}_i/\mathcal{I}_i > 1$ ) is reported to be 24.2%. A second example is provided in Figure 3.10(e)-(h) with an average luminance increase of 2.30% and an average local increase of 32.5%.

In Table 3.2, 8 natural images have been tabulated. The resulting colour error in terms of average and 99.5% percentile of  $\Delta E_{94}$  is listed together with the power consumption. The average increase in luminance ( $\mathcal{B}_i/\mathcal{I}_i$ ) and the average increase of luminance for pixels which are actually enhanced ( $\mathcal{B}_i/\mathcal{I}_i > 1$ ) is also shown.

The proposed method can reduce the 99.5%-percentile of  $\Delta E_{94}$  from 12.3 JND to 4.3 JND on average by introducing local backlight boosting. For the images of high saturation (1-5), an increase of 18-32% is achieved, whereas for desaturated images limited enhancement takes place. On average an increase of luminance of 16% is achieved, whereas the power consumption is reduced with 18% compared to an RGB display system with local backlight dimming, cf. to 41% for an RGBW display system without boosting. For all images, the proposed method is favorable compared to the RGB display system in terms of power consumption.

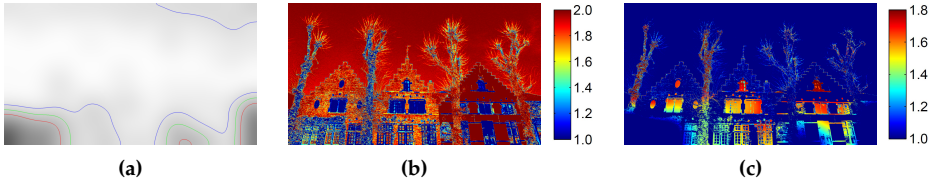
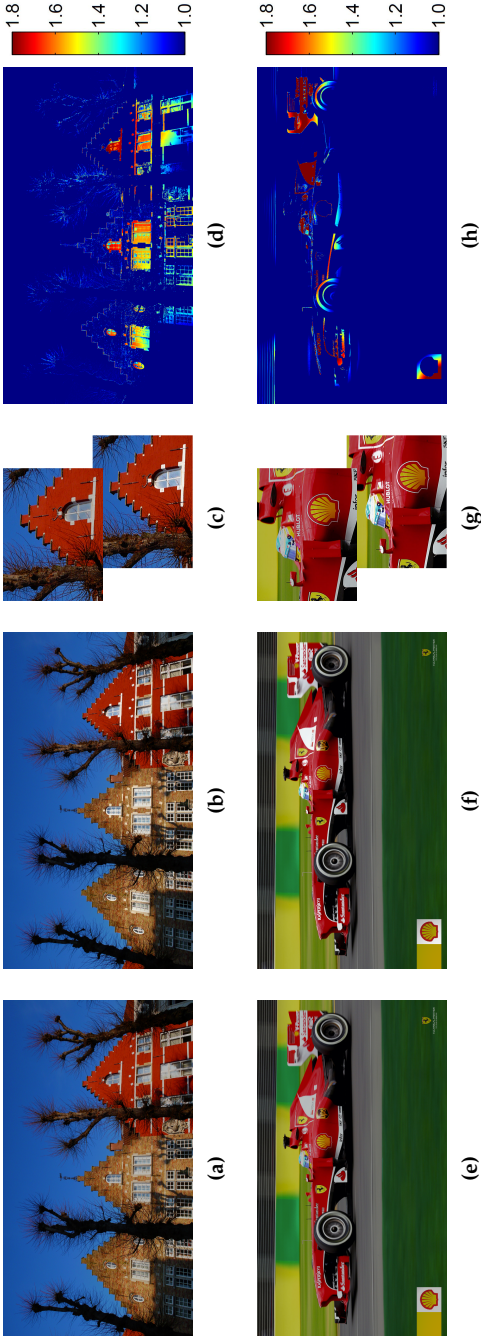


**Figure 3.9:** In (a) the backlight corresponding to the image in Figure 3.10(a). The intensity of the backlight is indicated with contours, red: 100%, green: 125%, and blue: 150% or higher. The pixel-wise and chromaticity-dependent needed boosting as defined in Eq. (3.17) is shown in (b). The backlight headroom and the needed boosting can be combined to show the possible pixel-wise gain, see Eq. (3.18), and is shown in (c).









### 3.5.4 32-inch Prototype Display

To verify the concepts presented in this work, a 32-inch RGBW LC-display prototype with 18 horizontal by 10 vertical backlight segments has been constructed. Using an imaging photometer the point-spread function of each of the backlight segments was measured and applied in the prediction and optimization procedures. The display opto-electrical response was carefully characterized for each subpixel independently and colorimetric measurements revealed that the white



**Figure 3.10:** In (a) the simulated output of an RGBW display system with local backlight boosting. In (b) the same image but including pixel-wise luminance enhancement. In (c) a zoomed version of the two images, and in (d) the pixel-wise gain is shown. Notice the difference with Figure 3.9(c) due to the non-linear tone-mapping preserving blacks. In Figure (e) to (h) the result for another image is shown.

**Table 3.2:** Color Error and Luminance Gain for an RGB display, an RGBW display with dimming (1), an RGBW display with boosting (2), and an RGBW display with boosting and luminance enhancement (3) ( $d_{\max} = 2.00$ )

									
$\Delta E_{94}$ (avg.)	RGBW 1	5.01	2.30	1.00	0.32	1.13	0.04	4.36	0.00
$\Delta E_{94}$ (99.5%)	RGBW 1	19.02	20.14	15.81	7.70	16.02	2.55	17.06	0.00
$\Delta E_{94}$ (avg.)	RGBW 2	0.08	0.46	0.35	0.13	0.11	0.03	0.15	0.00
$\Delta E_{94}$ (99.5%)	RGBW 2	3.81	9.43	6.98	6.14	3.97	1.55	2.58	0.00
Gain ( $B_i/I_i$ )	RGBW 3	3.95	2.30	2.88	0.25	7.23	0.00	0.29	0.00
Gain ( $B_i/I > 1$ )	RGBW 3	24.22	32.49	21.17	18.71	25.34	2.74	2.97	0.00
Power	RGB	88.6	55.0	70.2	57.6	89.3	17.9	55.2	2.69
Power	RGBW 1	48.1	30.1	40.9	43.1	46.9	14.3	31.9	1.70
Power	RGBW 2	80.9	44.2	51.1	45.8	66.1	15.4	50.8	1.84



subpixel had a slightly different chromaticity and intensity than the sum of the RGB subpixels.

## 3.6 Discussion

Prior work on local tone mapping for converting legacy video into high-dynamic range video is often characterized by smooth enhancement functions with wide support applied to bright pixels with nearly saturated values (Rempel *et al.*, 2007; Banterle *et al.*, 2006). This type of processing has strong resemblance to the proposed gamut-dependent local tone mapping. The spatial and temporal smoothness of the modulated backlight makes the need for computing large-support filters, such as used by Rempel *et al.* (2007), unnecessary. However, in our method large desaturated regions will not be boosted, neither will saturated pixels be boosted. Whereas our method should compare favorably to an HDR display in terms of power consumption, we suggest to carry out a viewer preference study on the image quality of an HDR display compared to our proposed RGBW display system.

## 3.7 Conclusion

In this work it was proposed to locally boost the backlight in order to address the luminance shortage for saturated pixels in an RGBW LCD system at a local scale. It was demonstrated that existing methods of deriving backlight drive levels either results in high contrast or temporal stability. Subsequently, we proposed a reformulation of the problem to a solution which provides both high contrast and temporal stability. In order to evaluate temporal stability of LC-display systems with spatially modulated backlights a novel method was introduced.

Further, a method was introduced which allowed an increase of luminance for non-saturated pixels (which *do not* need boosting) in regions of saturated pixels (which *do* need boosting). The method does not lead to an increase in power consumption, but results in HDR-like images.

A set of 8 images exhibiting either low or high saturation has been processed. By locally boosting the backlight, the 99.5%-percentile  $\Delta E_{94}$  was reduced from 12.3 JND to 4.3 JND on average. The power consumption was reduced by 18% compared to an RGB LCD with local backlight dimming, cf. 41% reduction for an RGBW display without boosting capabilities. For pixels for which luminance could be increased, an average increase of 16% was recorded.



# Local Luminance Boosting of a Colour-Sequential Display

The dynamic range of many real-world environments greatly exceeds the dynamic range of display systems based on liquid-crystal (LC) panels. Using a matrix of locally-addressable high-power LEDs, the black level can be improved substantially. With a colour-filter less LCD also the transmission can be improved substantially, but not the peak luminance. In this chapter, a method is described which allows an increase of the peak luminance of a segmented LCD without installing additional light.

## 4.1 Introduction

In the past decade numerous research activities have focused on the difference between the dynamic range of real-world environments and the dynamic range characteristics of state-of-the-art display systems. Common display systems such as LCDs are not capable of reproducing the pitch-black of a night scene or extreme brightness seen on a sunny day.

With local dimming backlights, which use a matrix of locally-addressable LEDs to adjust the backlight intensity to the image, the black-level can be reduced

---

Adapted from the publications M Hammer, KJG Hinnen, and EHA Langendijk (2012). „Boosting Luminance of a Colour-Sequential Display“. In: *Color and Imaging Conference*. Vol. 20. IS&T/SID, pp. 15–20 and M Hammer, KJG Hinnen, and EHA Langendijk (2013). „Balancing Luminance Boosting and Colour-Breakup Reduction for a Colour-Sequential Display“. In: *Digest Tech. Papers SID*. vol. 44, pp. 962–965.

by several orders of magnitude. However, high brightness displays are commonly designed by simply installing more light (Seetzen, Heidrich, *et al.*, 2004). As additional light requires more, or more powerful, LEDs, the bill-of-material goes up.

Colour-sequential display systems based on liquid-crystal (LC) panels, can eliminate the efficacy losses due to the colour filters. Without the colour filters and using a flashing backlight of red, green, and blue primary colours, for example using LEDs, it is potentially three times more efficient than a regular colour-filter based LCD (Hasebe and Kobayashi, 1985; Yamada *et al.*, 2002; Langendijk, 2005). Although the transmission level is increased, the luminance remains the same as each colour is limited to a one-third duty cycle.

The temporally flashing behaviour of colours leads to annoying colour breakup artefacts in case of (fast) eye movements. At high refresh rates, colour breakup is reduced and imperceptible to the human observer, but due to the slow temporal response of LC-panels, colour breakup remains an obstacle for the commercial breakthrough of colour-sequential systems based on LC-panels.

Advances in video processing have greatly reduced the presence of colour breakup (Lin, Zhang, and Langendijk, 2011; Zhang, Lin, and Langendijk, 2011; Zhang, Langendijk, Hammer, and Lin, 2011a; Zhang, Langendijk, Hammer, and Lin, 2011b). The proposed concepts are based on an advanced backlight with a matrix of red, green, and blue LED triplets which are locally addressable. Based on the video content, the backlight primaries are locally adjusted to reduce the colour differences between the primaries, thereby reducing the resulting colour breakup.

In this chapter, we propose a method that increases the luminance of a colour-sequential display system and also reduces the colour breakup. For a traditional 3-field colour-sequential system, luminance can be boosted with up to a factor three. In the following section we review related work on local dynamic gamuts for colour sequential displays. We then introduce the concept of local luminance boosting. In the subsequent section, we illustrate the performance of the proposed method. Finally, we investigate the potential increase of luminance across a large set of video data by estimating how often and how large the luminance gain is.

## Related Work

Traditional colour-sequential displays are based on forming colours by sequentially flashing the primary colours red, green, and blue in three separate fields. To address the issue of colour-breakup, it has been proposed to reduce the colour differences between the fields by adjusting the colour of the primaries (Lin, Zhang, and Langendijk, 2011; Zhang, Lin, and Langendijk, 2011). This is achieved by

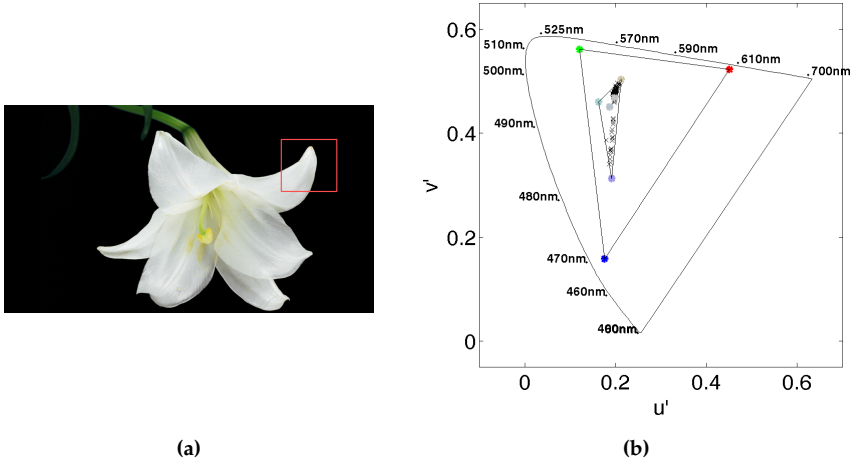


**Figure 4.1:** In (a) an input image for the illustration of local primary desaturation for a colour-sequential display system. The area in the red box is the segment under consideration. In (b), CIE 1976  $u'v'$  coordinates of the reference gamut (Rec. 709), the new local gamut, and the pixels in the red box show in (a).

flashing combinations of the red, green, and blue colours in each field. The new primaries are subject to form a gamut volume which is sufficiently large to encompass the image content.

In order to illustrate the concept of a local dynamic gamut, consider the input image of Figure 4.1(a). The segment in question has been marked with a red box. It is assumed that the input image and the display system are defined by the Rec. 709 primaries. By segmenting the backlight into smaller areas, we intend to reduce the (local) gamut in such a way that it just covers the range of chromaticities present in the image. In Figure 4.1(b), the CIE 1976  $u'v'$  chromaticity coordinates of the pixels in the red box of Figure 4.1(a) are shown as black dots. By applying local-primary desaturation, the new primaries are computed which create a smaller gamut. This smaller gamut is also indicated in Figure 4.1(b)

We will now define the forward model of a 3-field colour-sequential display system. Throughout the chapter, we assume a segmented backlight comprising a matrix of locally-addressable LEDs. Let the  $3 \times 3$  matrix  $\mathbf{A}$  represent the tri-stimulus values for the red, green, and blue LEDs measured through the LC-panel:

$$\mathbf{A} = \begin{bmatrix} X_R & X_G & X_B \\ Y_R & Y_G & Y_B \\ Z_R & Z_G & Z_B \end{bmatrix}. \quad (4.1)$$

The three drive levels for each field,  $f \in \{1, 2, 3\}$ , in the  $j^{\text{th}}$  segment are denoted by  $0 \leq \mathbf{d}_j^f \leq 1$  and  $\mathbf{D}_j = [\mathbf{d}_j^1 \ \mathbf{d}_j^2 \ \mathbf{d}_j^3] \in \mathbb{R}^{3 \times 3}$ . The transmission levels of the

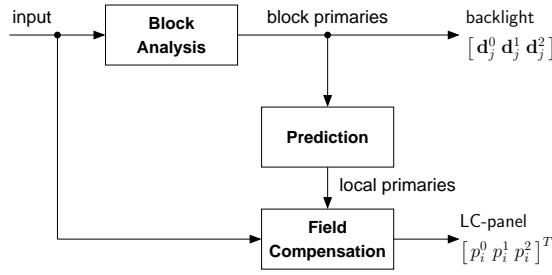


**Figure 4.2:** A block diagram for determining the local LED drive levels and the LC-panel drive levels for a colour-sequential display system with a backlight comprising a matrix of locally-addressable coloured LEDs.

panel,  $0 \leq p_i^f \leq 1$ , are defined by  $\mathbf{p}_i = [p_i^1 \ p_i^2 \ p_i^3]^T$  for the  $i^{\text{th}}$  pixel. Then the tri-stimulus output of the display is:

$$\begin{bmatrix} X_i \\ Y_i \\ Z_i \end{bmatrix} = \mathbf{A} \mathbf{D}_j \mathbf{p}_i . \quad (4.2)$$

If only one type of LEDs is turned on in each field, the drive level matrix,  $\mathbf{D}_j$ , reduces to the unity matrix. The gamut of this solution is given by the primaries (columns) of  $\mathbf{A}$ . If several types of LEDs are turned on in each field, the off-diagonal of  $\mathbf{D}_j$  is allowed to be non-zero. Consequently, the resulting fields can have different colours, such as orange, yellow, cyan, etc. If all LED drive levels in each field are identical, only one colour can be made, but at three times the nominal intensity.

A block diagram for determining the local LED drive levels and the LC-panel drive levels is shown in Figure 4.2. The input image is divided into blocks corresponding to the segmentation of the backlight. For each block, the primaries are determined that create a smaller gamut area (if possible). The resulting drive signals for the backlight segments are used to predict the amount of light falling onto each pixel of the LC-panel. This will form the local per-pixel primaries. In the prediction of the per-pixel primaries, the point-spread function of each backlight segment is taken into account. Let the relative amount of light from the  $j^{\text{th}}$  segment on the  $i^{\text{th}}$  pixel be given by  $0 \leq h_{i,j} \leq 1$ , then the forward model, including the point-spread function, is:

$$\hat{\mathbf{o}}_i = \left( \sum_{j=0}^{N-1} \mathbf{A} \mathbf{D}_j h_{i,j} \right) \mathbf{p}_i , \quad (4.3)$$

for a system with  $N$  segments and where  $\hat{\mathbf{o}}_i = [\hat{X}_i \ \hat{Y}_i \ \hat{Z}_i]^T$ . As the backlight segments may differ in drive signals (and therefore in primaries), the inter-segment cross-talk may affect the local primaries. It is therefore advantageous to

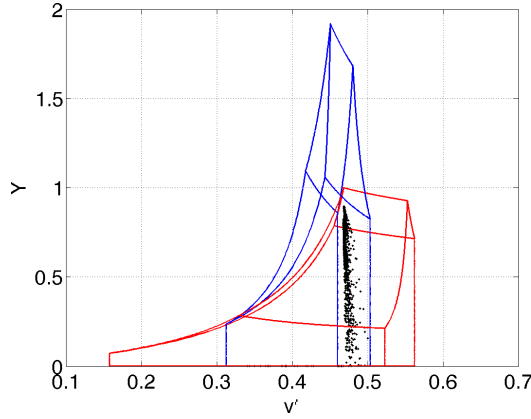


**Figure 4.3:** Side view of the gamut volume of regular colour-sequential mode (red-solid) and the de-saturated gamut volume (blue-solid) for the segment indicated in Figure 4.1(a). The gamut volumes are seen projected along the  $Y$ - $v'$  axis.

reduce the intensity of each local primary to a minimum, in order to reduce the influence on the chromaticity of neighbouring segments.

The effect of reducing the intensity of the local primaries can be illustrated by observing Figure 4.3. In this figure the gamut volume is shown projected along the luminance and the CIE 1976  $v'$  axes. The black dots represent the pixels of the segment in the red box indicated in Figure 4.1(a). The reference gamut is shown in red-solid and the de-saturated gamut is shown in blue-solid. Notice that both the reference and the desaturated gamut are too large. It is therefore possible to reduce the intensity of the backlight in all fields. This operation is similar to local dimming for a system with a white backlight, however, it is also possible to reduce the intensity of each field independently and thereby skew the local gamut and obtain the smallest possible volume which do encompass all pixels.

In order to achieve the correct colour for each pixel, the transmission levels of the LC-panel for each field,  $\mathbf{p}_i$ , must be computed. This can for example be done with quadratic programming as in:

$$\operatorname{argmin}_{0 \leq \mathbf{p}_i \leq 1} \left\| \mathbf{t}_i - \left( \sum_{j=0}^{N-1} \mathbf{A} \mathbf{D}_j h_{i,j} \right) \mathbf{p}_i \right\|^2, \quad (4.4)$$

where  $\mathbf{t}_i$  is the target tri-stimulus value for the  $i^{\text{th}}$  pixel. As a faster alternative, we found that employing the pseudo-inverse of the local primaries in combination with soft-clipping worked well.

Although the concept of local primaries is clearly illustrated in Figure 4.1(b), a method for determining such local primary chromaticity coordinates is not

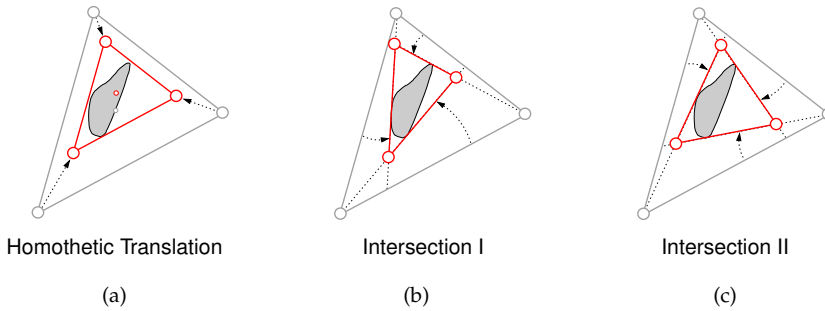


**Figure 4.4:** Illustration of local gamut determination based on geometric transformations. In (a), a homothetic transformation (translation and scaling) is shown. The lines connecting local primaries remain parallel to the original lines. In (b) and (c), the original lines are rotated in-wards until intersection with data. The rotation of (b), respectively, (c), is anti-clockwise and clockwise.

straightforward. The problem is further complicated by the inter-segment cross-talk, as illustrated in (4.3). Initially neglecting the cross-talk, a number of geometric transformations were used. The transformations are illustrated in Figure 4.4. In Figure 4.4(a), the local primaries are determined by a homothetic transformation (translation and scaling) leaving the lines connecting the local primaries parallel to the original lines. As this method proved limiting for particular situations, a second method based on in-wards rotation of the lines connecting the primaries (until intersection with data) was applied. This method is illustrated in Figure 4.4(b) and Figure 4.4(c) for a anti-clockwise and clockwise rotation, respectively. Due to the simplicity of the geometric transformations, all methods were applied and the best result chosen based on a weighed combination of area and circumference.

In order to illustrate the principles, the image of Figure 4.1(a) has been processed and the results are shown in Figure 4.5(d)-(g). A backlight with a segmentation of 20 by 12 (240 segments) was assumed. The spatial profiles of the segments were defined by a Gaussian profile and a full-white uniformity of 1%. The local primaries were computed based on the chromaticity of the pixels for the segment in question including the immediate neighbours (9 segments in total). The area over which pixels are taken into account is larger than the segment in order to take the inter-segment cross-talk into account and prevent excessive clipping. We applied image pre-filtering to remove noise and chromaticity distribution outliers.

Applying the outlined method results in the image shown in Figure 4.5(g). The corresponding fields of backlight modulated with the LC-panel, are shown in Figure 4.5(a), 4.5(b), and 4.5(c). The three fields showing the backlight only are shown in Figure 4.5(d), 4.5(e), and 4.5(f). Notice how the local primaries appear desaturated, the lack of saturated red, and how frequent white occurs as a local



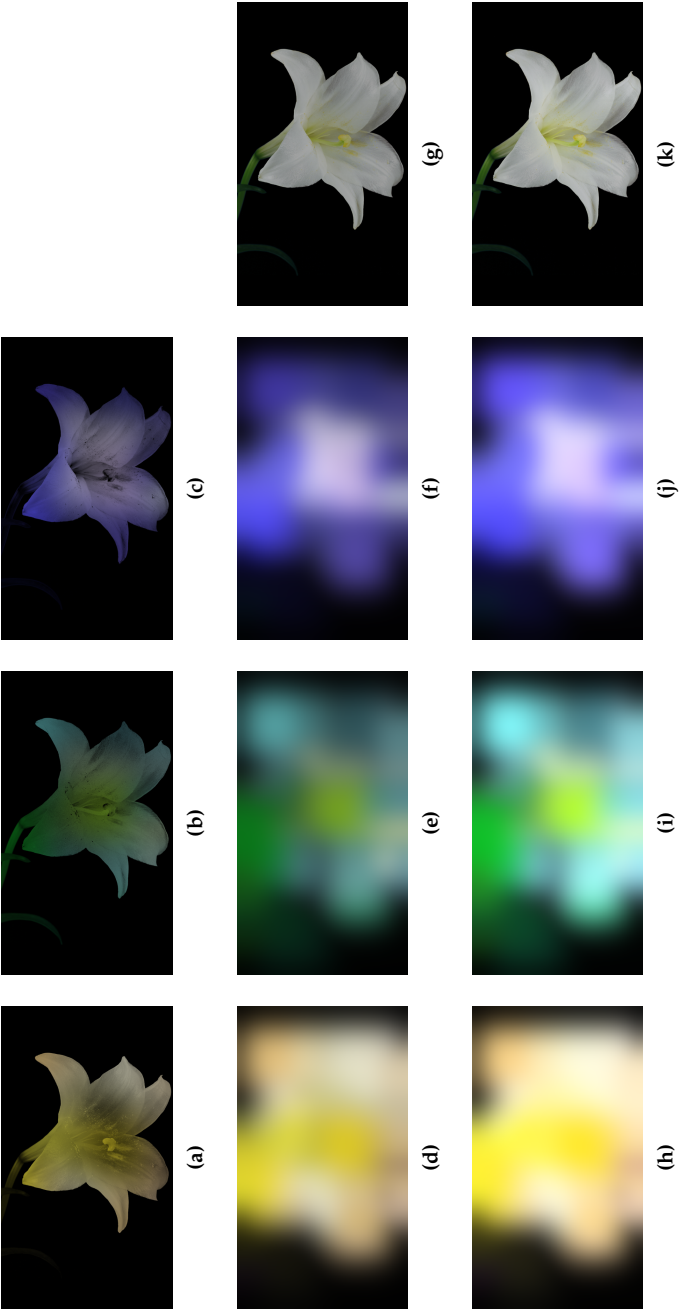


**Figure 4.5:** Illustration of the front-of-screen image for the three fields (top row, (a)-(c)) and the corresponding backlight image with (bottom row, (h)-(i)) and without (middle row, (d)-(f)) boosting. The resulting front-of-screen image is seen in the last row with (k) and without (g) boosting.

primary. Also notice how the backlight appears dark in regions where the image is black.

As illustrated in Figure 4.3, it is possible to reduce the intensity of the local primaries. The gamut volume can be made small while still large enough to contain the pixels. However, if one would not reduce the intensity of the desaturated primaries (gamut volume in dotted-blue), it would be possible to represent pixels at luminance levels considerably higher than the reference system (gamut volume in solid-red). In other words, it would be possible to increase the luminance of those pixels above the maximum luminance of the reference system. The following section describes a local tone-mapping method that increases the brightness of pixels in areas where the gamut volume allows.

## 4.2 Boosting Method

In this section, the increase in luminance is quantified as a function of the reduction of the local gamut. Furthermore a method is presented which utilise this capability for natural images by an increase of the backlight intensity and pixel-wise application of a local tone-mapping operator subject to the local gamut headroom.

The increase of luminance for a white desaturated colour will now be quantified. Consider a white region, similar to the petals of the lily of Figure 4.1(a), but with a more limited spread of chromaticity coordinates. Starting with a reference gamut and step-wise de-saturating the primaries toward white, will result in a gamut reduction as shown in Figure 4.6(a). As an indication of the potential luminance gain, consider the maximum intensity of white for the new gamut compared to the reference gamut. The resulting curve (black-dotted) as a function of the gamut coverage is shown in Figure 4.6(e). The gamut coverage is the ratio of the area of the new gamut compared to the area of the reference gamut expressed in CIE 1976  $u'v'$ . It can be observed that the maximum gain is 3 and the minimum is 1. It is also clear, that if it would be possible to reduce the size of the gamut to less than 20%, one would have 50% additional luminance. This curve corresponds well with earlier findings by Bergquist and Wennstam (2006).

The increase of luminance for a saturated colour will now be quantified. Consider an all-red image. If the gamut consists of three red fields, rather than a red, a green, and a blue field, the luminance gain would be 3. In Figure 4.6(e) the resulting gain-curve is shown (red-solid). Similar for green (green-dashed) and for blue (blue-dash-dotted). It can be observed that the gain factor depends on the chromaticity of the target. A smaller gamut coverage results in a larger luminance gain.

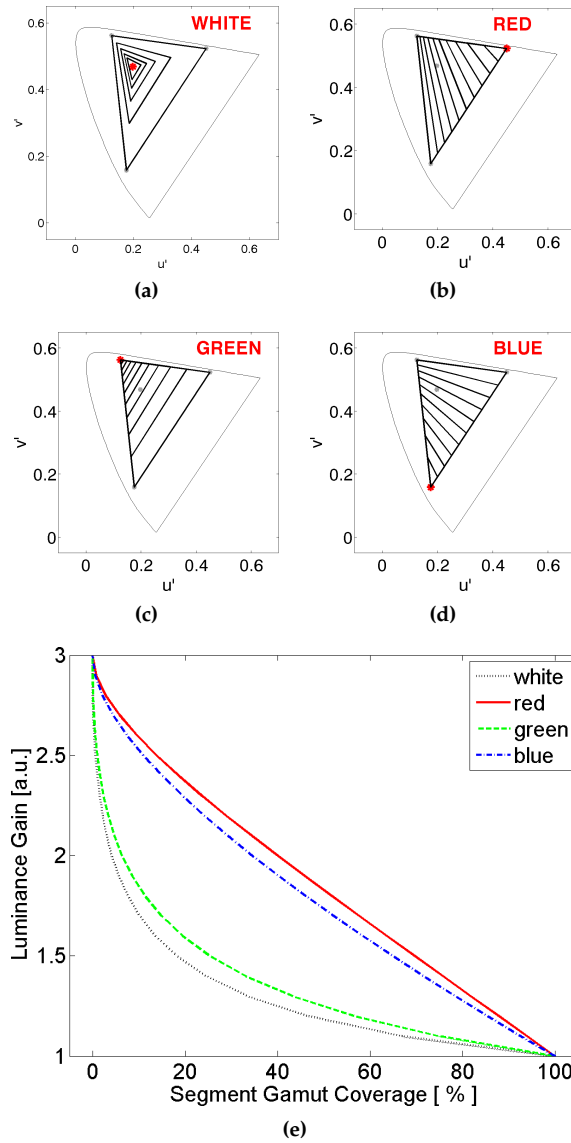


**Figure 4.6:** Illustration of step-wise desaturation towards a white-only gamut consisting of three white fields is seen in (a). In (e) luminance gain for a white (black-dotted) target chromaticity as a function of gamut coverage expressed as a CIE 1976 ' $u'v'$ ' ratio. Step-wise desaturation towards a red, a green, and a blue gamut is shown in (b), (c), and (d), respectively. The corresponding luminance gain for red (red-solid), green (green-dashed), and blue (blue-dash-dotted) is shown in (e).

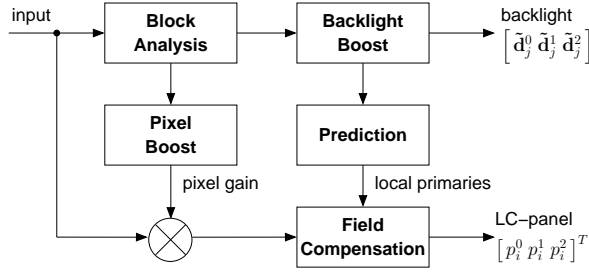


**Figure 4.7:** A block diagram of local primary desaturation with luminance boosting. Compared to the basic block diagram (Figure 4.2), two blocks have been added. *Backlight Boost*, which creates headroom where available, and *Pixel Boost*, which does per-pixel tone mapping.

The simplified observations on luminance gain shown in Figure 4.6 cannot easily be generalised to natural images. The relationship shown is only valid for one target chromaticity. Namely if the target chromaticity coincides with the local gamut white point (desaturation to white), or coincides with the only local gamut fixed primary (saturation to primary colour). Obviously, a multitude of chromaticities will be present in natural images.

The block diagram of Figure 4.7 shows how to utilise the boosting capabilities of a colour-sequential display system based on local primaries. The block diagram is similar to the method described in the previous section (Figure 4.2) except for the two additional blocks *Backlight Boost* and *Pixel Boost*. The block *Backlight Boost* creates headroom by increasing the intensity of the local primaries in order to allow boosting of the pixels. The block *Pixel Boost*, in turn, performs a local tone mapping depending on the local gamut headroom.

Increasing the intensity of the backlight primaries in the block *Backlight Boost* will reduce the overall contrast impression. In black regions, where the reduction of backlight intensity has positively contributed to a black level reduction, a blunt increase of backlight intensity will undo this benefit. It is therefore alternatively proposed to only increase the intensity of primaries which are already considerably bright. In order to preserve the chromaticity of the primaries, the backlight drive level of the  $j^{\text{th}}$  segment in the  $f^{\text{th}}$  field is modified to:

$$\tilde{d}_j^f = \frac{g\left(\max\left(\mathbf{d}_j^f\right)\right)}{\max\left(\mathbf{d}_j^f\right)} \mathbf{d}_j^f, \quad (4.5)$$

where the boosting function,  $g(x)$ , is defined by:

$$g(x) = \begin{cases} x/c, & x \leq c, \\ 1, & x > c. \end{cases} \quad (4.6)$$

Note that  $0 \leq x \leq 1$ , such that,  $0 \leq g(x) \leq 1$ . The constant,  $0 \leq c \leq 1$ , defines the level of boosting. Applying Eq. (4.5) leads to a taller gamut with the same chromaticity coordinates, but headroom for increasing the luminance of the input signal. If nothing else is changed, the resulting output would be exactly the same as without the boosting, due to the field compensation. In order to benefit from the headroom, the input image should be tone mapped taking into account the headroom.

## Conditional Tone Mapping

We have shown that the luminance increase depends on the desaturated gamut and on the target chromaticity. A simple method of tone mapping could consist of using the ratio of the reference gamut luminance (height) and the desaturated gamut luminance (height) at the target chromaticity. We show how to compute this per-pixel gain value. Let the maximised LC-panel drive level of the  $i^{\text{th}}$  pixel be given by,  $\mathbf{p}_i^{\text{max}} = \frac{\mathbf{p}_i}{\max(\mathbf{p}_i)}$ . Then the maximum luminance for the corresponding chromaticity coordinate in the desaturated gamut can be defined as:

$$Y_i^{\text{max}} = [Y_R \ Y_G \ Y_B] \left( \sum_{j=0}^{N-1} \tilde{\mathbf{D}}_j h_{i,j} \right) \mathbf{p}_i^{\text{max}}, \quad (4.7)$$

where  $\tilde{\mathbf{D}}_j \in \mathbb{R}^{3 \times 3}$  is the boosted backlight signal of the  $j^{\text{th}}$  segment. The vector  $[Y_R \ Y_G \ Y_B]$  is the second row of the primary matrix,  $\mathbf{A}$ . The maximum luminance of the reference gamut,  $Y_i^{\text{max-ref}}$ , can be computed by replacing the backlight signal,  $\tilde{\mathbf{D}}_j$ , with the identity matrix. We define the per-pixel gain,  $g_i$ , as the ratio of  $Y_i^{\text{max}}$  and  $Y_i^{\text{max-ref}}$ .

As it turns out, the per-pixel luminance headroom can vary considerably. This leads to large, high-frequency variations in the tone-mapped output. The strong dependence on chromaticity can also lead to undesirable changes in colour appearance. This problem can be reduced with low-pass filtering and other signal processing tricks. Instead, we have circumvented the problem by taking a different approach.

In this alternative approach, The actual headroom for each pixel in a segment at block level is computed first before taking the inter-segment cross-talk into account. The maximum luminance at block-level can be computed as:

$$\tilde{Y}_i^{\text{max}} = [Y_R \ Y_G \ Y_B] \tilde{\mathbf{D}}_j \mathbf{p}_i. \quad (4.8)$$

The per-pixel headroom is given by  $\frac{\tilde{Y}_i^{\text{max}}}{Y_i^{\text{max-ref}}}$ . We then average the headroom across all pixels in this segment and use this as the desired boosting factor. This may lead to an underutilised system for some pixels (above average headroom), while other pixels will be subject to clipping (below average headroom). One

could also employ the minimum, maximum, or 90<sup>th</sup> percentile, rather than the segment average. It is important to note that upsampling from segment resolution to pixel resolution is needed. One could simply interpolate to a higher resolution, but we found it useful to make use of the inter-segment cross-talk to compute the final per-pixel boosting value. Let  $\bar{v}_j$  be the average headroom of the  $j^{\text{th}}$  segment, then the per-pixel gain is defined as:

$$\tilde{g}_i = \sum_{j=0}^{N-1} \bar{v}_j h_{i,j} . \quad (4.9)$$

As the corresponding pixel may be black or subject to clipping, the resulting front-of-screen gain may differ. An obvious advantage of the second approach is that it is possible to do tone mapping and prediction of light falling onto the LC-panel in parallel.

## Artefact Reduction by Locally Balanced Boosting

The method described above generally results in more preferred images as the brightness is increased. The local enhancements are spatially smooth due to the interaction between the primary desaturation and the smooth backlight profiles. However, in particular cases, visible artefacts may occur. To illustrate such an artefact we provide the image of Figure 4.8(a). The simulated output for the sub-image shown in blue and processed by local primaries is shown in Figure 4.8(c). By applying luminance boosting the image of Figure 4.8(d) is created. To compare the results, the relative luminance is shown in Figure 4.8(b). Notice how luminance is increased in some regions and how the fall-off is smooth making the variation imperceptible. However, the luminance of the bright, white specular reflection in the balloon has not been increased. The greyish-looking reflection looks unnatural next to the bright saturated yellow balloon. The limited increase in luminance (about 20%) next to the specular reflection emphasises the importance of this problem.

We have observed that the artefacts typically manifest in areas of direct illumination, e.g. a photograph of a sunset, or with bright saturated colours next to specular reflections. The latter is frequently occurring as limitations in the dynamic range of conventional video acquisition often results in desaturated specular reflections.

The artefacts arising from luminance boosting relate to the local primaries. In Figure 4.9(a), the local primaries of the segment with the yellow balloon with a white specular reflection are shown (segment with red boundary in Figure 4.8(a)). It can be seen that all yellow tints can be made by mixing two primaries allowing an increase in luminance output. For white pixels, however, only one field can be used leaving no headroom for increase in luminance output. This is clearly

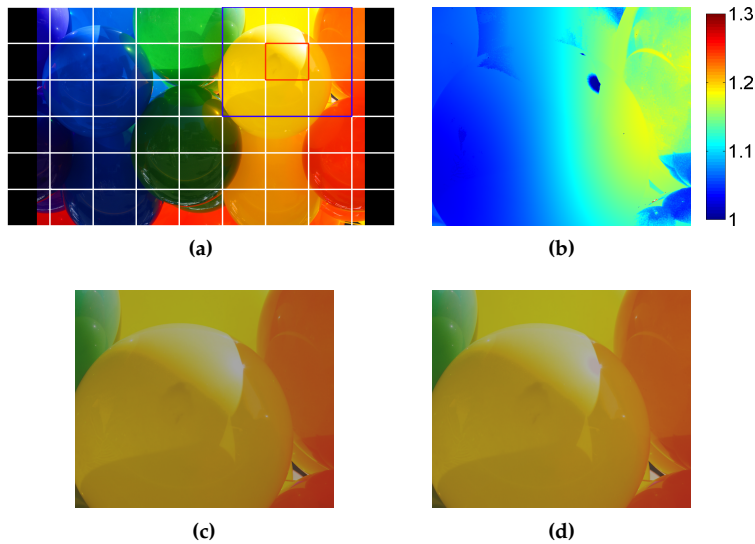


**Figure 4.8:** In (a) an input image divided into 9 by 6 segments. The output of the blue block after processing with local primaries is shown in (c) and with luminance boosting shown in (d). The luminance increase is shown in false colour in (b). The luminance increase of about 20% in the simulations can be difficult to see on a digital screen. Note the greyish-looking specular reflection.

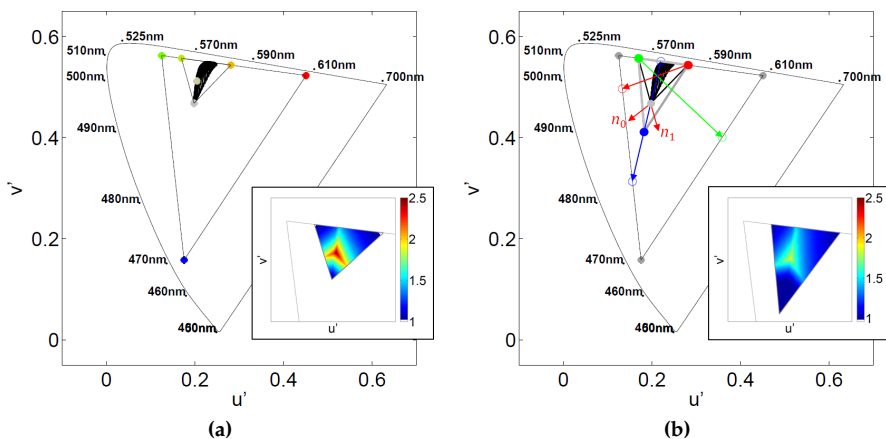


**Figure 4.9:** Chromaticity distribution of the pixels in the segment with red boundary in Figure 4.8(a) is shown. The corresponding input gamut and local primaries are also shown (a). The inset shows the local gamut luminance relative to the input gamut luminance, i.e. the headroom. By enlarging the local gamut (b), the white pixels show more headroom (see inset).

illustrated by the inset in Figure 4.9(a) which shows the local gamut luminance relative the input gamut luminance, i.e. the chromaticity-dependent headroom.

In order to reduce the visible artefacts, one could use a fall-back scenario in situations where luminance boosting is potentially limited for particular colours, such as white in the example provided. As luminance headroom can be predicted, this is a simple solution. However, rather than limiting luminance enhancement, it may be possible to increase the luminance output of the white areas. By enlarging the area of the triangle spanned by the local primaries, the white chromaticity can be constructed by mixing two primaries allowing for a (modest) increase in luminance. In Figure 4.9(b) we show how the white primary has been geometrically extended towards cyan. The algorithm we have applied for extending one local primary (in this case the white primary) consists of the following steps.

1. Determine the direction of extension (average of normal vectors  $n_0$  and  $n_1$  in Figure 4.9(b)).
2. Determine intersection(s) with the gamut boundary.
3. Detect amount of pixels close to primary.
4. Extend primary outwards in proportion to amount of pixels close to primary.
5. Clip new primaries along projected line to gamut boundary, if needed.

The steps in the algorithm are indicated by the solid red, green, and blue lines indicating the lines along which the gamut will be extended. The circles indicate intersections between the lines and the input gamut.

Whereas it may be counterintuitive to enlarge the gamut area, we must remember that the initial strategy of detecting problematic areas and reducing the maximum luminance would also have resulted in a lower luminance of the surround. Using the gamut enlargement, not only is the luminance of the surround reduced, the problematic area (white reflection) can be shown at an increased luminance than before enlargement. Consequently, the luminance is balanced at a higher luminance than if the gamut would not have been enlarged.

It should be noted, that as the area of the triangle is enlarged in order to increase luminance output, the risk of increasing visible colour-breakup artefacts arises. In order to balance luminance increase and the suppression of visible colour breakup, we found the step 3 and 4 particularly instrumental.



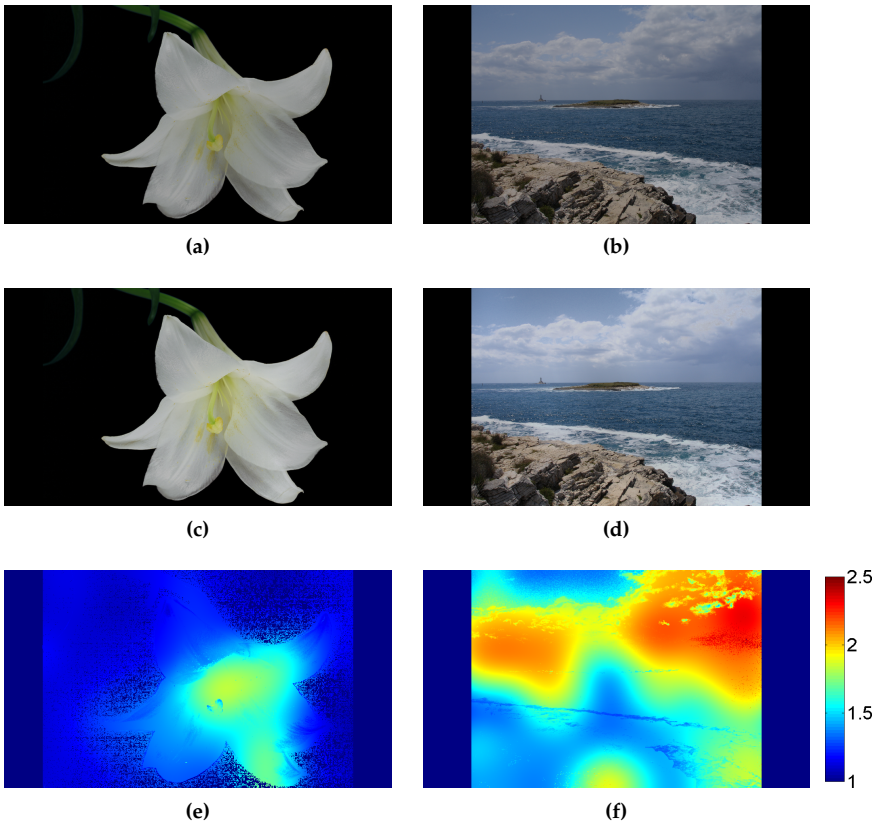


**Figure 4.10:** Illustration of the front-of-screen image with (c), (d) and without (a), (b) boosting. The corresponding luminance gain maps are seen in (e) and (f), respectively.

### 4.3 Results

The method of boosting the backlight intensity, described by Eq. (4.5), has been applied to the image of Figure 4.1(a). The boosted backlight fields are shown in Figure 4.5(h), 4.5(i), and 4.5(j). Note how the boosted backlight fields appear brighter compared to the fields with non-boosted backlights. Also the dark regions have remained dark, which is meant to ensure the black-level reduction known from local dimming. The tone mapping of the input has been based on the average headroom. This leads to the result shown in Figure 4.10(c) (cf. Figure 4.10(a)). Note that the display system will indeed consume more power when boosted, but it does not contain more installed light than the reference system. Compared to a conventional LCD, the proposed system will consume less power both with and without boosting. The luminance gain was calculated and is shown in Figure 4.10(e).

To evaluate the method about 15 images were processed, fully automatically, with identical algorithmic parameters. The results were visually inspected and more than 80% showed none or minimal artefacts. In Figure 4.10(d) such an image is shown. Notice the large gain in the sky and the sea of Figure 4.10(d) compared to Figure 4.10(b). In these regions, which are dominantly white-blue, considerable levels of luminance increase of up to a factor 2.4 has been achieved for large parts of the image, see Figure 4.10(f). Also note that the spatially-varying tone-mapping does not create visible artefacts in this example.

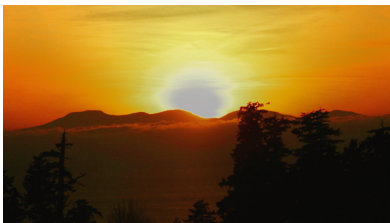
In less than 20% of the images, visual inspection revealed annoying artefacts. The most annoying example is shown in Figure 4.11(b). Whereas this image generally appears brighter than the reference (Figure 4.11(a)), the discrepancy between the luminance increase of the edges and the centre region of the sun is visually annoying. In Figure 4.11(c), it can be seen that the centre region is not boosted at all, while the edges are boosted with close to 70%. The cause of the problem lies in the local gamut. The local primaries in the sky and sun are rather constant. However, the luminance headroom is strongly dependent on the target chromaticity. For the red-yellow sky two (or more) fields can be used to form a pixel of correct chromaticity and high luminance, while the white sun can only be reproduced using a single field which limits the possibility of boosting luminance.

### Results with Locally-Balanced Boosting

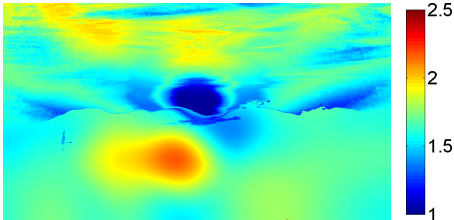
In order to address the luminance in-balance, we have proposed to enlarge the local gamut such that the luminance of problematic area will be increased while the luminance of the surround is slightly reduced. In the following, it is illustrated how this method works by means of examples. The image of Figure 4.8(a)



(a)



(b)



(c)

**Figure 4.11:** Illustration of the front-of-screen image with (d), (b) and without (b), (a) boosting. The corresponding luminance gain maps are seen in (f) and (c), respectively.

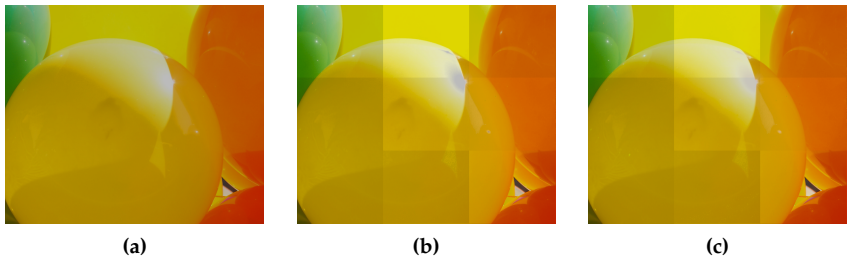


**Figure 4.12:** Simulation result of block-wise processing of the image Figure 4.8(a) by; (a) local primaries, (b) luminance boosting, and (c) improved luminance boosting. Inter-segment cross-talk has been omitted, which is the cause of the luminance difference between segments. Notice how the appearance of the specular reflection is improved between (b) and (c).

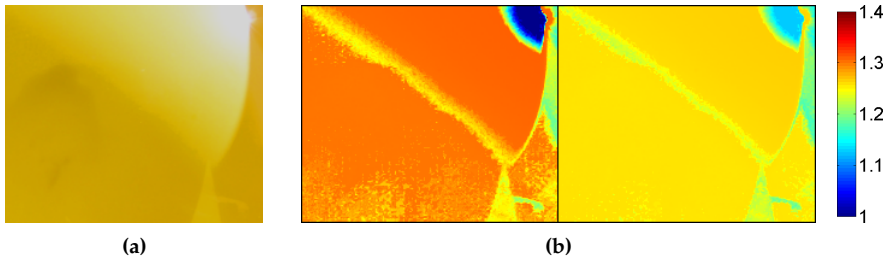


**Figure 4.13:** The red segment from Figure 4.8(a) is shown in (a). The luminance output relative the input image is shown in (b). To the Left is the first method with a small gamut and to the right the proposed method with local enlargement of the gamut. Notice that the average luminance increase has reduced, but the difference in luminance increase has been reduced.

has been processed in a block-wise fashion omitting the inter-segment cross-talk (modelled in Eq. (4.3)). By omitting inter-segment cross-talk, the effectiveness of the proposed method is highlighted as the smoothing effect of inter-segment cross-talk is excluded. This also creates a one-to-one relationship between the proposed method, illustrated in Figure 4.9, and the simulation result shown in Figure 4.12 and Figure 4.13. The luminance difference between segments in Figure 4.12 is caused by processing each segment independently.

The image processed with local primaries is shown in Figure 4.12(a) while traditional luminance boosting results in Figure 4.12(b). Notice how the reflection appears very grey and unnatural. By extending the white primary to cyan, the white reflection can be made brighter. This is shown in Figure 4.12(c). In order to compare the two luminance boosting methods, the luminance relative to the input image is shown in Figure 4.13(b). Left is the first method with a small gamut and to the right is the proposed method of enlarged gamut volume. Note that the increase in luminance is slightly less (on average) using the new method.

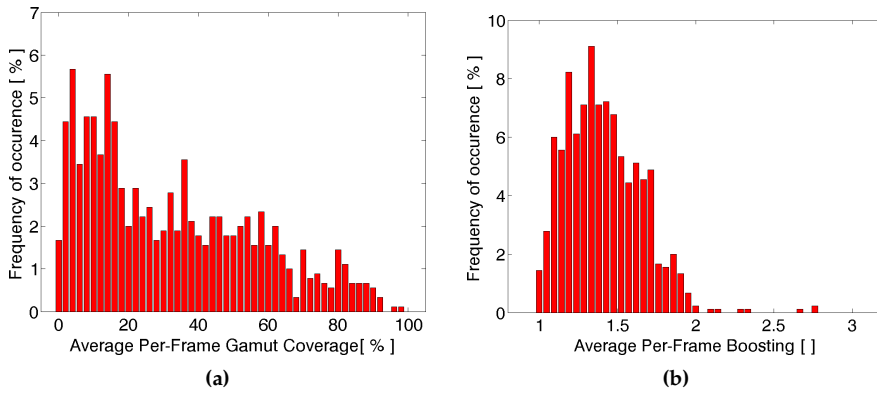


**Figure 4.14:** Results from the statistical experiment on the IEC 62087 video sequence (IEC, 2008). In (a) the frequency of occurrence of frame-average gamut coverage expressed in CIE 1976  $u'v'$ . In (b) Frame-average luminance headroom frequency of occurrence.

However, the white reflection is almost 15% brighter. Consequently the difference in luminance increase was reduced.

## Boosting Frequency

As shown in Section 4.2 (Figure 4.6), the theoretical headroom varies between 1 and 3. In the examples above, the actual level of gain varies between 1 and 2, sometimes a little higher. In order to understand how often boosting will be possible and how much boosting is possible, we conducted a small statistical experiment. The starting point of the experiment is a video data set collected for IEC 62087 (IEC, 2008) and originally intended to investigate the power consumption of domestic video equipment.

It is worthwhile noting that while the content is rather de-saturated, this does not need to be an advantage for the method. Extremely saturated content, like animations or computer programs like text editors, can also form good boosting candidates. The experiment was carried out as follows: 1) each frame was divided into 12 by 20 segments; 2) local primary desaturation was applied; 3) the backlight was boosted for bright segments; and 4) the average per-pixel headroom and the gamut coverage in CIE 1976  $u'v'$  was recorded.

The collected statistics can be used to understand the gamut coverage of the local primaries. As can be seen in Figure 4.6(e), one can expect the largest headroom for the smallest local gamut. It is therefore interesting to understand how often the local primaries will span a small gamut. We have plotted the histogram of the average gamut coverage per frame in Figure 4.14(a). The average gamut coverage is 33% and the 90<sup>th</sup> percentile is 68%. These results indicate that even

with a modest segmentation of 240 segments, the resulting local gamuts are considerably smaller compared to the reference gamut. As was found in earlier work, the approach of local primary desaturation should be quite effective at reducing colour breakup for most image content.

While colour breakup reduction is advantageous, we are actually interested in the resulting luminance headroom. In Figure 4.14(b) we show the histogram of the average headroom/boosting per frame. The average headroom is 1.43 and it can be observed that headroom up to a factor of 1.7 is frequently occurring. Notably is also that headroom above 2 does not occur frequently.

## 4.4 Discussion

The existing scheme for determining local primaries presented by Lin, Zhang, and Langendijk (2011), which consists in maximum reduction of the gamut area, may not be the best approach to increase front-of-screen luminance. New approaches, such as those presented in Section 4.2, which achieve less reduction in area may improve luminance by several factors. This offers an interesting trade-off between high-brightness and colour breakup artefacts. As annoyances of colour breakup are most frequent in high contrast regions with bright uniform areas, such as white text on a black surround, one could switch between approaches for luminance increase and colour breakup reduction, by analysing the video content.

The proposed method leads to impressive results for some images, while for others the visual appearance has changed. It may be worthwhile investigating other methods for tone mapping; in particular comparing existing inverse tone-mapping operators which are targeted at displays which do not exhibit constraints on the gamut size and shape.

In order to balance colour-breakup reduction and luminance boosting, we suggest incorporating a quantitative measure of colour-breakup such as presented by Zhang, Langendijk, Hammer, and Hinnen (2012). This challenge is of future work.

## 4.5 Conclusions

The concept of luminance boosting for a colour-sequential display has been introduced. The theoretical maximum luminance boosting is 300% without additionally installed light. Compared to a conventional LCD, the proposed display system is either considerable more efficient (no colour filters) at identical luminance, or consumes a comparable amount of energy at three times higher luminance.

A method to increase the luminance in bright regions, while maintaining the low black level in dark regions, was developed and evaluated. A local tone mapping, subject to constraints of the local gamut headroom, was proposed. Whenever the local gamut area was minimised, the local luminance enhancement was the largest. Visible artefacts, which for example may manifest in image areas of direct illumination, was shown to be reduced by enlarging the local gamut. A method was proposed for enlarging the local gamut area, whenever a significant amount of pixels would become subject to limitations on luminance increase.

It was determined that an average luminance boost of 143% could be expected for regular video content, and that more than 200% boosting does not occur frequently. For other image content such as text editors or animated movies the boosting could be considerably higher.





# Colour Reproduction on a 120-Hz Two-Field Color-Sequential LCD

## Abstract

Conventional displays use at least three primaries for full color image reproduction. In this contribution, we discuss the reproduction of color images using an LC-display system with two local dynamic primaries, based on a segmented backlight. The two primaries are chosen to minimise color error by means of total least squares. Simulation results indicate quite good color reproduction for a large set of video data even with a limited number of backlight segments. A statistical analysis of this video content shows that excellent color reproduction ( $\Delta uv < 0.020$  for more than 99.0% of the pixels per frame) can be achieved for 74.2% of the frames using 9216 backlight segments.

---

Reproduced from M Hammer *et al.* (2012). „Method to Improve Color Reproduction on a 120-Hz Two-Field Color-Sequential LCD“. in: *J. Soc. Inf. Display* 20.7, pp. 380–389.

## 5.1 Introduction

In order to increase the power efficiency of display systems based on liquid-crystal (LC) panels, the losses due to the color filters have caught much attention. For example, a color-sequential display where the color filters are omitted and replaced by a flashing backlight of red, green, and blue primary colors is a potentially very efficient solution (Hasebe and Kobayashi, 1985; Yamada *et al.*, 2002; Langendijk, 2005). To avoid annoying flicker, a color-sequential display requires a panel refresh rate of 180 Hz or higher. The temporal color synthesis is also the source of the well-known color breakup effect. These two issues, the high panel refresh rate and the color breakup, generally have been perceived as blocking for the commercialisation of color-sequential displays. Recently, advances in video processing has greatly reduced the presence of color breakup (Lin, Zhang, and Langendijk, 2011; Zhang, Lin, and Langendijk, 2011). The proposed concepts are based on an advanced backlight with three primary colors consisting of red, green, and blue light-emitting diodes (LED). The LEDs are segmented and locally addressable. Based on the video content, the primaries are locally adjusted to reduce the color differences between the primaries, thereby reducing the resulting color breakup. While a color-sequential display is several times more power efficient than a regular color-filter based display, the requirement for fast switching of the LC-panel remains an unsolved problem (Yamada *et al.*, 2002). As an alternative to a full color-sequential display operating at 180 Hz and without color filters, Langendijk, Roosendaal, *et al.* (2005) proposed a hybrid system comprising two wide-band color filters and two temporal fields. This results in flicker-free operation at a 120 Hz panel refresh rate. The display system is, however, less power efficient than a full color sequential system. The backlight could consist of two or more light sources, e.g. LEDs, which in combination with the color filters constitute 4 display primaries, two in each field. These spatio-temporal displays offer an interesting trade-off between power efficiency and panel refresh rate. Recently, Zhang, Langendijk, Hammer, and Lin (2011a) investigated how local dynamic primaries, by means of a backlight with locally addressable LEDs, can reduce color breakup for spatio-temporal display configurations. In this paper, we propose a two-field color-sequential display without color filters that can operate at a refresh rate of only 120 Hz. Using a fast-switching LC-panel and a segmented backlight consisting of colored LEDs, color reproduction relies on local primaries. While regular displays exhibit gamut volumes allowing correct color reproduction, the two-field scheme reduces the (local) gamut to a plane in a linear color space. Yet, in this paper we show that two-field color-sequential displays can have good color reproduction. In the following section, we review related work on two-field color sequential displays. We then introduce the concept of optimal primaries for a local two-primary system followed by simulation results for both simple and natural images. Finally, good color reproduction of a local

two-primary display system is statistically investigated for a large set of video frames followed by discussion and conclusions.

## 5.2 Related Work

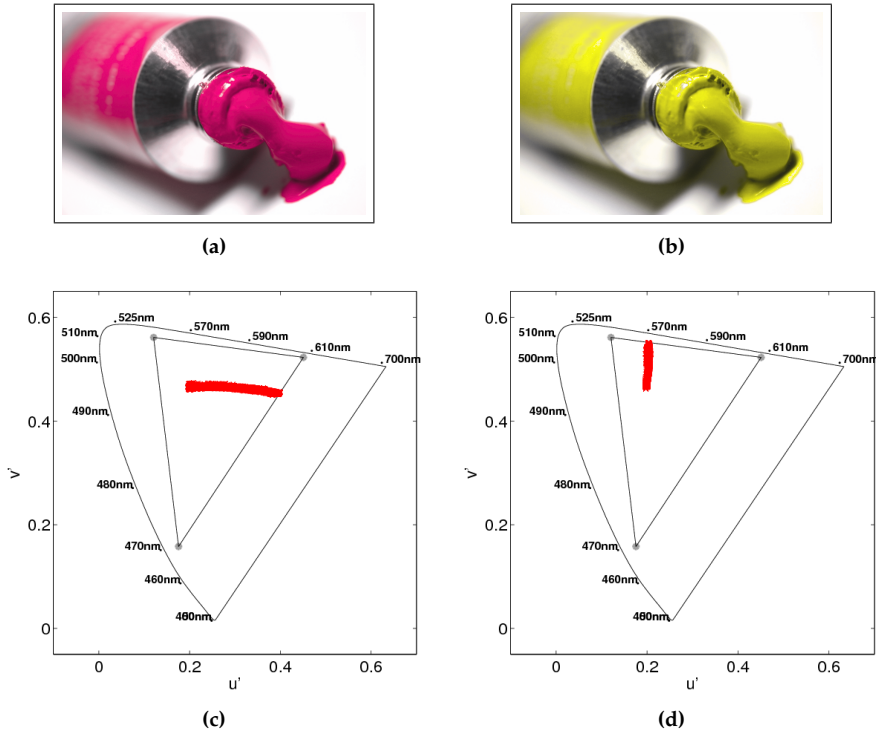


**Figure 5.1:** Simple images with magenta-white (a) and yellow-white (b). Below the images, in (c) and (d), the chromaticity diagrams of the image pixels are shown in CIE 1976  $u'v'$ .

It was initially Cheng, Huang, *et al.* (2009) who proposed a two-field color-sequential display without color filters in order to combine 120 Hz refresh rate with high power efficiency. Their system combines an LC-panel without color filters with a locally addressable red, green, and blue backlight. This allows them to create a colorful image with only two local primaries. In essence, they propose to independently calculate a red and a green field. The blue color is mixed into these two fields, as “[...] the human visual system is less sensitive to blue information [...]”, they reason. To show the working principles of this concept, we have included two images shown in Figure 5.1(a) (magenta-white) and Figure 5.1(b) (yellow-white). Below the images are the chromaticity diagrams of the pixels in CIE 1976  $u'v'$ . The triangle in the chromaticity diagram indicates the color gamut

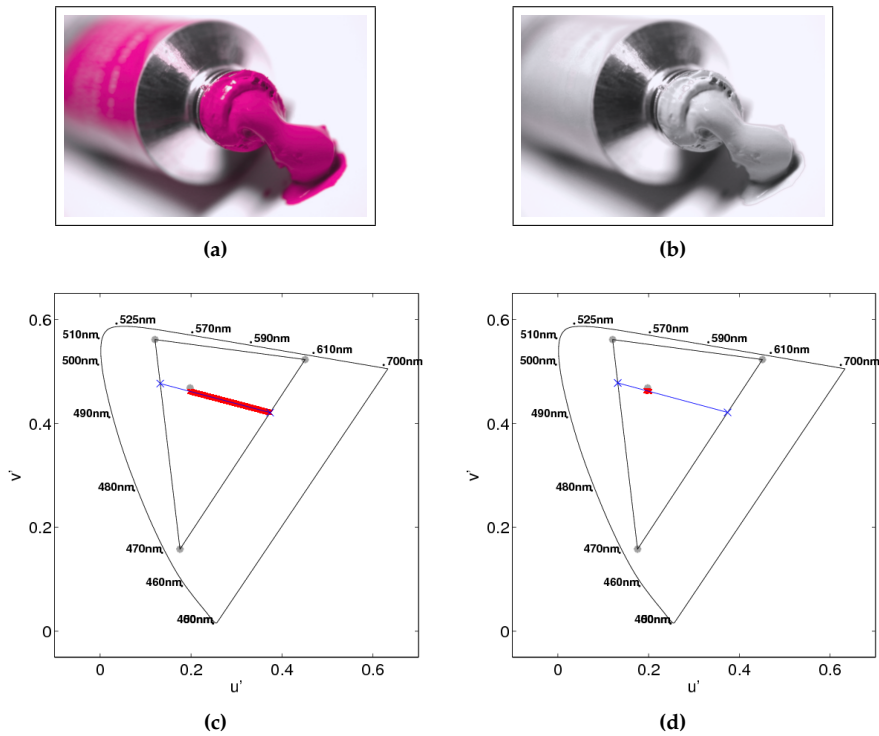


**Figure 5.2:** Simulated output of the images in Figure 5.1(a) and Figure 5.1(b) is shown in (a) and (b), respectively. The method applied corresponds to Cheng, Huang, *et al.* (2009). In (c) and (d) the corresponding output chromaticity is shown in a chromaticity diagram.

of the display backlight, in this paper assumed to be ITU Rec. 709 color primaries. We assume an ideal display without backlight segmentation for this example. The images have been processed using the concept described by Cheng, Huang, *et al.* (2009) applied to a global-addressable backlight and the result is shown in Figure 5.2(a) and Figure 5.2(b), respectively. Notice how the magenta-white image has been (almost) correctly reproduced with primaries located on the chromaticity lines red-blue and green-blue. For the yellow-white image, however, the color has not been reproduced at all. As the local primaries are forced to lie on the red-blue (field 1) and green-blue (field 2) chromaticity lines of the gamut triangle, the yellow-white image cannot be reproduced and the image appears black and white. Obviously the poor color reproduction for the yellow-white image is not inherent to the display system. In the following section we introduce a method for determining optimal primaries for a two-primary system by explicitly minimising the color error.

## 5.3 Methods

Good color reproduction of a two-field color-sequential display requires an optimal choice of the local backlight primaries as well as the LC-panel drive levels. For the moment, consider a non-segmented backlight with individually controllable red, green, and blue LEDs. We initially state the forward display model of the  $i^{\text{th}}$  pixel, which is given by:

$$\mathbf{o}_i = \mathbf{A} \begin{bmatrix} \mathbf{d}_0 & \mathbf{d}_1 \end{bmatrix} \begin{bmatrix} p_0^i \\ p_1^i \end{bmatrix} + \mathcal{E}_i, \quad (5.1)$$

where the  $3 \times 3$  matrix  $\mathbf{A}$  represents the tri-stimulus values for the red, green, and blue LEDs through the LC-panel. The three LED drive levels of field 0 and field 1 are defined as  $\mathbf{d}_0 \in \mathbb{R}^3$  and  $\mathbf{d}_1 \in \mathbb{R}^3$  and the scalar drive levels for the LC-panel are defined as  $p_0^i$  and  $p_1^i$ . With respect to the target tri-stimulus values  $\mathbf{o}_i \in \mathbb{R}^3$  the output can be associated with a tri-stimulus error  $\mathcal{E}_i \in \mathbb{R}^3$ . We have here assumed system linearity through the range of drive levels of both the LEDs and the LC-panel drive levels. Further we have neglected the effect of LC-panel contrast (normally an offset). We re-state Eq. (5.1) as a constraint optimisation problem:

$$\underset{0 \leq p_0^i, p_1^i, \mathbf{d}_0, \mathbf{d}_1 \leq 1}{\operatorname{argmin}} \left\| \mathbf{o}_i - \mathbf{A} \begin{bmatrix} \mathbf{d}_0 & \mathbf{d}_1 \end{bmatrix} \begin{bmatrix} p_0^i \\ p_1^i \end{bmatrix} \right\|^2. \quad (5.2)$$

It has been assumed that the drive levels are scaled between 0 and 1. The problem is characterised by its bi-linearity, which makes it difficult to solve. We therefore follow an alternative path in order to approximate the optimal solution by splitting the problem in two; 1) choosing the optimal backlight primaries, and 2) computing the corresponding optimal LC-panel drive levels. We further reduce the problem from obtaining the optimal display primary tri-stimulus values to determining the optimal primary chromaticity coordinates thereby initially disregarding the luminance component. For clarity we assume CIE 1931 chromaticity coordinates, without loss of generality. First a line is fit through the set of chromaticity target coordinates associated with the  $N$  input pixels. Let the line be defined by  $\mathcal{L} : ax + by + c = 0$  with slope  $-a/b$  and constant  $-c/b$ , then the parameters  $a, b, c$  of  $\mathcal{L}$  can be obtained in a total least squares sense by:

$$\underset{a, b, c}{\operatorname{argmin}} \sum_{i=0}^{N-1} \left\| \hat{\mathcal{E}}_i \right\|^2, \quad (5.3)$$

where

$$\hat{\mathcal{E}}_i = \mathbf{n}^T \begin{bmatrix} x_i \\ y_i \end{bmatrix} + c.$$

We have here made use of a unity vector  $\mathbf{n}^T \in \mathbb{R}^2$ . Based on the parameters of the line, a line segment can be computed by determining the intersection between

the line and the display gamut, defined by matrix  $\mathbf{A}$ . In fact, the chromaticity of the optimal primaries need not be located on the gamut boundary, i.e. along the edges of the color gamut triangle. Rather the primaries can be represented by the shortest possible line segment given by  $\mathcal{L}$  which sufficiently reproduces the chromaticity points in the data set. The advantage of reducing the length of the line is that the primaries will be located closer together and the visible color breakup may be reduced. Secondly, as a side effect, reducing the length of the line segment may also increase the maximum achievable luminance. Assume the line segment is defined by its end-points,  $(x_0, y_0)$  and  $(x_1, y_1)$ , then the tri-stimulus values of the primaries can be determined as follows:

$$\tilde{\mathbf{A}} = \mathbf{A} [\mathbf{d}_0 \quad \mathbf{d}_1] = \begin{bmatrix} \frac{x_0}{y_0} & \frac{x_1}{y_1} \\ 1 & 1 \\ \frac{z_0}{y_0} & \frac{z_1}{y_1} \end{bmatrix}, \quad (5.4)$$

where we have assumed  $Y_0 = Y_1 = 1$ . The matrix  $\tilde{\mathbf{A}}$  represents the tri-stimulus values of the new primaries. In order to determine the drive levels of the LC-panel corresponding to the new primaries, we have to solve:

$$\operatorname{argmin}_{0 \leq p_0^i, p_1^i \leq 1} \left\| \mathbf{o}_i - \tilde{\mathbf{A}} \begin{bmatrix} p_0^i \\ p_1^i \end{bmatrix} \right\|^2, \quad (5.5)$$

for each pixel. Without further derivation, we note that it is possible to replace the constraint least squares by unconstrained least squares. When a drive value is out of range (clipping), the value should be clipped to the upper/lower boundary and the other drive value computed as the projection of  $\mathbf{o}_i$  onto the line segment,  $\mathcal{L}$ .

## 5.4 Refinements of the Proposed Method

Using a line-fit through the chromaticity coordinates, as proposed in Eq. (5.3), leads to good results when the distribution of chromaticity resembles a line, for example for a single-hue image. For more complex stimuli, we found it useful to steer the line fit by means of per pixel weights. We modify Eq. (5.3) and get:

$$\operatorname{argmin}_{a,b,c} \sum_{i=0}^{N-1} w_i^2 \left\| \tilde{\mathbf{E}}_i \right\|^2, \quad (5.6)$$

where the per pixel weights  $w_i$  have been included. The weights could for example be proportional to saturation or luminance of the corresponding pixels. To create convincing results for natural images the method can be further refined by using a segmented backlight with individually controllable primaries. The

proposed method can in that case be applied directly in a block-wise fashion. However, when the backlight consists of individually controllable LED triplets, the backlight will suffer from optical cross-talk. In effect, the computed optimal backlight color may deviate from the realised color. Consider a single field of a display system with  $Q$  backlight segments and  $N$  pixels, then the tri-stimulus output values,  $q_i$ , stacked into columns of the  $3 \times N$  matrix  $\mathbf{Q}$ , relates to the drive levels as follows:

$$\mathbf{Q} = \mathbf{A} (\mathbf{H} \mathbf{D}_0)^T \mathbf{P}_0, \quad (5.7)$$

where  $(\mathbf{p}_0 = \text{diag}(p_0 \dots p_{N-1}))$  are the LC-panel drive levels and  $\mathbf{D}_0$  is a  $Q \times 3$  matrix of backlight triplet drive levels. The  $N \times Q$  matrix  $\mathbf{H}$  is the cross-talk matrix with entries corresponding to the relative contribution of a segment to a pixel. By definition the row-sum of  $\mathbf{H}$  equals one. In order to explicitly include the optical cross-talk into the computation of the local primaries one could for example make use of linear programming, as proposed in (Li *et al.*, 2007a). This is computationally expensive and we therefore propose a pragmatic approach of emphasising surrounding pixels from adjacent backlight segments into the optimisation of Eq. (5.6) and to weigh pixels farther away less according to the point-spread function of the backlight. Lastly it is worth noting, that due to the limited contrast of an LC-panel and referring to the problem of optical cross-talk, it is advantageous to reduce the intensity of the backlight primaries to a minimum. The assumption of unity-luminance used in Eq. (5.4) can result in bright primaries. To reduce the intensity of the primaries one can use Eq. (5.5) to compute the LC-panel drive levels, determine the local maximum drive level, and scale the intensity of the corresponding backlight segment accordingly. A disadvantage of this is the need to re-evaluate Eq. (5.5) after scaling the intensity of the backlight segments.

## 5.5 Results

### 5.5.1 Simple Images

For the image of Figure 5.1(a) we have computed the optimal primaries using Eq. (5.3) for a system with a global-addressable backlight. The computations are based on CIE 1976  $u'v'$  chromaticity coordinates. The result is depicted in Figure 5.3(a) and the reproduced chromaticity in Figure 5.3(c). Notice how the reproduced chromaticity points resemble the original of Figure 5.1(c). The local primaries have also been desaturated to the shortest possible line segment without introducing clipping. The primaries are represented by blue crosses in Figure 5.3(c). Similar, the optimal primaries have been computed for the yellow-white image of Figure 5.1(b). The resulting image is depicted in Figure 5.3(b) and the reproduced

chromaticity shown in Figure 5.3(d). Notice how the image appears colorful, unlike the image in Figure 5.2(b). Also notice the resemblance of the reproduced chromaticity points with the original chromaticity of Figure 5.1(d).

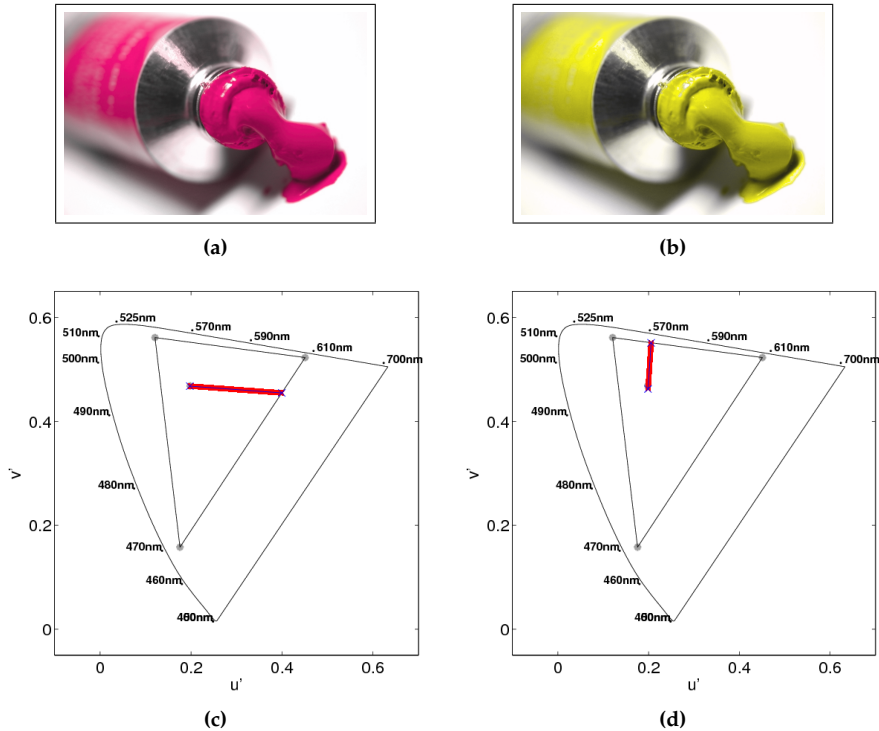


**Figure 5.3:** Simulated output of the images in Figure 5.1(a) and Figure 5.1(b) is shown in (a) and (b), respectively. The two primaries are established by minimising color error using total least squares. In (c) and (d) the corresponding output chromaticity is shown.

### 5.5.2 Complex Images

The distribution of chromaticity in the simple images of Figure 5.3 can easily be approximated by a line. For more complex stimuli, it is necessary to choose the chromaticity of the primaries wisely. Consider the image of Figure 5.4. The oranges are red and orange, while the background is dominantly white. This leads to poor results if we apply Eq. (5.3) directly, as can be seen in Figure 5.4(b). The chromaticity points of the input image (red-dots) are depicted together with the chromaticity of the primaries (blue-crosses) in Figure 5.4(e). Note how the red oranges are in the wrong tint and that the white background appears yellowish. If we apply weights to the optimisation of Eq. (5.6) proportional to intensity, in this case luminance, of the pixels, the result is very different. Observing Figure 5.4(c)



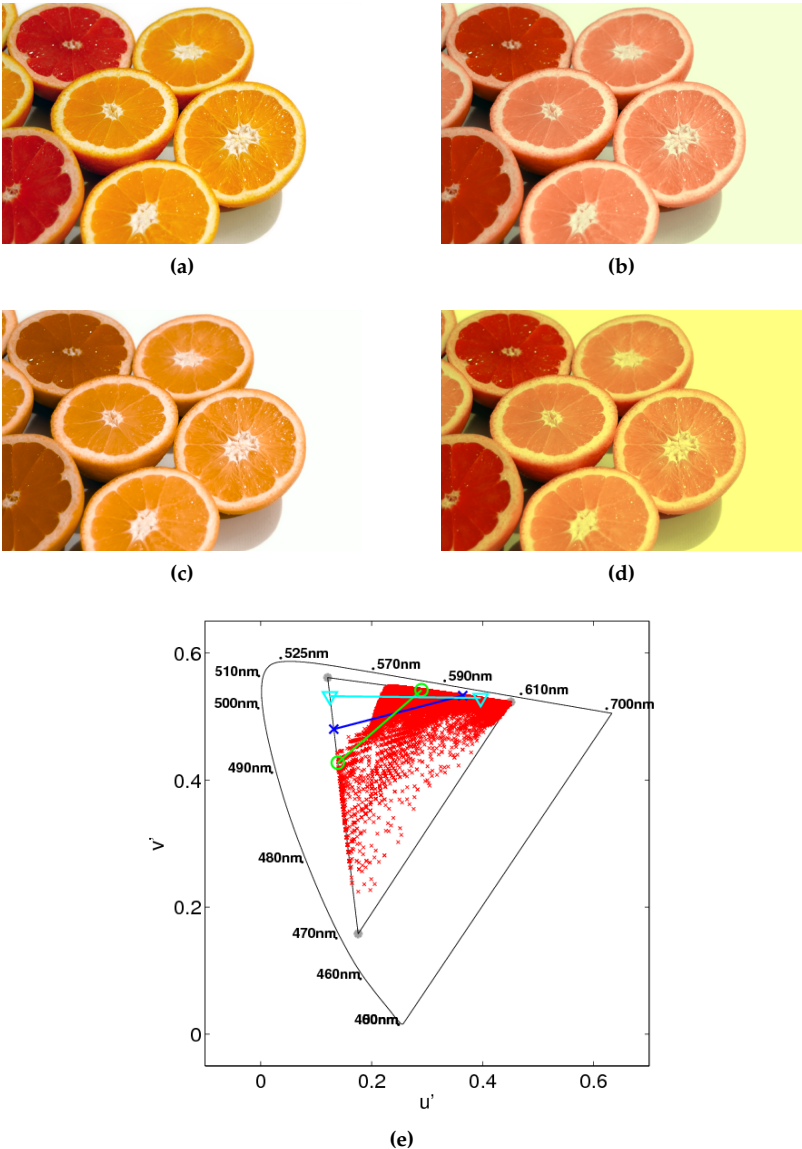


**Figure 5.4:** The simulated output of input image (a) has been processed with no-weight (b), intensity-weight (c), and saturation-weight (d). The corresponding chromaticity of the primaries (e) is shown in blue crosses, green circles, and cyan triangles, respectively.

one notices how the white background appears correct, however, the red oranges have turned yellow. The chromaticity of the primaries based on intensity weighting is shown in Figure 5.4 (green-circles). The result of applying saturation as weight for the optimisation is shown in Figure 5.4(d). For simplicity we used the following definition for saturation,  $[\max(\mathbf{q}) - \min(\mathbf{q})] / \max(\mathbf{q})$ , where  $\mathbf{q}$  is an RGB input triplet. The corresponding chromaticity of these primaries are shown in Figure 5.4 (cyan-triangles). Notice how the red and yellow oranges appears correct, but the white background has turned yellow-orange.

The sparse chromaticity distribution of the test images, which lends itself for approximate color reproduction by a chromaticity line, is not common to natural images. However, as it turns out, small segments of images contains smaller, more local chromaticity distributions, which can be approximated by a chromaticity line. In the following we apply the described optimal two-primary method to a system with a locally addressable backlight.

### 5.5.3 Natural Images

To illustrate the performance of the proposed optimal two-primary system, a number of images have been processed. We initially assumed a backlight segmentation of  $(y,x) = (9 \times 16)$ . Further the segments are characterised by a Gaussian light distribution. The panel is assumed to be ideal in terms of temporal and electrical response, and the backlight primaries correspond to the ITU Rec. 709 color primaries. An image with skin tones, shown in Figure 5.5(a), is used as input. The simulated output, shown in Figure 5.5(b), corresponds very well to the input in terms of color. The input image is seen to be dominated by desaturated colors. The backlight light distribution of field 1 and field 2 is shown in Figure 5.5(c) and Figure 5.5(e), respectively. It can be seen to consist of red, white, and cyan.

The difference between the input and the reproduced image is shown in Figure 5.5(d) and is expressed in  $\Delta u'v'$ . The color error is seen to be low. The largest color error around 0.040 appears in the eyes of the females. This is mainly due to a greenish tinted eye color. If watched without reference image, the output image seems correct. The error in the hair of the left female is due to the low intensity not perceivable. The results in terms of color error indicate that this type of natural image is suitable to be reproduced with already 144 segments. In Figure 5.6(e) a different input image is shown. The image contains many saturated colors and sharp color edges. This represents a very critical image to be reproduced by two local primaries. The simulated output, assuming  $(9 \times 16)$  backlight segments, is shown in Figure 5.6(b) and the backlight of field 1 and field 2 is shown in Figure 5.6(a) and Figure 5.6(d), respectively. The output image generally resembles the color impression of the original.



**Figure 5.5:** The input image (a) is described using the concept of optimal primaries and  $(9 \times 16)$  segments, shown in (b). In (c) and (e) the backlight of field 1 and field 2 is shown. The resulting color error map in  $\Delta u'v'$  is shown in (d).

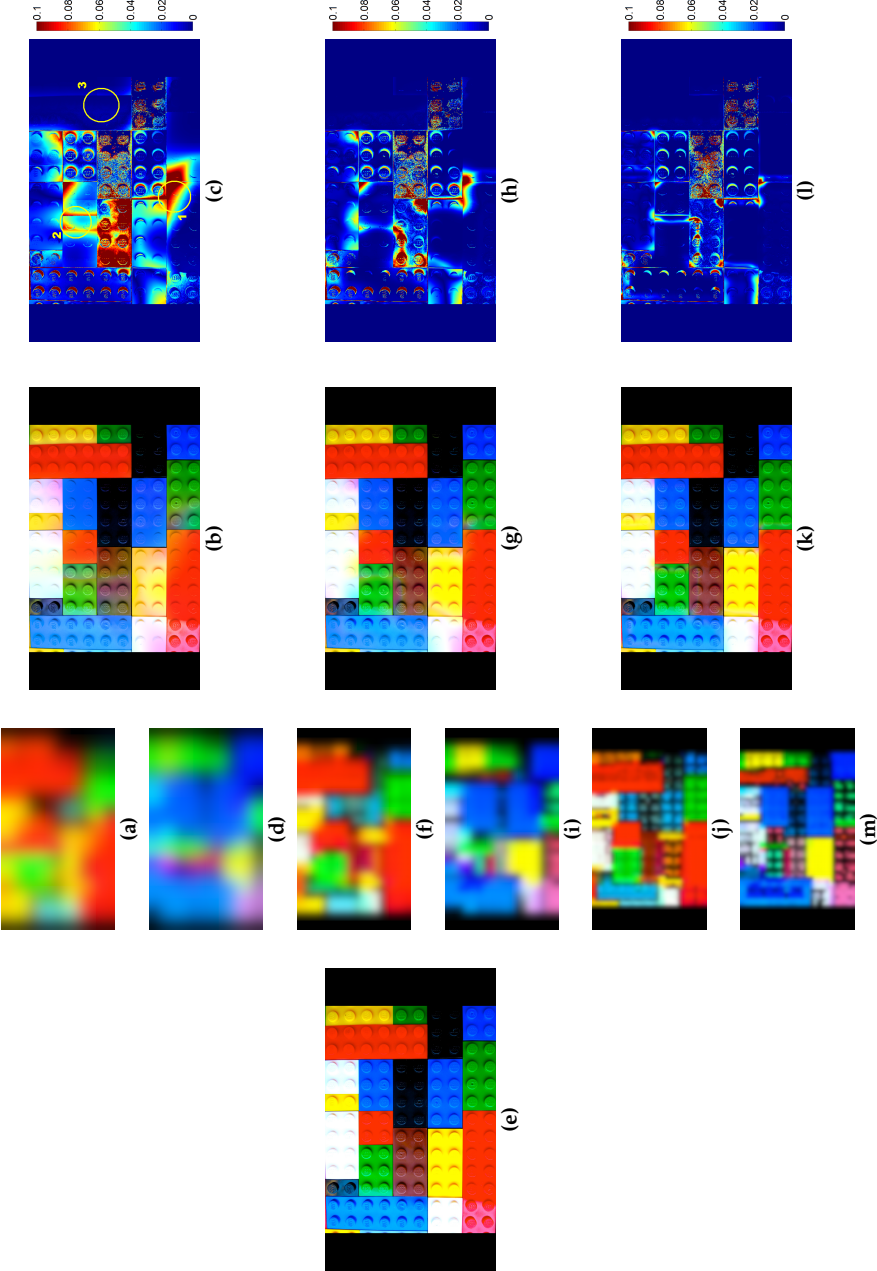


**Figure 5.6:** Simulation results of processing the input image (e) with 144 segments, (b), 576 segments, (g), and 2304 segments, (k). In the second column, the backlight of field 1 and 2 is shown. In the fourth column, the color error maps for the respective backlight divisions are shown.

However, the color error is seen to be very large for this image, shown in Figure 5.6(c). Some image regions even have errors larger than 0.1 in  $\Delta u'v'$ . In the color error map, three regions have been highlighted and marked (1), (2), and (3). These regions mark boundaries between three or more blocks. Due to the restriction of two primaries, the color reproduction near these edges can be very poor. For example, for (1) a blue-yellow and a red block are co-located. As the red block is not on the blue-yellow chromatic line, the red color appears rather yellow close to the boundary of the block. Similar for (2) where a green, red, and white block meet. The backlight primaries are not red, green, or white at this location, but rather yellowish-red and cyanish-green. This gives rise to a color error for both the red and the green block, while the white block can be reproduced correctly in terms of color, due to the fact that color mixing of field 1 and field 2 can yield white. For region (3), at the intersection of a red, green, and yellow block, the color error is below the threshold of visibility. The difference with region (1) and (2) is that red, green, and yellow lie on a line in the chromaticity space. It can therefore accurately be represented by two primaries, creating yellow as a mixture of the red and the green field. As it is expected that more backlight segments will lead to a reduction in color error for a local two-primary display system, we have repeated the simulation for different backlight segmentations. The image of Figure 5.6(e) has been processed with 144 ( $9 \times 16$ ), 576 ( $18 \times 32$ ), and 2304 ( $36 \times 64$ ) segments. The results of these simulations are shown in Figure 5.6. As the granularity of the backlight increases, the color errors are clearly reduced. The backlight of field 1 and field 2 (second column of Figure 6) also show how the correlation between the backlight color and the input image increases with more segments. In the color error map of Figure 5.6(l) (2304 segments), color errors above the visibility threshold are still present. However, these are all located at the edges of the blocks, or in black regions. The examples above have highlighted how the performance of the proposed two-field mode depends on the image and on the amount of backlight segments. In the following section, we report a statistical experiment to investigate the relationship between the number of backlight segments and color error across a large video data set.

## 5.6 Statistical Justification

The goal of the experiment is to statistically justify a local two-primary system with respect to color reproduction of natural video data. We do this, by computing the color error across a large set of video data. Further, the relationship between color error and backlight segmentation is investigated in order to determine the needed effective backlight color resolution. In the following experiment we have intentionally not included any display characteristics, rather we have assumed an ideal temporal display response and an ideal backlight separa-

tion, i.e. light distribution are square, non-overlapping blocks. This allows us to evaluate the amount of needed segments in the context of the video source. Of course for a realistic system with certain amounts of light cross-talk between the backlight segments, the results will be worse.

Table 5.1: Backlight segmentation in the experiment.

Case	#Segs.	Vert.	Horz.	Coverage
1	1	1	1	100.00%
2	28	4	7	3.60%
3	144	9	16	0.70%
4	576	18	32	0.17%
5	2304	36	64	0.04%
6	9216	72	128	0.01%

The starting point of the experiment is a video data set collected for IEC 62087 (IEC, 2008) and originally intended to investigate the power consumption of domestic video equipment. The video data is a collection ranging from news to cartoons, scenery to action movie. The sequence contains 17988 frames corresponding to approx. 10 minutes of video (resolution: 480 lines). The duration of the scenes in the collection varies from 30 to 40 frames.

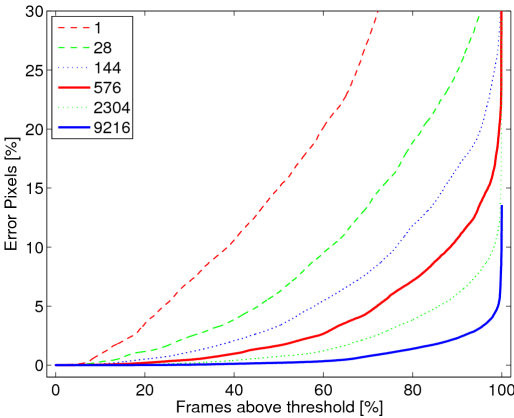


Figure 5.7: Results from statistical experiment on IEC 62087 video sequence. On the vertical axis, the averaged number of pixels per frame with a color error  $\Delta u'v' > 0.020$ . The horizontal axis shows the relative amount of frames above the color error threshold.

The experiment was carried out as follows: 1) each frame was divided into a number of fixed segments; 2) using total least squares, the chromaticity of the pixels for each segment was approximated by a line in CIE 1976  $u'v'$  and without weight; 3) the color error, expressed in  $\Delta u'v'$ , was computed for each segment. As a result, the per-pixel color error for all frames and all segments is obtained. To reduce the data set, we counted the amount of pixels within a frame with a

color error  $\Delta u'v' > \mathcal{E}$ , where  $\mathcal{E}$  is a color-error visibility threshold. For pixels with  $\max(R, G, B) < 4$  (gamma domain), the color error was reduced by means of a weighting function. Black was excluded from the color error computation. The experiment was repeated for a backlight segmentation  $(y, x)$  of  $(1 \times 1)$ ,  $(4 \times 7)$ ,  $(9 \times 16)$ ,  $(18 \times 32)$ ,  $(36 \times 64)$ , and  $(72 \times 128)$ . The six different segmentations are summarised in Table 1. The vertical and horizontal division is tabulated together with the total number of segments. The display coverage per segment is shown in the right-most column. The results of the experiment are summarised using a percentile plot in Figure 5.7. We have set a visibility threshold of  $\Delta u'v' > 0.020$ . On the vertical axis, the relative number of pixels with a color error above the visibility threshold within a frame. If the data can be represented by a two-primary system, only few pixels are above the color error visibility threshold. Ideally, the result would be a flat line at 0%. The more frames that can be represented with few pixels with color error, the better. The results clearly illustrates that more segments is beneficial for reducing color error. For example, for 576 segments (case 4, red-solid) 15.8% of the frames can be represented with maximum 0.1% pixels above the color error visibility threshold ( $\Delta u'v' > 0.020$ ). With 2304 segments this is 24.2% of the frames and for 9216 segments 38.5% of the frames. The reasoning behind the backlight segmentation is found in the characteristics of natural scenes. Based on similarity of color, scenes can be segmented into a finite number of super-pixels or objects (Omer and Werman, 2004). Such a representation is possible considering segments of any size and shape. In this experiment the size, shape, and location of the segments is fixed. When several objects of different color appear within a segment, color errors may appear. It is therefore expected that more segments would lead to a reduction in color error. This is indeed confirmed by the data shown in Figure 5.7. Assuming 9216 segments, 38.5% of the frames can be represented with maximum 0.1% pixels with visible color errors per frame. Allowing more color errors per frame, the amount of correct frames rises to 74.2% (1.0% error pixels) and to 99.2% (5.0% error pixels). For an image resolution of  $1920 \times 1080$  pixels, each segment will cover 225 pixels. We can therefore conclude that using two primaries on a local basis can result in reasonable color reproduction. Dividing a backlight into more segments comes at a higher cost due to more LEDs, more drivers and wiring, and more expensive processing. As the number of frames with few visible color errors increases with more segments, the trade-off between color errors and display cost is important. Considering current display products with local dimming, we choose 576 segments as a balanced choice. With 576 segments, 40.5% of the frames can be represented with 1.0% or less pixels per frame exhibiting visible color errors. For higher quality, i.e. maximum 0.1% pixels per frame with color error, the number of frames reduces to 15.8%. While this result is disappointing, it is important to relate the results of this quantitative study to the perceptual quality of image output. For example, consider the critical image of Figure 5.6(e) and compare this with the simulated

output of a two-field system with 576 segments as shown in Figure 5.6(g). The image generally appears colorful compared to the original, although color errors can be noticed along the edges of some blocks.

## 5.7 LCD Demonstrator

Based on the described 2-field color-sequential display concept we have built a display demonstrator. It consists of a 40" LC-panel operating at 120 Hz in combination with a segmented backlight. Each of the 1032 segments consists of an RGB LED triplet. The backlight is operated in a scanning fashion as to reduce temporal cross-talk.



**Figure 5.8:** To demonstrate the concept, a 120 Hz two-field color-sequential display has been constructed. Shown is a colorful test image (a) and a photograph of the display (b).

For the computation of the local primaries we used the CIE 1976  $u'v'$  chromaticity coordinates and a saturation-weighted optimisation Eq. (5.6). To implicitly account for the optical cross-talk between segments, a small surround of pixels corresponding to the 9 neighbouring segments - was included in the computation as proposed in the Methods section. A photograph of the display demonstrator showing a colorful image is shown in Figure 5.8(b). Compared to the input image, Figure 5.8(a), the display appears desaturated. This is due to the photograph and not the actual demonstrator, which is effectively wide-gamut. Compared to a monitor with primaries according to Rec. 709, the photographed display appeared more saturated.

## 5.8 Discussion

Obtaining the two optimal local primaries by minimising the chromaticity error in  $\Delta u'v'$  could be sub-optimal from a perceptual point of view. First of all be-



cause intensity is largely excluded from the optimisation. Secondly because the human perception of color is more complex than discriminating colors. The proposed method assumes a full-reference comparison. However, one could argue that true-color reproduction need not be the goal in all display applications. It is important to maintain spatial and temporal consistency in terms of color and intensity. For example, objects of constant color could be reproduced with constant, although changed, color. Combining local (varying) color mapping using image segmentation in combination with the two-primary optimisation might be a solution to this. We have consistently chosen to report the color error in  $\Delta u'v'$  as this corresponds to the optimisation criteria for determining the local primaries. However, as intensity is a very important aspect of color perception, it might be useful to re-evaluate the simulation results using a method sensitive to intensity. For example using the method described by Johnson and Fairchild (Johnson and Fairchild, 2003), which also further includes the spatial acuity of the human visual system. Based on the statistical experiment, we conclude that it is indeed possible to represent data with two local primaries, providing that the backlight is divided in sufficient segments. However, it is worth noting that the optical cross-talk between segments will change the local primaries and can therefore reduce the quality of the color reproduction. If the light distribution of a segment is very local, this reduces cross-talk, however, a wide light distribution might be beneficial for fast color transitions. Finally, for a display system, the finite contrast of the LC-panel should be taken into account. In this experiment, we have neglected the fact that the black level is in reality colored according to the local primaries. The visual effect of a locally varying color in the black level should not be underestimated. While it is expected that a two-primary color-sequential system will suffer less from color-breakup effects than, for example, a three-primary color-sequential system, this has to be investigated and perceptually validated.

## 5.9 Conclusions

In this paper, we have discussed a local two-primary display system operating in color-sequential mode at 120 Hz field rate. As it uses no color filters, the system is very power efficient, yet the field rate is lower than for full color-sequential displays with a field rate of 180 Hz or higher. The method is based on choosing two local primaries according to minimum chromaticity error using total least squares. In this sense the proposed method outperforms existing methods, which was demonstrated for simple imagery. For complex stimuli, a variation on the method was proposed which is based on a modified cost function using weighed chromaticity. By a statistical experiment we have shown that the more backlight segments, the better natural images can be approximated with a local two-primary system. For 576 backlight segments a local two-primary system can

represent 40.5% of the frames with maximum 1.0% pixels per frame above the threshold of visibility ( $\Delta u'v'$  of 0.020). With 9216 segments this is true for 74.2% of the frames. Simulation results of the front-of-screen performance validated the result of the statistical experiment. In contrast to common belief good color reproduction can be achieved with only two local primaries, provided that more than 9216 backlight segments are used. With fewer backlight segments, the method may lead to visible color errors and is not suitable for display applications requiring high-quality color reproduction. As a low-power mode or in particular applications, such as airport and train station signage, the method may be very well suited.

# Display Contrast Requirements Based on Human Eye Glare

## Abstract

Static contrast in LCDs can be improved by using local dimming backlight techniques, but it is still orders of magnitude lower than that of OLED. However, glare in the human eye limits the visible contrast and suggests that a very high contrast is not required. In this paper we estimate how much contrast is actually required in a display and compare that with today's OLEDs and local dimming LCDs.

## 6.1 Introduction

For years, the contrast in LCDs was much worse than that in emissive displays such as PDPs, CRTs, and OLEDs. Recently, local dimming backlights have been developed and brought to market that improve the contrast of LCDs considerably. In this technique, the backlight is divided into segments that can be dimmed individually. This improves the dynamic contrast (i.e. between different images) and the static contrast (i.e. within a single image), but only for the lower spatial frequencies (Langendijk, Muijs, and Beek, 2007; Langendijk, Muijs, and Beek,

---

Reproduced from EHA Langendijk and M Hammer (2010). „Contrast Requirements for OLEDs and LCDs Based on Human Eye Glare”. In: *Digest Tech. Papers SID*. vol. 41, pp. 192–194.

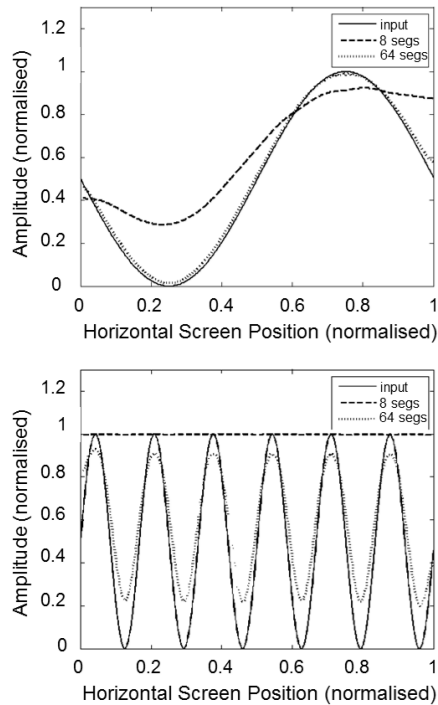


**Figure 6.1:** Reproduction of a sinusoidal test pattern with 1 (top panel) and 6 (bottom panel) cycle/screen for a backlight with 8 (dashed lines) and 64 segments (dotted lines). Adopted from (Langendijk, Muijs, and Beek, 2007).

2008). The dynamic contrast in high-end LCDs with local dimming backlights is on par with the before mentioned emissive display techniques. The static contrast in today’s LCDs, however, is not.

In (Langendijk, Muijs, and Beek, 2007) and (Langendijk, Muijs, and Beek, 2008), we showed that the static contrast in an LCD with local dimming backlight decreases exponentially with increasing spatial frequency of the image content. In Figure 6.1, for example, a spatial sinusoid with 1 cycle per screen width could be reproduced almost perfectly using a local dimming backlight with  $64 \times 36$  segments (horizontal  $\times$  vertical). Yet, for 6 cycles per screen width, the reproduction starts to deviate from the input and with 8 segments the backlight cannot follow the modulation of the input anymore and the contrast gain of the local dimming feature disappeared.

Although, we can now predict quite accurately what the static contrast is as a function of spatial frequency in both emissive displays and local dimming LCDs, the question remains what static contrast is actually required in a display. Or in other words, what is the maximum spatial luminance variation that a viewer can distinguish within a certain image and what is the maximum spatial luminance

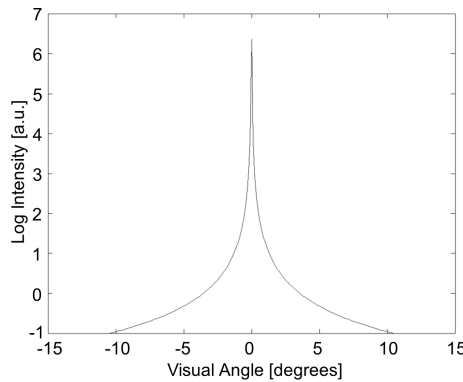


**Figure 6.2:** Glare as a function of visual angle

variation that a display can make? The objective of this study is to answer these questions and to apply this knowledge to LCDs with different numbers of local dimming backlight segments and to OLED displays.

## 6.2 Methods

The main factor that influences the maximum visible luminance variation within an image is the scattering of light in the human eye (Vos and van den Berg, 1999; Spencer *et al.*, 1995; Seetzen, Heidrich, *et al.*, 2004; McCann and Rizzi, 2009). This is called “glare”, and can be described by the glare function or point spread function (PSF) suggested by Vos (Vos and van den Berg, 1999) and plotted in Figure 6.2. The glare function illustrates the spatial smear of light across the retina.

In order to simulate how an actual image appears on the retina of a human eye, we convolved the input image using this glare function for a 42” display and a viewing distance of 3 times the height. For simplicity, we only considered the luminance channel. We also simulated the front-of-screen performance of an LCD display with  $8 \times 5$ ,  $16 \times 9$ ,  $32 \times 18$ ,  $64 \times 36$ , and  $128 \times 72$  backlight segments with quadratic Lorentzian shaped segment profiles and a panel contrast of 1000:1. As ideal reference display we took an OLED display with a static contrast of 1000000:1 for all spatial frequencies. Typically OLED displays are claimed to have such a high static contrast.

In order to better predict how well the visible luminance variations can be reproduced with a certain display, we also calculated the visible contrast and the display contrast as a function of the spatial modulation frequency. For that we simulated the luminance variations for images showing a spatial sinusoid with different cycles per screen width in the range from 1 to 24. Because the eye glare

depends on the object size we considered two extreme conditions. In the "minimum" glare condition, the sinusoidal variation was one pixel high (e.g. a line across the middle of the screen). In the "maximum" glare condition the sinusoid was as high as the screen height. Of course, even more extreme glare conditions can be defined, but the two presented here are expected to cover most natural image content. Figure 6.1 shows a cross-section for 1 and 6 cycles per screen width. The contrast ratio was calculated by dividing the maximum luminance and the minimum luminance in the image.

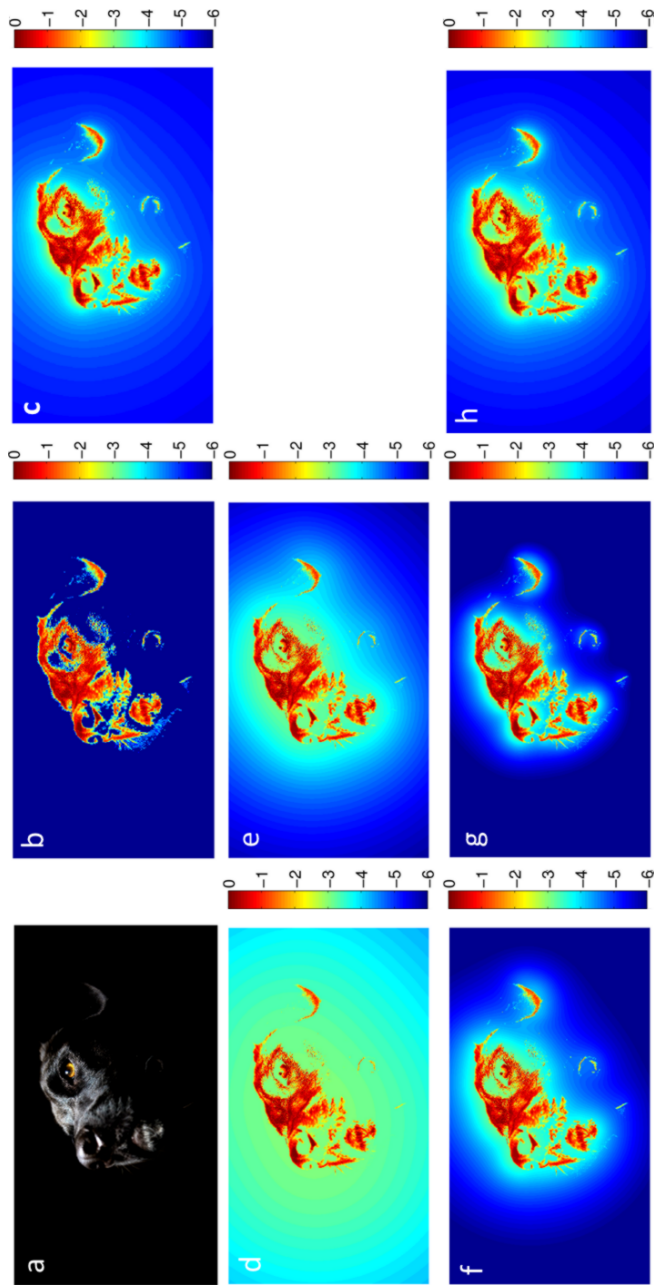
## 6.3 Results

Figure 6.3 illustrates the effect of glare and of local dimming for the Dog input image. The top left panel shows the normalized luminance variation of the Dog input image as it would be rendered on an OLED display. The top right panel shows the convolution of this image with the glare function and therefore illustrates the retinal image of the OLED display. Notice that the retinal image has a halo around the head and has less modulation depth within the head.

The middle and bottom panels of Figure 6.3 illustrate the luminance rendering in an LCD with local dimming backlight with different numbers of segments. With  $8 \times 5$  segments the LCD produces a much larger halo than the glare does and also the modulation depth in the head is lower. Increasing the number of backlight segments reduces the halo and increases the modulation depth of the rendered image, but even with  $128 \times 72$  segments the LCD cannot reproduce the exact luminance variations of the OLED. However, if human eye glare is included, the retinal image of the OLED and that of the LCD with  $128 \times 72$  backlight segments, are virtually the same (compare image c and h in Figure 6.3), and the perceived contrast in both displays is expected to be the same.

Figure 6.4 shows a cross-section of a selection of the images from Figure 6.3. It illustrates that LCDs with local dimming backlight can follow the high-frequency modulation up to a contrast of 1000 : 1, which is the panel contrast. With  $8 \times 5$  segments up to 1 order of magnitude is gained in static contrast especially towards the edge of the image, but the black level is still a few orders of magnitude higher than the visible black level. With  $64 \times 32$  backlight segments an LCD is still orders of magnitude higher in black level than an OLED display, but it is below that of the retinal image ("Display + Glare") suggesting that the perceived contrast in both displays will be the same.

In order to generalize the results, we plotted the static contrast ratio as a function of the spatial modulation frequency for an ideal display with human eye glare and the various LCDs with local dimming backlights. The results are shown in Figure 6.5. It illustrates that both the local dimming LCDs as well as the retinal



**Figure 6.3:** Illustration of the effect of human eye glare and of local dimming for the Dog input image (a). Panels show normalized log luminance of input image (b), input image with human eye glare (c), input image as shown on LCD displays with 8 × 5, 32 × 18, 64 × 36 and 128 × 72 backlight segments and 1 000 : 1 panel contrast (d-g, respectively), and “128 × 72” LCD with glare (h).

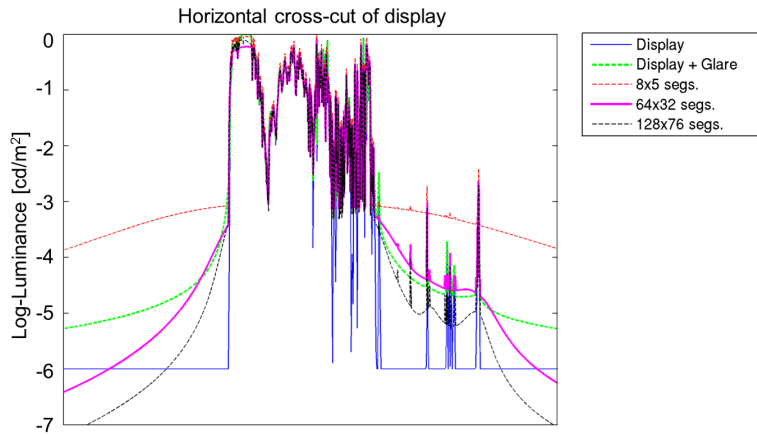


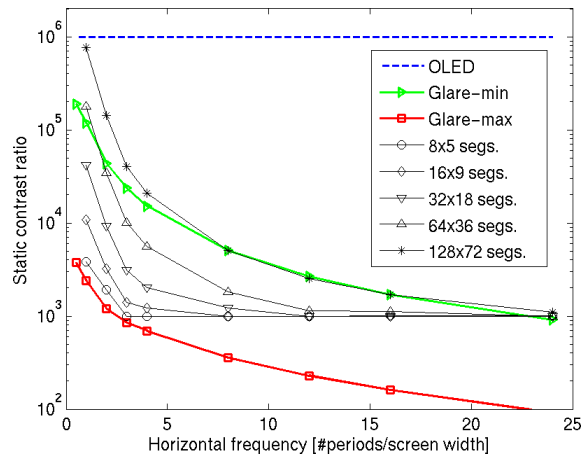
Figure 6.4: Cross-section of a selection of the images (b, c, d, f, g) from Figure 6.3

image of an ideal display have an exponentially decreasing contrast ratio. Yet, for the lowest modulation frequencies (1 and 2 cycles) more than  $64 \times 36$  back-light segments are required in the LCD and for the mid frequencies (3-16 cycles) almost  $128 \times 72$  segments are needed to be even better than the "minimum glare" condition. For the "maximum glare" condition  $8 \times 5$  segments is sufficient for all modulation frequencies. Above 16 cycles per screen width, the retinal contrast drops below the panel contrast (1000:1) indicating that for the higher spatial modulation frequencies typical LCDs without local dimming can already make sufficient contrast.

## 6.4 Discussion

In the present study, we assume that eye glare is the major cause of a reduction in the perceived contrast when looking at high contrast images. Other effects, like adaptation to the average luminance level, are ignored, because they are said to have less of an effect than the eye glare (Vos and van den Berg, 1999; Spencer *et al.*, 1995). The eye glare is caused by a number of different mechanisms, such as scattering in the cornea, lens, and retina, and diffraction in the coherent cell structures on the outer radial areas of the lens (Spencer *et al.*, 1995). These mechanisms can have different effects, such as bloom or "flare lines". In our model we only take the bloom for photopic vision (adaptation to luminance above  $3 \text{ cd/m}^2$ ) into account as described by Vos (Vos and van den Berg, 1999). Our study shows that eye glare has a large impact on the perceived contrast as is also indicated in the literature (Vos and van den Berg, 1999; Seetzen, Heidrich, *et al.*, 2004; McCann and Rizzi, 2009). On top of that it shows that high contrast is only required for lower spatial frequencies in an image and it quantifies the required static contrast as a function of the spatial modulation frequency.





**Figure 6.5:** Static contrast ratio as a function of modulation frequency. The "Glare-min" and "Glare-max" curves indicate the contrast of an ideal display with minimal and maximal eye glare as described in the text. The other curves indicate the contrast of local dimming LCDs with different numbers of backlight segments as indicated in the legend.

The present study ignores the effects of ambient illumination. In other words the results hold for a completely dark room. Under normal TV viewing conditions, with typically 50 lux ambient illumination, both the glare and the display contrast will be affected. For the display it will mainly depend on the amount of light that falls on the display and the reflectivity of the panel. Typically the reflected light will add a constant luminance to the black level independent of the image content or the number of segments in the backlight. The perceived glare will be effected by the amount and the spatial distribution of the ambient light in the room.

## 6.5 Conclusions

In the present study we investigated the effect of human eye glare on the perceived contrast and predicted how much contrast is actually required for a display. The results show that the contrast of a conventional LCD is not sufficient to accurately represent a high contrast image. An OLED display, on the other hand, makes more than sufficient contrast, even much more than can be seen in natural images. LCDs with local dimming functionality can make just enough contrast provided that they have enough backlight segments. Typically an LCD with  $16 \times 9$  backlight segments will be sufficient for the majority of images and with more than  $64 \times 36$  segments, virtually all images can be represented with sufficient contrast given the fact that the Dog image is a very critical image for contrast.



# What About OLED Displays?

The problem statement of this thesis is limited to LCDs, which is by far the most used display technology at this moment. However, with the recent introduction of OLED displays, a new display technology might take over this leading role in the next decade. As OLED displays are emissive and in principle capable of very high contrast and luminance, such displays may be attractive for HDR image reproductions.

## 7.1 Introduction

Whereas the contrast characteristics of OLED displays exceed those of most other display technologies the luminance is still lower than that of LCDs (Section 2.6.4). The light output of an OLED display is i.a. limited by low efficacy of the OLED materials, poor light extraction from the OLED emitter due to difference in refractive indices, and resistive losses in the active-matrix backplane. Energy losses generally lead to an elevated emitter temperature and consequently accelerate luminance depreciation (over time). As large-sized OLED displays have only recently been commercialised, the next decade is likely to bring several improvements on light output. Meanwhile, it is necessary to consider alternative methods in order to maximise light output.

In this chapter, an early-stage study showing experimental data of luminance and thermal characteristics of some OLED displays is reported. The data suggest that by using thermal management, it is possible to increase the light output of OLED display devices. Contrary to the previous chapters of this thesis, the results are at an early stage and should be seen as an indication of an interesting direction of future research, rather than a finished piece of work.

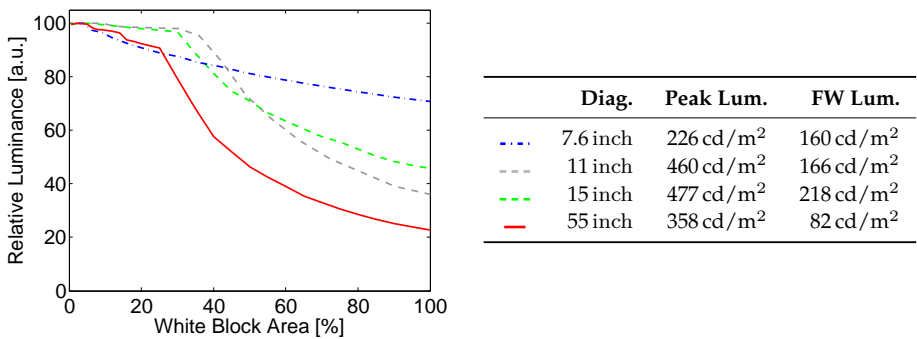


**Figure 7.1:** Measured relative luminance of a white block on four OLED display devices against area of the measured white block on a black background. The tabulated peak and full-white (FW) luminance illustrates that a larger display size results in a large decrease of luminance as the block size increases.

## 7.2 Observations of OLED Display Luminance

The luminance of state-of-the-art large-sized OLED displays is lower than that of LCDs. Nam *et al.* (2013) and Yoon *et al.* (2013) reported a 55 inch OLED display with 450 cd/m<sup>2</sup> peak luminance and Chen, Lin, *et al.* (2013) reported a 65 inch OLED with 200 cd/m<sup>2</sup> peak luminance. In comparison, the luminance of a conventional LCD is around 500 cd/m<sup>2</sup>, but it can be much higher. Contrary to the luminance of an LCD, the luminance of an OLED display is very image dependent. The luminance of images with many bright pixels is lower than the luminance of images with only a few bright pixels. For example, the 55 inch reported by Nam *et al.* (2013) shows a full-white luminance of merely 100 cd/m<sup>2</sup> (cf. to 450 cd/m<sup>2</sup> peak luminance).

In order to characterise the image-dependent luminance of an OLED display, an image with a white box of varying size on a black background was used (ICDM, 2012). In Figure 7.1, the relative luminance level is shown as a function of the area of the measured white block on four OLED displays. In the legend (right), the display diagonal, the peak luminance (0% area), and the full-white (FW, 100% area) luminance of each measured display is tabulated. It can be seen that the full-white luminance is about 30% to 80% lower compared to the peak luminance. The relative luminance of the measured displays is characterised by a short section of constant luminance, followed by a decrease of luminance with increasing white block area. This behaviour is also known from CRTs and plasma displays.

The characteristic behaviour shown in Figure 7.1 is probably introduced in order to prevent, or at least reduce, the presence of visible artefacts. When operating an OLED display, luminance depreciation and increase of threshold voltage

can be observed over time (Lee, Liu, and Wu, 2008). This is caused by intrinsic degradation of the organic layer and leads to visible variations of luminance. The degradation is even accelerated by increased temperature or increased current density (Ishii and Taga, 2002). Bright pixels (high current density) will therefore more quickly lead to visible luminance variations than dark pixels (low current density).

The reduction of full-white luminance compared to peak-luminance is relatively larger for large-sized displays than for small-sized displays, as can be seen in Figure 7.1. This can be explained by two effects. Firstly, the resistive losses in the long supply-lines of large-sized OLED displays will cause a larger voltage drop, which results in luminance non-uniformity and can be compensated by an increase of voltage (and increase of losses) (van der Vaart *et al.*, 2005; Lu *et al.*, 2008). In order to prevent losses, one can limit the maximum peak current by lowering the luminance when a large number of bright pixels is present, as shown in Figure 7.1. Secondly, studies have shown that the temperature rise of large-sized OLED displays will be substantially higher than that of small-sized OLED displays (Sturm, Wilson, and Iodice, 1998; Lu *et al.*, 2008). As the distance from the centre to the non-active area of a small-sized OLED display is small, the heat conduction is consequently relatively efficient (Lu *et al.*, 2008). For a large-sized OLED display, where heat dissipation is largely accomplished by convection and radiation, the operational temperature will therefore be higher than for a small-sized display. An elevated temperature will accelerate luminance depreciation. It is therefore necessary to limit the light output relatively more for large-sized displays, than for small-sized displays.

Besides the area-dependent luminance characteristic shown in Figure 7.1, the luminance of an OLED display is typically also reduced over time for static images. This is also done to prevent luminance non-uniformity. When only a few bright pixels are present, it is our experience that the light output is kept constant for about 1-2 minutes followed by a gradual reduction of luminance. For images with many bright pixels, the reduction over time is typically minimal as the initial luminance is already relatively low.

In this chapter, we will focus on the area-dependent luminance characteristic. As discussed, scientific literature indicates that this characteristic is introduced in order to prevent high current density and high operational temperature. In the following section we will focus on thermal aspects of OLED displays.

## 7.3 Observations of OLED Display Temperature

The temperature of an OLED display during operation depends on the dissipated heat (by the image) and the thermodynamic characteristics of the display unit. In

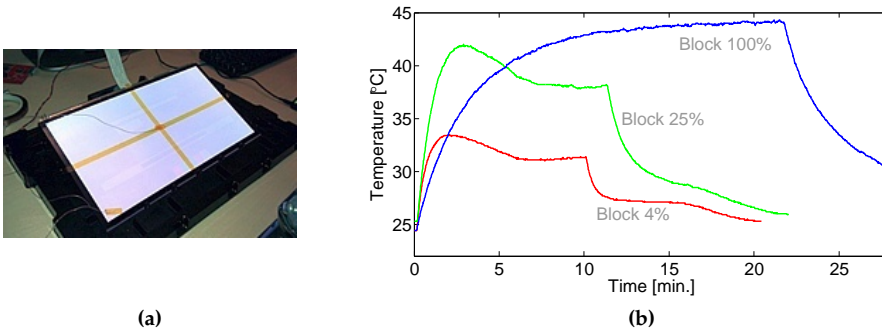


**Figure 7.2:** In (a), a photograph of an OLED device showing a full-white image. Using imaging thermography, the surface temperature was recorded during operation while a white block of 100% coverage was shown. A thermocouple was connected to the centre of the display and the resulting temperature is shown in (b) for three block sizes. The panel is switched on at  $t = 0$  and switched off after 10-20 minutes. Notice that steady-state temperature is dependent on block area.

order to better understand how the temperature of an OLED display changes over time, it was decided to conduct a small set of experiments.<sup>1</sup>

A 15 inch OLED unit without casing was used. The OLED panel was leaning backward at 60-70 degrees (almost lying down), as shown in the photograph in Figure 7.2(a). This position was chosen for convenience as the display did not have a vertical stand and we were worried about the thermal impact of creating a solid stand. The back side was not covered in order to allow airflow. Using imaging thermography, the surface temperature was recorded during operation while a white block was shown. The size of the block was varied in a number of repeated experiments, in between which the display was left to cool down to ambient temperature. Thermocouples were attached to the centre, bottom-left, and back side in order to verify the results of the imaging thermography.

In Figure 7.2(b), the temperature as a function of time is shown for a white block of 4% ( $20\% \times 20\%$ ), 25% ( $50\% \times 50\%$ ), and 100% area coverage. In the photograph of Figure 7.2(a) the coverage is 100%. The luminance of the three blocks was  $450 \text{ cd/m}^2$  for the two small blocks and  $210 \text{ cd/m}^2$  for the large block (in reasonable accordance with the luminance data of Figure 7.1).

The temperatures of both small blocks (4% and 25% area) are seen to increase steeply the first two minutes, then follow a more moderate increase of temperature before steady-state is attained at 7 minutes. The luminance output was constant for about 1 minute after which the luminance decreased steadily over

<sup>1</sup>I would like to acknowledge my colleagues GA Luiten (thermal specialist) and JGR van Mourik (display specialist), with whom I conducted these experiments.

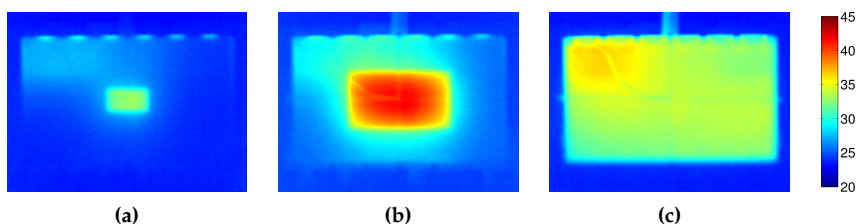


**Figure 7.3:** Thermograms of the 15 inch OLED display device showing a white block of 4%, 25%, and 100% area coverage in (a), (b), and (c), respectively. All three thermograms correspond to 120 s after power supply switch on. Notice the considerable lower temperature of the small block in (a) compared to (b), although the luminance is comparable. The higher temperature of the yellow area in the top left of (c) is due to the driving electronics just behind the panel.

time (a dynamic effect not illustrated in Figure 7.1, but well known in OLED displays). This is likely the cause of the moderate reduction of temperature from 2 minutes to 7 minutes. After 10-20 minutes, the power supply was turned off, which resulted in a steep reduction in temperature.

The temperature for the large block (100% area) increases slower than for the smaller blocks, but trends toward a substantially higher equilibrium temperature. After 22 minutes, the temperature equilibrium was still not fully achieved, after which the power supply was turned off. At this point, the temperature was a few degrees above the temperature of the middle-sized block (25% area). When the power supply was turned off, the temperature decreased slower in comparison to the curves for the smaller blocks. Note that although the luminance of the large block was less than half of the smaller blocks, the temperature of the large block was substantially higher.

In Figure 7.3, the thermograms for the three blocks are shown, all for the time instance 2 minutes. Due to the higher luminance of the small block and the particular resistance in the heat spreading, the temperature of the middle-sized block is the highest. Comparing the thermogram of the smallest block with the thermogram of the middle-sized block reveals a considerable difference in temperature, although the luminance is identical. The small block (4% area) is about 32 degrees, 9 degrees above ambient, while the middle-sized block (25% area) is close to 40 degrees, 17 degrees above ambient. The distance between the centre point and the edge of heat dissipation is considerably larger for the middle-sized block than for the small-sized block. Heat conduction is therefore limited for the middle-sized block, whereas the smaller block can obtain significant cooling via the nearby inactive areas.

In an OLED display, the temperature across the glass and organic material is nearly uniform, such that in-plane conduction becomes an important mechanism

to obtain sufficient cooling area (Sturm, Wilson, and Iodice, 1998). This is similar to the situation for large-sized thin form-factor LCDs (Luiten and Weeme, 2011). To that end, it may be beneficial to attach a graphite heat-spreader sheet in order to increase the in-plane thermal conductivity. This will lead to a reduced operating temperature (Kundrata and Baric, 2012) if the surrounding surface is not subject to heat dissipation, e.g. surrounding pixels are off. As we suspected that the rear glass of the measured OLED device was covered by a graphite heat-spreader sheet, we conducted experiments making thermograms of the back. A significant larger spreading of heat compared to the front supported this assumption.

In conclusion, the results presented in this section have illustrated that an area of low heat dissipation (dark pixels) can be used to reduce the operating temperature of a nearby region of high heat dissipation (bright pixels). With this in mind, the area-dependent luminance characteristic, shown in previous section, is a simple manner to prevent excessive operating temperature. In the following section we will consider alternative methods, which are aimed at increased luminance by exploiting this insight.

## 7.4 Suggestions for Improvements of Luminance

Without an area-dependent luminance characteristic, the luminance of state-of-the-art OLED displays would have to be limited to the worst-case scenario. This corresponds to a full-white image of all bright white pixels, such that both back-plane current density and steady-state temperature will be highest. Consequently, an OLED display would be 2-5 times darker, corresponding to the 100% area of Figure 7.1, for an image of only a few bright pixels than when luminance is adjusted according to the number of bright pixels.

The luminance control is typically adjusted based on a global histogram and has been known as “adaptive brightness control” (van der Vaart *et al.*, 2005), “power reduction method” (Shin *et al.*, 2005), but also occasionally as “automatic power control”. A histogram of the pixel values is used, as it is typically assumed that the power dissipation is proportional to the power consumption, which in turn can be approximated by a weighted average of the (linear) subpixel values (Lu *et al.*, 2008; Lee, Lee, and Kim, 2010).

For many images, the histogram-based luminance control will reduce the luminance unnecessarily. This is because such algorithms are not temperature aware. Consider the images of Figure 7.4. These images have an identical number of bright, white pixels and consequently the luminance of the white pixels will be identical. Yet, it is known from the previous section, that the temperature on top





**Figure 7.4:** Images of identical average pixel value. It is expected that the steady-state temperature of the white area on a display showing (a) will be substantially higher than the steady-state temperature of any of the white blocks when showing (b).

of the smaller blocks shown in Figure 7.4(b) will be much lower than the temperature on top of the large block shown in Figure 7.4(a).<sup>2</sup>

An obvious improvement of luminance could be achieved by measuring the temperature at multiple discrete locations and only limit the luminance whenever any region becomes critically warm. Although a display has several million small pixels generating heat, heat conduction will make the temperature profile spatially smooth and perhaps a few hundred temperature measurements on a large-sized OLED would suffice for the application. An obvious downside of this approach is the need for additional hardware. To that end, the homogeneity of the OLED display construction will likely allow a sufficiently accurate approximation of the local temperature using a computational model.

Another opportunity for improvement concerns the locality of the temperature problem. If one region reaches a critical temperature, a far-away region may still be well within limits, such that pixels in this region could be left unattenuated. In order to achieve this, it is necessary to only locally attenuate the bright pixels in regions of critical temperature.

Based on these two improvements, local temperature measurement and local attenuation of luminance, different luminance control approaches have been tabulated in Table 7.1. The frequently-used histogram-based luminance control (van der Vaart *et al.*, 2005; Shin *et al.*, 2005) is denoted (A). This method of global attenuation of luminance can be extended with temperature measurements or an equivalent computational approximation, denoted (B). An obvious advantage of global attenuation over local attenuation of an OLED display is the possibility to implement a global attenuation by adjusting the global maximum current, as a lower current density typically improves light efficacy of OLED emitters (Lee, Liu, and Wu, 2008).

It is expected that larger improvements of luminance can be achieved by using local, rather than global, attenuation of luminance, see (C) and (D) in Table 7.1.

<sup>2</sup>A similar argument could be used for backplane current density, which will also be lower for Figure 7.4(b) than for Figure 7.4(a). This section, however, is limited to temperature considerations.

This can be based on local temperature measurements, however, the attenuation map must contain sufficiently smooth spatial transitions as to not introduce visually annoying artefacts in uniform regions and preferably does not introduce halos.

The measured instantaneous (spatial) temperature profile of an OLED display, which depends on previously displayed images, will not (necessarily) correlate well with the luminance profile of the current image. Applying method (D), using local attenuation of luminance based on local temperature measurements, may therefore possibly lead to visually annoying artefacts. For example, one may experience that uniform image regions appear non-uniform, that a pair of equally bright car headlights will suddenly appear at different brightness, or that a spatially-static bright/dark spot appears.

Rather than using instantaneous temperature measurements, one can use a local approximation of the worst-case temperature. A worst-case temperature will typically occur when an image is static, such that bright pixels may result in a critically high thermal equilibrium. The approximation of temperature could be done using a computational model incorporating heat dissipation (from a pixel), heat radiation and convection (from the glass surface), and heat conduction (to neighbouring regions) and such an approach belongs to the category (C) in Table 7.1.

In a proposal to determine a local attenuation of luminance (type (C)), a two-step procedure is followed. First a worst-case estimate of local temperature is established based on a weighted average of the (linear) subpixel drive values followed by a linear low-pass filter. This filter should mimic heat conduction at a particular time-instance corresponding to the thermal equilibrium. For each OLED display, it is necessary to adjust the low-pass filter characteristics to the actual physical thermo-dynamic properties. Secondly, the approximation of temperature can be converted into a number indicative of whether or not a particular location will become too hot or not. This will automatically take both local heat dissipation as well as heat dissipation from neighbouring pixels into account. As the approximation of temperature will be of relatively low frequency compared to

**Table 7.1:** Classification of pixel-intensity control methods for OLED displays with or without temperature measurement(s)/prediction. The intensity attenuation is either a global or local operation. The histogram-based method is denoted (A).

<i>Attenuation</i>	<i>Temperature Meas./Prediction</i>		
	<b>None</b>	<b>Global</b>	<b>Local</b>
<b>Global</b>	(A)	(B)	(B)
<b>Local</b>	(C)		(D)

the image content, it is necessary to re-align the signals (image and temperature) such that visual artefacts are limited. This can be achieved using a joint-bilateral filter (Tomasi and Manduchi, 1998) on the temperature signal and using the image content (luminance channel, for example) as signal-range information. This concept has previously been disclosed by Hammer and de Greef (2012).

An example of the proposed method can be seen in Figure 7.5. In these examples a bilateral grid (Chen, Paris, and Durand, 2007), a computationally-efficient approximation to the full bilateral filter, has been employed. The reference image can be seen in the top row, where the intensity has been limited to one-half ( $1/2$ ). In the second row, the output images can be seen, and in the third row, the attenuation map. In the output images, the large and bright regions have been kept at the intensity of one-half, corresponding to black regions in the attenuation map, while the other regions have been increased in intensity to full range according to the white regions in the attenuation map. The factor 2 was arbitrarily chosen to illustrate the concept. By simulating the described behaviour on an LCD-based HDR display adjusted to about  $1000 \text{ cd/m}^2$  peak luminance, it was subjectively determined by expert viewers, that the visual artefacts are limited and below an acceptable threshold.

It is worth noting that proposed method (type (C)) may not entirely flatten the curve of Figure 7.1. In other words, the methods (A) and (C) are to some degree complementary and necessary in order to ensure that the display temperature is within safe limits at all times. Furthermore, in order to use OLED displays for HDR reproductions, the luminance should be increased 3-6 times. It is not likely that this can be achieved with the methods described above. However, advancements in power efficacy and light extraction can be expected to also improve the luminance performance of OLED displays and a combined result may deliver the desired increase of luminance.

## 7.5 Conclusions

In this chapter, we have considered OLED displays for reproducing HDR images. Whereas the contrast characteristics exceed those of most other display technologies, the luminance is still lower than that of LCDs. The luminance of a white region on an OLED display is often between 2 and 5 times lower for an image containing many bright pixel in comparison to an image with only a few bright pixels. This reduction in luminance can be ascribed to simple intensity control algorithms, which prevent extremely high current and temperature. As luminance depreciation of OLED materials is accelerated by increased temperature, we recommend to consider extending the existing intensity control algorithms to be temperature aware. One method based on a simple local temperature approximation was presented.

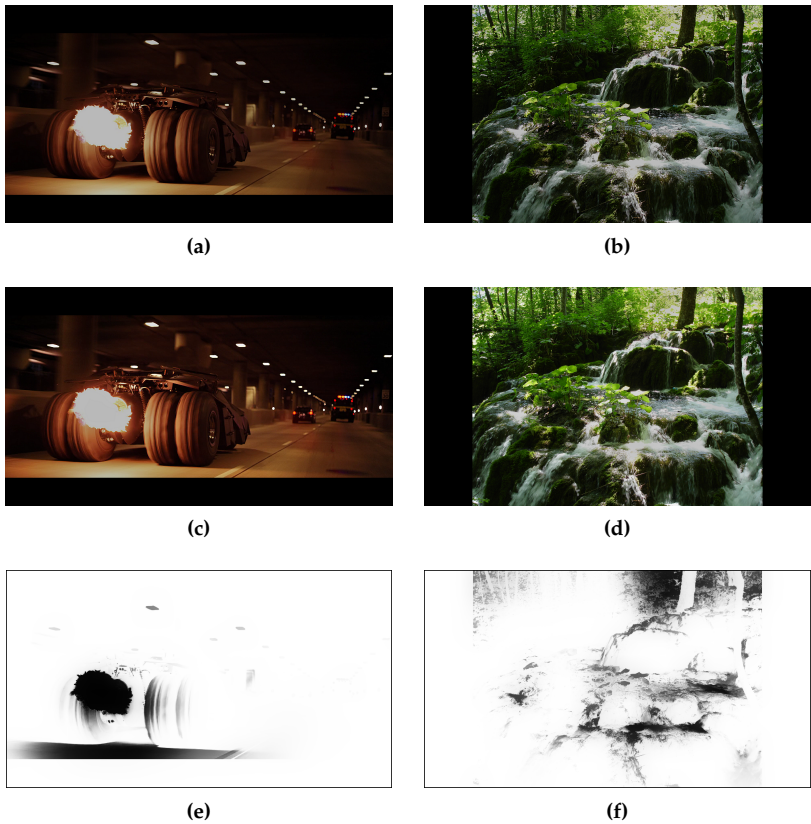


**Figure 7.5:** Illustration of local attenuation of intensity without temperature measurements, approach (C) in Table 7.1. The input images, processed images, and attenuation maps can be seen in the, top, middle, and bottom row, respectively. In the attenuation maps, the dark regions correspond to regions, which are limited in intensity, while bright regions are not affected by the method. Although this simulation is arbitrarily based on an attenuation by a factor 2, one can appreciate that the method results in brighter-looking images without introducing visually-annoying artefacts.

# Conclusions and Future Work

In this final chapter, the main contributions of this thesis are first summaries followed by a discussion on the research objectives stated in Chapter 1.

## Conclusions

The dynamic range (contrast and luminance) of state-of-the-art displays is considerably lower than what the human visual system effectively handles in daily life situations. Typically the contrast of a display is about 500:1 to 3000:1 and the luminance between  $100 \text{ cd/m}^2$  and  $500 \text{ cd/m}^2$ . However, Daly *et al.* (2013a) have found evidence of observer preference for contrast ratios of about 800 000:1 and luminance levels of close to  $4000 \text{ cd/m}^2$ . HDR display systems, such as spatially-modulated LCDs, exhibit contrast and luminance characteristics which could match these desired specifications.

Whereas HDR LCD systems provide high contrast and luminance, the power consumption is correspondingly higher compared to a conventional LCD system. The transmittance of an LC-panel is about 5-7% due to the crossed polarisers, small pixel aperture, and the presence of colour filters. A principal objective of this thesis was to investigate the combination of a high-transmission LC-panel with a spatially-modulated backlight in order to achieve increased luminance and contrast characteristics. To that end, a versatile high-dynamic-range display system was constructed to facilitate the research objective. In order to achieve high system efficiency, we investigated three display configurations; (1) an LC-panel with RGBW subpixel layout and local backlight boosting, (2) a colour-sequential display with local luminance boosting, and (3) a 120Hz, 2-field colour-sequential

system. In a last study, the contrast requirements for high-contrast display systems were investigated in relation to the limiting factor of human-eye glare.

In a first display configuration (Chapter 3) featuring an LC-panel with an RGBW subpixel layout, the problem of reduced luminance for bright saturated pixels was addressed. By applying local boosting in regions of luminance shortage using a spatially-modulated backlight, the colour error was successfully reduced. Furthermore, a method was introduced which allowed an increase of luminance for non-saturated pixels (which do not need boosting) in regions of saturated pixels (which do need boosting). This particular method did not lead to an increase in power consumption. In this context, it was also demonstrated that existing methods of deriving backlight drive levels either result in high contrast or temporal stability, but not both at the same time. In this thesis a new method was presented that does provides high contrast and temporal stability at the same time.

In a second display configuration (Chapter 4), a colour-sequential LC-panel (no colour filters) was combined with a backlight with locally-addressable RGB LEDs. A method was developed for local adjustments of the colour in each field to create small and tall local gamuts. A major advantage of this approach is that luminance can be increased up to 300% without installing additional light. As the display system reproduces colours without the use of colour filters, it is considerably more efficient than a conventional LCD system. The average luminance gain was validated on a large set of video data for a backlight with 240 segments and found to be more than 140%.

In a third display configuration (Chapter 5), a colour-sequential LC-panel (no colour filters) operating at 120 Hz was combined with a backlight with locally-addressable RGB LEDs. Full colour reproduction was achieved by dynamically adjusting only two local primaries per frame. Although normally at least three fields are required to display a colour image, the method enabled two-field colour reproduction. As colour-sequential operation of LC-panels has been complicated by their slow response time, the benefit of this method is the reduced field rate from 180 Hz to 120 Hz. A statistical analysis revealed excellent colour reproduction with 9216 backlight segments for close to 75% of the tested image and good to fair colour reproduction for the remaining 25%.

In Chapter 6, the effect of human eye glare on the perceived contrast was investigated and used to predict how much contrast is actually required for a display. The results showed that the contrast of a conventional LCD is not sufficient to accurately represent a high contrast image. It is also revealed that an OLED display makes more than sufficient contrast, even more than can be perceived by humans. Finally it revealed that spatially-modulated LCDs can make sufficient contrast provided that they have enough backlight segments. Typically such an LCD will be sufficient for the majority of images with  $16 \times 9$  backlight segments

and with more than  $64 \times 36$  segments, virtually all images can be represented with a contrast higher than the perception threshold.

In a final contribution (Chapter 7), OLED displays were considered for reproducing HDR images. Whereas the contrast characteristics of state-of-the-art OLED displays exceeds those of most other display technologies, the luminance is still lower than that of LCDs. Experimental data of four OLED displays show that luminance is 2 to 5 times lower for some images compared to others. This reduction is typically based on a global histogram. Experimental data shows that the thermal behaviour of an OLED display is substantially influenced by in-plane heat conduction. We therefore recommend to extend the existing luminance-reduction methods with a thermal model. Finally, a method was presented which is expected to allow improvements of luminance based on this insight.

In conclusion, this thesis contributed primarily to the field of display systems engineering with novel video processing and backlight control algorithms. A sophisticated backlight with HDR capabilities was constructed to facilitate the research objective and to demonstrate the performance of the algorithms. Existing methods for visualising HDR images considered display luminance and contrast characteristics constant. This thesis contributed by demonstrating that, when such characteristics are considered dynamic, it is possible to increase both contrast and luminance without physically modifying the display system.

## Discussion and Future Work

In this section, the results and methods presented in this thesis will be related to the research objectives stated in Chapter 1. The chosen methods will be motivated and alternatives discussed and possible improvements and extensions will be suggested as directions for future work.

### Spatially-Modulated Backlights

In order to increase the limited intrinsic contrast of LC-panels, it was an objective of this thesis to realise LCD solutions which utilise spatially-modulated backlights. The modulation of the backlight (contrast) should provide at least 2-3 orders of magnitude. With respect to this performance target, the design parameters of a backlight unit is first discussed followed by a discussion on how to quantify backlight contrast.

The performance of a segmented backlight is determined by the optical design and the method of control. The most important optical design parameters are the number of segments with respect to the display area and the spatial light distribution. The latter is a result of balancing overall uniformity in order to mask

variation between segments, and a desire for local light generation in order to maximise contrast. This can in turn be influenced by the type of LED, whether or not optical components, such as LED lenses and optical sheets, have been applied, and whether LEDs are mounted behind the screen or on the edge(s).

In scientific literature, methods for backlight modulation are often presented based on measured PSFs of a particular design. This makes reproduction of results complicated and therefore the results presented in Chapters 3 to 6 were based on simulated spatial light distributions using an analytical description of the PSFs. Furthermore, a simulated light distribution allows a convenient way of adjusting the number of backlight segments in order to quantify the importance of this design parameter.

Besides evaluating the proposed methods using simulations, the methods were also evaluated using a prototype display. For the majority of the work in this thesis, the display prototype was based on the HDR backlight design described in Chapter 2. In the following paragraphs the capabilities of this particular design in terms of backlight contrast are discussed.

A simple method for evaluating the contrast performance of a spatially-modulated backlight is difficult because the contrast of the backlight depends strongly on the image and the contrast perceived by an observer is influenced by attributes of the visual system. When a spatially-modulated backlight is adjusted to match a small bright image feature on a large black background, light from (a few) bright backlight segments may introduce small amounts of light into adjacent areas such that the black level varies across the screen. A spatially-varying luminance of black makes it impossible to define a meaningful global contrast measure. Furthermore, it is very likely that the spatially-varying luminance of black may be masked by the human visual system, for example due to limits of contrast discriminability or the presence of intra-ocular glare.

In Chapter 2, a number of methods for quantification of backlight contrast were presented which were designed to overcome the dependence on image stimuli. In a first method, estimation of backlight contrast is determined by exposing a computational model of the display (based on measured backlight PSFs) to sinusoidal patterns of varying frequency and phase. With this approach, the HDR prototype was shown to provide modulation of up to 2 orders of magnitude. In a second method, the backlight contrast was directly measured using a photometer and a set of corner-box stimuli (ICDM, 2012). With this approach, the HDR prototype (including LC-panel) was measured to provide a contrast range between 5 and 7 orders of magnitude. As about 3 orders of magnitude can be ascribed to the LC-panel, the remaining 2-4 orders of magnitude are due to backlight modulation. The large variation in the results is a consequence of the spatially-varying black level. A sinusoidal stimuli requires a large average light contribution from the backlight, such that the backlight contrast is limited.



The corner-box stimuli, on the other hand, requires a low average light contribution from the backlight, and as the distance from the display corner to the centrally-located measurement point is large, the backlight contrast measured using corner-box stimuli is larger than that estimated using sinusoidal stimuli. As neither of the stimuli are representative for natural images, it is difficult to predict the correlation between the contrast perceived by a human observer and the measured/estimated backlight contrast. However, the sinusoidal stimuli is likely to result in a conservative estimate, whereas the corner-box stimuli represents a somewhat idealised contrast value. Yet, due to the simplicity of the corner-box method, it is recommended to use this method for a quick comparison of backlight performance. In order to relate the corner-box method, and perhaps other measures of backlight contrast, to a more qualitative rating of backlight contrast, it is recommended to set up a well-designed comparative study.

With respect to human visual perception, the effect of intra-ocular glare on perceived contrast has been investigated in two ways. In Chapter 2 it was estimated that the tails of the spatial light distribution of a single backlight segment will be masked by the veiling glare generated by a white block. The size of the block was equal to the backlight segment pitch. For small(er) bright image features, the contribution of veiling glare to the retinal black level will be smaller such that the tails of the spatial light distribution may become visible. In order to prevent the backlight becoming visible for such critical images, one could either improve the LC-panel contrast, add more backlight segments, or improve the spatial light distribution of the backlight segments. In a second study (Chapter 6), the relationship between number of backlight segments and perceived contrast was investigated. For a given stimuli, the level of human eye glare was estimated and compared to the spatial light distribution of the display. In this study, it was concluded that about 2000 backlight segments would be required in order to mask the spatial light distribution even for very critical images. It is recognised that with only one critical image tested, the impact of the study results is limited and requires a more elaborate execution. However, it does illustrate the strength of the method and the simplicity of the method makes it a very useful tool when evaluating different design options of any display system.

With respect to backlight control, it was an objective of this thesis to investigate optimisation techniques, which have been shown to outperform existing schemes (Li *et al.*, 2007a; Li *et al.*, 2007b) in terms of resulting backlight contrast. However, such schemes suffer from poor temporal stability. In Chapter 3, a method was presented which was based on quadratic programming with spatio-temporal regularisation. The method was shown to outperform existing methods, for a range of different images, in terms of backlight contrast, and perform on-par with state-of-the-art methods in terms of temporal stability. Although the evaluation showed superior performance, the computational complexity has not

yet been investigated. It is suggested to pursue a real-time implementation, in the first place, and explorer approximate methods, in the second place.

A spatially-modulated backlight is widely perceived as *the* solution for improving the limited contrast of LCD systems. However, throughout this thesis, methods have been presented which illustrates that the benefits of a spatially-modulated backlight extends beyond this goal. For example, in combination with a multi-primary LC-panel, a spatially-modulated backlight can contribute to a significant reduction of colour errors (Chapter 3). In combination with a colour-sequential display it can contribute to a reduction of field-rate (Chapter 5) or an increase of luminance (Chapter 4). In the following sections these results will be discussed in detail.

### Multi-Primary LCD Systems

It is stated in Chapter 1, that it is an objective of this thesis to use multi-primary LC-panels to realise 50% higher luminance compared to a conventional LCD, while preserving same image fidelity and power consumption.

The focus of this thesis with respect to multi-primary displays has been limited to an RGBW configuration, in which a high-transmittance neutral colour filter (white) is added to the conventional RGB absorptive colour filters. Such systems exhibit about 50% more luminance for desaturated near-white colours, whereas saturated (primary) colours are about 25% darker. Compared to a conventional RGB LCD, colour images may appear out-of-balance due to this large discrepancy between the luminance of desaturated and the luminance of saturated colours. In Chapter 3 it was illustrated how a spatially-modulated backlight with white LEDs can be used to largely remove this discrepancy by applying local boosting of the backlight. To that end, the RGBW configuration was normalised such that the white point luminance was equal to a conventional RGB system. In that case, 50% reduction of power consumption is expected for an all white image. In the study it was shown that excluding the local boosting, the power consumption was 41% lower, whereas including the local boosting, the power consumption was about 20% lower. This shows that local boosting of the backlight is the largest contributing factor to the difference with the expected 50% lower power consumption. The smaller discrepancy (41% to 50%), is a consequence of the spatio-temporal regularisation and the optimisation. The optimisation directly takes into account contributions from neighbouring segments and may force additional segments to turn on in order to generate sufficient light. The regularisation may also turn on additional segments in order to enforce spatial and temporal smoothness. It should be emphasised that the 20% reduction in power consumption is equivalent to 20% increase of luminance for all colours.

Additional to the luminance increase of 20%, it was shown in Chapter 3 that it was also possible to increase the luminance of desaturated pixels in regions of

backlight boosting (necessary for the bright saturated pixels). On average, the luminance increase in such region was 30%. Consequently, the total increase of luminance in these regions can be more than 50%.

Although the work described in this thesis was limited to an RGBW configuration, other multi-primary colour-filter configurations may also benefit from a spatially-modulated backlight. Popular alternatives include the RGBY, RGBC, and RGBCMY configuration (Hinnen and Langendijk, 2010; Yoshida *et al.*, 2011; Teragawa *et al.*, 2011). For such configurations, the transmittance benefit for desaturated close-to-white colours is lower, however, the range of reproducible colours (chromaticity) will be enlarged. Such wide-gamut displays can therefore display very saturated colours. Despite that wide-gamut is not directly a contributor to the dynamic range, it is by many scientists considered a valuable and important improvement.

## Colour-Sequential LCD systems

An objective of this thesis with respect to colour sequential displays is to realise three times higher luminance compared to a conventional LCD with RGB colour filters with the same power consumption and comparable image fidelity.

The HDR display system presented in Chapter 2 has been designed to allow colour-sequential operation. Each segment consists of an RGB LED triplet for which both intensity and timing can be individually controlled. In combination with a prototype OCB-mode LC-panel, the display system can reach more than  $7000 \text{ cd/m}^2$ . In comparison with conventional LC-panels, the luminance has more than doubled in the colour-sequential configuration. This is significantly less than expected, but can be explained by the absence of high-end optical sheets for forward collimation and polarisation recycling, and to poor transmittance of the prototype OCB-mode LC-panel. The gamut area (area of chromaticity triangle expressed in CIE 1976  $u'v'$  coordinates) on the other hand, was 169% and very close to the 172% which was measured directly on the backlight. Such a wide gamut allows reproduction of very saturated colours which cannot be reproduced on a conventional LCD system. This is a significant benefit of using colour-sequential displays.

In Chapters 4 and 5, the colour-sequential prototype was used to demonstrate a method for increasing luminance and a method for reducing field rate, respectively. For both methods, the backlight is controlled in such a way that all LED colours (RGB) can be mixed in each field creating spatially- and temporally varying primaries. The chromaticity coordinates and the luminance of each segment are adjusted to the local image statistics and the final image (region) is reproduced by suitable modulation of the fast-switching LC-panel. This principle of backlight control satisfied a second objective with respect to colour-sequential displays: It

is an objective of this thesis to realise a colour-sequential display with spatially- and temporally-varying primaries as a means of reducing colour breakup artefacts. Although scientific literature has shown that such an approach can lead to reduced colour breakup (Lin, Zhang, and Langendijk, 2011; Zhang, Lin, and Langendijk, 2011), this has not been validated in the context of the research presented in this thesis.

Colour-sequential LCD systems should (in principle) allow 3 times higher transmittance, but in Chapter 4 a method is presented, which permits up to nine times higher luminance. The method is based on the principle of mixing light from multiple LED colours. In this way it is possible to reproduce white using three white-coloured fields, rather than a red, a green, and a blue field. When all three colours (LEDs) can be at full intensity throughout all three fields, the luminance has been increased by a factor three. Obviously, it is not possible to reduce the local primaries to a single colour at all locations in every image. However, in Chapter 4 it was illustrated that the gamut spanned by the local primaries was reduced by 66% on average. Such a reduction contributes to the possibility of increasing luminance, provided that the target colour is not located close to the local gamut primaries and preferably in the centre (the “white” point) such that the LC-panel can be set to maximum transmittance in all fields. On average, the method contributes to a 43% increase of luminance and up to 70% increase is frequently occurring. Combined with the improved transmittance of a colour-sequential display system, the luminance can then be increased with 400% to 500% compared to a conventional LCD. When neighbouring segments do not allow the same amount of LED colour mixing, there is a risk of introducing visible artefacts. This is caused by the spatially-varying gamut headroom (height). In the proposed method a heuristic algorithm was presented which could reduce the risk of introducing such artefacts. In a small study this proved to work very well, but we would encourage a more thorough visual evaluation and are open for alternative suggestions for improved backlight control.

A last objective with respect to colour-sequential displays was to investigate solutions with only two colour fields and no colour filters which would demonstrate three times higher luminance and same image fidelity compared to conventional LCDs. In Chapter 5 a method is presented which allows a field-rate reduction from 180 Hz to 120 Hz. The method is also based on mixing of the three LED colours, but only employs two fields. This provides the advantage of increased transmittance in combination with reduced field rate. When only two fields are used, it is often impossible to reproduce all colours of the input gamut. However, as the two primaries are spatially varying, it is shown in Chapter 5, that providing sufficient backlight segments, it is possible to reproduce most frames (close to 75%) with less than 1% of the pixels with a colour error above 0.020 CIE 1976  $\Delta u'v'$ . In this method of field-rate reduction, mixing of LED colours will lead to an increased gamut height. The shorter the line segment, the larger the

headroom. Provided that an input colour is located close to the gamut centre (the “white” point), the LC-panel can be set to maximum transmittance in both fields (ideally) resulting in a doubling of the luminance. This combines the benefit of field-rate reduction (Chapter 5) and luminance boosting (Chapter 4). This combination could be focus of a future investigation.

It is worth returning to the methods for determining the optimal local primaries. For both above-mentioned methods, the local primaries are determined without taking the inter-segment crosstalk into account. This means that the local primaries will deviate from the computed (ideal) primaries. This does, however, not immediately lead to clipping, as the inter-segment crosstalk is modelled prior to computing the LC-panel modulation values. A suitable gamut-mapping algorithm can therefore be applied in the case that clipping would occur. The disadvantage of this separation is apparent (a sub-optimal solution), however, the computational benefits are large, and necessary in order to efficiently compute the backlight and LC-panel drive levels.

### **Colour-Sequential Displays and Response Time of LC-Panels**

The results presented in Chapter 4 and Chapter 5 concerning a colour-sequential display system were based on the assumption of an idealised temporal electro-optical response of the LC-panel. Clearly, this assumption is violated in practice for most liquid-crystal alignment modes. Whenever high peak luminance is required (large LED duty cycle), the non-ideal temporal response of the LC-panel will lead to inter-field cross-talk. This will generally lead to colour errors (as illustrated in Figure 8.1). Dedicated LC-panel over-drive methods may be used to alleviate the colour errors by sacrificing overall contrast. However, in order to create spatially-consistent colour-error correction, it is necessary to extend the classical feed-forward first-order memory system to cover all fields.

In those situations where the field rate is a problem (LC-panel is slow) and where the risk of colour errors characteristic to the 2-field system described in Chapter 5 are unacceptable, it may be useful to consider a spatio-temporal configuration. In such a system two wide-band colour filters are used with two colour fields. This will trade off transmittance for a lower field rate. Similar to conventional colour-sequential LCDs, it is possible to use spatially-varying primaries in order to reduce the presence of colour breakup (Zhang, Langendijk, Hammer, and Lin, 2011b). Such a system can also benefit from the increased gamut height, similar to the method described in Chapter 4. Considering the slow technological progress of LC-panel response time, it may be worthwhile considering such a hybrid display system in order to increase the luminance and contrast.

Besides the aforementioned points of discussion, three items are considered very relevant as future work. First, the relationship between tone-mapping operators for tonal compression of HDR image to LDR image is related to the methods

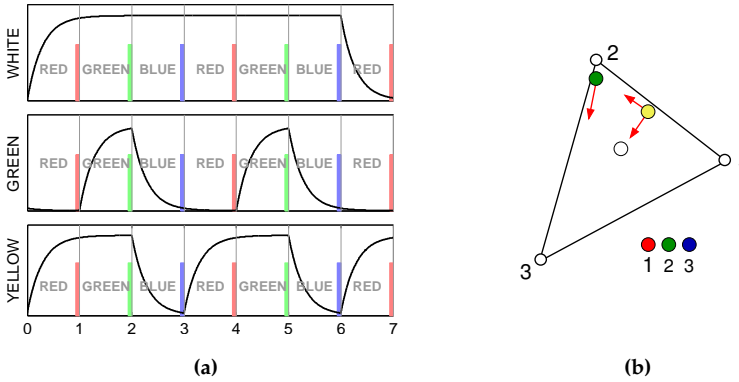


**Figure 8.1:** In (a), an illustration of LC-panel response for a white, green, and yellow pixel. The sequentially-flashing RGB backlight is shown with 15% pulse width. In total 7 fields (2 frames of 3 fields plus one additional red field) is shown. For a steady white pixel, the slow response time will have no effect, as the LC-panel does not have to change transmission state. For a green pixel, the slow increase in transmission may reduce the intensity of green, while the slow reduction in transmission in the blue field will result in a change of hue. In (b) this colour-change is illustrated. For a yellow pixel, the contribution of red relative to green will be reduced, while some blue may be added to the resulting colour. The yellow pixel will therefore to some degree more towards cyan, as illustrated in (b). Note that with a longer pulse width, the colour artefacts will increase.

presented in this thesis. Secondly, other display technologies, such as OLED displays and electro-wetting, are discussed.

### Display-Aware Tone Mapping

Reproduction of HDR images is ultimately the goal of increasing contrast and luminance of LCDs. Yet, the methods in this thesis have all been demonstrated using LDR images only. Whenever necessary, the tonal range of the LDR images were linearly expanded to match the display dynamic range, a method which has been shown to work well for mapping LDR images to HDR displays (Akyüz *et al.*, 2007). More advanced methods for tonal expansion has been extensively covered by others (Meylan, Daly, and Süssstrunk, 2006; Rempel *et al.*, 2007; Didyk *et al.*, 2008; Banterle *et al.*, 2008; Banterle, Debattista, *et al.*, 2009) and it is considered an interesting direction for future to research to investigate the importance of such methods in the context of HDR display design.

The dual problem of mapping HDR images to an LDR display is also relevant. When the dynamic range of an image exceeds that of the display unit, it is necessary to compress the tonal range. In order to preserve detail visibility while compressing the tonal range, perceptual limitations such as visual acuity,

contrast discriminability, and colour appearance are important. Consequently, so-called tone-mapping operators, such as those described by (Devlin *et al.*, 2002; Reinhard and Devlin, 2005; Reinhard, Ward, *et al.*, 2006), often employ computational models of the human visual system. This process can be simply stated as:

$$I_{\text{LDR}} = f(I_{\text{HDR}}, C_{\text{HVS}}) , \quad (8.1)$$

where an HDR image,  $I_{\text{HDR}}$ , is converted to an LDR image,  $I_{\text{LDR}}$ , under the constraints of the human visual system  $C_{\text{HVS}}$ .

Although an HDR display is characterised by a large dynamic range compared to a conventional (LDR) display, it is still necessary to apply tonal compression of HDR images to match the display dynamic range. This is a consequence of the large range of light intensities found in daily life which greatly exceeds the capabilities of state-of-the-art HDR displays.

In comparison with the tone-mapping of (8.1), the methods presented in this thesis can be expressed as:

$$I_{\text{HDR}} = f(I_{\text{LDR}}, C_{\text{disp}}) , \quad (8.2)$$

where the input LDR image,  $I_{\text{LDR}}$ , is expanded to an HDR reproduction,  $I_{\text{HDR}}$ , under the constraints of the display,  $C_{\text{disp}}$ . These display constraints pertain to colour gamut, luminance, and contrast. Due to a spatially-modulated backlight, these constraints are both spatially-varying and very image dependent. The tone-mapping operators (8.1) are in contrary typically based on a static definition of the target gamut, luminance, and contrast. When a tone-mapping operator (8.1) is simply cascaded by the display mapping operator (8.2), the operations will influence one another and result in a sub-optimal solution. Rather, if the methods are combined:

$$\hat{I}_{\text{HDR}} = f(I_{\text{HDR}}, C_{\text{HVS}}, C_{\text{disp}}) , \quad (8.3)$$

the compression of the dynamic range is based on both the spatially-varying luminance, contrast, and gamut characteristics, but also on the limitations of the human visual system. As an example of such an approach, one could compute the local luminance headroom (of the display) and feed this as an input to the tone-mapping operator. In this way, the tone-mapping operator can take the spatially-varying constraint into account and create a brighter result of higher dynamic range.

## OLED Displays

The emissive nature of OLED displays makes them attractive for HDR image reproductions, however, the luminance is still lower than that of LCDs. Luminance is limited by low light efficacy of the OLED materials and poor light extraction

from the OLED emitter. Resistive losses in the active-matrix backplane is also a source of problem which leads to elevated temperatures and accelerated luminance depreciation. As OLED displays have only recently achieved commercial breakthrough for large-sized panels, we can expect improvements on all elements during the next decade. Meanwhile, it is worth considering temperature measurements or predictions of the OLED device in order to maximise luminance. In this thesis a simple method was proposed, but clearly requires fine-tuning and a quantitative study of the luminance benefits.

### Other Transmissive Display Technologies

Besides LCDs, other transmissive display technologies may benefit from the methods presented in this thesis. For example, the transmissive panels with digitally-actuated micro shutters described by Hagood *et al.* (2007) operates without polarisers and colour filters, which results in a very high panel transmittance. A four-field (RGBW) colour-sequential prototype based on this technology has been reported by Payne (2013) and it is likely that the luminance of such a prototype could be increased using the concept of luminance boosting described in Chapter 3.

A second example is based on electro wetting, in which an optical shutter is created by electrically contracting a coloured oil film. Without polarisers and colour filters, such panels exhibit high transmittance and with a response time about 3-9 ms (Feenstra and Hayes, 2009) colour sequential operation is in principle possible. The concepts described in Chapter 3 could be applied to increase luminance. Furthermore with a close-to-critical response time (typically 5.6 ms is required), it may also be advantageous to use the concepts of Chapter 5 to allow a reduction of the minimal field rate from 180 Hz to 120 Hz.



# Bibliography

- Akyüz, AO, R Fleming, BE Riecke, E Reinhard, and HH Bülthoff (2007). „Do HDR Displays Support LDR Content? A Psychophysical Evaluation”. In: *ACM Trans. on Graphics* 26.3.
- Albrecht, M, A Karrenbauer, and C Xu (2009). „A Video-Capable Algorithm for Local-Dimming RGB Backlight”. In: *Digest Tech. Proc. SID*. Vol. 40, pp. 753–756.
- Banterle, F, K Debattista, A Artusi, S Pattanaik, K Myszkowski, P Ledda, and A Chalmers (2009). „High dynamic range imaging and low dynamic range expansion for generating HDR content”. In: *Computer graphics forum*. Vol. 28. 8, pp. 2343–2367.
- Banterle, F, P Ledda, K Debattista, and A Chalmers (2006). „Inverse Tone Mapping”. In: *Proc. Conf. Comput. Graph. and Inter. Tech. in Austral. and SE Asia*. Vol. 4. ACM, pp. 349–356.
- (2008). „Expanding low dynamic range videos for high dynamic range applications”. In: *Proc. 24th Spring Conf. on Comp. Graph*. Pp. 33–41.
- Bergquist, J and C Wennstam (2006). „Field-Sequential-Colour Display with Adaptive Gamut”. In: *Digest Tech. Proc. SID*. Vol. 37. 1, pp. 1594–1597.
- Berns, RS (2000). *Billmeyer and Saltzman’s Principles of Color Technology*. 3rd ed. John Wiley & Sons, Inc.
- Bitzakidis, S (1994). „Improvements in the moving-image quality of AMLCDs”. In: *J. Soc. Inf. Display* 2.3, pp. 149–154.
- Brightside Technologies (2012). *DR37-P Preliminary Specifications*. Downloaded from [web.archive.org/web/20070116130447/http://www.brightsidetech.com/products/info/dr37p\\_specs.pdf](http://web.archive.org/web/20070116130447/http://www.brightsidetech.com/products/info/dr37p_specs.pdf) on 01.05.2012.

- Chen, CY, LF Lin, JY Lee, *et al.* (2013). „A 65-inch Amorphous Oxide Thin Film Transistors Active-Matrix Organic Light-Emitting Diode Television Using Side by Side and Fine Metal Mask Technology”. In: *Digest Tech. Papers SID*. Vol. 44. 1, pp. 247–250.
- Chen, H, J Sung, T Ha, and Y Park (2007). „Locally pixel-compensated backlight dimming on LED-backlit LCD TV”. In: *J. Soc. Inf. Display* 15.12, pp. 981–988.
- Chen, J, S Paris, and F Durand (2007). „Real-time edge-aware image processing with the bilateral grid”. In: *ACM Trans. Graph.* Vol. 26. 3. ACM, p. 103.
- Chen, Y, J Yan, J Sun, ST Wu, X Liang, SH Liu, PJ Hsieh, KL Cheng, and JW Shiu (2011). „A microsecond-response polymer-stabilized blue phase liquid crystal”. In: *Applied Physics Letters* 99.20, p. 201105.
- Cheng, HH, A Bhowmik, and PJ Bos (2013). „Dual  $\pi$ -cell Fast Response LC Display”. In: *Digest Tech. Papers SID*. Vol. 44. 1, pp. 439–442.
- Cheng, YK, YP Huang, YR Cheng, and HPD Shieh (2009). „Two-Field Scheme: Spatiotemporal Modulation for Field Sequential Color LCDs”. In: *IEEE/OSA J. Display Technol.* 5.10, pp. 385–390.
- Cheng, YK and HPD Shieh (2009). „Colorimetric Characterization of High Dynamic Range Liquid Crystal Displays and Its Application”. In: *IEEE/OSA J. Display Technol.* 5.1, pp. 40–45.
- Daly, S, T Kunkel, X Sun, S Farrell, and P Crum (2013a). „Preference limits of the visual dynamic range for ultra high quality and aesthetic conveyance”. In: *IS&T/SPIE Electronic Imaging: Human Vision and Electronic Imaging*, 86510J.
- Daly, S, T Kunkel, X Sun, S Farrell, and P Crum (2013b). „Viewer Preferences for Shadow, Diffuse, Specular, and Emissive Luminance Limits of High Dynamic Range Displays”. In: *Digest Tech. Proc. SID*. Vol. 44. 1, pp. 563–566.
- Devlin, K, A Chalmers, A Wilkie, and W Purgathofer (Sept. 2002). „STAR: Tone Reproduction and Physically Based Spectral Rendering”. In: *State of the Art Reports, Eurographics 2002*, pp. 101–123.
- DICOM Part 14, Supp. 28 (1998). *Grayscale Standard Display Function*. National Electrical Manufacturers Association.
- Didyk, P, R Mantiuk, M Hein, and HP Seidel (2008). „Enhancement of bright video features for HDR displays”. In: *Computer Graphics Forum*. Vol. 27. 4, pp. 1265–1274.
- Dufaux, F, GJ Sullivan, and T Ebrahimi (2009). „The JPEG XR image coding standard”. In: *IEEE Signal Processing Magazine* 26.6, pp. 195–199.
- Eilertsen, G, J Unger, R Wanat, and R Mantiuk (2013). „Survey and Evaluation of Tone Mapping Operators for HDR-Video”. In: *Proc. Pacific Graphics*. Vol. 21. forthcoming.

- Elliot, CHB, MF Higgins, S Hwang, SJ Han, A Botzas, BS Hsu, M Im, and S Nishimura (2008). „PenTile RGBW Color Processing”. In: *Digest Tech. Proc. SID*. Vol. 39, pp. 1112–1115.
- Elliott, CHB, TL Credelle, and MF Higgins (May 2005). *Adding a White Subpixel*. SID Information Display.
- Fairchild, MD (2007). „The HDR Photographic Survey”. In: *Color and Imaging Conference*. Vol. 15. IS&T/SID, pp. 233–238.
- Feenstra, J and R Hayes (May 2009). *Electrowetting Displays*. Found on <http://www.liquavista.com/media/772/LQV0905291LL5-15.pdf> on 14.11.2013. Liquavista.
- Ferwerda, JA (2001). „Elements of early vision for computer graphics”. In: *IEEE Comput. Graph. Appl.* 21.5, pp. 22–33.
- (2011). „High Dynamic Range Displays and Low Vision”. In: *Color and Imaging Conference*. Vol. 19. IS&T/SID, pp. 181–185.
- Ferwerda, J and S Luka (2009). „A High Resolution, High Dynamic Range Display for Vision Research”. In: *Journal of Vision* 9.8, p. 346.
- Ge, Z, S Gauza, M Jiao, H Xianyu, and ST Wu (2009). „Electro-optics of polymer-stabilized blue phase liquid crystal displays”. In: *Appl. Phys. Lett.* 94.10, p. 101104.
- Greef, P de, HG Hulze, J Stessen, H van Mourik, and S Sluyterman (2006). „Adaptive scanning, 1-D dimming, and boosting backlight for LCD-TV systems”. In: *J. Soc. Inf. Display* 14.12, pp. 1103–1110.
- Greg Ward (2005). *High Dynamic Range Image Encodings*. Available from <http://www.anywhere.com/gward/hdrenc/>, date of access 07.09.2012.
- Hagood, N, R Barton, T Brosnihan, J Fijol, J Gandhi, M Halfman, R Payne, and JL Steyn (2007). „A Direct-View MEMS Display for Mobile Applications”. In: *Digest Tech. Papers SID*. Vol. 38. 1, pp. 1278–1281.
- Hammer, M, T Baar, KJ Hinnen, Y Zhang, and EHA Langendijk (21st Mar. 2013). „Driving of a Color Sequential Display”. WO/2013/037821.
- Hammer, M, T Baar, Y Zhang, KJG Hinnen, and EHA Langendijk (2012). „Method to Improve Color Reproduction on a 120-Hz Two-Field Color-Sequential LCD”. In: *J. Soc. Inf. Display* 20.7, pp. 380–389.
- Hammer, M, T Baar, Y Zhang, KJ Hinnen, and EHA Langendijk (2011). „Two-Field Colour-Sequential Display”. In: *Color and Imaging Conference*. Vol. 19. IS&T/SID, pp. 126–131.
- Hammer, M and P de Greef (23rd Feb. 2012). „Brightness Enhancement for Display”. First Filing, 2011P02578 US.

- Hammer, M and KJG Hinnen (2014). „Local Luminance Boosting of an RGBW LCD”. In: *IEEE/OSA J. Display Technol.* 10.1, pp. 33–42.
- Hammer, M, KJG Hinnen, and EHA Langendijk (2012). „Boosting Luminance of a Colour-Sequential Display”. In: *Color and Imaging Conference*. Vol. 20. IS&T/SID, pp. 15–20.
- (2013). „Balancing Luminance Boosting and Colour-Breakup Reduction for a Colour-Sequential Display”. In: *Digest Tech. Papers SID*. Vol. 44, pp. 962–965.
- Hammer, M and EHA Langendijk (2010). „Reduced Cross-Talk in Shutter-Glass-Based Stereoscopic LCD”. In: *J. Soc. Inf. Display* 18.8, pp. 577–582.
- Harbers, G, SJ Bierhuizen, and MR Krames (2007). „Performance of High Power Light Emitting Diodes in Display Illumination Applications”. In: *IEEE/OSA J. Display Technol.* 3.2, pp. 98–109.
- Hasebe, H and S Kobayashi (1985). „A full-color field sequential LCD using modulated backlight”. In: *Digest Tech. Papers SID*. Vol. 16, pp. 81–83.
- Hinnen, KJG, M Hammer, and EHA Langendijk (2011). „Ultra-Wide-Gamut LCD Using a Local Multi-Spectral Backlight”. In: *Digest Tech. Papers SID*. Vol. 42, pp. 669–672.
- (18th Oct. 2012). „Generation of Image Signals for a Display”. WO/2012/140551.
- Hinnen, K, M Klompenhouwer, Y Xie, R Rajagopalan, and EH Langendijk (2009). „Multi-Primary Displays From a Systems Perspective”. In: *Proc. Eurodisplay*. Vol. 29.
- Hinnen, K and EHA Langendijk (2010). „Design Considerations for Wide Gamut Displays”. In: *Color and Imaging Conference*. Vol. 18. IS&T/SID, pp. 11–16.
- Hong, H, H Shin, and I Chung (2007). „In-Plane Switching Technology for Liquid Crystal Display Television”. In: *IEEE/OSA J. Display Technol.* 3.4, pp. 361–370.
- Hong, JJ, SE Kim, and WJ Song (2010). „A clipping reduction algorithm using backlight luminance compensation for local dimming liquid crystal displays”. In: *IEEE Trans. Consum. Electron.* 56.1, pp. 240–246.
- Huang, SC, CL Chu, TL Chiu, and KH Chen (2011). „Multi-color LC/BL algorithm in field-sequential-color LCD for color-breakup suppression”. In: *J. Soc. Inf. Display* 19.2, pp. 170–177.
- ICDM, I (June 2012). *International Display Measurement and Metrology Standard (IDMS)*. Ed. by EF Kelley. v. 1.03. Downloaded from <http://icdm-sid.org/downloads/idms1.html> on 19.09.2012. Society for Information Display (SID).

- IEC (Oct. 2008). *IEC 62087 (100/1331/CDV), Methods of measurement for the power consumption of audio, video and related equipment*. English. IEC.
- Ishii, M and Y Taga (2002). „Influence of temperature and drive current on degradation mechanisms in organic light-emitting diodes”. In: *Appl. Phys. Lett.* 80.18, pp. 3430–3432.
- Iwata, Y, M Murata, K Tanaka, A Jinda, T Ohtake, T Shinomiya, and H Yoshida (2013). „Novel Super-Fast-Response, Ultra-Wide Temperature Range VA-LCD”. In: *Digest Tech. Papers SID*. Vol. 44. 1, pp. 431–434.
- Johnson, GM and MD Fairchild (Dec. 2003). „A top down description of S-CIELAB and CIEDE2000”. In: *Color Research and Application* 28.6, pp. 425–435.
- Jones, LA and HR Condit (1941). „The Brightness Scale of Exterior Scenes and the Computation of Correct Photographic Exposure”. In: *J. Opt. Soc. Am.* 31.11, pp. 651–678.
- Kang, SB, M Uyttendaele, S Winder, and R Szeliski (2003). „High dynamic range video”. In: *ACM Trans. Graph.* 22.3, pp. 319–325.
- Kao, MCA, PL Hsieh, and HT Lin (2010). „Advanced RGBW Display Image Process Using Sub-Pixel Rendering”. In: *Digest Tech. Proc. IDW, Japan*, pp. 1361–1364.
- (2011). „Dynamic Backlight Control Method for RGBW LCD”. In: *Digest Tech. Proc. SID*. Vol. 42, pp. 1296–1299.
- Kerofsky, L and S Daly (2006). „Brightness preservation for LCD backlight dimming”. In: *J. Soc. Inf. Disp.* 14.12, pp. 1111–1118.
- Kerofsky, L and J Zhou (2008). „Temporal Filtering in LCD Backlight Modulation”. In: *Digest Tech. Proc. SID*. Vol. 39, pp. 903–906.
- Kikuchi, H, H Higuchi, Y Haseba, and T Iwata (2007). „Fast Electro-Optical Switching in Polymer-Stabilized Liquid Crystalline Blue Phases for Display Application”. In: *Digest Tech. Proc. SID*. Vol. 38. 1, pp. 1737–1740.
- Kim, SE, JY An, JJ Hong, TW Lee, CG Kim, and WJ Song (2009). „How to reduce light leakage and clipping in local-dimming liquid-crystal displays”. In: *J. Soc. Inf. Disp.* 17.12, pp. 1051–1057.
- Klompshouwer, MA (2006). „Flat panel display signal processing : analysis and algorithms for improved static and dynamic resolution”. PhD thesis. Technical University of Eindhoven.
- Kundrata, J and A Baric (2012). „Electrical and Thermal Analysis of an OLED Module”. In: *COMSOL Conference Europe 2012*.

- Kunkel, T and E Reinhard (2010). „A reassessment of the simultaneous dynamic range of the human visual system”. In: *Proc. Symp. Appl. Percept. in Graph. and Vis.* Vol. 7, pp. 17–24.
- Lambooij, M and M Hammer (2013). „Visibility of Binocular Crosstalk for High-Dynamic Range Displays”. In: *IS&T/SPIE Electronic Imaging: Stereoscopic Displays and Applications*. Vol. 8648, pp. 864807–864807.
- Langendijk, EHA, G Cennini, and O Belik (2009). „Color-Breakup Evaluation of Spatio-Temporal Color Displays with Two- and Three-Color Fields”. In: *J. Soc. Inf. Display* 17.11, pp. 933–940.
- Langendijk, EHA (2005). „A comparison of three different field sequential color displays”. In: *Proc. Int. Disp. Workshops (IDW)* 12.2, pp. 1809–1812.
- Langendijk, EHA, O Belik, F Budzelaar, and FrankVossen (2007). „Dynamic Wide-Color-Gamut RGBW Display”. In: *Digest Tech. Proc. SID*, pp. 1458–1461.
- Langendijk, EHA and M Hammer (2010). „Contrast Requirements for OLEDs and LCDs Based on Human Eye Glare”. In: *Digest Tech. Papers SID*. Vol. 41, pp. 192–194.
- Langendijk, EHA, R Muijs, and W van Beek (2007). „Quantifying Contrast Improvements and Power Savings in Display with a 2D Dimming Backlight”. In: *Proc. IDW*. Vol. 14.
- (2008). „Contrast Gain and Power Savings using Local Dimming Backlights”. In: *J. Soc. Inf. Display* 16.12, pp. 1237–1242.
- Langendijk, EHA, SJ Roosendaal, MHG Peeters, and K Nasu (2005). „Design of a Novel Spectrum Sequential Display with a Wide Color Gamut and Reduced Color Breakup”. In: *Color and Imaging Conference*. Vol. 13. IS&T/SID, pp. 224–227.
- Ledda, P, G Ward, and A Chalmers (2003). „A wide field, high dynamic range, stereographic viewer”. In: *Proc. Conf. Comput. Graph. and Inter. Tech. in Austral. and SE Asia*, pp. 237–244.
- Lee, BW, C Park, S Kim, *et al.* (2003). „TFT-LCD with RGBW Color System”. In: *Digest Tech. Proc. SID*. Vol. 34, pp. 1212–1215.
- Lee, BW, K Song, Y Yang, *et al.* (2004). „Implementation of RGBW Color System in TFT-LCDs”. In: *Digest Tech. Proc. SID*. Vol. 35, pp. 111–113.
- Lee, C, C Lee, and CS Kim (2010). „Power-constrained contrast enhancement for OLED displays based on histogram equalization”. In: *IEEE Int. Conf. on Image Processing (ICIP)*, pp. 1689–1692.
- Lee, JH, DN Liu, and ST Wu (2008). *Introduction to Flat Panel Displays*. Wiley-SID Series in Display Technology. John Wiley & Sons, Ltd.

- Leyvi, E and K van Zon (2004). „A 180 Hz Frame Rate Video Format for Motion Compensated Frame Rate Upconverted Video Data”. In: *Digest Tech. Proc. SID-ADEAC*. Vol. 1, pp. 189–192.
- Li, F, X Feng, I Sezan, and S Daly (2007a). „Deriving LED Driving Signal for Area-Adaptive LED Backlight in HighDynamic Range LCD Displays”. In: *Digest Tech. Papers SID*. Vol. 38. SID, pp. 1794–1797.
- Li, F, X Feng, I Sezan, and S Daly (2007b). „Derive LED driving signals for high-dynamic-range LCD backlights”. In: *J. Soc. Inf. Disp.* 15.12, pp. 989–996.
- Liao, LY and YP Huang (2010). „Blur-Mask Approach for Real-Time Calculation of Light Spreading Function (LSF) on Spatial Modulated High Dynamic Range LCDs”. In: *IEEE/OSA J. Display Technol.* 6.4, pp. 121–127.
- Lin, FC, Y Zhang, and EHA Langendijk (2011). „Color Breakup Suppression by Local Primary Desaturation in Field-Sequential Color LCDs”. In: *IEEE/OSA J. Display Technol.* 7.2, pp. 55–61.
- Lin, FC, YP Huang, LY Liao, CY Liao, HPD Shieh, TM Wang, and SC Yeh (June 2008). „Dynamic Backlight Gamma on High Dynamic Range LCD TVs”. In: *IEEE/OSA J. Display Technol.* 4.2, pp. 139–146.
- Lu, MHM, M Hack, R Hewitt, MS Weaver, and JJ Brown (2008). „Power Consumption and Temperature Increase in Large Area Active matrix OLED Displays”. In: *IEEE/OSA J. Display Technol.* 3.1, pp. 47–53.
- Luiten, G and B ter Weeme (2011). „Thermal management of LED-LCD TV display”. In: *J. Soc. Inf. Display* 19.12, pp. 931–942.
- Luka, S and JA Ferwerda (2009). „Colorimetric Image Splitting for High-Dynamic-Range Displays”. In: *Digest Tech. Papers SID*. Vol. 40, pp. 1298–1301.
- Lyu, JJ, J Sohn, HY Kim, and SH Lee (2007). „Recent Trends on Patterned Vertical Alignment (PVA) and Fringe-Field Switching (FFS) Liquid Crystal Displays for Liquid Crystal Television Applications”. In: *IEEE/OSA J. Display Technol.* 3.4, pp. 404–412.
- Mantiuk, R (2006). „High-Fidelity Imaging - The Computational Models of the Human Visual Suystem in High Dynamic Range Video Compression, Visible Difference Prediction, and Image Processing”. PhD thesis. Universität des Saarlandes, Saarbrücken, Germany.
- Mantiuk, R, A Efremov, K Myszkowski, and HP Seidel (2006). „Backward compatible high dynamic range MPEG video compression”. In: *ACM Trans. on Graphics* 25.3, pp. 713–723.

- Mantiuk, R, G Krawczyk, R Mantiuk, and HP Seidel (2007). „High dynamic range imaging pipeline: Perception-motivated representation of visual content”. In: *IS&T/SPIE Electronic Imaging: Human Vision and Electronic Imaging*, p. 649212.
- McCann, JJ and A Rizzi (2009). „Retinal HDR Images: Intraocular Glare and Object Size”. In: *J. Soc. Inf. Display* 17.11, pp. 913–920.
- Meylan, L, S Daly, and S Süssstrunk (2006). „The reproduction of specular highlights on high dynamic range displays”. In: *Color Imaging Conference*. Vol. 14. IS&T/SID.
- Miller, ME and MJ Murdoch (2009). „RGB-to-RGBW conversion with current limiting”. In: *J. Soc. Inf. Disp.* 17.2, pp. 195–202.
- Mori, H (2005). „The Wide View (WV) Film for Enhancing the Field of View of LCDs”. In: *IEEE/OSA J. Display Technol.* 1.2, pp. 179–186.
- Morović, J (2008). *Color Gamut Mapping*. Wiley IS&T.
- Muijs, R, EHA Langendijk, and F Vossen (2008). „Spatio-Temporally Consistent Video Processing for Local Backlight Dimming”. In: *Digest Tech. Proc. SID*. Vol. 39, pp. 979–982.
- Murdoch, MJ and I Heynderickx (2012). „Veiling Glare and Perceived Black in High Dynamic Range Displays”. In: *J. opt. Soc. Am. A* 29, pp. 559–566.
- Murdoch, MJ, ME Miller, and PJ Kane (2006). „Perfecting the Color Reproduction of RGBW OLED”. In: *Proc. Int. Conf. of Imaging Science*, pp. 448–451.
- Myszkowski, K, R Mantiuk, and G Krawczyk (2008). *High Dynamic Range Video*. Ed. by BA Barsky. Morgan & Claypool Publishers.
- Nam, WJ, JS Shim, HJ Shin, *et al.* (2013). „55-inch OLED TV using InGaZnO TFTs with WRGB Pixel Design”. In: *Digest Tech. Papers SID*. Vol. 44, pp. 243–246.
- Omer, I and M Werman (2004). „Color lines: image specific color representation”. In: *Proc. IEEE Computer Vision and Pattern Recognition*. Vol. 2, pp. II–946.
- Payne, RS (2013). „The Joys of Being Digital for Low-Power, Mobile, Multi-Media Devices”. In: *Digest Tech. Papers SID*. Vol. 44. 1, pp. 859–862.
- Philips (2009). *Lumileds Rebel Datasheet no. 56*. Accessed Dec. 2009, has been replaced by datasheet 65.
- Pointer, M (1980). „The gamut of real surface colours”. In: *Color Research and Application* 5.3, pp. 145–155.
- Pólik, I, T Terlaky, and Y Zinchenko (July 2013). *SeDuMi: a package for conic optimization*. <http://sedumi.ie.lehigh.edu/>.



- Post, DL, AL Nagy, P Monnier, and CS Calhoun (1998). „Predicting Colour Breakup on Field-Sequential Displays: Part 2”. In: *Digest Tech. Papers SID*. Vol. 29. 1, pp. 1037–1040.
- Raman, N and G Hekstra (2005). „Dynamic contrast enhancement of liquid crystal displays with backlight modulation”. In: *IEEE Conf. Consumer Elec. (ICCE)*, pp. 197–198.
- Reinhard, E and K Devlin (2005). „Dynamic range reduction inspired by photoreceptor physiology”. In: *IEEE Trans. Vis. Comput. Graphic* 11.1, pp. 13–24.
- Reinhard, E, G Ward, S Pattanaik, and P Debevec (2006). *High Dynamic Range Imaging: Acquisition, Display, and Image-Based Lighting*. San Francisco, CA, USA: Morgan Kaufmann Publishers Inc.
- Rempel, A, M Trentacoste, H Seetzen, H Young, W Heidrich, L Whitehead, and G Ward (2007). „LDR2HDR: on-the-fly reverse tone mapping of legacy video and photographs”. In: *ACM Trans. on Graphics* 26.3.
- Rieke, F and ME Rudd (2009). „The challenges natural images pose for visual adaptation”. In: *Neuron* 64.5, pp. 605–616.
- Rüfenacht, D (2011). „Stereoscopic High Dynamic Range Imaging”. MA thesis. Ecole Polytechnique Fédérale de Lausanne (EPFL) and Philips BU-TV, the Netherlands.
- Sano, Y, R Nonaka, and M Baba (2012). „Wide gamut LCD using locally dimmable four-primary-color LED backlight”. In: *J. Soc. Inf. Display* 20.9, pp. 539–546.
- Seetzen, H, W Heidrich, W Stuerzlinger, G Ward, L Whitehead, M Trentacoste, A Ghosh, and A Vorozcovs (2004). „High dynamic range display systems”. In: *ACM Trans. on Graph.* 23.3, pp. 760–768.
- Seetzen, H, H Li, L Ye, W Heidrich, L Whitehead, and G Ward (2006). „Observations of Luminance, Contrast and Amplitude Resolution of Displays”. In: *SID Symp. Dig. Tech. Papers*. Vol. 37. SID, pp. 1229–1233.
- Seetzen, H, L Whitehead, and G Ward (2003). „A High Dynamic Range Display Using Low and High Resolution Modulators”. In: *SID Symp. Dig. Tech. Papers*. Vol. 34. SID, pp. 1450–1453.
- Sekiya, K, T Miyashita, and T Uchida (2006). „A Simple and Practical Way to Cope With Color Breakup on Field Sequential Color LCDs”. In: *Digest Tech. Proc. SID*. Vol. 37. 1, pp. 1661–1664.
- Shin, SR, HH Hwang, SH Kim, and JS Park (2005). „The Power Consumption Reduction Algorithm of OLED Display”. In: *Proc. IDW*. Vol. 12, pp. 763–764.

- Shu, X, X Wu, and S Forchhammer (2013). „Optimal Local Dimming for LC Image Formation with Controllable Backlighting”. In: *IEEE Trans. Image Proc.* 22.1, pp. 166–173.
- Silverstein, LD, SJ Roosendaal, and MJJ Jak (2006). „Hybrid spatial-temporal color synthesis and its applications”. In: *J. Soc. Inf. Display* 14.1, pp. 3–13.
- Sluyterman, A and E Boonekamp (2005). „Architectural Choices in a Scanning Backlight for Large LCD TVs”. In: *Digest Tech. Proc. SID*. Vol. 36. 1, pp. 996–999.
- Spencer, G, P Shirley, K Zimmerman, and DP Greenberg (1995). „Physically-Based Glare Effects for Digital Images”. In: *Proc. of the 22nd annual conference on Computer graphics and interactive techniques. SIGGRAPH '95*. ACM, pp. 325–334.
- Sturm, JC, W Wilson, and H Iodice (1998). „Thermal effects and scaling in organic light-emitting flat-panel displays”. In: *IEEE J. Sel. Topics Quantum Electron* 4.1, pp. 75–82.
- Swinkels, S, R Muijs, EHA Langendijk, and F Vossen (2006). „Effect of Backlight Segmentation on Perceived Image Quality for HDR Displays”. In: *Digest Tech. Proc. IDW, Japan*, pp. 1451–1454.
- Teragawa, M, A Yoshida, K Yoshiyama, S Tomizawa, and Y Yoshida (2011). „Multi-Primary-Color Displays: The Latest Technologies and Their Benefits”. In: *J. Soc. Inf. Disp.* 20.1, pp. 1–11.
- Tocci, MD, C Kiser, N Tocci, and P Sen (2011). „A versatile HDR video production system”. In: *ACM Trans. on Graphics* 30.4, p. 41.
- Tomasi, C and R Manduchi (1998). „Bilateral Filtering for Gray and Color Images”. In: *IEEE Int. Conf Computer Vision*. IEEE, pp. 839–846.
- Trentacoste, M, W Heidrich, L Whitehead, and G Seetzen H. and Ward (2007). „Photometric image processing for high dynamic range displays”. In: *J. Vis. Comun. Image Represent.* 18.5, pp. 439–451.
- Trentacoste, M (2006). „Photometric image processing for high dynamic range displays”. MA thesis. The University Of British Columbia.
- Unger, J and S Gustavson (2007). „High Dynamic Range Video for Photometric Measurement of Illumination”. In: *IS&T/SPIE Electronic Imaging: Sensors, Cameras and Systems for Scientific/Industrial Applications*. Vol. 6501.
- van der Vaart, NC, H Lifka, FPM Budzelaar, *et al.* (2005). „Towards Large-Area Full-Color Active-Matrix Printed Polymer OLED Television”. In: *J. Soc. Inf. Display* 13.1, pp. 9–16.
- van Hateren, JH (2006). „Encoding of High Dynamic Range Video with a Model of Human Cones”. In: *ACM Trans. on Graphics* 25.4, pp. 1380–1399.

- Vogels, I, I Heynderickx, and S Swinkels (2003). „The Visibility of a Local Deviation in Luminance and White-Point of a Display”. In: *Digest Tech. Papers SID*. Vol. 34, pp. 820–823.
- Vos, JJ (1984). „Disability Glare - A State of the Art Report”. In: *CIE Journal* 3, pp. 39–53.
- Vos, JJ and TJTP van den Berg (1999). „Disability Glare”. In: *CIE Research Note* 135.1.
- Wanat, R, J Petit, and R Mantiuk (2012). „Physical and perceptual limitations of a projector-based high dynamic range display”. In: *Theory and Practice of Computer Graphics*.
- Wang, L, Y Tu, L Chen, K Teunissen, and I Heynderickx (2007). „Trade-off between Luminance and Color in RGBW displays for mobile-phone usage”. In: *Digest Tech. Proc. SID*. Vol. 38, pp. 1142–1145.
- Ward, G (2002). „A Wide Field, High Dynamic Range, Stereographic Viewer”. In: *PICS 2002*. IS&T.
- Ward, G and M Simmons (2005). „JPEG-HDR: A backwards-compatible, high dynamic range extension to JPEG”. In: *Color and Imaging Conference*. Vol. 14. IS&T/SID, pp. 283–290.
- Wyszecki, G and WS Stiles (1982). *Color Science: Concepts and Methods, Quantitative Data and Formulae*. Second. Pure and Applied Optics. Wiley.
- Xu, D, L Rao, CD Tu, and ST Wu (2013). „A Nematic LCD with Submillisecond Gray-to-gray Response Time”. In: *Digest Tech. Papers SID*. Vol. 44. 1, pp. 435–438.
- Yamada, F, H Nakamura, Y Sakaguchi, and Y Taira (2002). „Sequential-color LCD based on OCB with an LED backlight”. In: *J. Soc. Inf. Display* 10.1, pp. 81–85.
- Yoon, JK, EM Park, JS Son, HW Shin, HE Kim, M Yee, HG Kim, CH Oh, and BC Ahn (2013). „The Study of Picture Quality of OLED TV with WRGB OLEDs Structure”. In: *Digest Tech. Papers SID*. Vol. 44, pp. 326–329.
- Yoshida, A, R Mantiuk, K Myszkowski, and HP Seidel (2006). „Analysis of Reproducing Real-World Appearance on Displays of Varying Dynamic Range”. In: *Computer Graphics Forum* 25.3.
- Yoshida, Otoi, Mori, and Tomizawa (2011). „Recent Trend of LED Backlight with Local Dimming and its Application for Multi-Primary-Color Displays”. In: *Digest Tech. Papers SID*. Vol. 42. 1, pp. 773–776.
- Zhai, J and J Llach (2009). „Non-Uniform Backlighting Computation for High Dynamic Range Displays”. In: *IEEE Conf Image Proc. (ICIP)*, pp. 4005–4008.

- Zhang, Y, EHA Langendijk, M Hammer, and KJ Hinnen (2012). „A new Color Brekaup measure based on Color Difference between Fields and Contrast to the Surrounding”. In: *IEEE/OSA J. Display Technol.* 8.3, pp. 145–153.
- Zhang, Y, EHA Langendijk, M Hammer, and FC Lin (2011a). „A 120 Hz Spatio-Temporal Color Display Without Color Breakup”. In: *Digest Tech. Papers SID*. Vol. 42, pp. 964–967.
- (2011b). „A Hybrid Spatial-Temporal Color Display with Local-Primary-Desaturation Backlight Scheme”. In: *IEEE/OSA J. Display Technol.* 7.12, pp. 665–673.
- Zhang, Y, FC Lin, and EHA Langendijk (2011). „A field-sequential-color display with a local-primary-desaturation backlight scheme”. In: *J. Soc. Inf. Display* 19.3, pp. 242–248.

# List of Publications

## Journal Papers

- Hammer, M and EHA Langendijk (2010). „Reduced Cross-Talk in Shutter-Glass-Based Stereoscopic LCD”. In: *J. Soc. Inf. Display* 18.8, pp. 577–582.
- Zhang, Y, EHA Langendijk, M Hammer, and FC Lin (2011b). „A Hybrid Spatial-Temporal Color Display with Local-Primary-Desaturation Backlight Scheme”. In: *IEEE/OSA J. Display Technol.* 7.12, pp. 665–673.
- Hammer, M, T Baar, Y Zhang, KJG Hinnen, and EHA Langendijk (2012). „Method to Improve Color Reproduction on a 120-Hz Two-Field Color-Sequential LCD”. In: *J. Soc. Inf. Display* 20.7, pp. 380–389.
- Zhang, Y, EHA Langendijk, M Hammer, and KJ Hinnen (2012). „A new Color Brekaup measure based on Color Difference between Fields and Contrast to the Surrounding”. In: *IEEE/OSA J. Display Technol.* 8.3, pp. 145–153.
- Hammer, M and KJG Hinnen (2014). „Local Luminance Boosting of an RGBW LCD”. In: *IEEE/OSA J. Display Technol.* 10.1, pp. 33–42.

## Conference Proceedings

- Hammer, M and EHA Langendijk (2009). „Time-Sequential Stereoscopic LCD Display with Scanning Backlight”. In: *Proc. Eurodisplay*. Vol. XX.
- Hammer, M, RTJ Muijs, and EHA Langendijk (2010). „Halo Artefact Visibility for Local Backlight Dimming LCD Systems”. In: *Proc. IDW*. Vol. 17. (invited paper).
- Langendijk, EHA and M Hammer (2010). „Contrast Requirements for OLEDs and LCDs Based on Human Eye Glare”. In: *Digest Tech. Papers SID*. Vol. 41, pp. 192–194.

- Hammer, M, T Baar, Y Zhang, KJ Hinnen, and EHA Langendijk (2011). „Two-Field Colour-Sequential Display”. In: *Color and Imaging Conference*. Vol. 19. IS&T/SID, pp. 126–131.
- Hinnen, KJG, M Hammer, and EHA Langendijk (2011). „Ultra-Wide-Gamut LCD Using a Local Multi-Spectral Backlight”. In: *Digest Tech. Papers SID*. Vol. 42, pp. 669–672.
- Zhang, Y, EHA Langendijk, M Hammer, and FC Lin (2011a). „A 120 Hz Spatio-Temporal Color Display Without Color Breakup”. In: *Digest Tech. Papers SID*. Vol. 42, pp. 964–967.
- Hammer, M, KJG Hinnen, and EHA Langendijk (2012). „Boosting Luminance of a Colour-Sequential Display”. In: *Color and Imaging Conference*. Vol. 20. IS&T/SID, pp. 15–20.
- (2013). „Balancing Luminance Boosting and Colour-Breakup Reduction for a Colour-Sequential Display”. In: *Digest Tech. Papers SID*. Vol. 44, pp. 962–965.
- Lambooij, M and M Hammer (2013). „Visibility of Binocular Crosstalk for High-Dynamic Range Displays”. In: *IS&T/SPIE Electronic Imaging: Stereoscopic Displays and Applications*. Vol. 8648, pp. 864807–864807.

## Granted and Filed Patents

- Damkat, C, G de Haan, MJW Mertens, M Hammer, and P. Newton (22nd Mar. 2010). „Apparatuses and Methods for Improved Encoding of Images”. WO/2012/035476.
- Hammer, M and P de Greef (23rd Feb. 2012). „Brightness Enhancement for Display”. First Filing, 2011P02578 US.
- Hammer, M and KJ Hinnen (19th June 2012). „Image Processing Method”. First Filing, EP12174542.6.
- Hinnen, KJG, M Hammer, and EHA Langendijk (18th Oct. 2012). „Generation of Image Signals for a Display”. WO/2012/140551.
- Muijs, RTJ, MJW Mertens, WHA Bruls, C Damkat, M Hammer, and CW Kwisthout (27th Sept. 2012). „Apparatuses and Method for Analyzing Image Gradings”. WO/2012/127401.
- Hammer, M (22nd Oct. 2013). „Consumer device and method for adapting the duration of a temporary control status related to the display of a user interface element”. First Filing, EP13189696.
- Hammer, M, T Baar, KJ Hinnen, Y Zhang, and EHA Langendijk (21st Mar. 2013). „Driving of a Color Sequential Display”. WO/2013/037821.

# Curriculum Vitae

Martin Hammer was born in Horsens, Denmark. After attending secondary school at Horsens Amtsgymnasium, he studied engineering at Aalborg University (Denmark). He received his Master's degree (civilingeniør) in Electrical Engineering in 2007 based on a thesis entitled "Dual-Microphone Noise Reduction with Applications to Speech and Real-Time Implementation". In 2005–2006, he was an Erasmus exchange student for two semesters at the Katholieke Universiteit Leuven (Belgium).



From 2007 to 2010, he was with Philips Research (the Netherlands) as a research scientist and from 2010 to 2013 with Philips Business-Unit Television (now TP Vision) as a senior scientist. His research has focused on signal processing applied to high-dynamic range displays, colour-sequential displays, and organic light-emitting diode displays. He has experience engineering novel display systems and has practised display metrology and calibration for many years. Currently he is employed at ASML (the Netherlands).

Martin Hammer has (co)authored 14 journal and conference publications, more than 20 business invention disclosures, and 7 patent applications. He is a member of SID and a reviewer of Journal of the SID and IEEE/OSA Journal of Display Technology. Seven students have combined their master thesis with an internship under his supervision, of whom two students are now pursuing doctorate degrees abroad.

